

Optimization of stability and rheological robustness of cosmetic salt-containing lamellar gel phase emulsions

Dissertation

zur Erlangung des akademischen Grades
Doctor rerum naturalium (Dr. rer. nat.)

vorgelegt der

Naturwissenschaftlichen Fakultät I - Biowissenschaften
der Martin-Luther-Universität Halle-Wittenberg

von

MSc. Chem. Lucile Bonnin
geboren am 11. Januar 1991 in La Roche sur Yon, Frankreich

Gutachter:

1. Prof. Dr. Dr. h.c. Reinhard Neubert
2. Prof. Dr. Thomas Gassenmeier
3. Prof. Dr. Rolf Daniels

Datum der Verteidigung: 06.03.2019

Abbreviations

ΔH	Melting enthalpy
$\Delta\eta_{\text{ionic}}$	Scattering of the viscosity for ionic samples
$\Delta\eta_{\text{nonionic}}$	Scattering of the viscosity for nonionic samples
ϵ	Static permittivity
$\epsilon(r)$	Relative static permittivity or dielectric constant
$\epsilon(0)$	Permittivity of a vacuum
$1/\kappa$	Debye-length
η	Viscosity
$ \eta^* $	Dynamic complex viscosity
τ	Shear stress
ω	Frequency
γ	Strain
$\dot{\gamma}$	Shear rate
γ_c	Critical strain
a	Surfactant cross-sectional area
av.	Average
AOT	Dioctyl sulfosuccinate sodium salt
APG	Alkyl polyglucoside
ATR-FTIR	Attenuated total reflection Fourier transform infrared
BH	Buffalo hair
C	Molar concentration
d	Particle radius
dc	Distance between emulsifier and FA in a surfactant bilayer
di	Interlamellar distance of a surfactant bilayer
DSC	Differential scanning calorimetry
DLVO	Derjaguin-Landau-Verwey-Overbeek
E	Weight percent of the EO unit
EDTA	Ethylenediaminetetraacetic acid
EO	Ethylene oxide
F	Faraday constant
FA	Fatty alcohol
FAc	Fatty acid

FF-TEM	Freeze-fracture transmission electron microscopy
G'	Elasticity/storage modulus
G''	Viscous/loss modulus
GC	Grey coverage
H	Distance between two particles (DLVO theory)
HLB	Hydrophilic-lipophilic balance
IH	Ideal hair
KBr	Potassium bromide
KCl	Potassium chloride
KI	Potassium iodide
l	Surfactant tail length
L_{α}	Lamellar phase
$[L_{\alpha}]$	Onion/vesicle phase or flexible bilayer phase
L_{β}	Semi-solid lamellar phase
LiCl	Lithium chloride
LVR	Linear viscoelastic region
m	Number of EO units
M	Molecular mass
MEA	Monoethanolamine
M_h	Molecular mass of the hydrophilic moiety
M_l	Molecular mass of the lipophilic moiety
n	Number of carbon atoms
NaCl	Sodium chloride
O/W	Oil-in-water
OE	Oxyethylated
PC	Phase contrast
PEG	Polyethylene glycol
PL	Polarized-light
POE	Polyoxyethylated (chemical function)
PP	Packing parameter
PPG	Polypropylene glycol
R	Gas constant
rpm	Revolution per minute
RT	Room temperature
SALS	Small angle light scattering
SAXD	Small angle X-ray diffraction
SAXS	Small angle X-ray spectroscopy
SDS	Sodium dodecyl sulfate

SEM	Scanning electron microscopy
SLES	Sodium laureth sulfate
Std. dev.	Standard deviation
T	Temperature
$T_{\alpha-\beta}$	α - β transition temperature for FA
T_c	Colloid critical temperature (melting)
$\tan\delta$	Loss factor
TEM	Transmission electron microscopy
TGA	Thermogravimetric analysis
t_R	Residence time
UAc	Uranyl acetate
V	Surfactant tail volume
V_A	Potential energy of attraction
V_{\max}	Highest potential energy level
V_{other}	Potential energy of other forces
V_R	Potential energy of repulsion
V_{TOT}	Total interaction potential
WH	White hair
W/O	Water-in-oil
Z	Ion valence

Content

Abbreviations	ii
Content	v
1. Introduction.....	1
1.1. Hair.....	1
1.2. Hair coloring products: generalities and modern challenges.....	1
1.3. Emulsifier systems.....	3
1.3.1. Amphiphile molecules	3
1.3.1.1. Ionic emulsifiers.....	4
1.3.1.2. Nonionic emulsifiers	5
1.3.2. Blended surfactants systems – Emulsifiers ratio	6
1.3.3. Hydrophilic-lipophilic Balance (HLB)	6
1.3.4. DLVO theory	7
1.3.5. Emulsifiers aggregates	11
1.3.5.1. Geometrical arrangements	11
1.3.5.2. Packing parameter (PP)	11
1.3.5.3. Lamellar structures.....	13
1.3.6. Polymorphism of emulsifiers	14
1.4. Physico-chemical properties of hair coloring products and characterization.....	15
1.4.1. Microstructure of emulsifiers' system forming bilayers	15
1.4.2. Swelling properties and hydration mechanism.....	17
1.4.3. Ageing properties	18
1.4.4. Manufacturing.....	19
1.4.5. Rheological behavior	20
1.4.6. Microscopic properties.....	22
1.4.6.1. Optical microscopy.....	22
1.4.6.2. TEM	24
1.4.7. Thermal properties	26
1.4.8. Spectroscopic imaging.....	27
1.4.9. The effect of electrolytes on lamellar phase systems.....	28

1.4.9.1.	Salt-like compounds.....	28
1.4.9.2.	Hair dyes.....	30
1.4.10.	Glossary for colloidal lamellar gel structure	31
1.5.	Objectives of the study	31
2.	Material and methods.....	34
2.1.	Materials	34
2.1.1.	Standard hair coloring product.....	34
2.1.2.	Optimization of the surfactant system: screening of nonionic emulsifiers.....	35
2.1.3.	Nonionic hair coloring product	36
2.2.	Methods	38
2.2.1.	Formulation process	38
2.2.2.	Microscopy.....	39
2.2.2.1.	Optical microscopy.....	39
2.2.2.2.	TEM/cryo-TEM	39
2.2.3.	Rheology	40
2.2.3.1.	Static rheological measurements	40
2.2.3.2.	Dynamic rheological measurements.....	40
2.2.4.	DSC	41
2.2.5.	ATR-FTIR	41
2.2.6.	Specific evaluations for hair coloring products	41
2.2.6.1.	Stability tests	42
2.2.6.2.	Color delivery	42
3.	Results and discussions	43
3.1.	Characterization of a classical hair coloring product	43
3.1.1.	Microscopy.....	43
3.1.1.1.	PL microscopy.....	43
3.1.1.2.	TEM	44
3.1.2.	Rheology	46
3.1.3.	DSC	51
3.1.3.1.	Thermal behavior of the raw materials contained in the ionic creams	51
3.1.3.2.	Thermal behavior of the ionic creams containing ammonium sulfate.....	52
3.1.3.3.	Thermal behavior of the ionic creams containing PTD	55
3.1.4.	Spectroscopic imaging.....	57
3.1.5.	Conclusion	60
3.2.	Optimization of the surfactant system.....	62
3.2.1.	Evaluation of the systems containing a single nonionic emulsifier	62
3.2.2.	Evaluation of the systems containing a combination of nonionic emulsifiers	64

3.2.3.	Influence of the nonionic surfactants molar ratio in the system containing a combination of two emulsifiers.....	67
3.2.4.	Conclusion	68
3.3.	Characterization of the nonionic hair coloring product	71
3.3.1.	Microscopy.....	71
3.3.1.1.	PL Microscopy	71
3.3.1.2.	Cryo-TEM	72
3.3.1.3.	Particle size measurement by means of PC-light microscopy.....	73
3.3.2.	Rheology	77
3.3.3.	DSC	83
3.3.3.1.	Thermal behavior of the raw materials contained in the nonionic creams	84
3.3.3.2.	Thermal behavior of the nonionic creams containing PTD	85
3.3.3.3.	Thermal behavior of the nonionic creams containing a mixture of hair-dyes	88
3.3.4.	Spectroscopic imaging.....	90
3.3.5.	Conclusion	93
4.	Summary	97
5.	Zusammenfassung	100
6.	Outlook	104
7.	Appendices.....	105
7.1.	List of 114 substances allowed for restricted use in hair dye products according to the European Commission. Regulation (EC) No. 1223/2009 updated in March 2017.	105
7.2.	Thermal behavior of the ionic system.....	110
7.2.1.	DSC thermograms of the raw materials contained in the ionic systems.....	110
7.2.2.	DSC thermograms of the ionic systems – Cooling run.....	112
7.3.	ATR-FTIR spectra of the raw materials contained in the ionic system	113
7.4.	Particle size measurement of the nonionic hair coloring product	116
7.5.	Thermal behavior of the nonionic system	120
7.5.1.	DSC thermograms of the raw materials contained in the nonionic system.....	120
7.5.2.	DSC thermograms of the nonionic systems – Cooling run	123
7.6.	ATF-FTIR spectra of the raw materials contained in the nonionic system	124
7.7.	Additional specific evaluations for cosmetic and industrial purposes	127
7.7.1.	Scale-up	128
7.7.2.	Stability tests.....	130
7.7.3.	Color delivery.....	132

7.7.4.	Scale-up data.....	134
7.7.5.	Storage tests results of the nonionic creams containing hair-dyes mixtures	137
7.7.6.	Color delivery data	139
7.8.	List of Tables.....	142
7.9.	List of Figures.....	144
7.10.	List of publications and patents.....	150
	Research Article	150
	Poster presentation.....	150
	Patents.....	150
7.11.	Acknowledgements.....	151
7.12.	Curriculum Vitae	153
7.13.	References	153
7.14.	Declaration of academic integrity.....	163

1. Introduction

1.1. Hair

All around the world and in various cultures, hair has always been a subject of fascination. Especially in women population, it is a powerful accessory for expressing traditions, beliefs and beauty habits. According to Technavio consumer and retail analysis: “the global hair color market is about to reach 29.14 billion by 2019, growing at a compound annual growth rate of more than 9%”. This quote is clearly highlighting the great market potential of this cosmetic branch. Interests for hair beauty products and consequently for the hair fiber itself is not something recent. Scientists observed for the first time hair fiber in the late 1800s, primarily for criminal investigation purposes and then for medical applications [1]. This led to extensive knowledge about the inner structure and chemical composition of the hair fiber. Hair is a protein filament which can be described as a three layers component: from the outside to the inside, the cuticle, the cortex and the medulla. The outer layer, the cuticle, is composed of scales of translucent cells which overlap. Depending on the composition and the condition of the hair, cuticles can be five to ten layers thick. Virgin hair is mostly formed by perfectly arranged scales which overlap, to protect the inner part of the hair and provide shine to the fiber. The middle part of the hair, the cortex, provides strength to the fiber and is containing the natural colorants called melanin. The cortex is composed of proteins, more specifically keratin and structural lipids. Keratin is made of eighteen different amino acids arranged in an alpha-helix configuration. These features give elasticity and strength to the hair fiber [2]. Finally, the most inner part of the hair fiber is called the medulla. This layer is the most fragile and soft part of the hair. It is almost transparent and plays a role of marrow in the hair fiber. Generally, humans have between 90 and 150 thousand hairs on the scalp that grow 1 to 2 cm a month with a cross-sectional diameter of 15 to 110 μm [3].

1.2. Hair coloring products: generalities and modern challenges

Hair coloration products are formulated to deliver artificial colorants in the cortex of the hair, and hence change the apparent color of the fiber. A pre-coloring step called “lift” is often required for highly pigmented hair. This consists of removing partially or completely the natural pigments from the hair fiber: the melanin. Simultaneously, the hair can be artificially re-colored with a proper delivery system [4]. Depending on durability, washing fastness, pH and the nature of the dye-mixture [5], hair coloring systems can be clustered into two distinct groups: the oxidative and the non-oxidative products. The non-oxidative hair dyes used in non-permanent colorations are leaving the hair after a few washings. They have a high molecular weight, deposit on the hair surface and do not reach the cortex. These compounds are mostly anionic and are selected to have the

minimum penetration in the hair and the maximum water solubility. On the contrary, permanent dyes can give the hair any kind of definitive new shade. They have a low molecular weight to reach the inner part of the hair fiber diffusing through the cuticles and are highly reactive to oxidation. The permanent coloration process is happening upon mixing two solutions. Firstly, the color base carrying the dyestuff containing also an alkalizing agent: ammonia and/or monoethanolamine (MEA), is promoting the opening of the cuticle for letting the dye penetrating in the cortex. In a second step, the developer, a stabilized solution containing hydrogen peroxide, is initiating the oxidation reaction of the hair dyes precursors. The polymerization reaction of the permanent hair dyes e.g. precursors together with couplers, lead to the formation of chromophores, responsible of the perceivable color by a human-eye [6]. The colorful oligomer macro-molecules are then sealed in the hair cortex by re-acidification of the hair fiber with hair-conditioning products. Dyestuffs are aromatic compounds derived from benzene. Commonly used dyestuff are the precursors: p-phenylene diamine, 2,5-diaminotoluene, p-aminophenol and the couplers: resorcinol, chloro-resorcinol, methyl-resorcinol, α -naphthol, m-aminophenol, m-phenylenediamine [7], [8]. These compounds will be described more precisely in [1.4.9.2. Hair dyes](#).

Hair coloration products are formulated to deliver dyestuff into the human hair fibers. Topical, functional hair coloration formulations contain generally: a dye mixture, one alkalizing agent e.g. ammonia or MEA, a buffer for constant basic pH, solvents, antioxidants/sequestrants, water, sometimes oil and surfactants to achieve the right viscosity for delivery, effortless application, stability and a satisfying cosmetic aspect and texture. Unfortunately, it is a well-known fact, that salts interact with some emulsifiers and impact on the rheology and the stability of emulsions. Many types of hair dyes are typical salt-like compounds which can interact with common emulsifier systems. Fatty alcohols (FA), ethoxylated fatty alcohols, glycols, glycol ethers, sulfuric acid derivatives, phosphoric acid derivatives and long chain carboxylic acids (fatty acids: FAc) are common emulsifiers used in hair coloring products. Kuss [9], Tucker [10] and Goldenberg [11] were the first to investigate the effect of the base components on the properties of oxidative dyes. The following non-exhaustive list is showing some examples of formulation challenges concerning hair coloring products:

- Solvents and surfactants used to dissolve and stabilize dyestuff are affecting the final color on hair. For instance, Goldenberg observed lower color deposit when increasing the propylene glycol concentration tenfold [11].
- Antioxidants can affect the final color results. For example: EDTA is used as sequestrant to ensure controlled release of oxygen from the developer upon mixing and keep the dyestuff in their reductive state in the color base. This antioxidant can

provoke an increase of the mixing temperature and a premature polymerization of the dyestuff when added in a too high concentration [11].

- Silicone compounds showed negative effect on the color delivery. Their addition is leading to darker color results [11].

Therefore, specific considerations must be taken while formulating hair coloring products: dyes stability, hair base stability and rheological robustness [12]. The color base must be monitored carefully as any changes in the formulation can affect the dye deposition and delivery, the final color results of the hair fiber, the dye solubility, the component interactions, etc. [13].

1.3. Emulsifier systems

1.3.1. Amphiphile molecules

Amphiphile molecules are characteristic compounds used to formulate emulsions. Their particularity is that they are composed of a polar hydrophilic ionic or nonionic head and a lipophilic tail. Due to this ambivalence, these molecules are surface-active and can self-assemble. They exist in many various forms. They are usually classified in two distinct groups which behave differently: the ionic and the nonionic amphiphiles. In a three-components system composed of e.g. water/oil/amphiphile, the amphiphiles are arranging differently depending on their concentration and affinity with both phases. At low concentration, the amphiphile compounds are rather in a dispersed state in one of the phase depending on their intrinsic polarity e.g. HLB value ([1.3.3. Hydrophilic-lipophilic Balance \(HLB\)](#)). When increasing the concentration, amphiphiles will start to form organized macro-molecular aggregate at the water/oil interface. This phenomenon is thermodynamically driven and reduces the global surface tension in the system [14]. This arrangement promotes the solubility of water in the presence of oil and inversely.

Hair colorations are specific emulsions due to their high pH [13]. Emulsifiers must then be chosen with caution to avoid side reactions in the system which would lead to destabilization and in the worst-case phase separation. For this reason, compounds having an ester functional group e.g. glyceryl stearate or sorbitan stearate compounds, which can be hydrolyzed under high pH, are not the first choice emulsifiers for formulating hair coloration [15]. Indeed, under alkaline conditions, large esters can be hydrolyzed. This reaction results in the two following products: carboxylate salt and alcohol. Because soaps can be prepared by the alkaline hydrolysis this reaction is more generally called saponification. Therefore, usage of esters in hair color products should be avoided. Moreover, for good conservation concerns, unsaturated compounds should

also not be used. In fact, ethylene derivatives are highly subject to spontaneous hydrogenation [16].

1.3.1.1. Ionic emulsifiers

All surfactants having a polar charged head group are classified in the ionic emulsifiers class. When the charge of ionic emulsifiers is dependent on pH, they can be called amphoteric [17]. Else, ionic emulsifiers can be anionic when charged negatively or cationic when charged positively. In this section, only the anionic emulsifiers will be reviewed as they are the class of interest for hair coloration for the following reasons:

- At high pH, anionic surfactants encourage the hair cuticles to swell, easing the penetration of the dyestuff into the fiber. In fact, in presence of ammonia, the carboxylic acid groups from the hair's amino acids are negatively charged [18] as well as the anionic polar head group from the surfactant.
- Anionic surfactants do not interact (attract) neither with the dyestuff molecules nor with the hair and act as a vehicle for the coloring process. It has also been demonstrated that the rate of polymerization of the dyes in a controlled bath is faster when containing anionic than cationic surfactants [19].
- Anionic surfactants have good cleansing properties: the negative charge from the surfactants entrapping the dirt is repelled by the negatively charged hair while rinsing.
- Even though not mild for the scalp, mainly due to the swelling effect on the stratum corneum (horny layer), anionic surfactants are less irritating than cationic surfactants. To achieve a milder mixture, anionic surfactants are often blended with nonionic or amphoteric surfactants [20].

Commonly used anionic surfactants are: ammonium lauryl/laureth sulfate, sodium laureth sulfate (SLES), sodium dodecyl sulfate (SDS), alpha-olefin sulfonate etc. The anionic class of emulsifiers can be subdivided into five major subgroups: acylated amino acids and acyl peptides, carboxylic acids, sulfonic acid derivatives, sulfuric acid derivatives and phosphoric acid derivatives.

In the cosmetic industry, the first class is seldom used due to preservation issue. In fact, they are subject to microbial attack, especially the peptides derivatives [17].

The carboxylic acid salts such as lauric, myristic, palmitic and stearic, having 12, 14, 16, 18 carbons, respectively, are found in the nature in their unsaturated form and can be synthesized to obtain the saturated molecule. More commonly called soaps, they are widely used for their high-water solubility and strong surface activity. The ester derivative of soap compounds will not be described as they are subject to hydrolysis/saponification at high pH [15].

The sulfonic acid derivatives are extremely stable. Alpha-olefin surfactants are part of this group and are used in shampoos and liquid soaps. A very commonly used surfactant in this group is called sodium C14-16 olefin sulfonate.

The sulfuric acid derivatives are half-esters and can be subject to hydrolysis in hair coloration products. Nevertheless, this reaction is more likely to occur at acidic than basic pH [17]. They are therefore usable compounds for formulating hair colorations. This group can be itself subdivided into two groups: the alkyl sulfates and alkylether sulfates in which SLES and SDS belong.

Finally, the last group called the phosphoric acid derivative are milder than their sulfuric equivalent. Lecithin derivatives are typical phosphoric acid derivative and are derived from mono and di-glycerides. They are seldom found pure in solution and are mostly mixtures of mono-, di- and tri-esters. Once again, these compounds are stable to hydrolysis except at acidic pH. Phospholipid-like surfactants are also part of the phosphoric acid derivative. This latter and lecithin are also well-known for forming bilayers and/or liposomes alone in solution [17]. They are nevertheless also sensitive to alkaline hydrolysis and are, therefore, not the first compounds of interest for formulating hair coloration products.

1.3.1.2. Nonionic emulsifiers

Nonionic surfactants do not have a charged polar head group and are therefore not influenced by the pH conditions. Nonionic surfactants can be classified in five different subgroups: alcohols, esters, ethers, alkanolamides and amine oxides. As mentioned earlier, esters will not be described as they are not the first compounds of interest for formulating hair coloring products.

The first group, the alcohols, are used in blend with co-emulsifiers as are unstable alone in solution. The following notation can be used to describe them: C_nOH , with n defining the number of carbon atoms in the apolar moiety. They are usually commercially available in mixtures with carbon chain length ranging from $n = 8$ to 18.

The ethers are not subject to hydrolysis. They are therefore stable in formulation and can be used for hair coloring products. Ethoxylated alcohols are very common in cosmetics and can be described as follow: C_nE_m , with n defining the number of carbon atoms in the lipophilic tail and m the number of oxyethylene (OE) function in the polar head group. Such a compound is called a polyoxyethylated (POE) surfactant or polyethylene glycol (PEG) derivative. Their solubility in water is dependent on the m value: the higher m the more hydrophilic the surfactant. This characteristic is essential for the formation of self-assemble systems such as bilayers. It has been shown that increasing the value of m of two units can lead to a drastic change of morphology and hence rheological behaviour [21]. The OE unit can also be branched such as in polypropylene oxide (PPG) compounds,

thus giving the opportunity to vary the hydrophilic/lipophilic ratio (HLB) of the surfactant. Alkyl polyglucosides (APG) are mild to the skin and are interesting for hair cosmetic applications. They are stable at high pH and sensitive to low pH where they hydrolyze to sugar and FA [22]. They are FA sugar derivatives, usually glucose, and are good foaming agents. These compound are also able to stabilize emulsions by forming a lamellar gel phase in a ternary water/oil/surfactant system [23].

Finally, the two last groups: alkanolamides and amine oxides are rarely used as structural emulsifiers in cosmetics but rather as foaming agents.

Most of the nonionic surfactants have a water solubility which is directly correlated with the degree of ethoxylation.

1.3.2. Blended surfactants systems – Emulsifiers ratio

To achieve sufficient viscosities, it is usual to find in commercial emulsions blended emulsifiers systems. Topical functional emulsions often contain an excess of FA blended with ionic and/or nonionic surfactants. The British Pharmacopoeia recommends using one part by weight of surfactant to nine (ionic) and four (nonionic) parts of cetearyl alcohol [24]. This corresponds to a molar ratio, for ionic and nonionic surfactant systems, of about 1:9 and 1:20, respectively.

The three to more- components systems forming self-assemble organized aggregates are very stable and well-documented in the literature under the name of colloids.

1.3.3. Hydrophilic-lipophilic Balance (HLB)

Estimation of the stability of surfactant-based systems can be done using the hydrophilic-lipophilic balance. This factor can be calculated for each surfactant and measures the relative contribution of the hydrophilic and lipophilic part of a surfactant. The HLB value is given along an arbitrary scale which allows classification of surfactants from zero to twenty: from oil soluble to water soluble compound. The HLB value can be calculated from different formula depending on the nature of the emulsifier. The empirical generic formula was given by Griffin [25]:

$$HLB = 20 \times \left(1 - \frac{M_l}{M}\right) = 20 \times \left(\frac{M_h}{M}\right) \quad (1)$$

Where M_l , M_h and M stand for the molecular mass of the lipophilic, hydrophilic moiety and the whole molecule, respectively. If the hydrophilic portion consists only of EO, equation (1) becomes the simplified equation (2).

$$HLB = \frac{E}{5} \quad (2)$$

Where E stands for the weight percent of the EO unit. These two formulas were generated mainly for nonionic surfactants like FA, FAC, polyols and PEG. The HLB number is a useful formulation tool for simple and mixed emulsifier-based emulsions [26].

The [Table 1.1](#) is giving the common HLB classification.

Table 1.1. Emulsifiers typical usage according to their HLB values - Classification

HLB RANGE	EMULSIFIERS' TYPICAL USAGE
4-6	w/o
7-9	Wetting agent
8-18	o/w
13-15	Detergent
15-18	Solubilizer

Most of the nonionic emulsifiers' HLB values can be determined thanks to the above formulas (1) and (2). However, the HLB value of ionic compounds must be empirically estimated. This method is rather complex and time-consuming. It is therefore recommended, for such compounds, to evaluate the HLB value from the water solubility as a first screening-test. The analysis of the chemical functions can also be an efficient way to achieve a good HLB estimation. Davies developed in 1957, a cumulative theory, where the HLB value is calculated from the individual contribution of the hydrophilic and hydrophobic moieties of the surfactant. This method is strictly restricted to ionic surfactants. He established an equation from which the HLB values can be calculated by substituting the hydrophilic groups by their group numbers as following [27], [28]:

$$HLB = 7 + \sum (\text{hydrophilic group numbers}) - n \times 0.475 \quad (3)$$

With n , the number of lipophilic groups in the molecule.

1.3.4. DLVO theory

When the estimation of the HLB value is not sufficient, one can use the Derjaguin-Landau-Verwey-Overbeek (DLVO) theory. This method was presented in 1941 by Derjaguin, Landau, Verwey and Overbeek to describe colloidal stability. It considers two long-range forces: the electrostatic repulsive forces and van der Waals' attractive forces. The DLVO theory explains that two surfaces e.g. two dispersed particles, at a relative long finite distance, must be stable when a balance between the repulsive forces and attractive forces exists. The minimum free energy level corresponds to the balanced state. According to this theory, repulsive interactions are created by similarly charged electric double layers

surrounding the particles or to particle-solvent interactions. Attractive interactions are mainly due to Van der Waals forces between the particles [29], [30]. Therefore, to disperse particles, the system must have greater repulsive forces than attractive ones. On the contrary, to aggregate particles, the system must have greater attractive forces than repulsive ones. According to the classical DLVO theory, the total interaction potential (V_{TOT}) of a system is composed of two distinct terms:

$$V_{TOT} = V_A + V_R \quad (4)$$

where V_A is the potential energy of attraction and V_R is the potential energy of repulsion. They are expressed as a function of H : the distance between two particles (from surface to surface). The value of V_R is equal to zero when the particles are infinitively far apart and is increasing when the particles are approaching each other. Therefore, V_R is always positive. The value of V_A is equal to zero when the particles are infinitively far apart and is decreasing when the particles are approaching each other. Therefore, V_A is always negative. The total energy of the system depends on different parameters: the particle size compared to the thickness of the electrical double layer, the electrolyte concentration and the surface potential. A typical plot of V_R and V_A as a function of H is shown in [Figure 1.1.](#) V_{max} stands for the highest potential energy level. According to the DLVO theory, this unstable energy state is found in between the two lower energy levels called the primary and secondary minimum. This means that two particles in solutions must overcome the highest potential energy level V_{max} , also called the potential barrier, to get closer to each other and aggregate in an irreversible way. This happens when two particles receive enough energy from the Brownian motion [30]. When two particles are at a distance H corresponding to the secondary minimum, the attractive forces are weak, and the bonding can be reversed by stirring or shaking the solution.

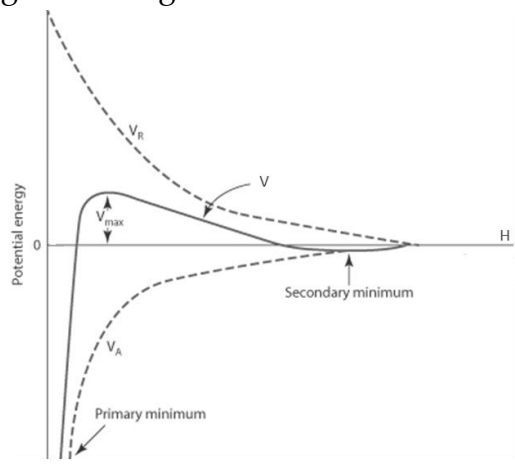


Figure 1.1. Schematic plot of the total potential energy $V=V_{TOT}$ (plain line) between two particles as a function of the distance H . The dotted lines represent V_A and V_R . (modified from Rosen et al. [29]).

The potential energy of attraction is defined by:

$$V_A = \frac{-Ad}{12H} \quad (5)$$

where A is the Hamaker constant relative to the Van der Waals forces, H the distance between two particles (surface to surface) and d the particle radius.

When two phases enter in contact, e.g. particle and solvent, the interface between them is called the double electrical layer. In this region, unequal repartition of electrical charges exists. This nonequilibrium gives rise to a potential energy which maintains overall neutrality. The most used model was explained by Stern in 1924 [31]. He divided this interface into two parts: The Stern layer, close to the particle (charged surface), where counterions are strongly held, and the diffuse layer, further in the solvent phase, where counterions are not held to the particle. The thickness of the Stern layer is called the Debye length and is given by the equation (6).

$$\frac{1}{\kappa} = \sqrt{\frac{\varepsilon(r)\varepsilon(0)RT}{4\pi F^2 \sum_i z_i^2 c_i}} \quad (6)$$

Where $\varepsilon(r) = \frac{\varepsilon}{\varepsilon(0)}$ is the relative static permittivity or dielectric constant of the solution, $\varepsilon(0)$ the permittivity of a vacuum, ε the static permittivity of the solution, R the gas constant, T the temperature, F the Faraday constant, Z the ion valence and C the molar concentration of any ions in solution. This expression shows that the Debye length is inversely proportional to the valence Z and the concentration C of ions contain in the solution. Therefore, colloidal interactions are highly dependent on these two factors. When increasing the overall concentration of electrolytes in the solution, the Debye length decreases. Consequently, the electrical double layer is compressed, and V_{\max} decreases and can even disappear (when $\kappa \rightarrow 0$). A graph illustrating the double layer compression is shown in [Figure 1.2](#). This means, that according to the DLVO theory, at a high critical electrolytes concentration, two particles would aggregate more easily.

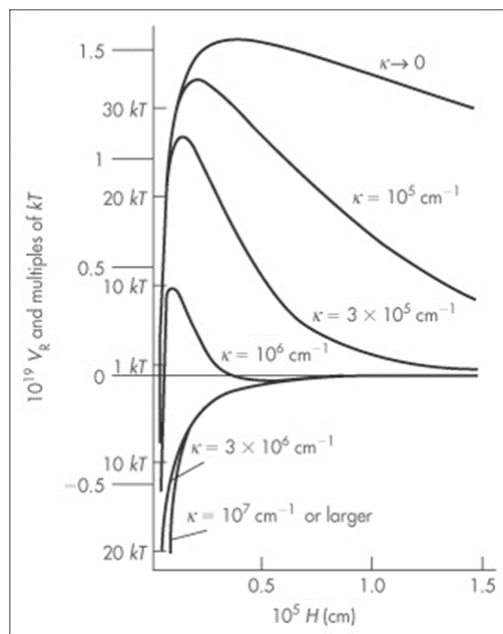


Figure 1.2. Influence of electrolytes concentration on the energy of interaction V_{TOT} between two spherical particles as a function of the distance H . (Taken from Rosen et al. [29])

The DLVO theory has its limitations. Indeed, systems stabilized by nonionic surfactants would, according to this theory, be limited to the comprehension of the Van der Waals and the electrostatic forces. The extended DLVO theory from Ohki and Oshima [32] describes colloids' potential energy with three terms: V_R , V_A and V_{other} , where V_{other} represents all other possible interactions such as steric forces, hydration forces or short-range forces. The sum of these three terms is defining the new total potential energy of the system:

$$V_{TOT} = V_A + V_R + V_{OTHER} \quad (7)$$

Multitude of examples in the literature are describing the DLVO theory's limitations. Restricting the estimation of a colloidal systems' behavior to the electrostatic and Van der Waals forces can lead to underestimation of the systems' stability. One well-known example concerns nonionic emulsifiers system. Indeed, POE compounds can form a nonelectrical steric barrier which stabilizes the system against aggregation [33]. In this specific situation, electrostatic repulsive forces are replaced by nonelectrical steric repulsive forces. The nonelectrical steric barrier is formed when the large nonionic polar headgroup binds strongly with water (two molecules of water per OE unit [34]), which prevent the colloid to aggregate. More precisely, the hydration forces drag the water molecules away from the lipophilic phase promoting strong attractive Van der Waals forces in the hydrophilic part of the bilayers. This improves the stability of emulsifier systems independently from the electrolyte content [29]. Hydration repulsion forces are

playing a key role in the explanation of colloids stability. In fact, when neglecting their existence, the DLVO theory would predict aggregation at high electrolytes concentration. Nevertheless, as hydration forces increase with increasing electrolytes content, especially for ionic surfactants systems, the rate of aggregation is significantly lowered, and the system is stabilized [35]. However, beyond a critical electrolyte concentration, the system aggregates. This occurs slower for nonionic surfactant systems as hydration forces are driven by the POE/water interaction and not by electrostatic strong repulsions. Another example was described by Park et al. [36]. They demonstrated that the stability of a system containing vesicles formed with a single quaternary ammonium surfactant, was threefold higher than the DLVO estimations. Therefore, even though the DLVO theory is very useful for predicting the main interactions in colloidal systems, other factors must be considered to have a complete quantitative approach.

1.3.5. Emulsifiers aggregates

1.3.5.1. Geometrical arrangements

Once the general interactions in the colloid are understood, one can estimate more precisely the molecular geometrical arrangement of the system. Due to their surface-active characteristics, emulsifiers can undergo various supramolecular morphologies [37]. Surfactants' morphology dynamic was intensively investigated due to its key role in many applications e.g. drug dosage and delivery and cosmetic and food formulation [38], [39]. As mentioned in [1.3.4. DLVO theory](#), emulsifiers' self-assembly is driven mainly by two forces:

- the hydrophobic attractions (Van der Waals) between the hydrocarbon tails contributing to reduce the surface tensions of the system
- the repulsive interactions between the hydrophilic heads and the lipophilic phase, the electrostatic repulsions between the head moieties and the steric repulsions

Due to these forces emulsifiers and amphiphilic compounds can aggregate in bilayers, which form the building block of lamellar phases. This formation creates an interface between the solvent and the lamellar phases. To minimize the free energy of the system, the lamellar phases self-arrange in the geometrical most optimal way: this is called the "optimal surface area" per head group [40].

1.3.5.2. Packing parameter (PP)

Estimation of the geometrical arrangement of emulsifiers' aggregates is done thanks to the packing parameter (PP) described first by Israelachvili et al.. They showed that surfactants can assemble into different patterns depending on the emulsifiers' composition and the salt content. The PP is defined by equation (8).

$$PP = \frac{V}{(a \cdot l)} \quad (8)$$

where V is the surfactant tail volume, l is the tail length, and a the cross-sectional area of the surfactants' head-group. It has been shown, that the value of the dimensionless PP will determine whether the colloidal phase will arrange in spherical micelles ($p < 1/3$), cylindrical micelles ($1/3 < p < 1/2$), vesicles and/or flexible bilayers ($1/2 < p < 1$), planar bilayers ($p \sim 1$) or inverted micelles ($p > 1$) [40].

Thanks to the PP and considering other factors e.g. temperature, ionic strength, hydrocarbon chain length, surfactant head functional chemical group and pH, the theory can predict the geometrical arrangement of surfactant systems. The diverse types of aggregates are presented in [Figure 1.3.](#):

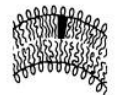
Packing parameter	Shape of the cross-section	Expected structure of associates
$< 1/3$	cone 	spherical micelle 
$1/3 - 1/2$	truncated cone 	rodlike micelle 
$1/2 - 1$	truncated cone 	flexible bilayer, vesicle 
$= 1$	cylinder 	planar bilayer 

Figure 1.3. Illustration of the geometrical PP and the related shapes of surfactants aggregates (Taken from Hiemenz et al. [41])

The onion/vesicle phase or flexible bilayer and the planar bilayer or ordinary lamellar phase are denoted by $[L_{\alpha}]$ and L_{α} , respectively. Other less common morphologies exist for emulsifier systems: the hexagonal phase (H_I), the inverted hexagonal phase (H_{II}), the bilayer cubic phase ($Im3m$, $Pn3m$, $la3d$) etc.. These morphologies are described in [Figure 1.4.](#).

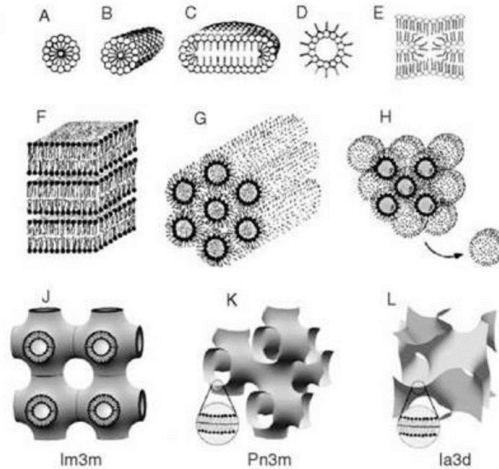


Figure 1.4. Liquid crystalline aggregate with different morphologies: (A) spherical micelles, (B) rodlike micelles, (C) disks, (D) inverted micelles L_2 , (E) fragment of a rhombohedral phase, (F) lamellae planar bilayer L_α , (G) inverted hexagonal phase H_{II} , (H) inverted micellar cubic phase I_{HI} , (J) bilayer cubic $Im3m$ phase, (K) bilayer cubic $Pn3m$ phase also called sponge phase, (L) bilayer cubic $Ia3d$ phase. (Taken from Tenchov [42])

As above mentioned, the geometry of the aggregate is highly dependent on the emulsifiers' nature and concentration or the phase conditions. Phase transition can be observed when changing one single emulsifier's type or concentration in the system [43], [44]. Moreover, the addition of polyelectrolytes in a simple SDS solution, provokes a $L_\alpha \rightarrow [L_\alpha]$ (bilayers to uni- or multi-lamellar vesicles) transition [45].

1.3.5.3. Lamellar structures

The specific lamellar structure formed upon mixing FA and/or co-emulsifiers in water is described in [Figure 1.5](#). This colloidal arrangement is common in high concentrated surfactant formulations. Surfactants aggregate together to form a single phase composed of alternating FA and more hydrophilic compounds.

This topic was deeply investigated by Eccleston [24] who studied a ternary nonionic system containing ceteth 20, cetearyl alcohol and water. DSC experimentations showed that the increase of the cetearyl alcohol concentration (surfactant/FA ratio from 1:9 to 1:120) causes the disappearance of the low temperature crystalline endotherm at the expense of the high temperature endotherm. These results prove that the ternary system is organized in a single phase i.e. lamellar gel phases. Grewe et al. worked on the same topic with systems containing ionic surfactants [46] and observed a similar phase behavior. These results are consistent evidence of the formation of a lamellar gel phase when precise ratios of surfactant and FA are blended together. Surfactant-based lamellar structures will be described more precisely in [1.4.1. Microstructure of emulsifier's system forming bilayers](#).

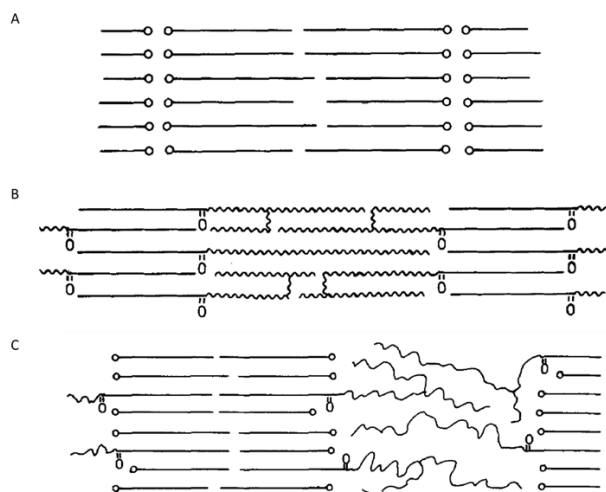


Figure 1.5 Schematic representation of a colloidal arrangement containing (A) pure FA (cetyl and stearyl alcohol 1:1), (B) pure nonionic type emulsifier and (C) a mixture of FA and nonionic type surfactants used as co-emulsifiers in water. \circ are the FA polar head, — the long hydrophobic carbon tail of the FA, \sim the POE or hydrophilic moiety and \sim the hydrated POE or hydrophilic moiety (Redrawn from de Vringer et al. [47]).

1.3.6. Polymorphism of emulsifiers

Fatty alcohols (FA) are widely used in cosmetics as amphiphiles and are compounds of interest in this specific study. They are often associated to a co-emulsifier for forming multiple phase emulsions [17]. For understanding this phase formation, it is important to know about the polymorphism behavior of the long-chain alcohols. FA generally range from eight to eighteen carbon atoms and exist under two stable crystal forms [48]. At room temperature (RT), an orthorhombic phase, the β -form, is found in excess. The γ -phase also called the tilted phase can co-exist with the β -form at ambient temperature. At higher temperature, a hexagonal phase exists: the α -form. The transition temperature between the two phases, called $T_{\alpha-\beta}$ depends on the purity and the hydration of the sample. To form a swollen lamellar gel phase, the hydrocarbon chains of the cetearyl alcohol must be in the crystalline-solidified state: α -form [49]. The addition of water into a FA simple phase, forms a crystalline hydrate phase where the crystals have a limited possibility to swell. This is due to the considerable Van der Waals forces between the amphiphile layers balancing the strong hydration repulsion. On the contrary, when associated to co-emulsifiers having larger polar moiety, the lipophilic phase can swell under addition of water. The thermal behavior of FA will be more precisely described in [1.4.7. Thermal properties](#).

Alcohols are not the only nonionic amphiphile molecules to exhibit a polymorphism behavior. The polymorphism of lipids is also a factor influencing multiple phase

emulsions systems. These compounds are nonpolar solvent and include fats, waxes, fat-soluble-vitamins, mono-, di-, triglycerides and phospholipids. They exist under two forms: the β -form at lower temperature under $T_{\alpha-\beta}$ and the α -form which is usually existing after cooling the melted form [50]. The stability of these two forms depends on the nature of the lipid. The polymorphism of lipids is well documented in the literature. Glycerides have been described by Chapman already in the early 60's [51], FAc lipid derivatives by Wong et al. [52], wax-based lipids and vitamins by Jennings et al. [53]– [55]. This polymorphism influences the stability of the system as the most stable form of the lipid is not always the one present at RT. Therefore, lipids can undergo phase transition over time and cause ageing and/or destabilization of the phase [56]. While formulating emulsions containing multiple amphiphile molecules, it is therefore important to understand the precise polymorphism behavior of the compounds to predict possible phase transitions. In general, a differential scanning calorimetry (DSC) investigation is performed to understand this behavior ([1.4.7. Thermal properties](#)).

1.4. Physico-chemical properties of hair coloring products and characterization

Modern cosmetic products containing a high concentration of surfactants are mostly semisolid lamellar gel phases [57]. Hair coloring products can be clustered in this category. They can be called semisolid lamellar multiphase systems or colloidal gel structures. This means that they are in the solid state at RT and change to their liquid state when heated up or mechanically stressed [58]. These structures differ from classical more fluid emulsions, often called milk, because they contain crystalline phases. They cannot be described as simple two-phases micellar oil-and-water (o/w) emulsions where the surfactant is forming a monomolecular layer around the oil droplet [24]. Thus, this study will focus on typical lamellar gel phases. These phases are three-dimensional networks containing a high concentration of combined ionic and/or nonionic surfactants and FA. They are mostly used for their high stability and good cosmetics application properties.

Note: This manuscript will refer to apolar amphiphiles under the following appellation: FA. FA such as cetearyl alcohols are common compounds used in the hair coloring products.

1.4.1. Microstructure of emulsifiers' system forming bilayers

In dermatological researches, lipids, such as lecithin, are widely used in preference of synthetic surfactants. These compounds having a double hydrocarbon chain, form lamellar gel phases alone in solution. On the contrary, artificial surfactants used in hair colorations, form, alone in solution, micelles. FA are also not able to form gel phases alone in solution. They are therefore used in blends.

The microstructure of multiple phase emulsions containing mixed emulsifiers has been studied in detail at an early stage by Eccleston [24], [59], de Vringer [60]– [62] and Junginger [58]. Gel phases are composed of surface- active materials, FA, water and oil. They arrange in bilayers separated by water forming an anisotropic long-range orientated network structure of crystalline phases. As a result, they reflect polarized-light (PL) and show birefringence under microscope. They can increase the viscosity of an emulsion, and stabilize it [58]. The stabilization of the phase is maintained by the equilibrium between the attractive and repulsive forces reviewed in the [1.3.4. DLVO theory](#). The Van der Waals forces existing between the molecules of different polarities are mainly responsible of the lamellar gel phase formation. These kind of phases are called lyotropic liquid crystal phases [59].

Upon mixing ionic and/or nonionic surfactants with FA, water and oil above $T_{\alpha-\beta}$, a swollen gel phase is formed. The bilayers of the gel phase are more precisely composed of alternating surfactants and long chain alcohols in the α -form. Although close to a liquid crystalline phase, the hydrocarbon long chains are solid. This brings rigidity, higher viscosity and stability to the system [46]. Hence, the microstructure of multiple emulsions can be precisely described as a four-phases system:

- Crystalline/hydrophilic successive gel phase, is composed of bilayers of alternating surfactants and FA. Water molecules are inserted between the bilayers, thus forming inter-lamellar water layers (see [Fig. 1.5](#)).
- The bulk-water consists in unbound water molecules in equilibrium with the inter-lamellar fixed water in the gel phase. It is assumed that inter-lamellar water and bulk-water have different physicochemical properties. The inter-lamellar water together with the above-listed phase form the lamellar gel phase.
- The crystalline phase consists of the excess of the lipophilic amphiphiles and is not part of the hydrophilic gel-phase.
- The dispersed oil-phase is mainly surrounded and/or dissolved by the lipophilic gel-phase.

[Figure 1.6](#). outlines the four-phases lamellar gel phase system.

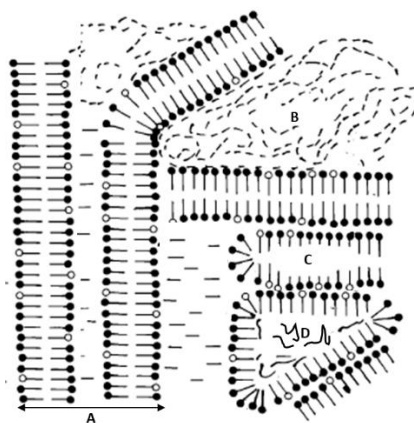


Figure 1.6. Schematic diagram of a multiple-phase-o/w emulsion containing ionic surfactant to illustrate the composition of the viscoelastic continuous phase with (A) the crystalline/hydrophilic successive gel phase, (B) the bulk-water, (C) the crystalline phase and (D) the dispersed oil-phase (redrawn and modified Eccleston [24]). Refer to [Figure 1.5](#) for more details of phase (A).

The hydrophobic carbon chains from the surfactants and the FA in the lamellar phase are orientated such as they are directed towards each other. Thus, strong Van der Waals attractive forces exist in the hydrophilic gel phase between the long-chain alcohols. This can lead to aggregation. Stabilization of the colloid is achieved thanks to the addition of surfactants having a larger polar moiety e.g. higher HLB. Indeed, the hydrophilic contribution of the surfactant in the lamellar gel phase drives the system to integrate water between the bilayers [63]. Moreover, due to the increase of viscosity caused by the swelling of the liquid crystalline gel phase, the film-thinning process usually responsible of coalescence is delayed [64]. This mechanism ensures additional stabilization of the systems. These phases are easily formed upon mixing FA with ionic and/or nonionic POE surfactants in water [65]. Utilization of POE-free nonionic surfactants forms lamellar gel phase which have limited abilities to swell. In fact, there is a lack of hydration driving forces [65]. Hence, the water stays in the bulk-water phase and will not fix into the bilayers.

1.4.2. Swelling properties and hydration mechanism

The swelling properties of the lamellar gel phase depend on the overall water content. This topic has been investigated by Junginger [58] for systems containing ionic and nonionic emulsifiers. DSC measurements of ternary systems containing ionic surfactants, demonstrated that the inter-lamellar water content linearly increases until maximum swelling. Beyond this point, the colloidal structure is not stable anymore. This swelling mechanism is driven by strong electrostatic attractions between the large charged ionic hydrophilic surfactants' head and water. For systems containing nonionic POE surfactants, lamellar swelling also occurs but is driven by hydration forces. This topic was studied by means of small angle X-ray (SAXS) diffraction, DSC, thermogravimetric

analysis (TGA) and freeze-fracture transmission electron microscopy (FF-TEM) [60]. It was found that a minimum water content is needed to form a homogeneous lamellar gel phase in the first place. Beyond this point the system is swelling until destabilization. Before reaching the minimum water content, the system contains a mixture of partially hydrated POE surfactants and FA forming a crystalline phase. The ability of swelling is determined by the POE chain length. Nevertheless, a system containing nonionic POE surfactants will not swell as much as ionic systems [65]. Nonionic lamellar gel phases can also be described as a four-phases system (see [Fig. 1.7.](#)).

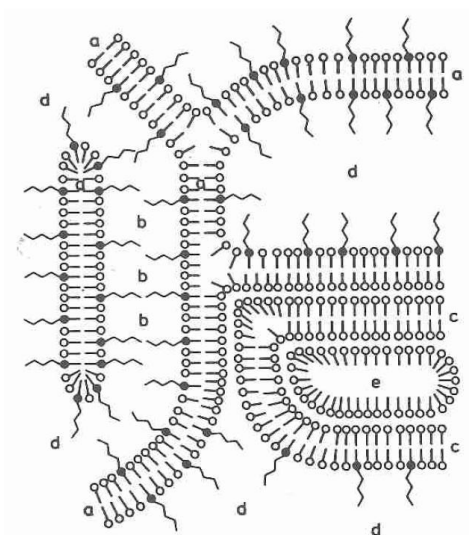


Figure 1.7. Schematic diagram of a multiple-phase-o/w emulsion containing nonionic e.g. PEG surfactants illustrating the composition of the viscoelastic continuous phase with (a) mixed crystal bilayers of PEG surfactants and FA, (b) interlamellarly fixed water (a+b form together the lamellar gel phase), (c) the lipophilic gel phase, (d) the bulk-water, (e) lipophilic components (taken from Eccleston [24]).

The interlamellar water bound in the lamellar gel phase is also dependent on the surfactants/FA ratio. Indeed, systems having a constant surfactant amount but an increasing FA concentration, have a larger portion of the overall water in the bulk-water than in the hydrophilic gel phase. This can be explained by the increase of the lipophilic Van der Waals attractive forces upon addition of long-chain alcohols. On the contrary, at equal molar ratio, the increase of the overall nonionic surfactant concentration increases the fixed interlamellar water quantity at the expense of the bulk-water [65].

To summarize, the swelling ability of a lamellar gel phase depends on the surfactants' nature, overall quantity and composition.

1.4.3. Ageing properties

The stability, over time, of multiple phase emulsions, depends of the FA repartition in the separate phases. The bilayers contain a mixture of FA and surfactants. The repartitions of these two compounds in the lamellae can either be homogeneous or heterogeneous depending on the manufacturing conditions and the surfactants/FA molar ratio. A homogeneous lamella is very stable and not subject to changes over time. On the contrary, inhomogeneous lamellae are subject to a lateral re-organization by diffusion of the unordered FA in between the surfactants. This mechanism is very slow when the system contains nonionic surfactant due to the dominant hydrophobic forces tiding up hydrocarbon tails together. Systems containing ionic surfactant re-arrange faster due to the strong dominant electrostatic forces. This mechanism had been explained by de Vringer by means of SAXS [62]. However, diffusion is not happening only along the bilayers in lamellar gel phases. Surfactants can also, over time, migrate from the lipophilic phase or the bulk phase to the lamellar gel phase and inversely. If this diffusion occurs rapidly in micelles, this mechanism happens rather slowly in bilayers. The typical phase migration motion for classical ternary systems has been estimated by Israelachvili. The residence time (t_R) would be for micelles and bilayers in the range of 10^{-4} and 10^{+4} seconds, respectively [30].

If properly built, lamellar structures are very stable and appear to have a steady rheological behavior. If not, one can observe collapsing or ripening of the bilayers which would lead to decrease of the dynamic viscosity and storage modulus until progressive phase separation. These systems are nevertheless more stable than micelles which can be subject to film thinning and coalescence processes [64].

1.4.4. Manufacturing

Multiple phase emulsions are manufactured similarly to classical emulsions. The molten components (surfactants, FA and oil) are mixed together with a portion of water and then cooled down to ambient temperature. During cooling the amphiphiles compounds are diffusing from the lipophilic phase to the lamellar liquid phase. When the temperature reaches the critical temperature (T_c), the crystalline surfactant/FA phase becomes a viscoelastic gel phase. Processing parameters like heating rate, shear rate ($\dot{\gamma}$) and the order of mixing raw materials can affect the rheology of the final products and its stability.

As the rate of diffusion of the FA in the lamellar phase is very slow in nonionic systems ([1.4.3. Ageing properties](#)), more attention is required for the preparation of these systems. Moreover, PEG compounds are more soluble at ambient temperature than elevated temperature. Therefore, above T_c , PEG compounds do not form hydrated crystalline phases. Approaching T_c , if the hydration forces are strong enough, crystalline phases will

separate and diffuse to form the mixed surfactant/FA lamellar gel phase [66]. As a result, a careful monitoring of the temperature during nonionic multiple phase emulsions formation is required. Indeed, if the cooling process is too fast, the final cream will be very mobile and will probably exhibit low viscosity due to inhomogeneous bilayers' formation. On the contrary, if the system is slowly cooled down to ambient temperature, the viscosity of the final cream will be high due to the stable homogeneous lamellar formation.

1.4.5. Rheological behavior

To characterize swollen lamellar gel phase, it is necessary to perform both steady and dynamic stress tests. Steady rheological tests are deforming the material under continuous rotation in a single direction. The shear rate ($\dot{\gamma}$) or shear stress (τ) can be constant or not. Viscosity (η) can be measured during a classical rotational sweep measurement. During this test, the viscosity is monitored as a function of the linearly increasing shear rate. The following equation (9) is explaining the mathematical relation between shear rate ($\dot{\gamma}$), shear stress (τ) and viscosity (η):

$$\tau = \eta\dot{\gamma} \quad (9)$$

The viscosity of a fluid is translating the concept of "thickness". The higher the viscosity of a fluid the more strength is necessary to make this fluid flow in between two parallel surfaces moving with a different finite velocity. Typically, a viscometer or a rheometer, will be composed of two parallel plates or cylinders: one rotating and the other one static. Swollen lamellar gel phases often have a thixotropic behavior. This means that the viscosity of the system, at constant temperature and constant shear-rate, decreases over time and returns to its original value in a finite time when the shear is removed. This reversible behavior is stressing the ability of complex fluids to lose, under constant shear, the bonding forces between molecules and restore them when the shear is removed [67], [68]. Systems containing lamellar gel phases can be also qualified of non-Newtonian fluids as their viscosity is dependent on the shear rate. This rheological behavior is also called shear-thinning [69].

To characterize more precisely the structure of a fluid in a nearly non-destructive way, dynamic rheological measurements are necessary. In this case, the fluid is subject to an oscillating, and not continuous, shear rate or stress. This different deformation gives insights about the structure of the fluid. The most common tests are the amplitude variation test also called strain (γ) test and the frequency tests. The first one is performed at a fixed frequency (ω) to define the linear viscoelastic region (LVR). This region is

defined thanks to the plot of the storage modulus (G') and the loss/viscous modulus (G'') against the strain deformation. The area where the moduli are leaving the linear range (for higher values of γ) defines the border of the LVR. The LVR limit can also be defined by the cross-over point of G' and G'' in the strain test. This limit is called the critical strain (γ_c). This test is usually run as a pre-screening test and is important for defining the appropriate amplitude to perform the next oscillatory measurements. Indeed, rheological measurement can be compared only if the studied fluids are in the same linear and steady amplitude region, before the critical strain (γ_c) [69]. The frequency tests are performed at constant amplitude ($\gamma < \gamma_c$ i.e. in the LVR) with the frequency increasing logarithmically. Thanks to this test, two important structural factors can be defined: the storage modulus (G') and the loss/viscous modulus (G''). The storage modulus or elasticity is related to the stored energy from the system during one cycle under stress. The loss/viscous modulus is related to the dissipation of the energy during the same cycle. These values are connected to the stability potential of a colloid and its structural properties. Lamellar gel phases always exhibit larger G' compared to G'' over a large frequency range [70]. When G' is larger than G'' , the fluid can be qualified as solid-like. When the contrary is observed, the fluid is qualified as liquid-like.

An empirical relation between the static and dynamic rheology was stated by Cox and Merz in 1958 [71]. This relation correlates the dynamic viscosity $|\eta^*|$, at a given frequency ω , to the viscosity η , at a given shear rate $\dot{\gamma}$. Consequently, if $\dot{\gamma} = \omega$, one can write the following equation (10).

$$|\eta^*|(\omega) = \frac{\sqrt{G' \omega^2 + G'' \omega^2}}{\omega} = \eta(\dot{\gamma}) \quad (10)$$

Experimental work showed that this relation was a good approximation for different polymers, linear and branched macromolecules, high and low molecular weight molecules with narrow and broad molecular weight distributions, solutions and melts [72].

In general, swollen lamellar gel phases are viscoelastic systems. This means that they exhibit a high viscosity with high elastic properties in the LVR compared to classical emulsions. This is observed for both ionic systems [21], [46], [73]– [76] and nonionic surfactants systems [74], [75], [77], [78]. Amplitude sweep measurement on lamellar gel phases containing ionic surfactants enables to determine the surfactant/FA ratio dependency of the rheological behavior. It was shown that the LVR, therefore the cross-over point between G' and G'' , shifts to lower amplitudes i.e. strain deformation γ , when

the ionic surfactant molar concentration increases above the FA molar concentration. This means that the solid-like properties of the lamellar gel phases are lessened when the ionic surfactant/FA molar ratio is larger than one [21], [46]. Consequently, the dynamic rheology decreases. The same rheological behavior was observed also for nonionic systems [74].

Additionally, it is interesting to connect the swelling properties of lamellar gel systems to their rheological behavior. In fact, the repartition of the water either in the bulk-water or fixed in the hydrophilic lamellar gel phase, determines if the system is more solid-like (higher elastic character, G') or liquid-like (higher viscous character, G''). Systems containing a large amount of water in the lamellar gel phase are more solid-like than the one containing a large amount of bulk-water phase. Therefore, it should be easier to form solid-like systems with ionic surfactants than with nonionic POE-surfactants and even more than with nonionic POE-free-surfactants [65]. There is hence a synergy between the rheological properties and the ionic surfactants concentration contained in the system. In a mixed ionic/nonionic surfactants system, the maximum elasticity is observed when the bilayers are in the most charged state [75]. In other words, addition of ionic surfactants brings more repulsive interaction in the system leading to higher viscosity. Upon reaching this maximum, the strong screening effect caused by the counter ions leads to no further rise of the repulsion forces. This point of saturation is accompanied by a decrease of G' .

A very detailed review was written by Berni et al. about the rheological behavior of surfactants systems containing nonionic, anionic and cationic surfactants while focusing on the $L_\alpha \rightarrow [L_\alpha]$ shear induced transition [79]. This transition is accompanied by shear thickening.

1.4.6. Microscopic properties

1.4.6.1. Optical microscopy

A direct and non-destructive way to characterize colloidal phases is to use PL microscopy. These observations are based on the distinction of isotropic and anisotropic phases which reflect the normal and PL differently. Isotropic phases, such as micelles or cubic phases, are transparent and do not scatter light. On the contrary, anisotropic phases, such as hexagonal and lamellar phases, scatter light and appear bright under microscope and opaque at a macroscopic scale. "Maltese crosses" under PL microscopy are a clear indication of the presence of lamellar gel phases, especially vesicles and bilayers [46], [80]. These patterns are similar to skin lipids and double-tailed natural surfactants such as lecithin. Typical photomicrographs are presented in [Figure 1.8.](#)

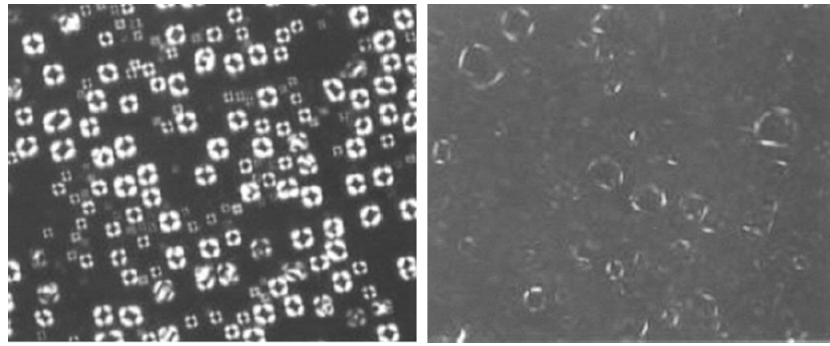


Figure 1.8. Photomicrograph of (left) Maltese crosses and (right) faint Maltese crosses, typical patterns formed by lamellar phases, under PL (Taken from Park et al. [81]).

It is not always easy to distinguish planar lamellar phases from flexible bilayers and/or vesicles under PL microscopy. Indeed, they all form bright Maltese crosses-like patterns. The investigation of the $L_{\alpha} \rightarrow [L_{\alpha}]$ transition by means of small angle light scattering (SALS) highlighted the pattern modification under shear stress. [Figure 1.9](#) shows the evolution of the Maltese crosses shape from bilayer to vesicle.

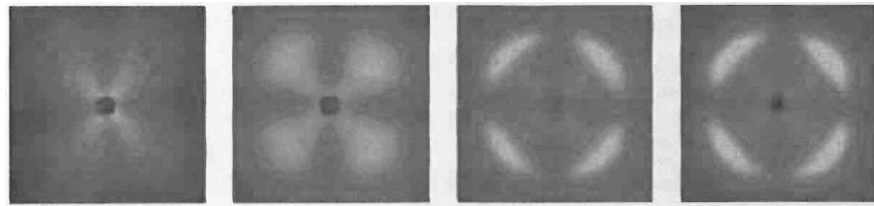


Figure 1.9. Different Maltese crosses shape under SALS from planar bilayers to single vesicles densely packed vesicles phase (taken from (Taken from Richtering [82])).

It is not possible to attribute one single pattern to a specific anisotropic phase. In fact, emulsifiers do not always arrange under a single geometry but rather a mixture or an intermediate form. Moreover, the precise geometry between the planar form and the circular one, induced by shear rate, is not well identified. According to the small angle neutron scattering (SANS) results from Richtering et al. [82], this intermediate geometry could have a cylindrical symmetry.

The morphological transition can also be observed under the microscope by changing the emulsifier concentration. This was done by Nagai et al. [83], by means of optical and confocal microscopy. They demonstrated that under addition of a nonionic POE surfactant ($C_{16}E_7$), in a system containing a fixed concentration of $C_{16}E_6$, the colloidal phase is arranging under: first linear lamellar, then lamellar with a certain curvature (entangled or not) and finally circular vesicles. This mechanism is dependent on the hydrophobicity of the bilayers. More hydrophobic system would tend to form inflexible entangled planar

lamellar structure whereas more hydrophilic system would tend to form vesicles (see [Fig. 1.10.A.](#)). All phases are coexisting with the neighboring one as shown in [Figure 1.10.B.](#) The PP theory is predicting the same behavior: p is decreasing when a , the cross-sectional area (polar moiety contribution), is increasing ([1.3.5.2. Packing parameter](#)). Nagai et al. also demonstrated the existence of a cylindrical symmetrical surfactant structure between the linear form and the circular one. They called this domain: discoid lamellar [83].

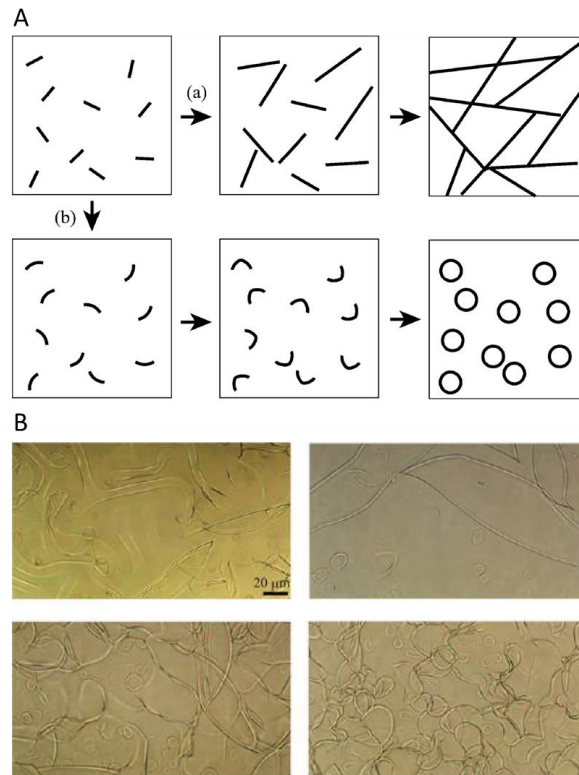


Figure 1.10. (A) Schematic representation of the formation of different lamellar domains from planar lamellar to entangled not flexible bilayers (a) or flexible bilayers and/or round vesicles (b). (B) Typical region of vesicles and lamellar coexistence under optical microscopy (taken from Nagai [83]).

1.4.6.2. TEM

TEM remains a classical method for characterizing colloids. It provides direct structural information of macro-molecule arrangement or nanoparticles. However, TEM can be subject to artefacts. Sample preparation is complex and time-consuming, and pictures can be interpreted erroneously. Thus, this method must be used cautiously.

For colloidal systems, samples can be prepared according to the following techniques: drying, freeze-drying, freeze-fracture, negative or positive staining, quick-freeze and cryo-TEM. These techniques can also be used in combination [84]. Drying remains the most readily accessible method of preparation, especially for highly stable systems.

Typically, a drop of the sample is applied onto a coated grid and dried from several minutes to several hours. This technique is unfortunately risky as the water content plays in most colloids a significant role in the geometrical arrangement (see [1.4.2. Swelling properties and hydration mechanism](#)). The relevance of the TEM pictures can be called into question. Staining is less subject to artefact. Uranyl acetate (UAc) is the most used stain for soft matter. The stain is usually applied directly on the sample onto the grid to avoid dehydration. Finally, cryo-TEM is one of the best way to produce relevant pictures of colloidal systems. For this technique, a thin layer of the sample is blotted on a grid and directly freeze-cooled by pouring it into a solution at its melting temperature. The freeze-fracture sample preparation requires specific equipment. Due to unavailability of this equipment, this technique will not be described in this manuscript [84].

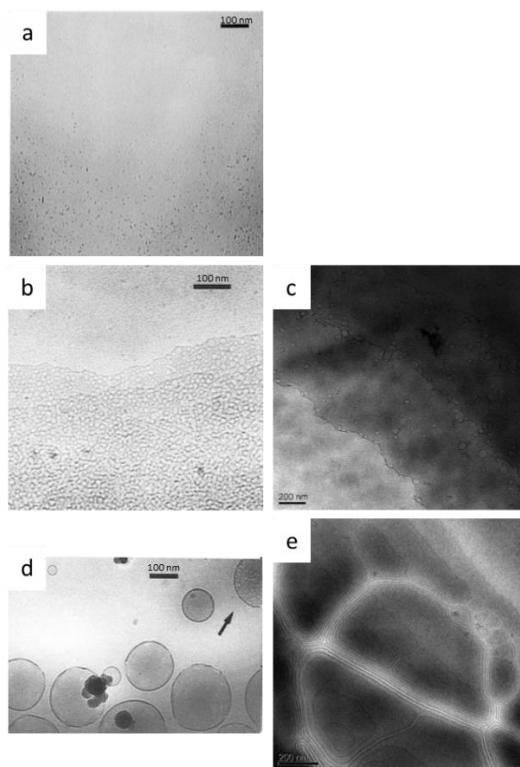


Figure 1.11. Cryo-TEM micrographs of (a) small micelles, (b) and (c) bilayers, (d) uni-lamellar vesicles (the arrow shows a perforated vesicle) and (e) multi-lamellar vesicles ((a),(b),(d) taken from Gustaffson et al. [85] and (c),(e) taken from Yuan et al. [86]). (a), (b) and (d) Colloidal system are formed by egg lecithin and cetyltrimethylammonium chloride in brine (NaCl). (c) and (e) Colloidal system are formed by cationic surfactant di-(2-ethylhexyl) phosphoric acid and cationic trimethyltetradecylammonium hydroxide in a salt-free solution.

All colloidal structures, from classical micelles ($p < 1/3$) to vesicle aggregates ($p \approx 1$), can be observed under cryo-TEM. Depending on the surfactants concentration of the samples, structural patterns are more-or-less easy to recognize. [Figure 1.11.](#) is showing

cryo-TEM photomicrographs of two different colloidal systems from the literature [85], [86].

1.4.7. Thermal properties

Lamellar gel phases are often containing FA at high concentration. To understand the thermal behavior of more complex systems, it is first necessary to focus on the melting behavior of FA (refer first to [1.3.6. Polymorphism of emulsifiers](#)). Pure long-chain alcohols exhibit a single narrow endotherm peaking corresponding to the melting of the long-chain alcohols. The melting temperature is increasing with increasing carbon-chain length [87]. Upon cooling, two exothermic peaks are generally observed. The earlier peak corresponds to the crystallization of the long-chain alcohols, the later peak corresponds to the α - β polymorphism transition [87]. When the FA are not pure (mixture of different chain lengths, typically cetyl and stearyl alcohol, C₁₆OH and C₁₈OH, respectively), the heating and cooling thermograms show two distinct peaks. Upon a second heating, the first endotherm peak shifts to lower temperature. This can be explained by the formation of a FA aggregate with alteration of C₁₆OH and C₁₈OH. In fact, the α -form exists over a longer range of temperature as the alcohols have different chain lengths. Upon addition of water and surfactants, called ternary system, a single lamellar phase is formed. Hence, the thermogram exhibits a single endotherm. The usage of a blend of C₁₆OH and C₁₈OH in the appropriate ratio is widely used for forming stable emulsions. In fact, C₁₆OH or C₁₈OH alone in solution are unstable [88]. [Figure 1.12](#) illustrates the expected behavior of C₁₆OH and C₁₈OH firstly pure, blended and integrated into a ternary system.

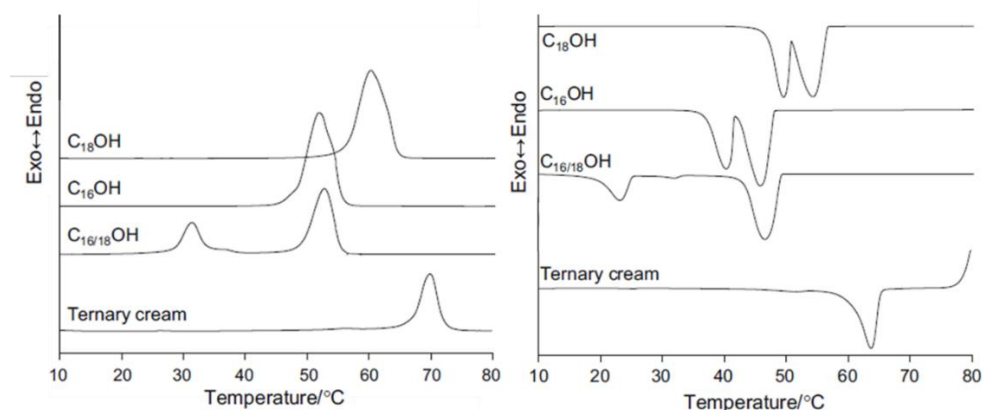


Figure 1.12. Thermal behavior of C₁₆OH and C₁₈OH pure, blended in a 1:1 mixture and in a ternary system containing 6% ionic surfactants and a large amount of water during (left) the second heating run (heating rate: 5°C/min) and (right) the first cooling run (cooling rate: 5°C/min). (Redrawn from Wunsch et al. [87]).

DSC measurements of a lamellar gel phase formed by a blend of emulsifiers usually result in a broad endotherm and is therefore difficult to interpret. When the different surfactants form a single phase, a single peaking is observed during melting [49]. The enthalpy of these systems is generally low [24]. Additionally, when the system contains a nonionic

emulsifier with a hydroxyl group, the melting temperature of the solid-like system is usually higher than the $T_{\alpha-\beta}$ transition of the FA [76]. This characteristic thermal behavior is observed for all kinds of surfactants. It does not depend on whether the system contains anionic [76], cationic [74], [89] or nonionic [89] surfactants.

Nevertheless, the concentration of ionic surfactants, as seen on the rheological behavior, has an influence on the thermal behavior of the lamellar gel phases. When the surfactant concentration increases, the system tends to be more liquid-like and exhibit a lower melting point [74], [76].

1.4.8. Spectroscopic imaging

Attenuated-total-reflection Fourier-transform-infrared (ATR-FTIR) spectroscopy is a non-destructive analytical method which can be used for a various range of molecular systems. It studies the interaction of light with a matter e.g. soft-matter. The method is based on the absorbance/reflectance of a beam of IR light which is dependent on the molecular vibration of the compounds contained in the system. This method can be used in theory to investigate structure formation and chemical composition. For studying multi-phase emulsions containing lamellar phases (non-transparent), ATR-FTIR spectroscopy must be used in reflectance. More precisely, the IR light is directed at the interface of a sample squeezed in between two plates made of a transparent IR material. This transparent material must have a high refractive index (1.38 - 4) and is called the internal reflection element (IRE). It can be a prism made of zinc selenide, diamond, silicon or germanium. In ATR-FTIR, the incident angle of the IR light beam is greater than the critical angle and thus, cause total internal reflection. In other words, the wave i.e. IR light, is propagated through the IRE and strikes the sample/IRE interface with a greater incident angle than the critical one. As the refractive index of the sample is lower than the IRE refractive index the wave cannot pass through and is entirely reflected. The portion of the wave entering in contact with the sample is called the evanescent wave and can penetrate the sample to a certain depth depending on the refractive indexes of the prism and the sample and the incident angle [90]– [92]. The equation (11) describes the depth of penetration d_p .

$$d_p = \frac{\lambda}{2\pi n_1 \sqrt{\left(\sin^2 \theta - \left(\frac{n_2}{n_1}\right)^2\right)}} \quad (11)$$

Where n_1 , n_2 , λ and θ are the refractive index of the IRE, the refractive index of the sample, the wavelength of the IR-light and the critical incident angle, respectively.

[Figure 1.13](#). is showing the ATR-FTIR sample set-up.

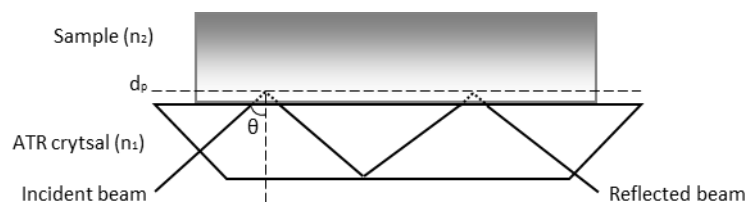


Figure 1.13. Schematic diagram of the sample set-up for ATR-FTIR measurements and the IR light path from the light source to the detector.

The depth of penetration ranges usually from 0.5 to 2 μm [90].

ATR-FITR is so far mainly used for characterizing medical samples, proteins and lipids nanoparticles and liquid crystals [91], especially for dynamic drug release investigations. The usage of this method for characterizing multiple phase emulsions is seldom documented in the literature. Nevertheless, this method showed successful results on distinguishing various kind of interactions and structural surfactant arrangements in lamellar gel phases systems. FTIR alone is more common in colloid science, especially for lipid systems. It can deliver relevant results about phase transitions and structural information [93].

1.4.9. The effect of electrolytes on lamellar phase systems

1.4.9.1. Salt-like compounds

It is a well-known fact, that salt-like compounds or additives interact with emulsifiers and show an impact on the stability of emulsions. Salt-like compounds used in the hair coloration can interact with common emulsifier systems. When added to a phase, salt-like compounds are contributing to the overall electrolyte concentration of the system. Therefore, according to the DLVO theory, the value of the electrostatic potential V_R is increasing (see [Fig. 1.2.](#)).

In nonionic surfactant systems, electrolytes influence in a much greater effect the surfactant alkyl tail than the hydrophilic head group. Indeed, the addition of various salts e.g. LiCl, NaCl, KCl, KBr and KI in PEG solutions, induces a decrease of the solubility of the alkyl moieties of the surfactants in water. This results in increasing the surface activity of the surfactant and decreasing the overall surface tension in the solution [94], [95]. The effect of salt-like compounds on ionic surfactant systems is twofold: (i) electrostatic interactions between the salt-like compounds and the polar moiety, (ii) salting out effect of the alkyl moiety. Nonionic and ionic surfactant systems were compared by Martinez et al. [96]. They observed stabilization of both systems under addition of NaCl and highlighted the lack of sensitivity of nonionic surfactant systems to ionic strength

increase. The stability of commercial ionic surfactant systems under addition of sodium disilicate and NaCl was also studied by Brooks [97]. They showed a stability improvement of the densely packed phases. They demonstrated that, without salts, the lamellar phases are larger and less perfect.

In each case, the stabilization effect by salt addition can be explained by the interfacial theory and by changes of the rheological properties of the medium from liquid-like to solid-like systems. The diffusion of salts counterions to the charged interface i.e. Stern layer of the surfactant bilayers, screens the surfactant's head group charges responsible of the electrostatic repulsions and enhance the surface-active properties of the surfactants. This allows them to pack closer in a more stable geometry. As a result, the viscosity increases, and the systems becomes more solid-like (G' largely greater than G''). This transformation makes diffusion of the particles in the medium more difficult which leads to less coagulation and therefore more stability. Many papers are describing the stabilizing effect of salts in specific emulsions composed of surfactants bilayers and/or monolayers [94], [96]– [98].

The valence, the concentration and the nature of the salts influence strongly surfactant aggregates. As demonstrated in [1.3.4. DLVO theory](#), the Stern layer is more compressed, meaning the interfacial surface tension decreases more effectively, with increasing the ions valence value [99]. The influence of the ion can have two effects: “salting in” or “salting out”. This effect is more dependent on the anion nature than on the cation nature. In fact, because of their low hydration requirement, the anions tend to be more present at the surfactants interface (Stern layer) than the cations, which are more easily dispersed in water. The following classification ranges anions from the most “salting out” one to the most “salting in”:



Therefore, in the presence of NaCl, the polar moieties of the surfactants are forced in the aqueous phase and the alkyl chains in the non-aqueous phase, forming a more solid-like system. On the contrary, in the presence of NH_4NO_3 the “salting in” effect drives the polar and the unpolar moieties of the surfactants in the aqueous phase, leading the system to arrange under a more liquid-like system [100], [101]. These findings are putting in evidence that, depending on their nature, addition of salts can also destabilize surfactant systems.

Addition of salts can also drive the system to rearrange under new configurations. Morphological changes in a system containing ionic surfactants e.g. dioctyl sulfosuccinate sodium salt (AOT) was observed upon addition of NaCl [102]. The system showed a spontaneous $[L_{\alpha}] \rightarrow L_{\alpha}$ complete transition after addition of 0.7% NaCl without alteration of the bilayer spacing. This transition was explained according to two theories: (i) the preferred curvature orientation of the surfactants, (ii) the electrostatic contribution of the salt compressing the Stern layer (see [1.3.4. DLVO theory](#)).

Salt-like compounds can interact with surfactants aggregates towards either stabilization or destabilization of the system. The latter is often due to a configuration transition from solid-like to liquid-like.

1.4.9.2. Hair dyes

It is challenging to predict the impact of the hair dyes on multiple phases emulsions. In fact, there is limited information in the literature about hair dyes stability and interactions [12]. Due to regulatory issues and toxicological regulation, the list of the European Cosmetic Directive for available hair dyes is now limited to 114 substances (see [Appendix 7.1](#)). Among them, the most used are listed in [Table 1.2](#).

Table 1.2. Authorized and most common hair dyestuffs for hair coloring products.

INCI Name	CAS No.	Molecular Weight	Linear Formula	Solubility*	Function**
Toluene-2,5-diamine sulfate (PTD)	95-70-5	220.3	C ₇ H ₁₂ N ₂ O ₄ S	H	P
Resorcinol	108-46-3	110.1	C ₆ H ₆ O ₂	H	C
m-aminophenol	591-27-5	109.1	C ₆ H ₇ NO	H	C
2,4-diaminophenoxyethanol HCl	66422-95-5	241.1	C ₈ H ₁₄ C ₁₂ N ₂ O ₂	H	C
2-methylresorcinol	608-25-3	124.1	C ₇ H ₈ O ₂	H	C
p-amino-o-cresol	-	123.1	C ₇ H ₉ NO	L	C
4-chlororesorcinol	95-88-5	144.5	C ₆ H ₅ ClO ₂	H	C
1-naphtol	90-15-3	144.2	C ₁₀ H ₈ O	L	C
1,5-naphthalenediol	83-56-7	160.2	C ₁₀ H ₆ (OH) ₂	L	C
2,7-naphthalenediol	582-17-2	160.2	C ₁₀ H ₆ (OH) ₂	H	C
p-aminophenol (PAD)	123-30-8	109.1	C ₆ H ₇ NO	H	P
4-amino-m-cresol	2835-99-6	123.2	C ₇ H ₉ NO	H	P
2-amino-6-chloro-4-nitrophenol	6358-09-4	188.6	C ₆ H ₅ ClN ₂ O ₃	H	C
2-amino-3-hydroxypyridine	16867-03-1	110.1	C ₅ H ₆ N ₂ O	H	C
1-hydroxyethyl 4,5-diamino pyrazole sulfate	155601-30-2	240.2	C ₅ H ₁₂ N ₄ O ₅ S	H	P

* The solubility of the dyestuff is clustered into two groups: the lipophilic (L) and the hydrophilic (H) dyes. It is important to note that the hydrophilic phase, e.g. water, is in the case of this study alkaline (pH 9-11).

** The function of the dyestuff is clustered into two groups: the precursors (P) and the couplers (C).

As seen in [Table 1.2](#), hair dyes are aromatic compounds. The oxidation reaction taking place for coloring the hair is involving a primary intermediate such as PTD and/or PAD, hydrogen peroxide and a coupler from the class of m-aminophenols, resorcinols, 1-naphtols and/or meta-substituted difunctional benzene derivatives [12]. Therefore, hair

dyes as additives are mostly di- or trifunctional hydroxylated, alkylated, aminated and/or chlorinated aromatic compounds. Hair dyes, as salt-like compounds, are also interacting with the surfactants forming the multiple phase emulsion. The most studied interaction is the one concerning a phenol compound with POE surfactants. The existence of hydrogen bonds between the hydroxyl functional group from the phenol and the EO from the POE surfactant, results into the formation of a lipophilic complex [103]– [105]. This latter diffuses from the water phase to the lipophilic lamellar phase. The creation of this complex helps for dye solubilization [106] but lead also to a loss of activity. Hence, the color delivery can be jeopardized. This theory is supported by the Pharmacist Chamber of North Rhine Westphalia [107].

Other kinds of dying substances are used in the food industry. Natural or chemical colorants are organic compounds with limited solubility in water [108]. They can therefore, to some extent, be compared to organic hair dyes. Natural colorants containing a phenol functionality such as curcumin or β -carotin, can be formulated in nonionic emulsions with polysorbate-20 as main emulsifier. Constantinides et al. [109] reported that despite the phenol/POE surfactants interactions, nonionic surfactants remain the best solution for minor pH and ionic strength sensitivity and best chemical stability.

1.4.10. Glossary for colloidal lamellar gel structure

The disordered liquid-like phase existing above T_c is called, for a lamellar gel phase, the L_α phase. The semi-solid ordered phase below T_c is called the L_β phase. The designation L means lamellar. These appellations are not to be mistaken with the nomenclature used for describing fatty alcohol crystal polymorphism behavior: α -phase and β -phase, respectively above and below $T_{\alpha-\beta}$ ([1.3.6. Polymorphism of nonionic emulsifiers](#)).

1.5. Objectives of the study

Hair coloring products are finished goods of great interest for the cosmetic industry. In fact, in 2015, more than 75% of women were coloring their hair [110]. This process requires to be repeated due to the regrowth of the hair. Hair coloring products are hence a source of constant revenue for the cosmetic industry. Even though world-wide formulated since decades, the interaction dyestuff/emulsifier is not yet fully understood. For instance, the rheological behavior of hair coloration is highly dependent on the dyestuff concentration and nature. This aspect is seldom reviewed in the literature.

This study aims to characterize the physicochemical behavior of classical hair coloration emulsions. Subsequently, it will focus on identifying the key-parameters responsible of

the rheological instability of these specific emulsions. Finally, these emulsions will be optimized to obtain more robust and stable emulsions in terms of rheological and thermal behavior.

Most of modern hair coloring products contain a high amount of emulsifiers and FA. Their characterization by PL microscopy, DSC and rheological tests together with the above literature review led to the first conclusion that hair coloring products are mostly semi-solid systems composed of lamellar gel phases. To identify the key-parameters impacting the viscosity, simplified emulsions have been studied. The simplification of a classical hair coloration formulation enabled to focus on the specific interactions existing between electrolytes and emulsifiers. Therefore, rheology modifier polymers as well as the cosmetic claim ingredients or preservatives have been removed from the classical hair coloring formulation. The alkalizing agent was kept in the formulation so that the emulsifiers and the electrolytes remain in the same electrical state. The water phase and the oil phase were preserved. The electrolyte composition was monitored in the following way:

- 1- Formulation of the simplified hair coloring product with one inorganic salt: ammonium sulfate. This salt was chosen for its anion. Indeed, sulfate is the counter-anion of many common dyestuffs. As reviewed in the above literature, anions have the most influence on the colloidal structure ([1.4.9.1. Salt-like compounds](#)). It was therefore highly relevant to choose ammonium sulfate for this study.
- 2- Formulation of the simplified hair coloring product with one organic salt: PTD. This common dyestuff has the same anion than the above mentioned inorganic salt. A similar investigation studying simplified hair coloring products has been done by Wis-Surel [12]. They managed to highlight relevant hair coloring products properties by using a single colorant in the system.
- 3- Formulation of the simplified hair coloring product with more than one organic salt: a hair dyes mixture. This last step was twofold. Firstly, studying the behavior of a nonionic and/or ionic surfactant system containing a mixture of hair dyes having various chemical functional groups. In fact, it has been reviewed in [1.4.9.2. Hair dyes](#) that POE nonionic emulsifiers interact with phenol derivatives e.g. 1-naphtol. Second, this step aimed to check on the good delivery of the dyestuff by performing color measurements on real human hair fibers. In fact, optimization of the system must lead to a stable and rheological robust system while still offering a good color delivery into the hair cortex.

Characterization of the standard hair coloring system and evaluation of the optimized one have been done by means of static and dynamic rheological measurements, microscopic observations: cryo-TEM, TEM and PL, phase-contrast (PC) microscopy, DSC measurements and ATR-FTIR spectroscopic imaging.

2. Material and methods

2.1. Materials

2.1.1. Standard hair coloring product

Deionized water was used throughout. Cetearyl alcohol (Lanette O[®]) and glyceryl monostearate (Cutina GMS SE[®]) were obtained from BASF, Ludwigshafen, Germany. The ionic surfactant, sodium laureth sulfate (SLES) 27% (Genapol LRO Liquid[®]) was obtained from Clariant Corporate, Oberhausen, Germany. The nonionic surfactant, PEG-20 cetyl/stearyl ether (Eumulgin B 2[®]) was obtained from BASF, Ludwigshafen, Germany. Octyldodecanol (Eutanol G[®]) was used as the lipophilic phase and obtained from BASF, Ludwigshafen, Germany. The salt concentration was adjusted with ammonium sulfate special grade (99%) from BASF, Ludwigshafen, Germany. All the excipients were used as received.

Note: Cutina GMS SE[®] contains sodium stearate. The sodium stearate free version is commercialized under the name of Cutina GMS V[®] used in the following chapters.

The ionic creams were composed of 2.0 w% octyldodecanol, 3.0 w% and 2.0 w% emulsifiers (blended PEG-20 cetyl/stearyl ether and SLES, respectively) and 17.0 w% of FA and/or amphiphiles (cetearyl alcohol and glyceryl monostearate SE). Different amounts of ammonium sulfate (0.1 – 0.5 – 1.0 – 2.0 – 3.0 – 4.0 – 5.0 w%) were added to the ionic creams. They were labelled E1, E2, E3, E4, E5, E6, and E7, respectively, as described in [Table 2.1](#). The water amount was adjusted to 100 w%. 1.5 w% of ammonia was added to regulate the pH-value of the simplified hair coloring products.

Table 2.1. Classical hair coloring products containing a blend of ionic and nonionic emulsifiers and different amounts of ammonium sulfate.

	E0	E1	E2	E3	E4	E5	E6	E7
Ammonium sulfate [w%]	0	0.1	0.5	1.0	2.0	3.0	4.0	5.0

All the ionic creams containing inorganic salts were studied by means of microscopy, rheology, DSC and spectroscopy.

The ionic systems were also formulated with hair-dyes. The organic salt concentration was monitored with a classical precursor: toluene-2,5-diamine sulfate (PTD). PTD was provided by Henkel KGaA, Düsseldorf, Germany, and was used as received. These ionic creams were labelled F1 to F6 and contained from 0.2 to 6.7 w% of PTD. The PTD concentrations were calculated to be equivalent to the molar amount of ammonium sulfate added in E1 to E7. An overview of the ionic systems containing organic salts is presented in [Table 2.2](#).

Table 2.2. Classical hair coloring products containing a blend of ionic and nonionic emulsifiers and different amounts of PTD.

	E0	F1	F2	F3	F4	F5	F6
PTD [w%]	0	0.2	0.8	1.7	3.3	5.0	6.7

All the ionic creams containing organic salts were studied by means of DSC.

2.1.2. Optimization of the surfactant system: screening of nonionic emulsifiers

The nonionic surfactants studied in this manuscript are described in [Table 2.3](#). They have been chosen according to the following criteria:

- PEG nonionic polar moiety
- Long chain alcohol n= 12-18
- Ether rather than ester functional group
- Cosmetics acceptance

Note: Due to unavailability of pure APG surfactants having a C16-18 carbon chain length, this compound is not part of this study.

Table 2.3. Nonionic emulsifiers used for the optimization of the surfactant system of the classical hair coloring product.

Chemical Name	INCI Name	Trade Name	Provider
PEG-2 Cetyl/Stearyl Ether	Ceteareth-2	Lowenol® C-279	Jos. H. Lowenstein & Sons, Inc., NY, USA
PEG-20 Cetyl/Stearyl Ether	Ceteareth-20	Eumulgin® B 2	BASF Corp., Ludwigshafen, Germany
PEG-50 Cetyl/Stearyl Ether	Ceteareth-50	Genapol® T 500 P	Clariant Int. Ltd., Muttenz, Switzerland
PEG-100 Cetyl/Stearyl Ether	Ceteareth-100	Brij® S 100	Merck KGaA, Darmstadt, Germany
PEG-23 Lauryl Ether	Laureth-23	Brij® L23	Croda Inc., Snaith, UK
PEG-20 Oleyl Ether	Oleth-20	Brij® O20	Croda Inc., Snaith, UK

As for the ionic creams, the new nonionic creams were composed of: deionized water adjusted to 100 w%, cetearyl alcohol and glyceryl monostearate (Cutina GMS V®) as FA substances and octyldodecanol as the lipophilic phase in the same concentrations than above-mentioned. The salt concentration was adjusted with 1.0 w% ammonium sulfate, in all the nonionic creams. 1.5 w% of ammonia was added to regulate the pH-value.

The nonionic emulsifiers were tested alone and in combination. The nonionic surfactants/FA molar ratio was calculated according to Eccleston [24]: 1:20. This ratio is detailed in equation (13).

$$\frac{1}{20} \approx \frac{n_{\text{TOT. Surfactants}}}{n_{\text{TOT. Amphiphile}}} = \frac{\sum_i n_{\text{Surfactant } i}}{n_{\text{FA}} + n_{\text{Glyceryl stearate}}}$$

With $n_{\text{TOT. Surfactants}}$, the total number of mole of the nonionic surfactants ($i = 1$ or 2) and $n_{\text{TOT. Amphiphile}}$, the total number of mole of glyceryl monostearate ($n_{\text{Glyceryl stearate}}$) and cetearyl alcohol (n_{FA}). Additionally, the influence of the length and the degree of saturation of the carbon chain of the nonionic surfactant was studied. For answering this problematic, the following nonionic surfactants were used: PEG-23 lauryl ether and PEG-20 oleth ether, alone (see [Table 2.4](#), S11 and S12, respectively) and in combination with PEG-20 cetyl/stearyl ether and PEG-50 cetyl/stearyl ether.

All the studied systems are described in [Table 2.4](#). For the systems containing a combination of two surfactants, the molar ratio between both surfactants was kept equal to 1.

In a second step, the influence of the molar ratio between the two nonionic surfactants was studied (while keeping $n_{\text{TOT. Surfactants}}$ constant). This step was performed only for the most promising system indicated by a red cross (X) in [Table 2.4](#). The nonionic surfactant ratio was calculated according to equation (14).

$$0 \leq \frac{n_{\text{Surfactant 1}}}{n_{\text{Surfactant 2}}} < 1.1 \quad 14$$

With $n_{\text{Surfactant 1}}$ the number of mole of the nonionic surfactant having the shorter polar moiety and $n_{\text{Surfactant 2}}$, the number of mole of the nonionic surfactant having longer polar moiety. The following nonionic surfactants molar ratio were investigated: 0, 0.15, 0.40, 1.01, corresponding to S3, S13, S14 and S8, respectively.

Table 2.4. Nonionic simplified hair coloring systems containing either one or two PEG surfactants.

Chemical Name	INCI Name	HLB	Nonionic systems												
			S1	S2	S3	S4	S5	S6	S7	S8	S9	S10	S11	S12	
PEG-2 Cetyl/Stearyl Ether	Ceteareth-2	4.9 [111], [112]	X				X				X*		X		
PEG-20 Cetyl/Stearyl Ether	Ceteareth-20	15.5 [111]		X					X			X	X		
PEG-50 Cetyl/Stearyl Ether	Ceteareth-50	See 3.3.5			X					X	X*	X			
PEG-100 Cetyl/Stearyl Ether	Ceteareth-100	18.8 [111]				X	X	X							
PEG-23 Lauryl Ether	Laureth-23	16.7 [113]												X	
PEG-20 Oleyl Ether	Oleth-20	15.3 [113]													X

* The red crosses (X) indicate the systems for which the influence of the molar ratio between both nonionic surfactants was studied.

For each system, the viscosity η , the critical strain γ_c , the storage G' and the loss G'' modulus were monitored at t_0 (24 hours after formulation). Moreover, photomicrographs were taken under PL microscopy. Both rheological and microscopic measurements were repeated after six months of storage at RT.

2.1.3. Nonionic hair coloring product

The most satisfying nonionic system: S14, from the previous screening study, was characterized in more details in this chapter. As for the ionic systems, the salt concentration was monitored with either ammonium sulfate or PTD, a common precursor. The nonionic creams were labelled G0 and G1 when containing no salt or 1.0 w% of ammonium sulfate, respectively. The nonionic creams were labelled H1 to H6 when containing from 0.2 to 6.7 w% of PTD. The PTD concentrations were calculated to be equivalent to the molar amount of ammonium sulfate added in E1 to E7. An overview of the nonionic systems is presented in [Table 2.5](#).

Table 2.5. Nonionic hair coloring products containing a blend of nonionic emulsifiers and different amount of salts: either inorganic (ammonium sulfate) or organic (PTD).

	G0	G3*	H1	H2	H3	H4	H5	H6
Ammonium sulfate [w%]	0	1.0	-	-	-	-	-	-
Toluene-2,5-diamine [w%]	-	-	0.2	0.8	1.7	3.3	5.0	6.7

* The nonionic system G3 is the same than S14.

All the nonionic creams were studied by means of microscopy, rheology, DSC and spectroscopy. Additionally, H3, H5 and H6 were also re-formulated in bigger batches (15 kilos) in the scale-up study (see [7.7.1. Scale-up](#)).

In a second step, the nonionic creams were formulated with hair-dyes mixtures. Some details about the composition of these nonionic shades: black, brown, orange, red and blond, are given in [Table 2.6](#). All the hair-dyes were provided by Henkel KGaA, Düsseldorf, Germany, and used as received. To evaluate the proper cosmetic properties of the nonionic shades, reference hair coloring products, used by hair-dressers, were chosen. These products are listed in [Table 2.6](#) and were provided by Henkel KGaA, Düsseldorf, Germany. The reference hair coloring products contain a mixture of ionic and nonionic emulsifiers and can be considered as classical professional hair coloring products.

Table 2.6. Nonionic hair coloring products containing a blend of nonionic emulsifiers and different hair-dyes mixtures. The reference hair coloring products contain a blend of ionic and nonionic emulsifiers and the same hair-dyes mixtures than the nonionic formulations.

	Black	Brown	Orange	Red	Blond
PTD	X	X	X		X
Resorcinol	X	X	X		X
m-aminophenol	X	X		X	X
4-chlororesorcinol	X				
2,4-diaminophenoxyethanol HCl	X				X
2-methylresorcinol		X	X		
2-amino-3-hydroxypyridine		X	X		
4-amino-m-cresol			X	X	

1-naphthol			X		
p-Amino-o-cresol			X	X	
2-amino-6-chloro-4-nitrophenol			X		
1-hydroxyethyl 4,5-diamino pyrazole sulfate				X	
TOTAL [w%]	5.4	1.8	1.4	2.8	0.1

All the nonionic creams containing hair-dyes mixtures were studied by means of DSC and evaluated according to cosmetic and industrial standards.

2.2. Methods

2.2.1. Formulation process

The creams were prepared following a hot-hot emulsification process per batch of 200 grams. Firstly, the lipophilic and the aqueous phase were heated up separately to 75°C. The lipophilic phase was composed of the octyldodecanol, FA, glyceryl monostearate and the surfactants. Subsequently, the lipophilic phase was added to the water phase under constant stirring. Agitation was ensured by a lab stirrer (Hei-Torque Value 400®, Heidolph, Schwabach, Germany) equipped with a propeller rotating at 1000 rpm. Stirring was maintained until the creams reached 30°C. Salts and ammonia were added at low temperature. Each cream was formulated three times in the exact same conditions. This formulation process was used for all the creams at the exception of the nonionic shades (containing hair-dyes mixtures) and the systems studied in the scale-up chapter.

The nonionic shades were formulated following the same hot-hot emulsification process per batch of 2 kilos. For these systems, stirring was ensured by a laboratory mixer (EWTKV 0,5®/EWTMV 0,5®, Vollrath GmbH, Hürth, Germany). After the final addition of the hair-dyes mixtures, the creams were homogenized for three minutes at RT using a disperser at 5000 rpm (T25 digital ULTRA-TURRAX®, IKA Works, Inc., Wilmington, USA). Each cream was formulated two times in the exact same conditions.

Finally, 15 kilos of the creams H3, H5 and H6 were prepared for the scale-up study. Each cream was formulated three times in the exact same conditions. The same hot-hot emulsification process was followed. The creams were prepared in a vacuum-, mixing- and homogenizing system from Symex (production mixer CML 20, Bremerhaven, Germany). First, the lipophilic and half of the aqueous phase were heated up to 75°C in the reactor. The mixture was then cooled down to 35°C under constant stirring (25 rpm, under vacuum). The cooling ratio was controlled by the jacket of the reactor and maintained at 1°C/min. Subsequently, the rest of the water, the salts and the ammonia

were added. Finally, the creams were homogenized for 3 minutes at 5000 rpm. Stirring (25 rpm) and the vacuum were kept constant throughout the all process.

2.2.2. Microscopy

2.2.2.1. Optical microscopy

A small amount of the creams was dropped on the glass slide and spread over by covering it with a transparent coverslip. Optical anisotropy was observed under the cross-polarized-light microscope Axio Scope.A1 (Carl Zeiss Microscopy, Jena, Germany) equipped with an optical 40x objective (Carl Zeiss Microscopy, Jena, Germany). Images were treated with the Imaging Software for microscopy ZEN 2.1 (Carl Zeiss Microscopy, Jena, Germany). Particle size distribution was estimated using the optical light microscope in phase contrast (PC) mode. Images were treated using the image analysis expansion module “Blue” from the ZEN 2.1. software (Carl Zeiss Microscopy, Jena, Germany).

2.2.2.2. TEM/cryo-TEM

After multiple attempts, it was not possible to observe the ionic creams (E0 to E7, especially E3) under TEM without a pre-treatment. This is often an issue in applied chemistry when the studied systems are too thick or too opaque [84]. To overcome this issue with available methods, a particle extraction protocol was set up: immediately prior to the TEM measurements, the samples were diluted in distilled water and centrifuged. The rate of dilution was 1:1 for all the creams. The diluted samples were then centrifuged for 90 min at 9000 rpm. The lower liquid rich water phase was extracted. Subsequently, 3 μ l of the lower water phase was then spread on a copper grid (Cu-grid) coated with a Formvar film. After one minute of adsorption, the excess liquid was blotted off with filter paper. The grids were air-dried for thirty seconds and washed three times for one minute with water. Subsequently, a droplet of 2% aqueous uranyl acetate was dropped on the grids. The grids were finally drained for one minute. The dried specimens were examined with an EM 900 transmission electron microscope (Carl Zeiss Microscopy, Jena, Germany) at an acceleration voltage of 80 kV. Electron micrographs were taken with a Variosped SSCCD camera SM-1k-120 (TRS, Moorenweis, Germany). After such pre-treatment, results should be interpreted with caution. Indeed, TEM can be subject to artefacts and dilution of the creams could lead to the expansion or swelling of the bilayers or drive the system to self-assemble into different structural arrangement [84], [114]. Therefore, right after the extraction, we checked under PL microscopy the aspect of the diluted emulsions. These observations were carried on over a week and revealed that Maltese crosses are still

present in the diluted creams after at least five days (see [Fig. 3.3.](#)). No phase separation was observed in the diluted creams during this week. Finally, for the above-mentioned reasons, the TEM results will be taken only for qualitative understandings and not for quantitative evaluation of the system.

On the contrary, the observation of the nonionic creams (G3) was successful under cryo-TEM without staining or dilution. Therefore, the cream was used as such and directly spread with a filter paper on an uncoated copper grid (Cu-grid). Vitrification was conducted by plunging the grid into liquid propane at its freezing point. The frozen specimen was placed with help of a single tilt liquid nitrogen cryo-transfer holder model 626 (Gatan, Pleasanton, USA) in the cryo-TEM TEC-NAI 10 (Philips Electron Optics, Eindhoven, Holland) at an accelerating voltage of 100 kV. Electron photomicrographs were taken with a Tengra camera (Emsis, Muenster, Germany).

2.2.3. Rheology

2.2.3.1. Static rheological measurements

Rotational sweep measurements were performed with the Haake Rheostress 6000 version 2007 (Thermo Fisher Scientific, Waltham, USA) equipped with a cone C35/1 geometry (35mm diameter and 1,014° angle). The viscosity η was measured at a shear rate of 7.2 s⁻¹ at 20°C, in the yield stress region. The factor $\Delta\eta$ was calculated within one group of creams (either E1 to E7, or H1 to H6) according to equation (15).

$$\Delta\eta = \eta_{MAX} - \eta_{MIN} \quad 15$$

With η_{MAX} and η_{MIN} the maximum and minimum, respectively, viscosities measured within one group of creams over six months storage at RT. These factors enabled to evaluate the overall fluctuation of viscosities of the one system.

2.2.3.2. Dynamic rheological measurements

In a first step, a strain sweep measurement was performed to determine the linear viscoelastic region (LVR) of the creams. This region corresponds to the area where the rheological properties of the system are independent of the strain. Below this strain the system can be qualified as viscoelastic. 100% of the strain corresponded to a displacement angle of 0.0885 rad. All the creams exhibited a critical strain such as: $0.01 < \gamma_c < 0.2$ This corresponded to 0.2% and 4% of the strain, respectively.

In a second step, a frequency sweep test between 0.1 and 300 rad/s and below the critical strain γ_c ($\gamma = 0.001$ corresponding to a 0.02% of the strain and a displacement angle of $1.77\text{E-}05$ rad), in the LVR, was performed. The storage modulus (G' in Pa) and the loss modulus (G'' in Pa) were monitored. The ratio of G'' over G' is called the loss factor: $\tan\delta$ and is equal to 1 when $G'' = G'$.

For all samples and tests the measurements were performed with the Haake Rheostress 6000 version 2007 (Thermo Fisher Scientific, Waltham, USA) equipped with a cone C35/1 geometry (35mm diameter and $1,014^\circ$ angle) at 20°C .

2.2.4. DSC

The raw materials and the creams were analyzed by means of DSC over three heating runs from 20°C to 85°C with a heating rate of $2\text{K}/\text{min}$ in sealed aluminium-crucibles. The samples were preliminary weighted to get 6 to 7 mg assays. The cooling process between the three heating runs, was also monitored at the same rate. The measurements were performed with the DSC Q2000 with autosampler and a refrigerated cooling system RCS90, all from TA-Instruments (TA Instruments, New Castle, USA). The measurements were repeated three times. All the DSC measurements were performed within the first week after preparation of the creams.

Note: To demonstrate the lack of side-reactions between the ammonium sulfate from the creams and the aluminum oxide from the crucible, a separate DSC measurement of E7 (5.0 w% ammonium sulfate) in a sealed stainless-steel crucible was performed under the above-defined conditions. The thermograms did not show any significant difference compared to the DSC performed in aluminium-crucibles. These results indicated that no side-reaction occurred between the ammonium sulfate from the creams and the aluminum oxide from the crucible. This aspect will not be further discussed in this study.

2.2.5. ATR-FTIR

The creams were placed on the sample introduction system using the UATR-accessory (Universal ATR technique from PerkinElmer, Waltham, USA) at RT. The absorbance spectra were obtained using a FT-NIR spectrometer Spectrum 100 (PerkinElmer, Waltham, USA) equipped with a diamond-thallium bromoiodide crystal (diamond-KRS-5, PerkinElmer, Waltham, USA) system. In total, eight scans were measured per sample. A spectral resolution of 4 cm^{-1} was used as a compromise between scan speed and resolution. The intensity imaging of the samples was done with the IR-microscope system Spotlight 400 (PerkinElmer, Waltham, USA) equipped with a germanium crystal with a contact surface of $600\text{ }\mu\text{m}$ in diameter. The creams were pre-dried at ambient temperature prior the measurements.

2.2.6. Specific evaluations for hair coloring products

2.2.6.1. Stability tests

The samples were stored at RT, -10°C and +40°C and observed at t0, week 4, 8, 12 and 24. At every stage of the storage test, the viscosity η was monitored as above-described in [2.2.3. Rheology](#). Moreover, the pH value was monitored using a 761 pH-meter Calimatic (Knick, Berlin, German) at RT. Finally, visual evaluations at a macroscopic level enabled to assess stability, appearance and color under a binary classification: OK/not OK.

2.2.6.2. Color delivery

The nonionic creams were applied on different human hair strands purchased from a hair provider (Kerling International Haarfabrik GmbH, Backnang-Waldrems, Germany). The application mixture was composed of the hair coloring cream and the developer (the stabilized solution containing hydrogen peroxide) in a 1:1 weight ratio. The developer, containing 6% of hydrogen peroxide, was provided by Henkel KGaA, Düsseldorf, Germany. Two kinds of hair were colored: Buffalo hair (BF) and Ideal Hair base (IH). The level of pigmentation i.e. the colors of the IH strands, were chosen according to the recommendation done on the reference hair coloring products' packaging. Each strand weighted approximately 1 gram. For each shade, two strands were colored: one BH strand and one IH strand. The mixture was applied on the dry strands on a Plexiglas® plate and left at 37°C for 30 minutes. Subsequently, the strands were rinsed with lukewarm water and blow-dried. The color of the colored strands was evaluated with a spectrometer Spectraflash® SF450 (DataColor, Lucerne, Switzerland). Six measurements per strands were performed. The two factors: the color difference between two strands (ΔE_{1-2}) and the grey coverage (GC) were calculated as explained in the following equations (16) and (17), respectively.

$$\Delta E_{1-2} = \sqrt{(L_2 - L_1)^2 + (a_2 - a_1)^2 + (b_2 - b_1)^2} \quad 16$$

$$GC = \left(1 - \frac{\Delta E_{(BH-IH)}}{\Delta E_{(WH-IH)}}\right) \times 100 \quad 17$$

With L, a and b, the lightness, the green/red component and the blue/yellow component, respectively, from the Lab color space and WH, the white hair strands, composed of 100% sorted white hair, not colored.

The specific evaluations for cosmetic and industrial purposes of the hair coloring products are not part of the core of this manuscript. The results are therefore presented in [Appendix 7.7.](#)

3. Results and discussions

3.1. Characterization of a classical hair coloring product

3.1.1. Microscopy

3.1.1.1. PL microscopy

All the ionic creams, E0 to E7, were observed under PL microscopy 24 hours after preparation ([Figure 3.1](#)). E0 showed no anisotropic pattern. The rest of the ionic creams all exhibited Maltese crosses of different shapes and sizes.

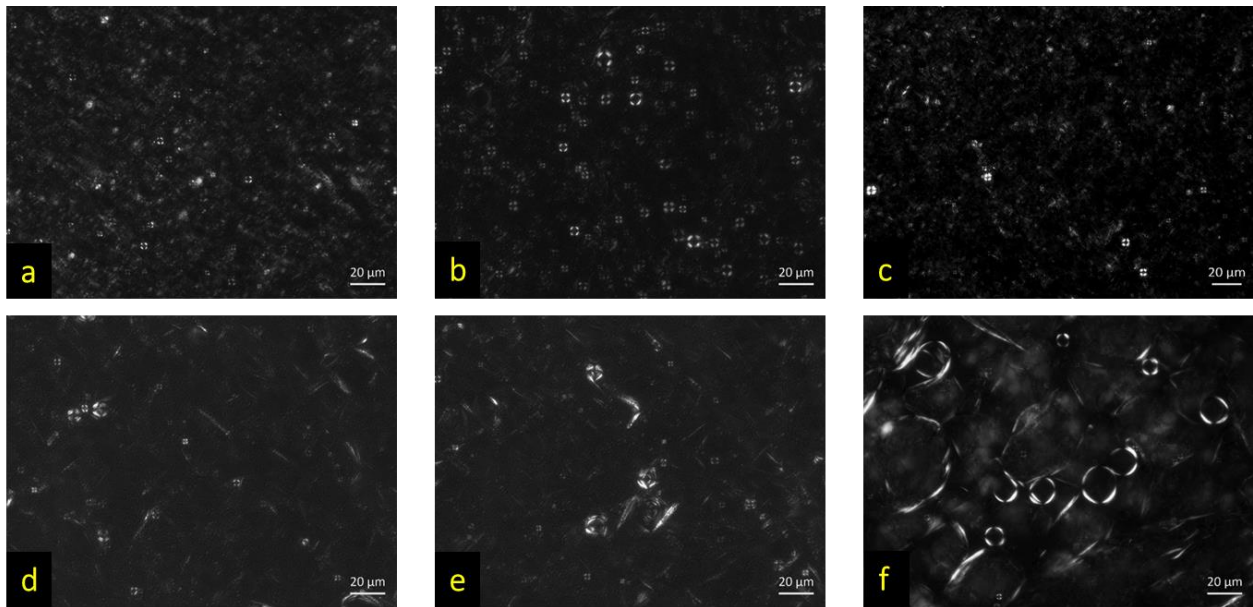


Figure 3.1. Photomicrographs of the creams (a) E1, (b) E3, (c) E4, (d) E5, (e) E6 and (f) E7 using PL microscopy 24 hours after preparation (magnification x200).

The microstructure of the creams changed between low and high amounts of ammonium sulfate. At low salt concentration (E1), the emulsion showed characteristic small Maltese extinction crosses ($\sim 3 \mu\text{m}$). These self-assembled structures highlighted the presence of lamellar phases [75], [102]. These phases can also be described as a swollen lamellar gel phase [21]. As the concentration increased (E2 and E3), the extinction crosses expanded ($\sim 4 - 6 \mu\text{m}$) and the size distribution became less homogeneous. The following increase in inorganic salt concentration (E4 to E6) drove the Maltese crosses to expand even more. Some of these structures appeared with numerous concentric layers. Their sizes enlarged from approximately $5 \mu\text{m}$ to $20 \mu\text{m}$. Upon approaching the highest salt content (E7), the extinction crosses reached their maximal size. As the salt concentration increased, the colloidal structures tend to expand and exhibited multiple visible layers: larger and/or more lamellae. The arrangement of the surfactants in these latest patterns could be due to:

- The larger colloidal structures formed under the influence of the changing electrostatic forces.
- The higher amount of lipophilic compounds such as octyldodecanol bound in the bilayers.

The photomicrograph of the cream E4 under PL microscope after one year of storage at RT is shown in [Figure 3.2.](#) Aging led to obvious structural changes. Indeed, the anisotropic structures are much larger and more numerous. This phenomenon may occur via aggregation of the bilayers [32], [36]. All the other creams containing from 0.1 to 5.0 w% of ammonium sulfate showed the same kind of structural changes after one year of storage.

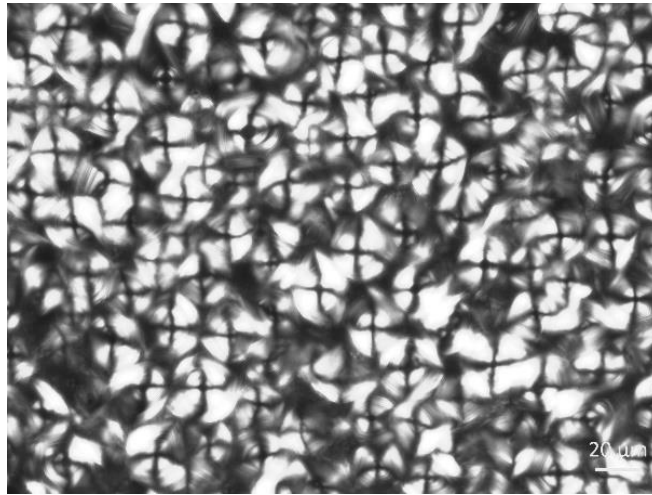


Figure 3.2. Photomicrographs of the cream E4 under PL microscopy after one-year storage at RT (magnification x200).

3.1.1.2. TEM

Prior to the TEM, the creams were diluted and centrifuged. To determine whether the extracted phases contained similar structures than the original creams, they were observed under polarized-light microscopy (see [Fig. 3.3.](#)). The photomicrographs before and after dilution showed similar Maltese crosses. Even though less abundant, the same anisotropic structures were found in [Figure 3.1.](#) (b) than in [Figure 3.3.](#) (a) and in [Figure 3.1.](#) (e) than in [Figure 3.3.](#) (b). Thus, one can assume that similar structures existed in the creams. It is important to observe that the larger structures present in the original E6 cream ([Figure 3.1.](#) (e)), were not visible anymore. We assumed that these structures were hydrated and hence diluted through the extraction protocol or could have been modified due to the mechanical stress induced by mixing.

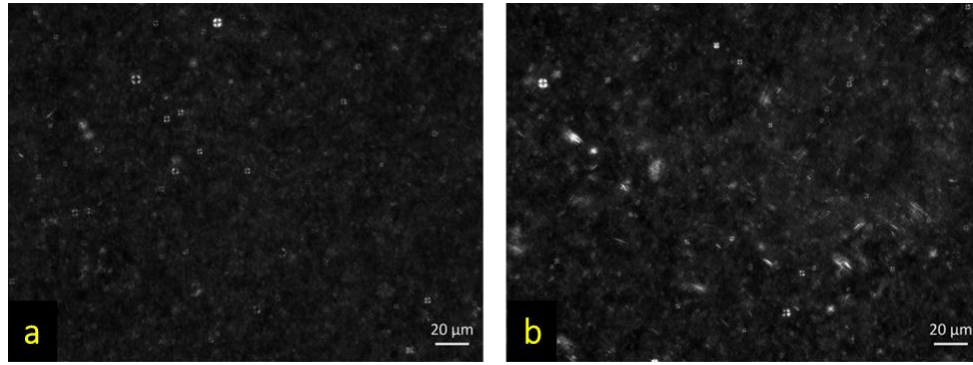


Figure 3.3. Photomicrographs of the creams (a) E3 and (b) E6 using PL microscopy after dilution 1:1 for the TEM study (magnification x200).

The photomicrographs of the diluted, centrifuged and negatively stained creams E3 and E6 under TEM are shown in [Figure 3.4](#). Both photomicrographs showed structures composed of a large core, which may contain mostly water, surrounded by bilayers forming the shell.

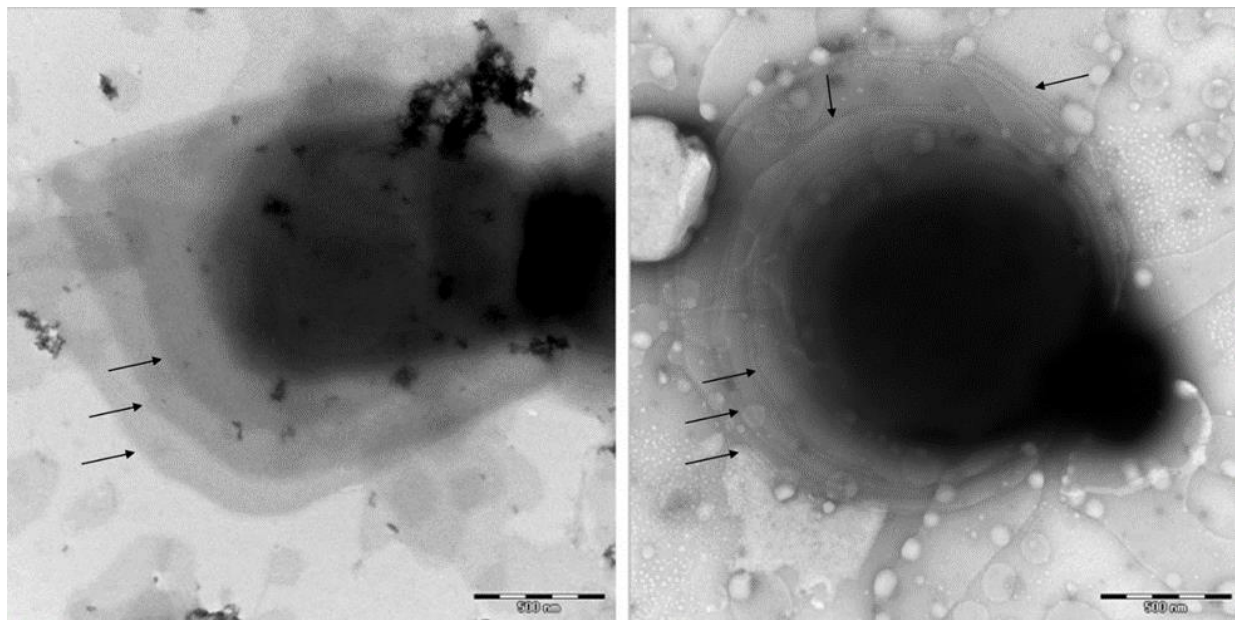


Figure 3.4. Photomicrographs of the diluted (1:1), centrifuged and negatively stained creams (left) E3 (right) E6, under TEM. The arrows are indicating the lamellar phases (magnification of the TEM x20000).

As mentioned earlier, TEM can be subject to artefact, especially when drying or staining the samples. Therefore, the results of this chapter must be interpreted with caution. These results will be only used as an additional indication of the existence of the bilayers. Quantitative characterization cannot be done thanks to this method.

3.1.2. Rheology

Twenty-four hours after preparation and at a fixed shear rate of 7.2 s^{-1} , the viscosities of the creams E0 to E7 scattered between 20 and 38 Pa.s. They exhibited a typical shear thinning and solid-like behavior (see [Fig. 3.5.](#)) [115]. Thanks to these measurements, the factor $\Delta\eta$ was calculated. $\Delta\eta$ defines the scattering of the viscosities for the sample E0 to E7. At a fixed shear rate ($\dot{\gamma} = 7.2 \text{ s}^{-1}$): $\Delta\eta_{\text{ionic}} = 16.29 \text{ Pa.s.}$

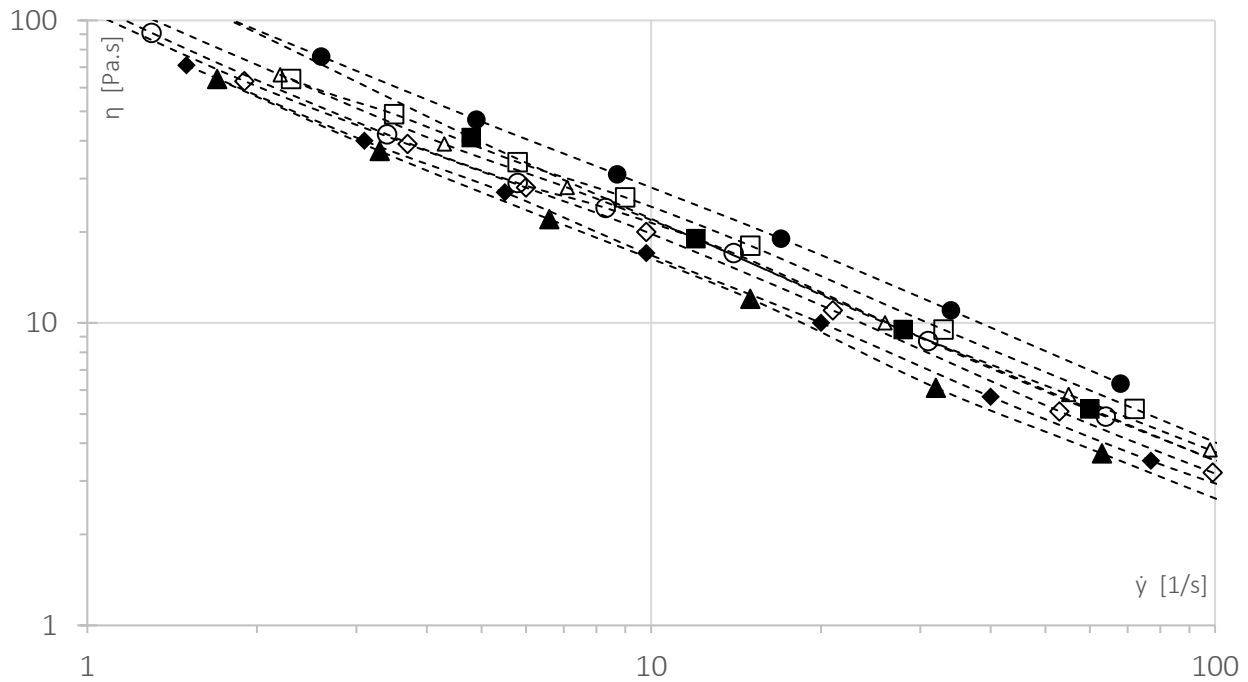


Figure 3.5. Rotational sweep measurement of the creams ● E0, ■ E1, ▲ E2, ◆ E3, ○ E4, □ E5, △ E6 ◇ E7, 24 hours after preparation at 20°C.

The same rotational sweep tests were performed over time from the first day after preparation until the sixth month of storage at RT. The viscosity measurements of the creams E0 to E7 during aging are summarized in [Figure 3.6.](#) It showed two tendencies. First, the viscosity η is decreasing significantly under addition of ammonium sulfate. Moreover, at a defined salt content, the viscosities of the creams E0 to E5 tend to increase over time. E6 and E7 remained lower in viscosities and no significant increase over time was observed. Even though ionic systems are less sensible than nonionic systems to aging processes (see [1.4.3. Aging properties](#)), the lamellae can randomly re-arrange. An increase in viscosity is more likely to happen under aggregation of the bilayers than due to a ripening mechanism. Therefore, the viscosity rises over time observed for the creams E0 to E5 might be due to an aggregation process. This hypothesis is in line with [Figure 3.2.](#), which showed more anisotropic structures in the cream E4 after one-year storage at RT.

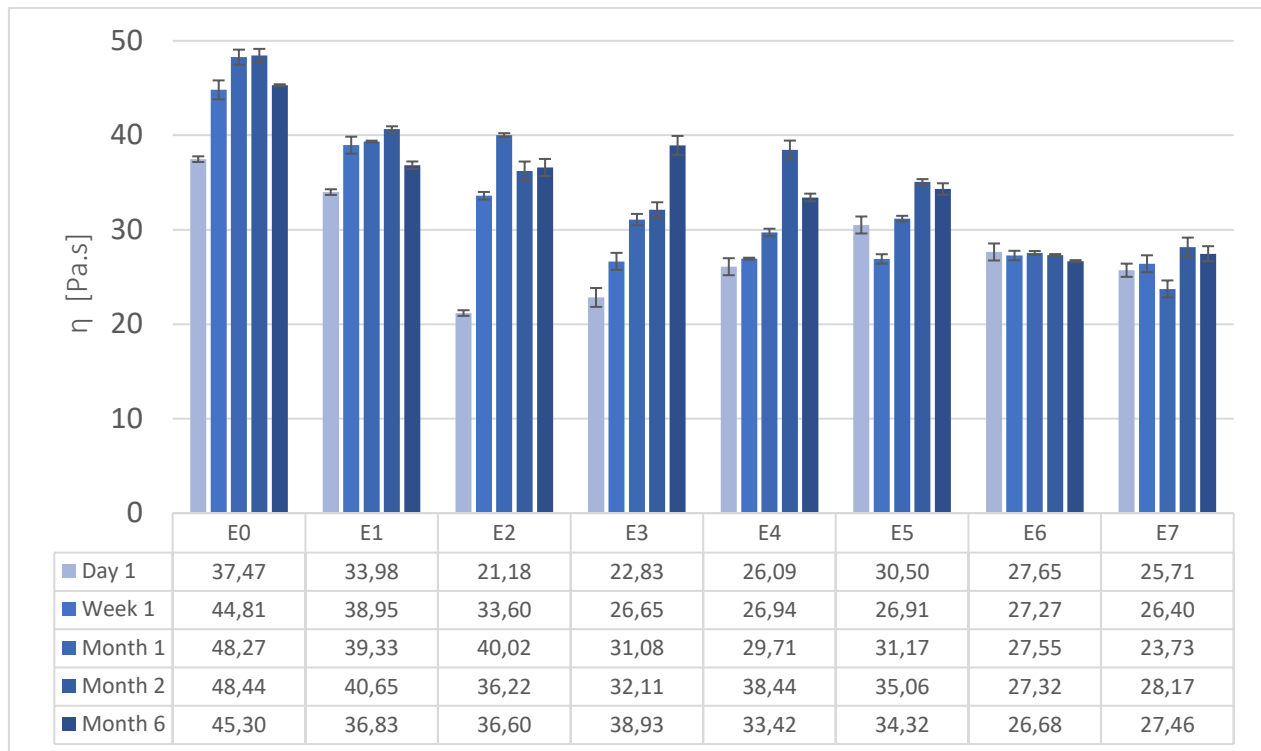


Figure 3.6. Viscosity of the creams E0 to E7 from t_0 to month 6 of storage at RT. The viscosity is measured at $\dot{\gamma} = 7,2 \text{ s}^{-1}$ at 20°C . The whiskers above and below the average values define the $\text{av.} \pm \text{std. dev.}$

Note: all the viscosity values are in Pa.s.

A strain test was performed for the creams E0 to E7. The cross-over point between G' and G'' indicated the critical strain γ_c . This value is plotted for all the ionic creams in [Figure 3.7](#), one day after preparation and after 6 months storage at RT. The critical strain γ_c is indicated in the graphic as a percent of the total strain applied during the strain test.



Figure 3.7. Critical strain γ_c of the creams E0 to E7 one day (X) and 6 months (-) after preparation (storage at RT). γ_c is expressed as a percent of the total strain range during the amplitude test (γ from 0 to 5) and taken at $\tan\delta = 1$, $\omega = 1.6 \text{ Hz}$.

It is important to remind that the critical strain of different systems can be compared only if a single ingredient in the composition is changing. Hence, the absolute γ_c value of the ionic system cannot be compared with the γ_c of other systems observed in the following chapters. One day after preparation, γ_c decreased drastically as the salt content increased (E1 to E7). The tendency stayed the same after 6 months storage at RT. The critical strain can be used as a stability indicator [69]: the lower the critical strain, the less stable the system. Therefore, the ionic creams are becoming less stable under addition of inorganic salts. The sample E0 exhibited a lower γ_c than E1 and E2. Consequently, the ionic system might be more stable with addition of 0.1 w% to 0.5 w% ammonium sulfate than salt-free. This behavior can be explained thanks to the DLVO theory. When few electrolytes are contained in the system, the electrostatic repulsion forces between the charged polar heads of SLES are not screened, and form, therefore, less stiff and stable lamellae. Additionally, the gap in γ_c between low and high salt-content, was minimized after 6 months storage at RT. This could be due to a loss in stability over time. Finally, no clear correlation existed between the viscosities of E0 to E7 and their respective critical strains. In fact, even though E0 exhibited the highest viscosity, its critical strain remained low compared to the one of E1 and E2. Hence, the most stable systems were not the one having the highest viscosities. This information confirmed that oscillatory rheological measurements are crucial for characterizing a colloidal system in a correct and precise way.

Subsequently, the storage and loss modulus of the creams E0 to E7 were plotted against the frequency: [Figure 3.8.](#) and [Figure 3.9.](#), respectively. They showed that the elastic properties of all the creams remained higher than the viscous properties on the entire range of frequencies. Moreover, G' and G'' slightly and linearly increased with the frequency without crossing each-other. This rheological behavior is typical for a lamellar gel phase [70]. These findings showed that all samples are metastable semisolids and may be composed of self-assembled semisolid bilayers [69], [116]. Moreover, G' and G'' increased under addition of salts over the full range of frequencies. In other words, at a defined frequency ω , E1 exhibited a lower G' and G'' than E2, E2 than E3 etc. These results could be explained by the microstructural changes in the creams. Indeed, as seen in [Figure 3.1.](#), more and larger anisotropic structures (Maltese crosses) appeared under microscopy as the electrolytes concentration increased. This would mean that the presence of more and/or larger lamellar structures would drive the storage and loss modulus to increase. This rise cannot be correlated with the stability of the systems.

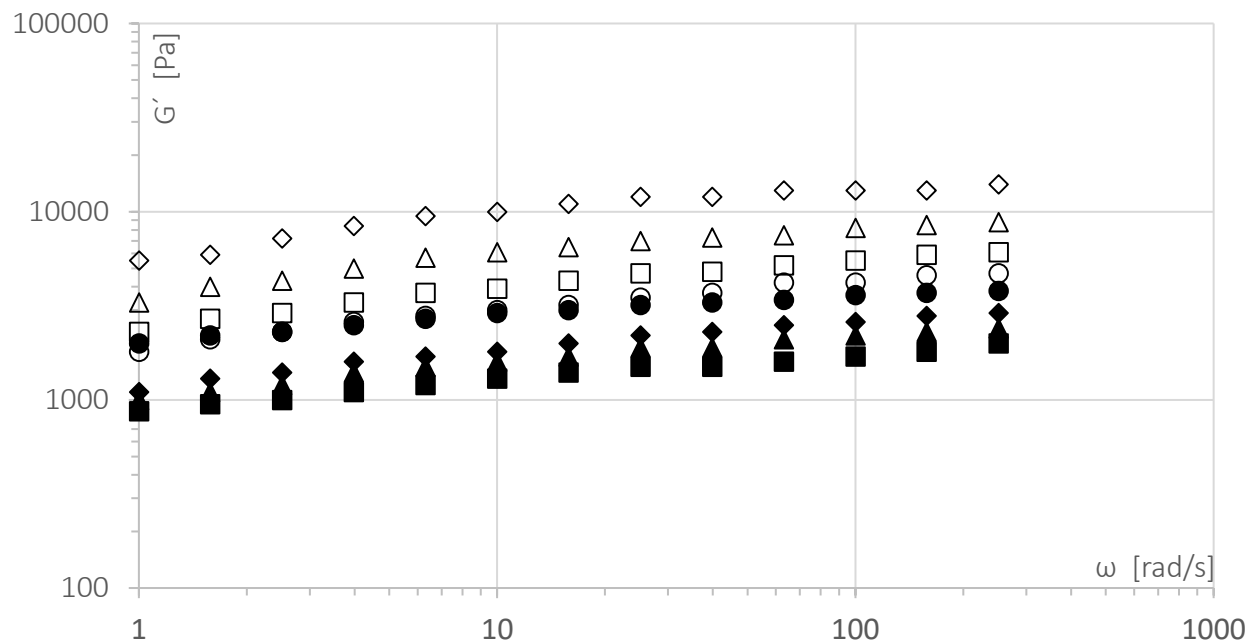


Figure 3.8. Storage modulus G' during the frequency sweep test of the creams \bullet E0, \blacksquare E1, \blacktriangle E2, \blacklozenge E3, \circ E4, \square E5, \triangle E6 and \diamond E7, 24 hours after preparation in the LVR at 20°C. The frequency ω increases logarithmically from 0.1 to 300 rad/s and the strain $\gamma = 0.001$ corresponds to a displacement angle of $1.77\text{E-}05$ rad, such as $\gamma \ll \gamma_c$.

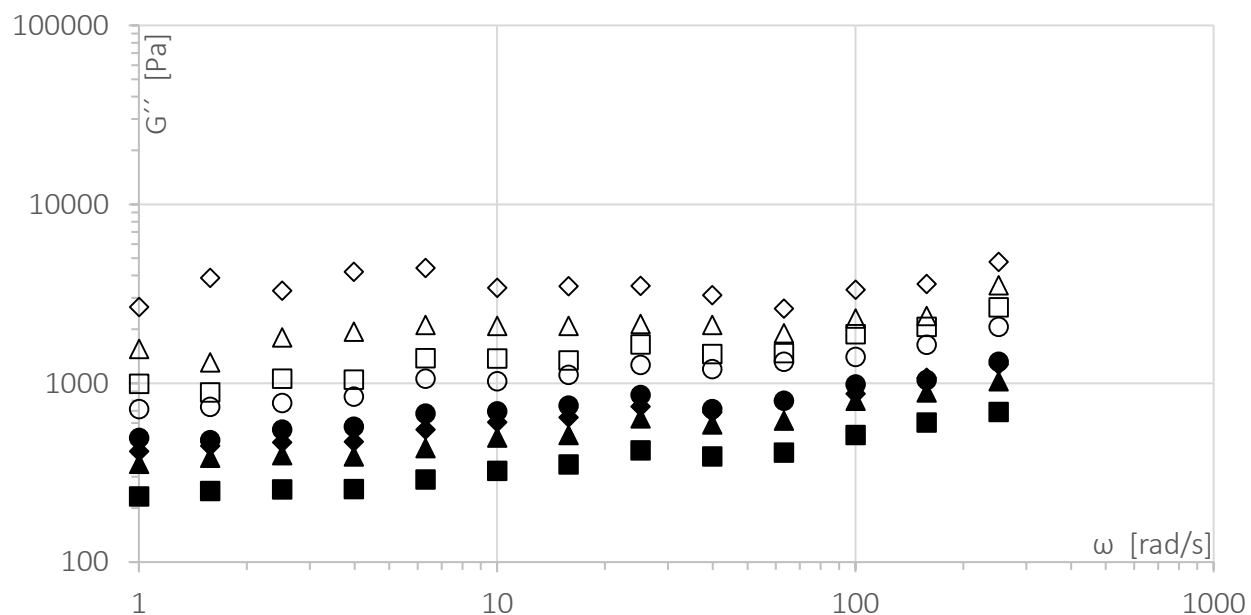


Figure 3.9. Loss modulus G'' during the frequency sweep test of the creams \bullet E0, \blacksquare E1, \blacktriangle E2, \blacklozenge E3, \circ E4, \square E5, \triangle E6 and \diamond E7, 24 hours after preparation in the LVR at 20°C. The frequency ω increases logarithmically from 0.1 to 300 rad/s and the strain $\gamma = 0.001$ corresponds to a displacement angle of $1.77\text{E-}05$ rad, such as $\gamma \ll \gamma_c$.

However, the ratio of G'' over G' (the loss factor: $\tan\delta$) can be relevant for the assessment of the stability. In the frequency sweep test, the strain is considered small enough ($\gamma \ll 1$) to not disturb the fluid structures [115]. Hence, the fluctuations measured are only related to the re-arrangement or relaxation of the bilayers in the system. If the loss factor shows large fluctuations at a fixed frequency, this would mean that the system endeavor to re-arrange. If the loss factor approaches the finite value 1, then the system would change its structural configuration from solid- to liquid-like [69], [115]. $\tan\delta$ was plotted in the high frequency region ($\omega = 250$ rad/s) for the ionic creams: E1 to E7 in [Figure 3.10](#). The loss factor scattered between 0.30 and 0.45. No significant differences were observed between the creams E1 to E7. Aging showed also no significant difference in the loss factor.

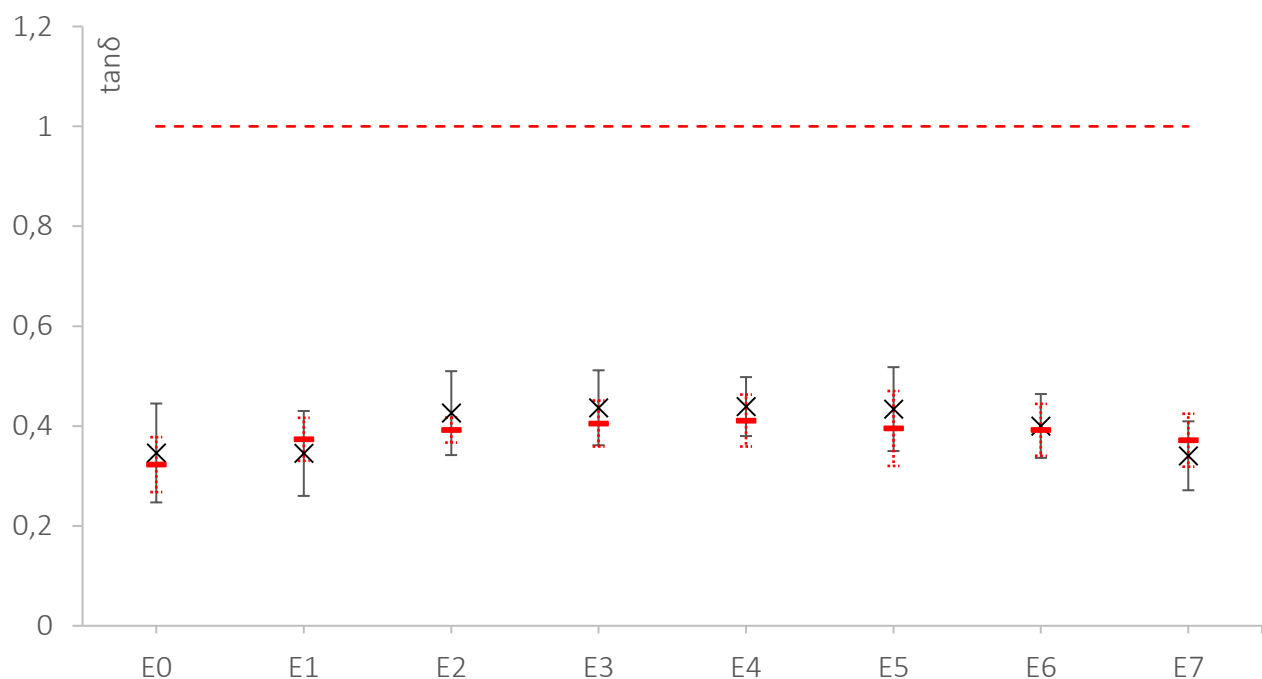


Figure 3.10. Loss factor ($\tan\delta$) at high frequency ($\omega = 250$ rad/s) for the creams E0 to E7 one day (X) and six months (—) after preparation. The whiskers above and below the average values define the $av. \pm$ std. dev.

The observation of the rheological behavior of the ionic creams at high frequencies did not indicate instability potential which could lead to phase separation. The strain stress study led to more relevant information than the frequency sweep test.

All rheological data considered, the ionic creams E0 to E7 showed a typical solid-like behavior likely to be composed of lamellar phases. The rheological properties of the ionic samples are strongly dependent on the overall electrolytes concentration and aging.

3.1.3. DSC

3.1.3.1. Thermal behavior of the raw materials contained in the ionic creams

DSC was primarily used to determine the thermal behavior of the raw surfactants and FA contained in the ionic systems. Thermal cycling was performed. The results were taken during the third heating run and the second cooling run. All measurements were repeated three times. SLES is liquid at RT, therefore no DSC was performed for this compound. The thermograms of PEG-20 cetyl/stearyl ether and glyceryl monostearate showed a single endothermic peak at 42 and 60°C, respectively. Therefore, these two compounds have a single melting point. However, glyceryl monostearate showed two overlapping exotherms during cooling. The onset temperature of this peak was measured at 59°C. Hence, glyceryl monostearate exhibits a polymorphism behavior with two close transition temperatures. This behavior was not observed during the melting process. This is probably due to the overlap between the first transition and the melting. During cooling, PEG-20 cetyl/stearyl ether showed one single narrow exotherm with an onset temperature at 35°C. Cetearyl alcohol used in this study showed a β - α transition at 30°C and a melting temperature at 51°C ([Figure 3.11.](#)). Accordingly, the cooling run of cetearyl alcohol indicated two transitions at 50 and 26°C. The melting enthalpy of PEG-20 cetyl/stearyl ether, glyceryl monostearate and cetearyl alcohol was: 130 J/g, 80 J/g and 74-118 J/g (first and second endotherms), respectively. Additionally, ammonium sulfate showed, at elevated temperatures, a single narrow endotherm at 366°C with a melting enthalpy equal to 29 J/g. PTD did not exhibit any endotherm peaking even at elevated temperature. These results are summarized in [Table 3.1.](#) The thermogram of cetearyl alcohol is shown in [Figure 3.11.](#) The thermograms of all the other raw materials are shown in [Appendix 7.2.1.](#)

Table 3.1. Thermal behavior of the raw materials contained in the ionic creams (E0 to E7) during the third heating and second cooling run (2K/min).

	$T_{\text{Melt. Max. 1}}$ [°C]	$T_{\text{Melt. Max. 2}}$ [°C]	$\Delta H_{\text{Melt. Tot.}}$ [J/g] *	$T_{\text{Cryst. Onset 1}}$ [°C]	$T_{\text{Cryst. Onset 2}}$ [°C]
Cetearyl Alcohol	29.62 ± 0.02	51.47 ± 0.04	191.63 ± 1.30	49.69 ± 0.04	25.62 ± 0.12
PEG-20 cetyl/stearyl ether	41.41 ± 0.16	-	130.53 ± 1.50	34.81 ± 0.41	-
Glyceryl monostearate	60.26 ± 0.10	-	80.96 ± 1.85	58.56 ± 0.03	-

* The melting enthalpies reported in this table are the total melting enthalpies of each raw materials. For cetearyl alcohol, exhibiting two melting endotherms, the $\Delta H_{\text{Melt. Tot.}}$ is the sum of $\Delta H_{\text{Melt. 1}}$ and $\Delta H_{\text{Melt. 2}}$.

Characterization of the raw materials contained in the ionic creams by means of DSC is a crucial step to understand the solid-like systems. In fact, it was found that cetearyl alcohol and glyceryl monostearate exhibit a polymorphism behavior. This information will help later to determine whether these compounds are integrated in the surfactants' bilayers in the crystal- or in the liquid-form.

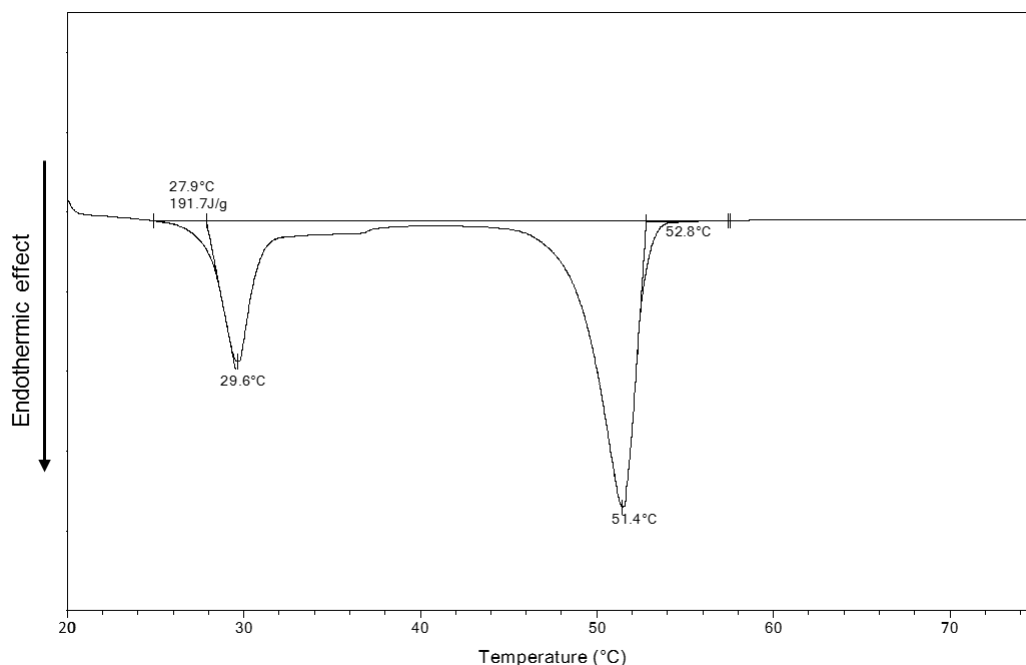


Figure 3.11. DSC thermograms of ceteryl alcohol measured between 20°C and 70°C at a heating rate of 2K/min.

3.1.3.2. Thermal behavior of the ionic creams containing ammonium sulfate

Subsequently, DSC was used to establish the melting behavior of the ionic creams. Thermal cycling was performed. Data were taken during the third heating run and the second cooling run. All measurements were repeated three times. First, all the creams showed a reproducible melting behavior for the three repeated measurements. During the third heating run, a single broad and tailed endotherm was observed for all the ionic creams (see [Fig. 3.12.](#)). The absence of a phase transition in the 30°C region indicated that the hydrocarbon chains of ceteryl alcohol are in the crystal α -form. Accordingly, the same assumption can be done for glyceryl monostearate. The presence of a single broad endotherm demonstrated that the surfactants and the fatty alcohols form together a single phase possibly composed of multiple bilayers called the hydrophilic gel phase [49]. Moreover, the melting enthalpy of all the creams remained lower than 20 J/g (see [Fig. 3.13.](#)). A thermal behavior showing: a broad single melting endotherm and a low melting enthalpy, has been earlier described in the literature for surfactants' bilayers formed by a blend of fatty alcohol and anionic [76] or cationic emulsifiers [74]. The DSC measurements showed that the studied ionic creams behave like typical viscoelastic gels [46] likely to contain surfactants bilayers.

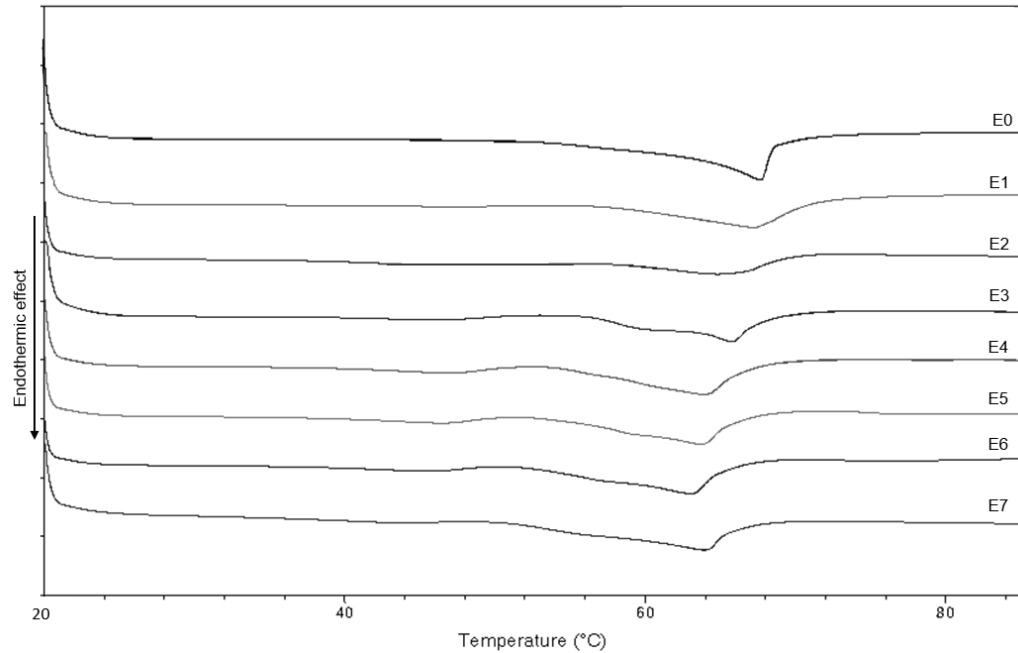


Figure 3.12. DSC thermograms of the ionic samples E0 to E7 containing from 0 to 5.0 w% ammonium sulfate in the third heating run. Heating run from 20 to 85°C at a constant a heating rate of 2K/min.

The endotherms differed for different ammonium sulfate concentrations. [Figure 3.13.](#) shows the melting temperature and the melting enthalpy of E0 to E7.

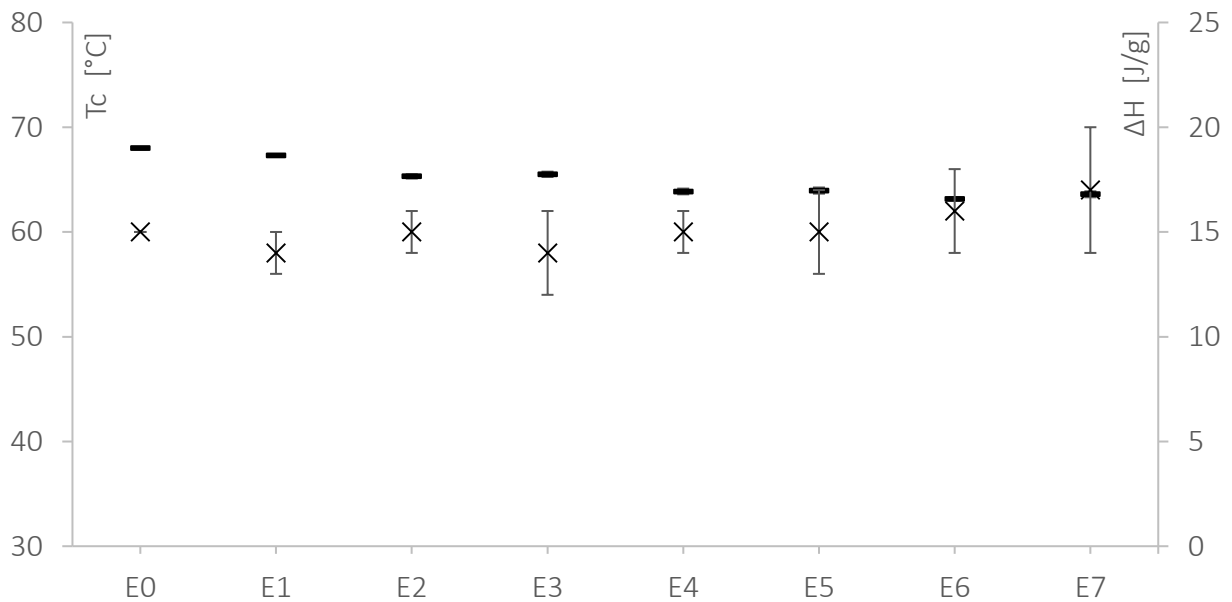


Figure 3.13. Melting temperatures T_c (—) and melting enthalpies ΔH (X) of the creams E0 to E7. The measurements were repeated three times. The whiskers above and below the average values define the av. \pm std. dev. The values presented were taken during the third heating run (2K/min).

The melting process is occurring between 60 and 70 °C. The melting endotherms slightly shifted to lower temperatures as the salt concentration increased. The melting enthalpy was not significantly different for E0 to E7. However, the standard deviation of the melting enthalpy, calculated on the three repetitions of the DSC measurements, became larger for high amounts of salt. These variations can be the sign of inhomogeneous or unstable systems.

To fully understand the thermal behavior of the nonionic creams, the crystallization behavior of the creams E0 to E7 are presented in [Table 3.2.](#)

Table 3.2. Crystallization temperatures of the creams E0 to E7 during the second cooling run (2K/min).

	E0	E1	E2	E3	E4	E5	E6	E7
Onset crystallization temperature [°C] *	61	61	64-50	63-48	63-47	63-47	62-46	62-45
Std. dev. [°C] *	0.1	0.1	0.2-0.1	0.6-0.2	0.6-0.1	0.1-0.2	0.1-0.1	0.7-0.2

* Av. values and std. dev. calculated from the three repeated measurements.

At the exception of E0 and E1, the ionic creams showed two broad exotherms during the cooling run. The first exotherms were intense compared to the second exotherms which were almost laying on the thermograms baseline. While increasing the salt concentration, the second onset temperatures lowered from 50 to 45°C. This region corresponds to the crystallization temperature of cetearyl alcohol. The same temperature range was found for hydrated cetearyl alcohol by Wunsch et al. [87]. These results may reveal the existence of a crystalline phase in E2 to E7. This phase could be composed of essentially hydrated FA in their crystalline α -form as described in [Figure 1.5.](#) (A) and [Figure 1.6.](#) (C). This second exotherm shifted from 50°C, at low salt concentration, to 45°C, at high salt concentration. This could be due to the degree of hydration of the crystalline phase i.e. its water content. It was demonstrated that the melting temperature of cetearyl alcohol shifts to higher temperature when they are more hydrated [76], [87]. This means that crystalline phases of FA exhibit a higher melting temperature when they contain more water. Accordingly, the crystalline phases of E2 may contain more water than the crystalline phase of E7. Thus, the diffusion of water to the hydrophobic crystalline phases, would be more favorable when less electrolytes are diluted in the bulk-water phase. This could be explained by the higher polarity of the bulk-water phase when the overall electrolytes concentration increases. Concerning E0 and E1, two assumptions can be done:

- These systems contain a lipophilic phase, composed of FA-amphiphiles and/or surfactants, which was not identified by means of DSC due to its too low concentration.

- The FA contained in E0 and E1 are fully integrated into the lamellar gel phase. Therefore, no crystalline hydrated phase exists in E0 and E1.

The first assumption is more likely to happen as the FA are in large excess in the ionic creams.

3.1.3.3. Thermal behavior of the ionic creams containing PTD

To understand the thermal behavior of the ionic creams containing organic salts, the DSC measurements were repeated for F1 to F6. This step was added to obtain insights about the melting behavior of the ionic creams in view to formulate a hair coloring product. Thermal cycling was performed. Data were taken during the third heating run and the second cooling run. All measurements were repeated three times. [Figure 3.14.](#) is showing the thermograms of E0 and F1 to F6 and [Figure 3.15.](#), the melting temperature and the melting enthalpy of the same ionic creams.

As for E0 to E7, the onset, the melting and the offset temperatures shifted to lower temperatures as the salt concentration increased. The melting process was occurring between 60 and 70 °C. The melting behavior of E1 to E7 and F1 to F6 are comparable. The endotherms of the creams containing PTD appeared bulkier than the one containing ammonium sulfate. However, the melting enthalpies from F1 to F6 remained low: from 14 to 19 J/g. These values are in the same range than the melting enthalpies of the ionic creams containing ammonium sulfate. Hence, the required energy to melt the ionic creams does not depend on whether the salt is inorganic e.g. ammonium sulfate or organic e.g. PTD. This observation is important to validate the relevance of this study. In fact, this reveals that the simulation of the overall salt content by using ammonium sulfate was a consistent choice. The creams F1 to F6 showed a typical lamellar gel phase behavior i.e. large single endotherm exhibiting a low melting enthalpy.

The rise of melting enthalpy, while increasing the PTD concentration, was not as linear as for E0 to E7. The low salt concentration group F1 to F3 and the higher salt concentration group F4 to F6 did not show significant differences in their melting enthalpies, within one group. However, the melting enthalpies of both groups were significantly different. This could be due to a higher inhomogeneity in all the samples. However, the melting enthalpy range remained the same than for the creams containing inorganic salt.

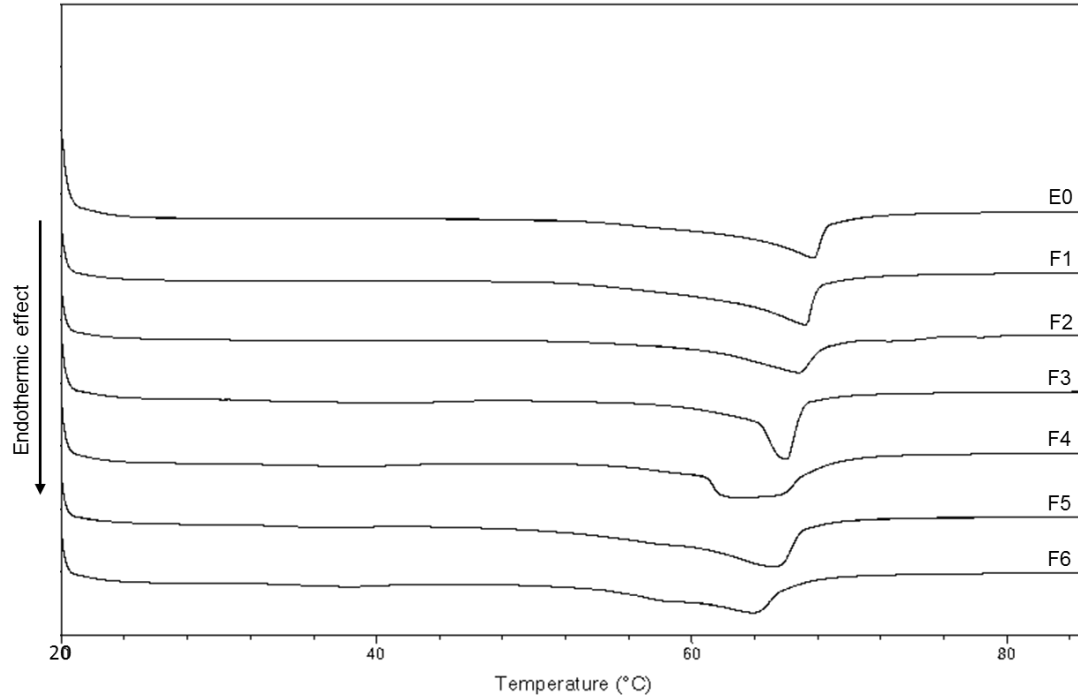


Figure 3.14. DSC thermograms of the ionic samples E0 and F1 to F6 containing from 0 to 7.0 w% PTD in the third heating run. Heating run from 20 to 85°C at a constant a heating rate of 2K/min.

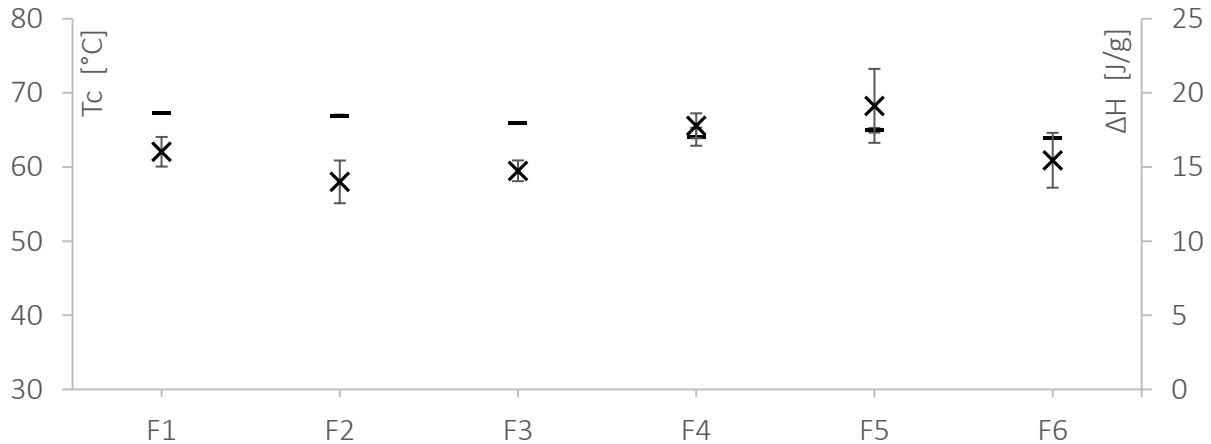


Figure 3.15. Melting temperatures T_c (—) and melting enthalpies ΔH (X) of the creams F1 to F7. The measurements were repeated three times. The whiskers above and below the average values define the av. \pm std. dev. The values presented were taken during the third heating run (2K/min).

The crystallization behavior of the creams F1 to F6 are summarized in [Table 3.3.](#) and shown in [Appendix 7.2.2.](#)

Table 3.3. Crystallization temperatures of the creams F1 to F6 during the second cooling run (2K/min).

	F1	F2	F3	F4	F5	F6
Onset crystallization temperature [°C] *	66	65	65	64	64	63
Std. dev. [°C] *	0.0	0.1	0.1	0.1	0.1	0.0

* Av. values and std. dev. calculated from the three repeated measurements.

All creams exhibited a single broad tailed exotherm during cooling. The onset of the crystallization shifted to lower temperatures with increasing the PTD concentration. This is in line with the melting behavior observed earlier. Contrary to E2 to E7, none of the creams showed a double exotherm during the cooling run. This does not mean that the crystalline phase is not existing. A possible explanation would be, once again, that this phase exists at a too low concentration to be detected by means of DSC. This will be further investigated in chapter: [3.1.4. Spectroscopic imaging](#).

The thermal behavior of the creams containing organic salt is similar to the creams containing inorganic salts. This step highlighted the relevance of replacing the dye stuff mixture in the simple hair coloring formulation by either ammonium sulfate or PTD.

3.1.4. Spectroscopic imaging

The main IR absorption bands of the raw materials used for formulating the ionic creams are summarized in [Table 3.4](#). The ATR-FTIR spectra of the raw material are shown in [Appendix 7.3](#). It is clear from [Table 3.4](#) that the region of interest for the ionic creams is found between 3500-3000 cm^{-1} and between 1500-1000 cm^{-1} .

Table 3.4. Main IR absorption bands of the raw materials contained in the ionic creams E0 to E7.

Wavenumber region [cm^{-1}]	4000-3500	3500-3000	2000-1500	1500-1000	1000-500
Cetearyl alcohol		3270*, 2916, 2849		1472, 1060	730, 719
Glyceryl monostearate		3305*, 2915, 2850	1730	1470, 1178	719
PEG-20 cetyl/stearyl ether		3425*, 2916, 2885, 2850		1467, 1343, 1280, 1241, 1104	962, 842
SLES		3458*, 2923, 2854	1642	1213, 1021	
Am. Sulf.		3015*		1403, 1061	610
Water	3500		1650		

* Broad overtone of medium intensity.

Note: The absorption bands typed in bold are the most intense bands of the spectrum.

The ionic cream E3 was observed under ATR-FTIR spectroscopy and microscopy. The microscopic intensity image at 1420 cm^{-1} and the associated spectra are presented in [Figure 3.16](#). and [Figure 3.17](#)., respectively.

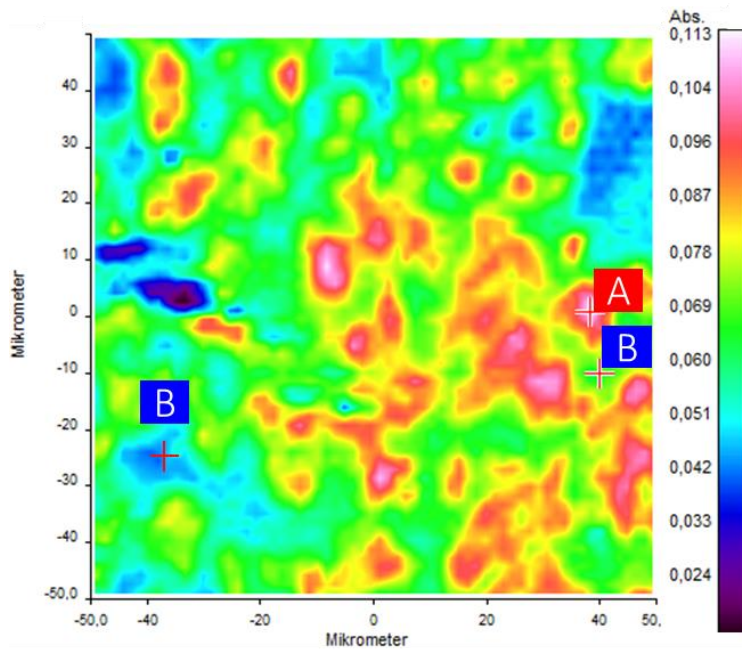


Figure 3.16. Intensity image under ATR-FTIR microscopy at 1420 cm^{-1} of the ionic cream E3 containing 1.0 w% ammonium sulfate. The marked regions A and B correspond to the “concentrated” and the “diffuse” area, respectively. The color pattern corresponds to the color code used in [Figure 3.17.](#)

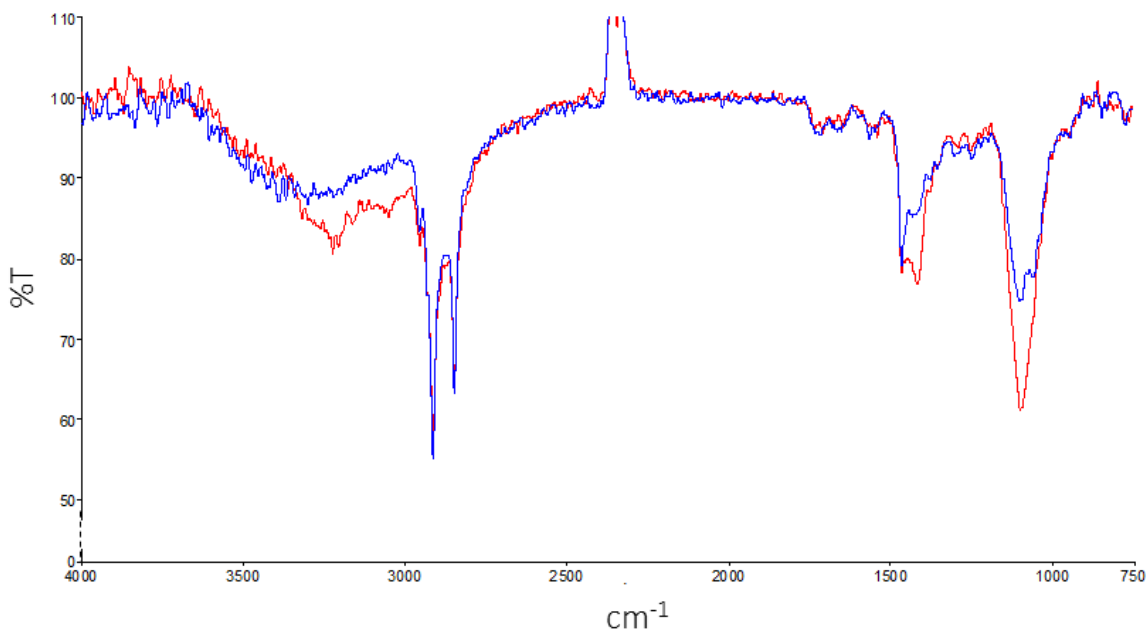


Figure 3.17. ATR-FTIR spectra of the ionic cream E3 (1.0 w% ammonium sulfate) in two different regions of the sample: the “concentrated” (red) and the “diffuse” (blue) area. The color pattern corresponds to the color code used in [Figure 3.16.](#) The spectra are measured at RT using UATR-technique with a diamond-KRS-5 (Thallium Bromoiodide) crystal.

The microscopic intensity images, at 1420 cm^{-1} , revealed the presence of two distinct areas in the sample: a concentrated area (A in [Figure 3.16.](#)) and a diffuse area (B in [Figure 3.16.](#)), present predominantly in the sample. The intensity image was taken at 1420 cm^{-1} because both areas showed different absorption bands at this specific wavenumber. The spectra of both identified areas displayed very similar profile at the exception of their intensities. The spectra of both B marked regions, showed the same absorption bands. Therefore, they both belong to the diffuse area. This region showed typical absorbance bands of fatty alcohols ($2916, 2849\text{ cm}^{-1}$), long chain alcohol compounds e.g. PEG-20 cetyl/stearyl ether ($2916, 2850, 1104\text{ cm}^{-1}$), SLES ($2923, 2854, 1021\text{ cm}^{-1}$), and ammonium sulfate (large band at 3015 overlapping with the water absorption at $3500, 1403\text{ cm}^{-1}$). The diffuse area might correspond to the bulk-water phase ([Figure 1.6.](#) (B)).

The concentrated area also showed typical absorbance bands of fatty alcohols ($2916, 2849\text{ cm}^{-1}$), long chain alcohol compounds e.g. PEG-20 cetyl/stearyl ether ($2916, 2850, 1104\text{ cm}^{-1}$), SLES ($2923, 2854, 1021\text{ cm}^{-1}$), and ammonium sulfate (large band at 3015 overlapping with the water absorption at $3500, 1403\text{ cm}^{-1}$). This region showed more intense absorption bands in the characteristic wavenumber regions of ammonium sulfate. In fact, the corresponding spectrum showed a large intense absorption band between 3200 and 2900 cm^{-1} and two characteristic intense bands at 1410 cm^{-1} and 1090 cm^{-1} . Considering that the concentrated area is the lamellar gel phases ([Figure 1.6.](#) (A)), this demonstrated that the concentration of ammonium sulfate is higher in the lamellar gel phase than in the bulk-water phase or at least, that ammonium sulfate diffuses in both phases.

ATR-FTIR spectroscopy and microscopy confirmed that ammonium sulfate is present everywhere in the sample including in the ionic surfactants' bilayers forming the lamellar gel phase. Therefore, the salts might interact with the ionic surfactants in a strong manner. This is in line with the rest of the chapter 3.1. which revealed a strong dependency of the microstructure, hence the rheological and the thermal behavior, towards salts addition. Moreover, the presence of the characteristic absorption bands of long chain alcohols, in both areas, highlighted that the FA and/or the surfactants are not only present in the lamellar gel phase. This may be the crystalline hydrate phase ([Figure 1.6.](#) (C)) also identified by means of DSC. This phase could correspond to the bulky anisotropic structures (other than Maltese crosses) observed in the PL photomicrographs. Nevertheless, this phase was not further investigated by means of optical PL microscopy.

3.1.5. Conclusion

The results showed that the microstructure of the ionic systems is strongly dependent on the ammonium sulfate content, thus, the overall electrostatic forces contained in the system. The analysis demonstrated that the ionic creams, composed of surfactants' bilayers, were behaving as typical lamellar gel phases. TEM photomicrographs especially brought out the presence of vesicles and/or bilayers. As discussed earlier, TEM is subject to artefact. Therefore, it is relevant to confirm this hypothesis by calculating the theoretical PP of the systems (see [1.3.5.2. Packing parameter](#)):

Israelachvili described SLES in earlier work as a twelve carbons chain compound with OE functional groups having a tail volume V and length l equal to 350 \AA^3 and 17 \AA , respectively. Due to the screening effects occurring under addition of more counter-ions, the cross-sectional area a of the polar head of SLES varies between 62 and 45 \AA^2 , respectively [40]. These approximations lead to a PP at low and high salt concentration of 0.33 and 0.5 , respectively. Hence, SLES alone in solution would rather pack into cylindrical micelles at low salt content and into flexible bilayers and/or vesicles at high salt concentration. The ionic system contained additionally the nonionic cetearyl alcohol. This FA has a smaller head-group which reduces the theoretical value of a , and a longer bulky tail which prevents the fatty alcohol and the surfactants to pack under small micellar aggregates. Therefore, the PP of the complete combined surfactants system shift to values superior to 0.5 . Theoretically, the ionic creams E0 to E7 are more likely to be composed of vesicles, flexible bilayers and planar bilayers. Glyceryl monostearate and PEG-20 cetyl/stearyl ether are typical o/w emulsifiers and would rather form lamellar structures and/or vesicles than inversed micelles. Therefore, it is very unlikely that the system arranged under inversed-micelles ($p > 1$). This assumption correlates well with all the above observations.

In summary, the ionic systems showed under addition of ammonium sulfate:

- An expansion of the Maltese crosses under PL microscopy
- A decrease of the viscosity η
- A decrease of the critical strain γ_c
- A decrease of the melting temperature T_c

To explain these phenomena, the DLVO theory can be used (see [1.3.4. DLVO theory](#)): the strong repulsive forces which drives normally SLES polar heads to repeal themselves, are screened by the counter-ions from the ammonium sulfate salts. The Stern layer is formed around the head of the surfactants and shields the short-range repulsive electrostatic

forces. This allows the Van der Waals attractive forces to contribute in the formation of bilayers. This mechanism occurs for all the creams from E0 to E7 which exhibit a high viscosity. When the counter-ions from the salts are compensating all the electrostatic repulsive interactions from the SLES, the surfactants come to assemble in the most stable and stiff pattern: E1 and E2, for which the critical strain is reaching a maximum. As the salt concentration gets higher, the additional ionic compounds incorporated into the system do not promote anymore the surfactants and the fatty alcohols to pack even closer and stiffer. On the contrary, this addition of ions brings strong additional ionic repulsion forces in the system. This may lead to the swelling of the hydrophilic gel phases in less firm microstructures. Therefore, the viscosity together with the critical strain decreased and the anisotropic structures under PL microscopy expanded. This swelling mechanism may also prevent the insertion of long-chain alcohol in the hydrophilic gel phase by restricting hydrophobic packing driving forces. Therefore, the cetearyl alcohol would more favorably form additional crystalline lipophilic phases. This phase was possibly identified by means of DSC for the samples E2 to E7. The ATR-FTIR imaging spectroscopic results were supporting this assumption. The same speculations were made by Ballmann and Müller who studied a similar system [117]. The presence of a crystalline hydrate phase becoming more abundant while increasing the salt concentration would explain the decrease of the melting temperature.

The characterization of the classical simplified hair coloration products proved that the unstable rheological behavior of these systems is due to structural changes in the lamellar gel phase under addition of salts and ageing. These changes are due to the strong electrostatic interactions between the ionic surfactants and the electrolytes. In fact, this chapter demonstrated that the lamellar gel phases swell under addition of inorganic salt and that the lamellae may aggregate over time. A strong electrolytes concentration dependency of the structural arrangement of surfactants' bilayers was also observed in the literature for other systems [75], [118]. Additionally, the changes in the microstructure after 6 months showed that a non-favorable equilibrium already existed in the fresh samples. This can be due to either a not optimal formulation process or an incorrect surfactant/FA ratio. The following chapters are aiming to correct these instability factors by:

- Using exclusively nonionic surfactants
- Optimizing the surfactant/FA ratio of the system

3.2. Optimization of the surfactant system

The aim of the surfactants' screening study is to evaluate the stability and rheological robustness of new nonionic systems. Therefore, the following criteria/specifications were used for selecting the most promising nonionic surfactant combinations in view to develop stable creams containing hair-dyes:

- (i) $10.0 < \eta < 30.0$ Pa.s (according to the hair coloration cosmetic standards)
- (ii) Viscosity homogeneity and robustness over time
- (iii) High critical strain
- (iv) Higher G' modulus than G'' modulus on the full range of frequencies (solid-like)
- (v) Homogeneity of the anisotropic microstructures under PL microscopy at t_0 and after 6 months storage at RT

3.2.1. Evaluation of the systems containing a single nonionic emulsifier

This chapter is focusing on characterizing the system S1, S2, S3, S4, S11 and S12 containing a single nonionic emulsifier and described in [2.1.2. Optimization of the surfactant systems: screening of nonionic emulsifiers](#). Directly after preparation, S2, S3 and S4, S12 were stable. On the contrary, S1 and S11 showed a phase separation. The rheological properties of the nonionic systems are summarized in [Table 3.5.](#)

Table 3.5. Rheological properties of the nonionic systems containing a single emulsifier.

	S1	S2	S3	S4	S11	S12
η_{10} [Pa.s] ¹		8.14	14.36	15.50		1.27
$\Delta\eta$ [%] ²	Phase separation	+13	+14	+17	Phase separation	+400
γ_c ³		0.070	0.087	0.088		0.028
$\tan\delta < 1$ ⁴		Solid-like	Solid-like	Solid-like		Solid-like

¹ Viscosity at a fixed shear rate of 7.2 s^{-1} at 20°C , one day after the preparation t_0 .

² Maximum intervals in viscosity between t_0 and 6 months storage at RT. These intervals are expressed as a percentage with η_{10} equivalent to 100%.

³ γ_c , the critical strain, taken at $\tan\delta = 1$, $\omega = 1.6$ Hz.

⁴ Control of the solid-like nature of the system. When $G' > G''$, meaning $\tan\delta < 1$, on the full range of frequencies ($\omega = 0.01$ to 250 rad/s), the system is solid-like, else, the system is liquid-like.

The systems S1 and S11 containing as unique nonionic surfactant: PEG-2 cetyl/stearyl ether and PEG-23 lauryl ether, respectively, were not stable. In the first case, one can assume that the polar moiety of the PEG-2 cetyl/stearyl ether was not long enough to provide hydrophilicity to the system. This result could have been expected as the HLB value of PEG-2 cetyl/stearyl ether is low: 4.9 [111], [112]. In the second case, the difference in carbon chain length between the FA and the PEG-23 lauryl ether might explain the phase separation. Indeed, if the apolar moiety of the nonionic emulsifier is reduced to 12 carbons, the Van der Waals hydrophobic forces decrease. The spontaneous phase separations which occurred for S1 and S11 are illustrating the importance of conserving

in the system a reasonable balance in the nonionic surfactant system between polar and apolar moieties. Indeed, both the nonelectrical steric barrier formed by the POE polar moieties and the hydrophobic Van de Waals attractive forces must co-exist for enhancing stability and drive a sustainable bilayers formation. S2, S3 and S4 were all solid-like stable creams. The critical strain value and the viscosity increased with the OE unit number of the nonionic surfactant. However, S4 showed the largest fluctuations in viscosity after 6 months storage at RT. These observations could be correlated with the bulkiness of the PEG-20, 50, 100 polar moieties: on the one hand, a voluminous POE polar head promotes a high η and γ_c due to large steric hindrances and nonelectrical steric barrier forces, respectively. On the other hand, surfactants' bilayers composed of bulky POE units, seems to be favorable to spontaneous re-arrangement. Hence, even though S4 showed the best potential for stability and robust rheological behavior at t_0 , the results after 6 months storage at RT confirmed that the system is, in fact, subject to significant fluctuations. The system S12 containing PEG-20 oleth ether showed solid-like properties but exhibited the lowest viscosity, a dramatic increase of viscosity over time and the lowest critical strain. PEG-20 oleth ether is composed of an unsaturated carbon chain. Therefore, the apolar moiety adopts a curved geometry which impacts the volume of the tail, V . This results in less packed surfactants bilayers. The formation of imperfect lamellae could explain the low viscosity at t_0 . The reduced Van der Waals hydrophobic interactions could explain the significant fluctuations in viscosity over time.

The control of the homogeneity of the microscopic pictures from t_0 to 6 months after preparation are presented in [Figure 3.18](#). For evaluating the inhomogeneity, the following factors were observed: appearance of crystal-like structures, large anisotropic structures, needle-like structures or drastic microscopic changes over time.

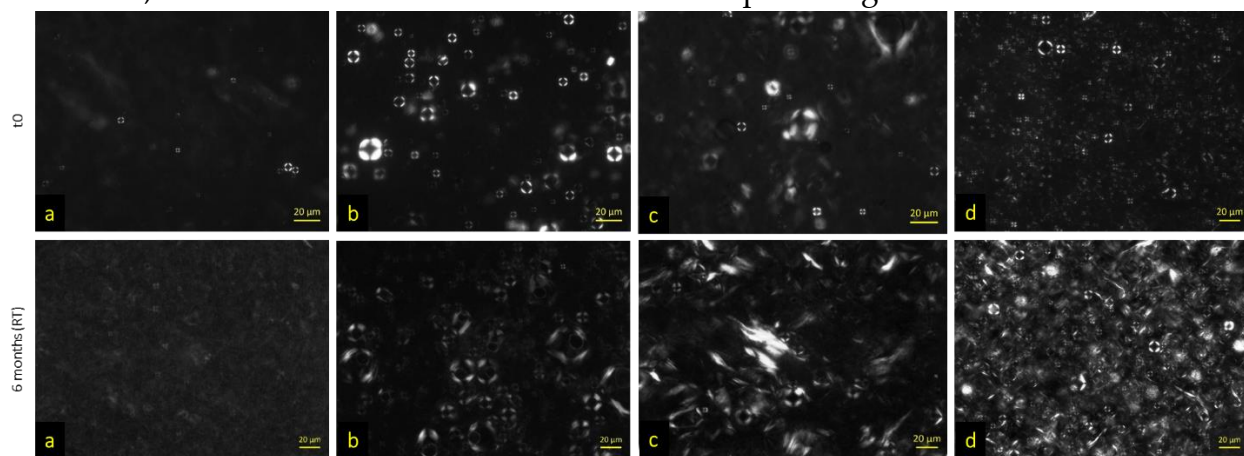


Figure 3.18. Photomicrographs of (a) S2, (b) S3, (c) S4 and (d) S12 one day after preparation t_0 (above row) and after 6 months storage at RT (below row) under PL microscopy (magnification x200).

S2, S3, S4 and S12 all showed typical Maltese crosses under PL microscopy at t_0 . Sizes and aspects were different from one sample to another one. After six months storage, it seemed that anisotropic patterns became more intense and present in the samples. No sign of inhomogeneity was observed. It is important to note that photomicrographs cannot be taken alone to draw conclusions about the robustness and stability of the nonionic samples. Therefore, rheological and microscopic measurements were associated in this chapter.

Saturated PEG-ether derivatives such as PEG-20, 50 and 100 cetyl/stearyl ether, are interesting compounds for achieving stable solid-like nonionic creams. The use of a unique nonionic emulsifier is, however, not sufficient for achieving rheological robustness. The next chapter will hence aim to evaluate nonionic systems containing PEG-ether derivative in combination.

3.2.2. Evaluation of the systems containing a combination of nonionic emulsifiers

This chapter is focusing on characterizing the system S5, S6, S7, S8, S9 and S10 containing a combination of two nonionic emulsifiers and described in [2.1.2. Optimization of the surfactant systems: screening of nonionic emulsifiers](#). Directly after preparation, S6 to S10 were stable. On the contrary, S5 showed a spontaneous phase separation. The rheological properties of the nonionic systems containing a combination of emulsifiers are summarized in [Table 3.6](#).

Table 3.6. Rheological properties of the nonionic systems containing a combination of two emulsifiers.

	S5	S6	S7	S8	S9	S10
η_{10} [Pa.s] ¹		13.90	17.91	10.66	12.13	4.16
$\Delta\eta$ [%] ²	Phase separation	+10	+11	+5	+7	-2
γ_c ³		0.164	0.186	0.103	0.129	0.0261
$\tan\delta < 1$ ⁴		Solid-like	Solid-like	Solid-like	Solid-like	Solid-like

¹ Viscosity at a fixed shear rate of 7.2 s^{-1} at 20°C , one day after the preparation t_0 .

² Maximum intervals in viscosity between t_0 and 6 months storage at RT. These intervals are expressed as a percentage with η_{10} equivalent to 100%.

³ γ_c , the critical strain, taken at $\tan\delta = 1$, $\omega = 1.6 \text{ Hz}$.

⁴ Control of the solid-like nature of the system. When $G' > G''$, meaning $\tan\delta < 1$, on the full range of frequencies ($\omega = 0.01$ to 250 rad/s), the system is solid-like, else, the system is liquid-like.

S5 showed a spontaneous phase separation. This may be due to the large differences in HLB values between PEG-2 cetyl/stearyl ether and PEG-100 cetyl/stearyl ether, 4.9 and 18.8, respectively.

The nonionic surfactants combinations led to the following observations:

- The viscosity increased when the overall OE units present in the system increased: $\eta_{S10} < \eta_{S8} < \eta_{S9} < \eta_{S6} < \eta_{S7}$
- The critical strain increased when the overall OE units present in the system increased: $\gamma_{c,S10} < \gamma_{c,S8} < \gamma_{c,S9} < \gamma_{c,S6} < \gamma_{c,S7}$. The critical strain increased substantially between S10 and S8. S8, S9, S6 and S7 showed minor differences in γ_c . In general, the systems containing a combination of nonionic surfactants (S6 to S10) rather than a single nonionic surfactant (S2, S3, S4 and S12) exhibited a higher critical strain.
- The systems containing a combination of nonionic surfactants (S6 to S10) rather than a single nonionic surfactant (S2, S3, S4 and S12) were subject to less viscosity fluctuations over time. These fluctuations were more pronounced when the overall OE units present in the system increased.

The first observation can be explained using the classical theory about colloidal systems. In fact, the polar moiety of the nonionic surfactants is dragging water in the interlamellar space: the ability of the bilayers to swell becomes greater when the number of OE units present in the bilayers increases. This means that, at equal surfactants molar ratio, the increase of the overall nonionic surfactant concentration increases the fixed interlamellar water quantity at the expense of the bulk-water [65]. Consequently, the viscosity increases. In parallel, the critical strain increased at t_0 in the same manner. In fact, more polar moiety may provide more nonelectrical steric forces, which enhance stability. Nevertheless, systems exhibiting a high γ_c at t_0 , were subject to more fluctuations in viscosity over time. This could be due to rather slow re-arrangement of the nonionic bilayers. To summarize: to one extent, the nonionic polar moiety brings stability by creating a nonelectrical steric barrier in the system. However, when too bulky, this stabilizing effect disappears over time. In general, combining different PEG-ether derivatives in the same mixture brought stability. The alternation of long and short polar moieties seemed to enhance the bilayers structure robustness. This alternation may allow the bilayers to pack closer and stiffer than when containing a single nonionic surfactant (S2, S3, S4). In fact, by combining two nonionic surfactants having short and long POE units, the strong stabilizing hydrophobic attractions are preserved between the FA and the apolar moieties of the short POE unit's surfactants. In parallel, the polarity of the interlamellar space, hence, the swelling ability of the lamellae, increases thanks to the polar moieties of the long POE unit's surfactants. This assumption will be further explained in [3.2.4. Conclusion](#) and illustrated in [Figure 3.21.](#)

The photomicrographs of S6 to S10 at t_0 and after six months storage at RT, under PL microscopy, are shown in [Figure 3.19.](#) At the exception of S8, the photomicrographs of the samples S6, S7, S9 and S10 revealed rather large anisotropic structures. It was not clear

if these structures were big Maltese crosses, crystalline phases or aggregates. After six months storage, S9 and S10 exhibited even larger anisotropic structures than at t0. This can be considered as an inhomogeneity factor. S8 showed typical Maltese crosses with diameters below 20 μm . These structures did not enlarge after six months storage at RT. The system S8 showed the best anisotropic patterns, under PL microscopy.

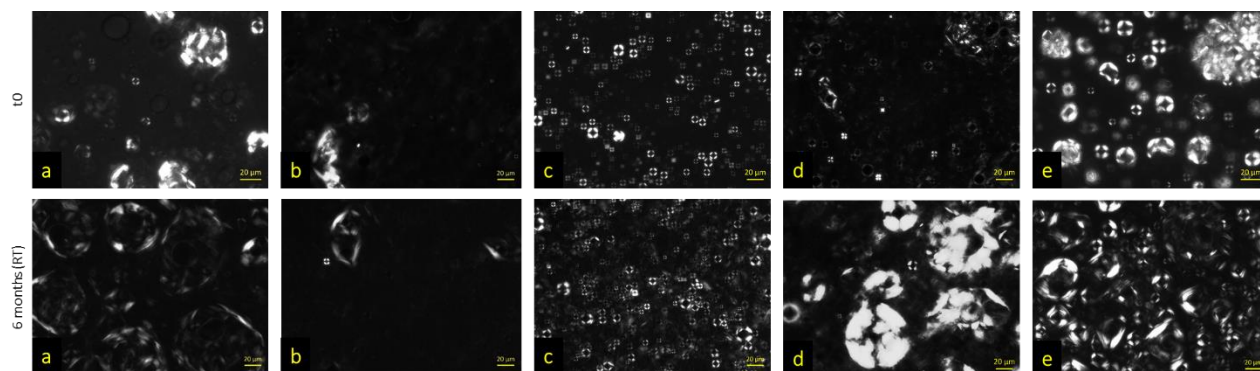


Figure 3.19. Photomicrographs of (a) S6, (b) S7, (c) S8, (d) S9 and (e) S10 one day after preparation t0 (above row) and after 6 months storage at RT (below row) under PL microscopy (magnification x200).

PEG-20 oleyl ether and PEG-23 lauryl were also tested in combination with PEG-20 cetyl/stearyl ether and PEG-50 cetyl/stearyl ether. The rheological properties of these systems are presented in [Table 3.7](#):

Table 3.7. Rheological properties of nonionic additional systems containing a combination of two emulsifiers (including PEG-20 oleyl ether or PEG-23 lauryl ether).

	Additional nonionic systems			
PEG-20 Cetyl/stearyl Ether	X		X	
PEG-50 Cetyl/stearyl Ether		X		X
PEG-20 Oleyl Ether	X	X		
PEG-23 Lauryl Ether			X	X
η^{10} [Pa.s] ¹	6.67	9.12	12.27	13.05
$\Delta\eta$ [%] ²	+55	+48	+21	+20
γ_c^3	0.026	0.037	0.059	0.063
$\tan\delta < 1^4$	Solid-like	Solid-like	Solid-like	Solid-like

¹ Viscosity at a fixed shear rate of 7.2 s^{-1} at 20°C , one day after the preparation t0.

² Maximum intervals in viscosity between t0 and 6 months storage at RT. These intervals are expressed as a percentage with η^{10} equivalent to 100%.

³ γ_c , the critical strain, taken at $\tan\delta = 1$, $\omega = 1.6 \text{ Hz}$.

⁴ Control of the solid-like nature of the system. When $G' > G''$, meaning $\tan\delta < 1$, on the full range of frequencies ($\omega = 0.01$ to 250 rad/s), the system is solid-like, else, the system is liquid-like.

The molar ratio between both nonionic surfactants was kept equal to 1. While combining PEG-20 oleyl ether with PEG-20 and PEG-50 cetyl/stearyl ether, the viscosity and critical strain decreased in comparison to S2 and S3. Moreover, larger viscosity fluctuations were observed over time. However, in comparison with S12, the viscosity and the critical strain were enhanced. Hence, PEG-20 and 50 cetyl/stearyl ether stabilized the bilayers composed

of PEG-20 oleyl ether only. Nevertheless, the performance of the systems containing PEG-20 oleyl ether remained unsatisfying compared to S6 to S10. The combination of PEG-23 lauryl ether together with either PEG-20 or PEG-50 cetyl/stearyl ether led to the same conclusions.

According to the specifications listed in the beginning of this chapter, the rheological and microscopical results showed that S8 seemed to be the most optimal candidate. This system contained, so far, the same mole number of PEG-50 cetyl/stearyl ether and PEG-2 cetyl/stearyl ether. In the following chapter, the influence of the molar ratio between both nonionic emulsifiers will be studied. While keeping the nonionic surfactants/FA molar ratio equal to 1:20 (see [2.12. Screening of nonionic emulsifiers](#), equation (13)).

3.2.3. Influence of the nonionic surfactants molar ratio in the system containing a combination of two emulsifiers

To finalize the emulsifiers screening, the influence of the molar ratio [PEG-2 cetyl/stearyl ether: PEG-50 cetyl/stearyl ether] was studied. The results are presented in [Table 3.8](#). The nonionic surfactants/FA molar ratio remained equal to 1:20. The compositions of these systems are described in detail in [2.1.2. Optimization of the surfactant system: screening of nonionic emulsifiers](#).

Table 3.8. Rheological properties of the nonionic systems containing PEG-2 and PEG-50 cetyl/stearyl ether in combination, at different molar ratio.

	Ratio [PEG-2 cetyl/stearyl ether : PEG-50 cetyl/stearyl ether]			
	0 (S3)	0.15 (S13)	0.40 (S14)	1.01 (S8)
η_{t0} [Pa.s] ¹	14.36	13.86	12.66	10.66
$\Delta\eta$ [%] ²	+14	+10	+6	+5
γ_c ³	0.087	0.089	0.091	0.103
$\tan\delta < 1$ ⁴	Solid-like	Solid-like	Solid-like	Solid-like

¹ Viscosity at a fixed shear rate of 7.2 s⁻¹ at 20°C, one day after the preparation t₀.

² Maximum intervals in viscosity between t₀ and 6 months storage at RT. These intervals are expressed as a percentage with η_{t0} equivalent to 100%.

³ γ_c , the critical strain, taken at $\tan\delta = 1$, $\omega = 1.6$ Hz.

⁴ Control of the solid-like nature of the system. When $G' > G''$, meaning $\tan\delta < 1$, on the full range of frequencies ($\omega = 0.01$ to 250 rad/s), the system is solid-like, else, the system is liquid-like.

All the systems were stable after six-month storage at RT and exhibited a solid-like rheological behavior. The increase of PEG-2 cetyl/stearyl ether in the systems led to a decrease in viscosity, less fluctuation in viscosity over time and an increase in the critical strain. These results are in line with the above-mentioned observations.

The photomicrographs of S3, S13, S14 and S8 at t₀ and after six months storage at RT, under PL microscopy, are shown in [Figure 3.20](#). All the systems showed typical Maltese

crosses under PL microscopy. No inhomogeneity sign in the anisotropic pattern was observed after six months storage at RT.

In conclusion, all systems: S13, S14 and S8 were potential candidates for developing robust hair coloring products. As above-listed in [3.2. Optimization of the surfactant system](#), the viscosity of the nonionic system must belong to the following interval: $10.0 < \eta < 30.0$ Pa.s. Accordingly, the system S14 was chosen for its lower viscosity fluctuation than S13 and its higher viscosity value than S8. This system will be further characterized in the following chapter [3.3. Characterization of the nonionic hair coloring product](#).

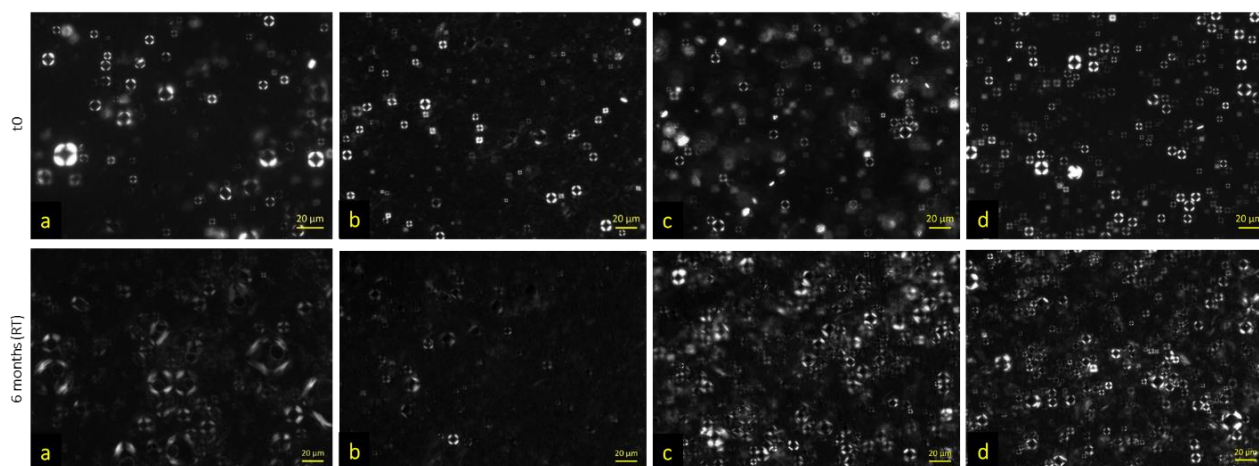


Figure 3.20. Photomicrographs of (a) S3, (b) S13, (c) S14 and (d) S8 one day after preparation t_0 (above row) and after 6 months storage at RT (below row) under PL microscopy (magnification x200).

3.2.4. Conclusion

To summarize, the stability of all solid-like systems and their abilities to form robust bilayers, was enhanced by using a combination of PEG ether derivatives rather than a single nonionic surfactant. This stabilization effect may be driven by two synergetic forces:

- The preserved nonelectrical steric barriers existing in the interlamellar space enabling swelling of the bilayers. This hydrophilic region is stabilized via hydrogen bonds existing between the oxygen of the POE units from the nonionic surfactants and water [119].
- The reduction of the steric hindrances while using a short and a long PEG surfactant rather than only a long polar moiety.

A similar well-known stabilizing effect was described by Fukushima et. al [57], [88]. They reported that mixing cetyl alcohol and stearyl alcohol in the appropriate ratio rather than using them alone enhanced significantly the stability [88]. The change of the apolar moiety in length and geometry did not improve the stability of the nonionic lamellar systems (S11 and S12). The best stability was achieved by using exclusively cetostearyl carbon chains.

To conclude, [Figure 3.21](#). presents a model of the bilayers arrangement for different nonionic emulsifiers content and nature. For easier comprehension, the system was simplified: therefore, only cetearyl alcohol and the PEG ether derivatives were represented. Thanks to this schematic representation, is it easier to visualize and understand the differences between all nonionic systems. As mentioned earlier, the main forces driving the stable and lasting nonionic bilayers' formation, are: the hydrophobic attractive Van der Waals forces and the nonelectrical steric repulsive barrier. These forces work in synergy and are dependent on the length of the POE moiety and the ability of the hydrophobic chains to pack close together. [Figure 3.21](#). (A), illustrates a system which is driven by strong Van der Waals attractions (small dc_1 , with dc : distance between a nonionic emulsifier and a successive FA in the hydrophobic part of a bilayer) but which does not have the ability to drag water in the interlamellar hydrophilic part of the bilayer (small di_1 , with di : interlamellar distance of the hydrophilic part of a surfactant bilayer). Therefore, bilayers cannot swell and both parts are not in equilibrium. Accordingly, S1 showed phase separation. On the contrary, [Figure 3.21](#). (B), represents a system which is driven by middle range Van der Waals attractions (medium dc_2) and strong repulsive nonelectrical steric forces (large di_2). The large polar moieties enable to drag water in the interlamellar space. Hence, systems such as S3 or S4, are stable but likely to be composed of rather mobile bilayers. [Figure 3.21](#). (C), shows a system where the bulky curved unsaturated apolar moieties prevent the cetyl/stearyl carbon chain to arrange in a close-packed manner (large dc_3). This system (S12) is stable but subject to substantial fluctuations (mobility of the bilayers) and low viscosity. Finally, [Figure 3.21](#). (D), represents a system where both the hydrophobic and hydrophilic parts of the bilayers are very stable. In fact, the large interlamellar distance (di_2) allows water to be dragged in and stabilize the polar moieties whereas the medium to small distances between the carbon chains (dc_1 and dc_2) are ensuring strong attractive Van der Waals forces. This stabilizing effect occurred for the system containing a combination of long and short POE chains such as S8, or medium and long POE chains such as S6, S7, S9 and S10.

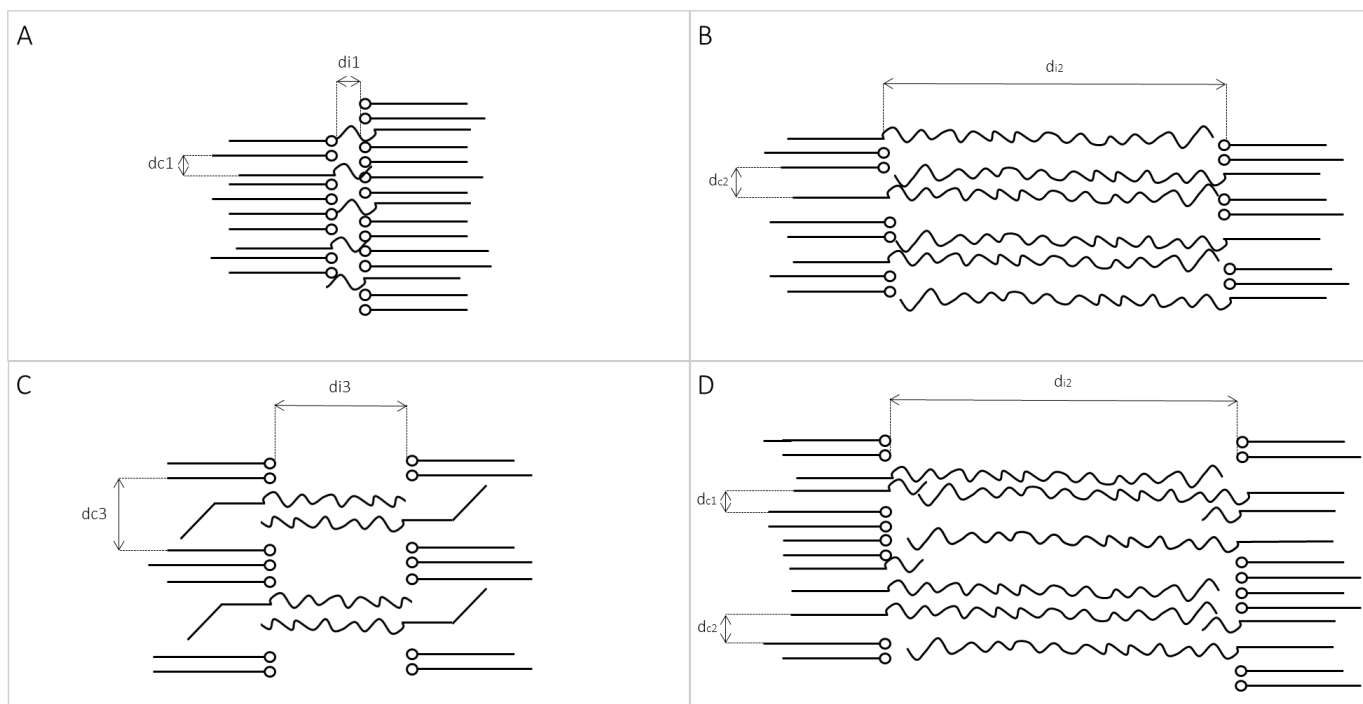


Figure 3.21. Schematic representation of the bilayers containing (A) a short POE chain single nonionic emulsifier like S1, (B) a long POE chain single nonionic emulsifier like S3 or S4, (C) a medium POE chain single emulsifier having an unsaturated carbon chain like S12 and (D) a short POE chain nonionic emulsifier combined with a long to medium POE chain nonionic emulsifier like S6, S7, S8, S9 and S10. \bullet are the FA polar heads, — the C16-18 saturated FA hydrophobic tail, — the C16-18 unsaturated (curved) FA hydrophobic tails, ~ the POE hydrophilic chain of the PEG surfactants. d_{i1} , d_{i2} and d_{i3} are the interlamellar distances of the hydrophilic part of the bilayers (where the water is fixed) in system like S1, S3 or S4 or S6 or S7 or S8 or S9 or S10 and S12, respectively. d_{c1} , d_{c2} and d_{c3} are the distances between a nonionic emulsifier and successive FA in the hydrophobic part of the bilayer in system like S1, S3 or S4 or S6 or S7 or S8 or S9 or S10 and S12, respectively. Distances are drawn so that $d_{i1} < d_{i3} < d_{i2}$ and $d_{c1} < d_{c2} < d_{c3}$.

3.3. Characterization of the nonionic hair coloring product

To achieve more relevant results in view of formulating hair coloration products, the following systems will be formulated with only 1.0 w% ammonium sulfate (G3) and subsequently with 0 to 7.0 w% PTD (H1 to H6).

3.3.1. Microscopy

3.3.1.1. PL Microscopy

The nonionic creams G0, G3 and H1 to H6 were observed under PL microscopy ([Figure 3.22](#).) 24 hours after preparation. The compositions of these systems are described in detail in [2.1.3. Nonionic hair coloring product](#).

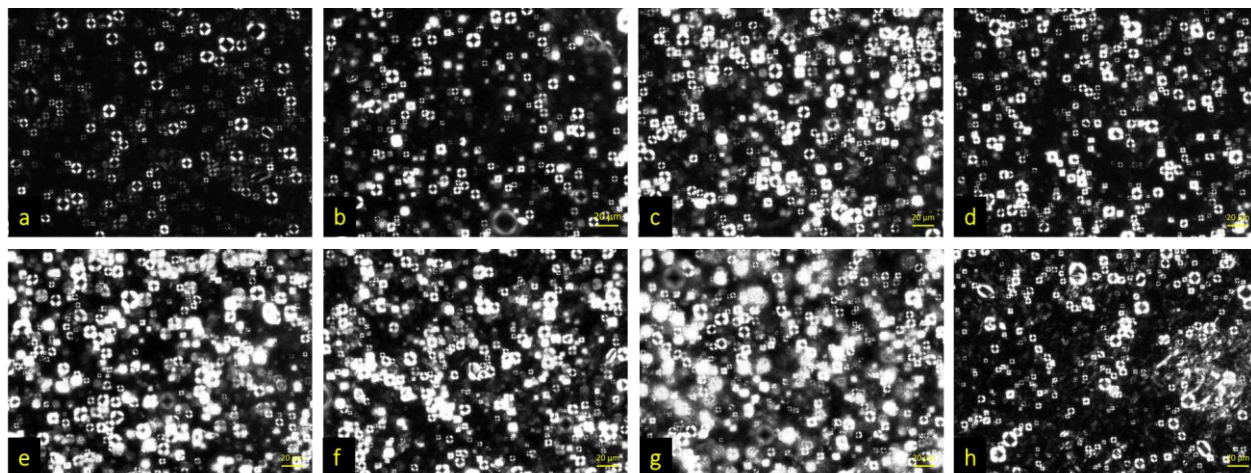


Figure 3.22. Photomicrographs of the creams (a) G0, (b) G3, (c) H1, (d) H2, (e) H3, (f) H4, (g) H5 and (h) H6, 24 hours after production, using PL microscopy (magnification x200).

All the creams exhibited numerous Maltese crosses all over the sample. These anisotropic structures are typical for flexible bilayers L_{α} and/or onion phases $[L_{\alpha}]$. Hence, the nonionic creams are likely to form self-assembled lamellar structures. The Maltese crosses exhibited a diameter between 1 and 20 μm . The photomicrographs presented in [Figure 3.22](#) cannot be used to draw quantitative conclusions about the size of the microstructures. In fact, the amount of extinction crosses in one microscopic picture is dependent on two factors: the thickness of the cream laying between the glass slide and the transparent coverslip, and the position of the objective on the slide. Therefore, one microscopic picture containing more extinction crosses than another one does not reveal that this sample contains more self-assembled structures. However, it was possible to determine the size distribution of the particles in each sample i.e. vesicles. thanks to PC-light microscopy. This is described in the next chapter [3.3.1.3. Particle size measurement](#).

The nonionic creams G0, G1 and H1 to H6 were observed after 6 months storage at RT under PL microscopy. The results are presented in [Figure 3.23](#):

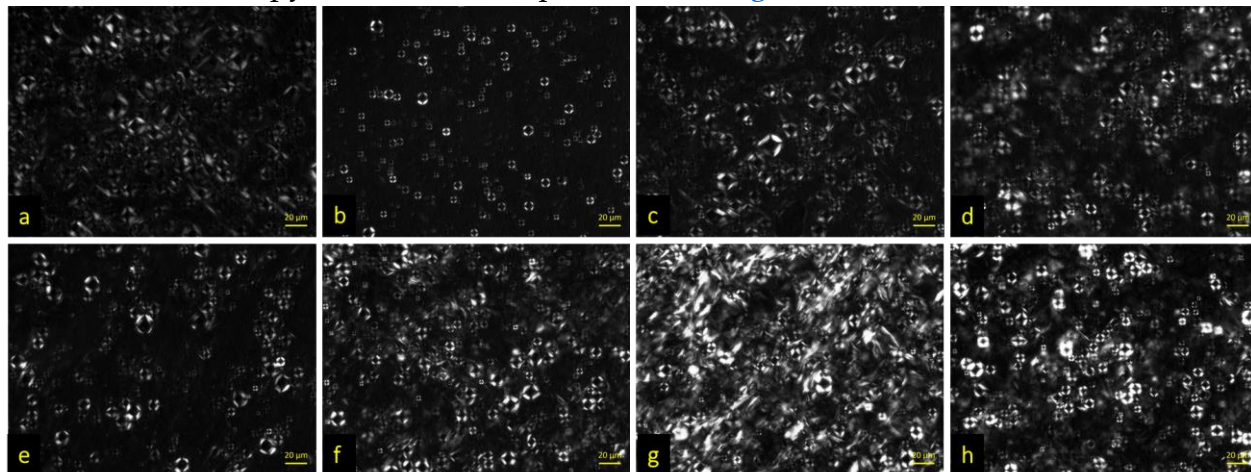


Figure 3.23. Photomicrographs of the creams (a) G0, (b) G3, (c) H1, (d) H2, (e) H3, (f) H4, (g) H5 and (h) H6, 6 months after production using PL microscopy (magnification x200).

After 6 months storage at RT the nonionic creams photomicrographs were slightly different compared to 24 hours after preparation. In fact, the photomicrographs showed less birefringence i.e. less intense visible anisotropic structures. This could be explained by a partial $[L_{\alpha}] \rightarrow L_{\alpha}$ transition occurring spontaneously in all samples. Similar transitions were observed and described by Linden [102] and Yuan [86]. It is, so far, not possible to make a clear statement whether the lamellar gel phase is composed essentially of vesicles $[L_{\alpha}]$, or flexible bilayers L_{α} , or both. The following chapters will aim to clarify this uncertainty. The extinction crosses did not show dramatic changes in shape and size after 6 months storage at RT: the diameter of the anisotropic pattern did not exceed 20 μm .

3.3.1.2. Cryo-TEM

The nonionic creams were observed under cryo-TEM at different magnifications. The photomicrographs of the cream H3 are presented in [Figure 3.24](#). Cryo-TEM was performed successfully without using any pre-treatment such as dilution of the samples or staining. As the samples remained highly concentrated, the photomicrographs are dark and dense and exhibited multiple self-assembled structures in the same region (see [Fig. 3.24](#). (f)). The photomicrographs of the nonionic cream H3 revealed two kinds of colloidal structures: flexible bilayers having circular geometry also called onion phase $[L_{\alpha}]$ (see [Fig. 3.24](#). (a), (b) and (c)) and linear bilayers forming lamellae L_{α} (see [Fig. 3.24](#). (d) and (e)). The radius of the vesicles was ranging between 0.1 and 1.5 μm . Most of these structures were not visible under PL-microscopy. Bilayers or linear lamellar patterns were also found.

Their widths varied from 1 to 10 nm, which correspond to a typical surfactant bilayer membrane thickness [120]. The L_{α} phase was not observed by means of classical light microscopy. Similar self-arranged structures formed by various surfactants systems are largely described and observed with cryo-TEM in the literature [85], [86], [121]– [123]. The transition between $L_{\alpha} \leftrightarrow [L_{\alpha}]$ will be discussed later in [3.3.7. Conclusion](#). However, it seems that both L_{α} and $[L_{\alpha}]$ coexisted in the nonionic samples. Further characterization of the vesicles e.g. radius and distribution will be discussed in the following chapter [3.3.1.3. Particle size measurement](#).

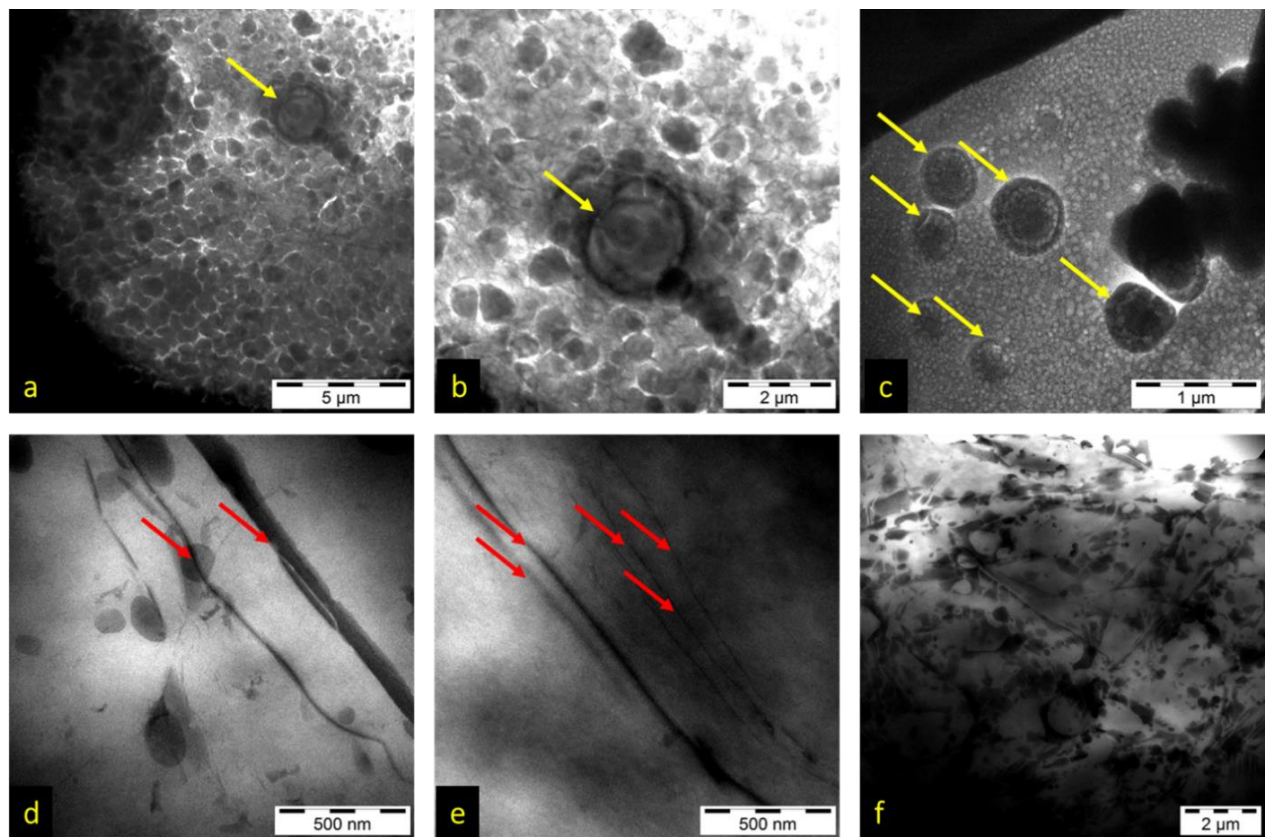


Figure 3.24. Cryo-TEM photomicrographs of the nonionic cream H3 at different magnification. The yellow arrows point the vesicles/flexible bilayers (uni- or multi-lamellar): $[L_{\alpha}]$ phase in (a), (b) and (c). The red arrows point the linear bilayers forming lamellae: L_{α} phase in (d) and (e). The magnifications of the TEM microscope are as follow: (a) $\times 2100$, (b) $\times 4200$, (c) $\times 10000$, (d) 20000 , (e) $\times 20000$, and (f) $\times 2900$.

3.3.1.3. Particle size measurement by means of PC-light microscopy

The particle size measurement of the nonionic creams G0 and H1 to H6 was performed with PC-light-microscopic pictures with a 200 times total magnification and without PL. Due to the opacity of the samples, other classical particle size measurement methods, such as DLS, did not deliver satisfying results. For each cream, 20 to 40 photomicrographs were

taken 24 hours after preparation. To evaluate the particle size distribution evolution of the creams over time, this process was repeated after 3 months. Samples were stored at RT. As an example, one highly contrasted photomicrograph of each nonionic cream (G0 and H1 to H6) is shown in [Figure 3.25](#). Moreover, a photomicrograph of the previous ionic cream (F1) is shown in [Figure 3.25](#). (h). This cream did not exhibit large enough particles to set up an automatic particle recognition program. For this reason, the particle size measurement study was only performed for the nonionic optimized hair coloring products.

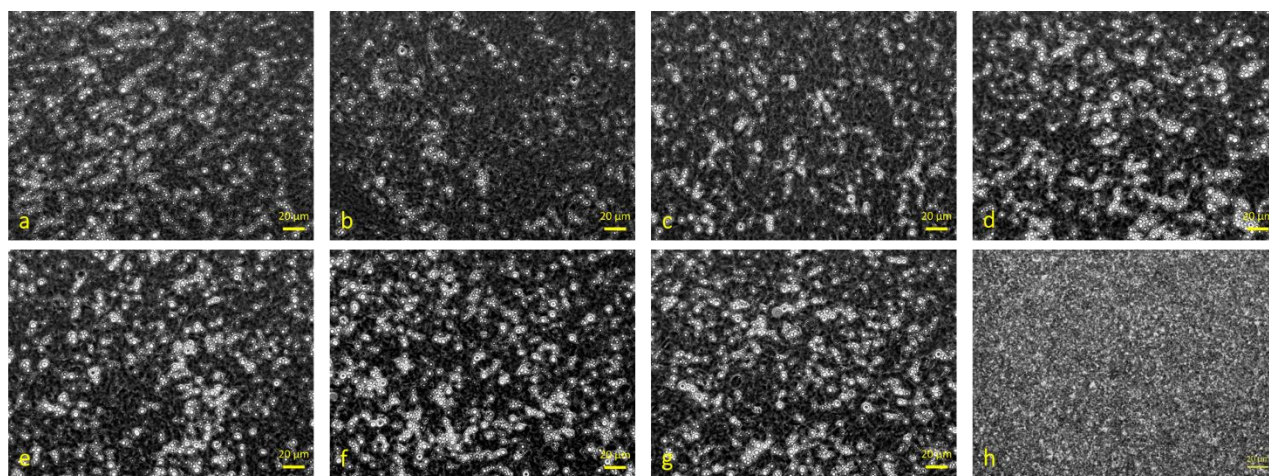


Figure 3.25. Photomicrographs of the creams (a) G0, (b) H1, (c) H2, (d) H2 (e) H4, (f) H5, (g) H6 and (h) F1, 24 hours after preparation under PC light microscopy (magnification x200).

For each nonionic cream, the highly contrasted photomicrographs exhibited multiple droplets/particles all over the slide. By contrasting this picture even more, it was possible to automatically isolate the particles from the backgrounds. The image analysis software was then able to recognize them as “objects”. This detailed procedure is illustrated in [Figure 3.26](#).



Figure 3.26. Description of the automatic particle recognition process for particle size distribution calculation in the nonionic creams using the software ZEN (image analysis module Blue) from Zeiss. Left and middle photomicrographs: PC pictures of the cream H3 before and after isolation of the “objects” (i.e. isolation of the particles from the background). Right: Automatic particle recognition. The yellow dots show

the particle with a radius such as $R \geq 2.0 \mu\text{m}$, the green dots show the particles with a radius such as $1 \mu\text{m} \leq R < 2 \mu\text{m}$. The red dots show the particles with a radius such as $R < 1 \mu\text{m}$.

Thanks to this process, it was possible to isolate several thousand of particles in each sample. The particle size distribution calculation of the nonionic creams was based on these particles. The results of the fresh and aged nonionic samples are presented in [Table 3.9](#) and [Table 3.10](#), respectively. The plot of the particle size distributions of all samples at t0 and 3 months storage at RT are shown in [Appendix 7.4](#).

Table 3.9. Particle size distribution in the creams G0 and H1 to H6, 24 hours after production.

	G0	H1	H2	H3	H4	H5	H6
Av. R [μm]	0.72	0.73	0.78	0.81	0.81	0.83	0.79
Min. R [μm]	0.22	0.22	0.22	0.22	0.22	0.22	0.22
Max. R [μm]	10.32	8.20	11.27	8.67	8.35	12.87	8.96
Median	0.63	0.62	0.64	0.68	0.66	0.67	0.62
Std. dev.	0.48	0.54	0.62	0.63	0.60	0.69	0.67
Number of counted particles	13873	10392	10689	12434	12457	13452	12973

Table 3.10. Particle size distribution in the creams G0 and H1 to H6, 3 months after preparation (storage at RT).

	G0	H1	H2	H3	H4	H5	H6
Av. R [μm]	0.70	0.74	0.77	0.71	0.80	0.74	0.76
Min. R [μm]	0.21	0.22	0.22	0.22	0.20	0.22	0.21
Max. R [μm]	10.25	5.71	11.52	6.50	8.17	12.81	8.83
Median	0.71	0.69	0.63	0.63	0.65	0.69	0.61
Std. dev.	0.46	0.33	0.61	0.43	0.64	0.32	0.58
Number of counted particles	12661	8582	7229	7428	8824	7854	8484

The average radius of the particles in all nonionic samples did not show significant fluctuations under salt concentration increase or over time. The average radius of the particles from the fresh and aged nonionic samples ranged from 0.72 to 0.83 μm and from 0.70 to 0.80, respectively. The standard deviation remained substantially high for all creams compared to the calculated average radius: from 0.48 to 0.69 in the fresh samples and from 0.33 to 0.64 in the 3 months old samples. This can be due to:

- The broad distribution in particle size in every nonionic samples
- The limit of detection of the microscope. Indeed, with a total $\times 200$ magnification, only particles larger than 0.22 μm (in radius) can be detected

The number of counted particles was considered consistent for achieving a relevant evaluation of the particle size distribution. However, due to the limit of detection from the objective and the microscope, particles below $0.22\ \mu\text{m}$ in radius are not visible (see Min. R. in [Table 3.9.](#) and [Table 3.10.](#)). This limit might have a bias on the results in favor of bigger particles. Moreover, because of this limitation, the particle size distribution was not normally distributed (see [Appendix 7.4.](#)). This is a limiting factor for doing further elementary statistics. Moreover, for the same number of photomicrographs, fewer particles were counted in the aged samples than in the fresh ones under PC-microscopy. Indeed, the average number of particles counted in the fresh and the old samples were 12324 and 8723 particles, respectively. This is in line with the observation made in [Figure 3.23.](#), where less anisotropic structures were observed after 6 months storage at RT. These results are summarized in [Figure 3.27.](#). The latter shows that the average radius of the nonionic creams fluctuates around $1\ \mu\text{m}$. This is the case for both fresh and aged samples. Increasing the organic salt content did not show significant differences in the average of the particles' radius. As the distribution of these samples was large, it is also important to compare the minimum and maximum radius of the particles under addition of electrolytes and over time. These results are presented in [Figure 3.28.](#)

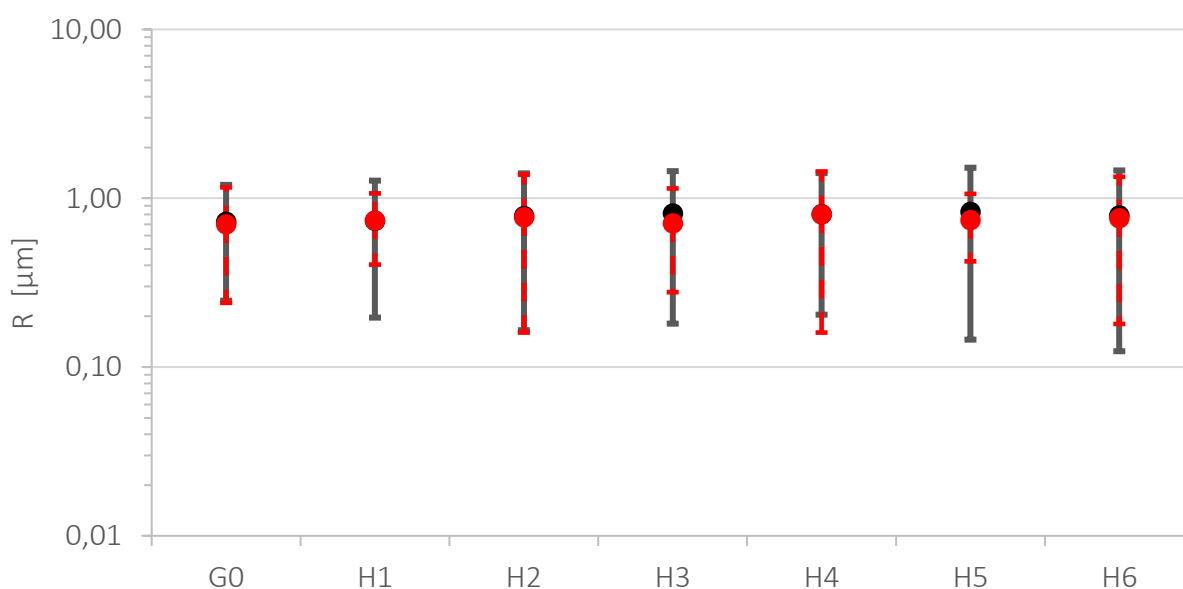


Figure 3.27. Average value of the radius of the particles R , for the cream G0 and H1 to H6, (●) one day and (●) 3 months after preparation. The whiskers above and below the average value define the $\text{av.} \pm \text{std. dev.}$

The minimum radius of the particles is limited by the magnification capabilities. In fact, it was assumed that particles having a radius lower than $0.22\ \mu\text{m}$ were not detected. The maximum radius of the particles ranged for all samples between 5.7 and $13.0\ \mu\text{m}$. This

confirmed the assumption that the particle size distributions of all the samples, fresh or aged, were broad.

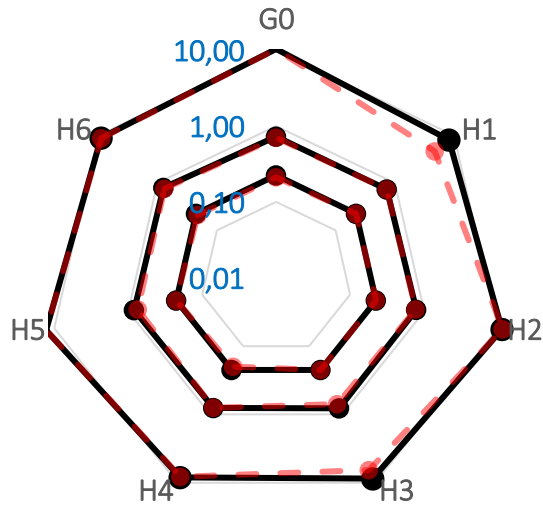


Figure 3.28. Average, min. and max. radius of the particles for the cream G0 and H1 to H6, (●) one day and (●) 3 months after preparation. The inner circles represent the min. radius, the outer circles represent the max. radius and the circles in between represent the average of the particles' radius in μm .

To conclude, the automated particle size measurement, established with the highly contrasted photomicrographs, helped to define the particle size distribution in all nonionic samples. These samples seemed to have a broad particle size distribution centered around $1 \mu\text{m}$. These results are in line with the estimation done earlier with cryo-TEM and PL microscopy which demonstrated that the nonionic samples were structured with a mixture of self-assembled bilayers (linear lamellar structures) and vesicles, having an estimated maximal diameter of $10 \mu\text{m}$. No size distribution shift was observed after three months storage at RT or under addition of organic salts. This aspect is important for assessing the robustness of the viscosity and the stability of the creams. Indeed, vesicles' sizes and distributions are playing a major role in the rheological behavior of self-arranged lamellar gel phases [73].

3.3.2. Rheology

Twenty-four hours after preparation and at a fixed shear rate of 7.2 s^{-1} , the viscosities of the creams G0 and H1 to H6 scattered between 15 and 21 Pa.s. They exhibited a typical shear thinning and solid-like behavior (see [Fig. 3.29.](#)) [115].

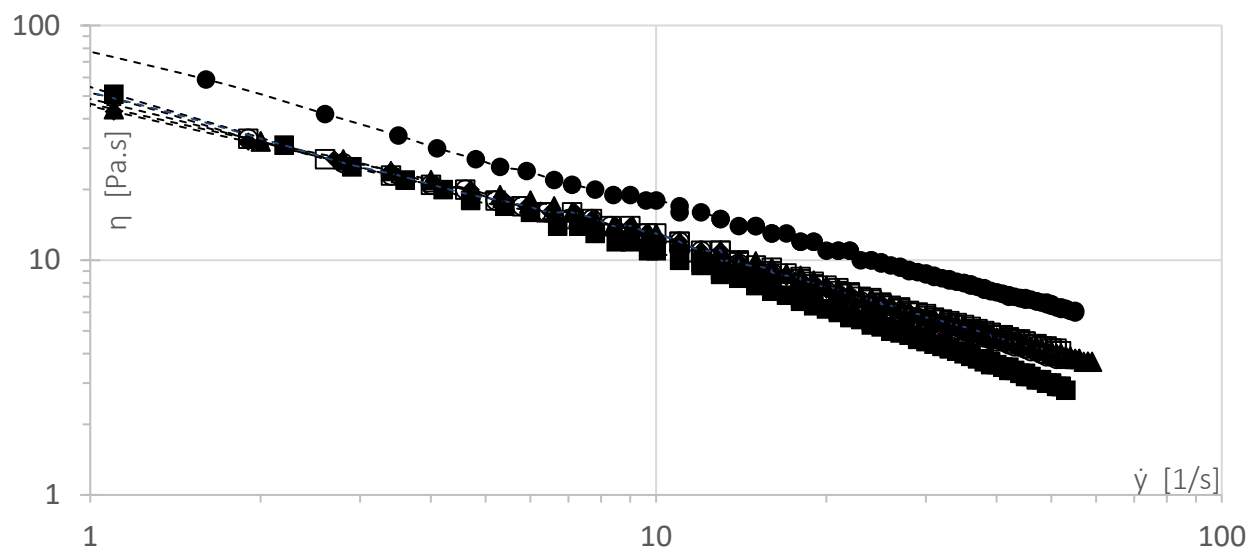


Figure 3.29. Rotational sweep measurement of the creams • G0, ■ H1, ▲ H2, ◆ H3, ○ H4, □ H5, △ H6, 24 hours after production at 20°C.

The difference in viscosities under addition of salts have been reduced from $\Delta\eta_{\text{ionic}} = 16.29$ Pa.s (for E0 to E7) to $\Delta\eta_{\text{nonionic}} = 6.24$ Pa.s (for G0 and H1 to H6). Static rheological measurements already revealed improvement in the robustness of the nonionic creams toward salt addition. Knowing that marketable products would contain at least 0.1 w% of salts due to the presence of sequestrants or other salt-like admixtures, the factor $\Delta\eta$ can be recalculated without taking E0 and G0 in account. The improvement is even more obvious as $\Delta\eta_{\text{ionic}} = 12.80$ Pa.s and $\Delta\eta_{\text{nonionic}} = 1.06$ Pa.s.

The same rotational sweep tests were performed over time from the first day after preparation until the sixth month. The viscosity measurements of the creams G0 and H1 to H6 during aging are summarized in [Figure 3.30](#). G0, the salt-free formulation, exhibited a significant higher viscosity than the rest of the samples. Under addition of PTD, the creams H1 to H6 did not show significant differences in viscosity. However, over time a significant decrease of viscosity was observed after 6 months storage at RT for all the creams. The loss in viscosity after 6 months storage at RT could be due to the $[L_{\alpha}] \rightarrow L_{\alpha}$ transition. This phenomenon was already mentioned and noticed in the aged photomicrographs under PL. This transition is likely to occur slowly in nonionic systems (see [1.4.3. Aging properties](#)). It is therefore not surprising that this viscosity drop was observed only after 6 months. However, the viscosities of all creams remained acceptable regarding the listed conditions in [3.2. Optimization of the surfactant system](#). In fact, the viscosities of the nonionic systems containing at least 0.1 w% of PTD, scattered between 14 and 18 Pa.s.

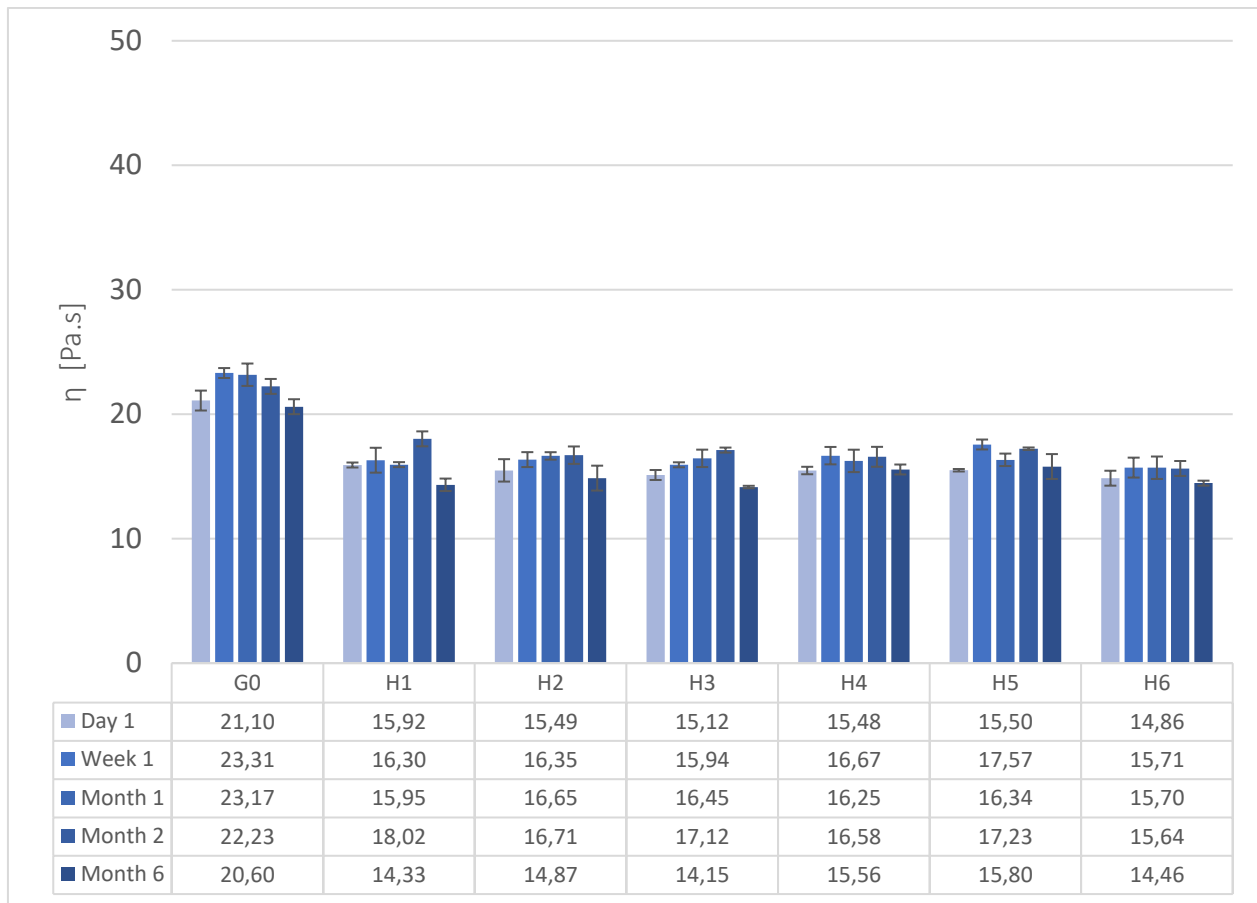


Figure 3.30. Viscosity of the creams G0 and H1 to H6 from day 1 to month 6 storage at RT. The viscosity η is measured at $\dot{\gamma} = 7,2 \text{ s}^{-1}$ at 20°C . The whiskers above and below the average values define the $\text{av.} \pm \text{std. dev.}$

Note: all the viscosity values are in Pa.s.

Subsequently, a strain test was performed for the creams G0 and H1 to H6. The cross-over point between G' and G'' indicated the critical strain γ_c . This value is plotted for all the nonionic creams in [Figure 3.31](#), one day after preparation and after 6 months storage at RT. As mentioned earlier, one can compare the critical strains of creams having only one single ingredient which differ in the formulation. Therefore, the absolute γ_c values of the ionic and the nonionic systems cannot be compared. G0 and H1 exhibited a slightly higher γ_c than all the other creams. This revealed that addition of organic salts altered the stability of the system. However, further increase in salt concentration did not influence the stability of the system even more. In fact, there were no significant differences observed between γ_c from H2 and H6. Moreover, the critical strain remained steady after 6 months storage at RT. The systems are therefore robust against aging. The assumed $[L_\alpha] \rightarrow L_\alpha$ transition occurring after 6 months storage at RT was not observable thanks to this rheological test.



Figure 3.31. Critical strain γ_c of the creams G0 and H1 to H6 one day after the preparation (X) and after 6 months storage (-) at RT. γ_c is expressed as a percent of the strain range during the strain test (γ from 0 to 5) and taken at $\tan\delta = 1$.

The storage and loss modulus of the creams G0 and H1 to H6 were plotted against the frequency in [Figure 3.32.](#) and [Figure 3.33.](#), respectively. They showed that the elastic properties of all the creams remained higher than the viscous properties on the entire range of frequencies. Moreover, G' and G'' slightly and linearly increased with the frequency without crossing each-other. This rheological behavior is typical for a lamellar gel phase [70]. These findings showed that all samples are metastable and may be composed of self-assembled semisolid bilayers [69], [116]. G' and G'' plots of creams H1 to H5 overlapped over the full range of frequencies. H6 exhibited slightly higher G' and G'' . All in all, the nonionic creams showed a more homogeneous rheological behavior, for both moduli, compared to the ionic creams.

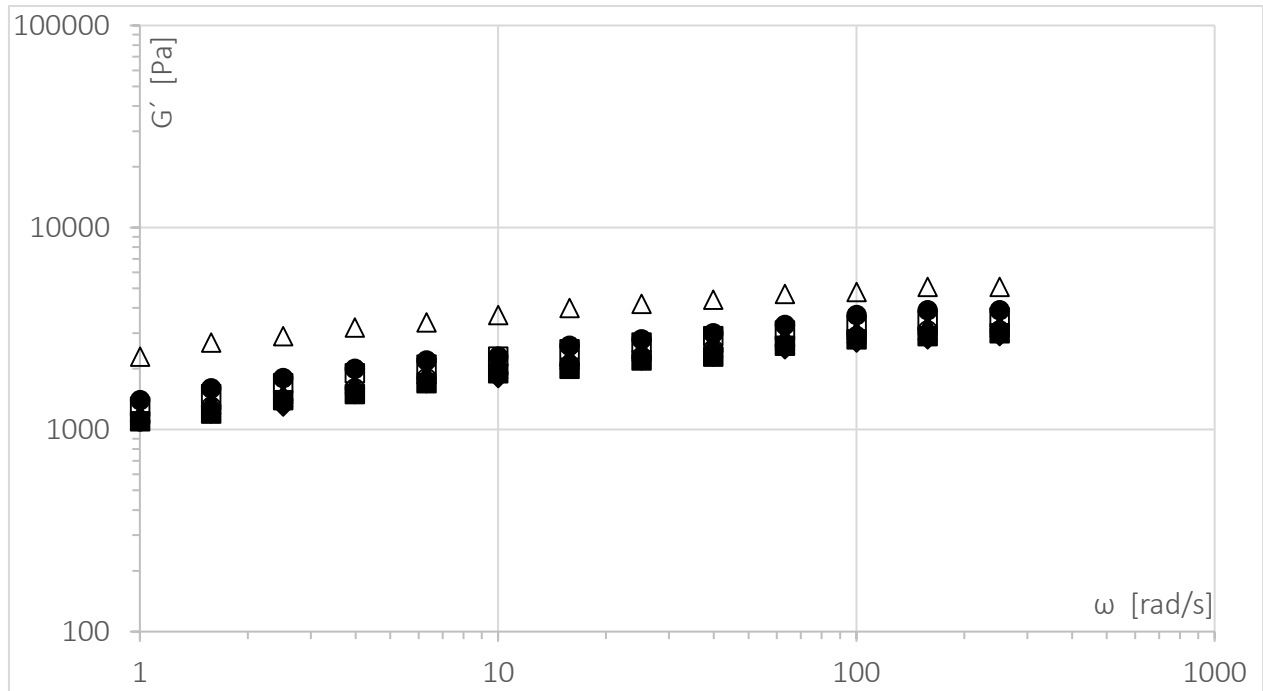


Figure 3.32. Storage modulus G' during the frequency sweep test of the creams \bullet G0, \blacksquare H1, \blacktriangle H2, \blacklozenge H3, \circ H4, \square H5 and \triangle H6, 24 hours after preparation in the LVR at 20°C. The frequency ω increases logarithmically from 0.1 to 300 rad/s and the strain $\gamma = 0.001$ corresponds to a displacement angle of 1.77E-05 rad, such as $\gamma \ll \gamma_c$.

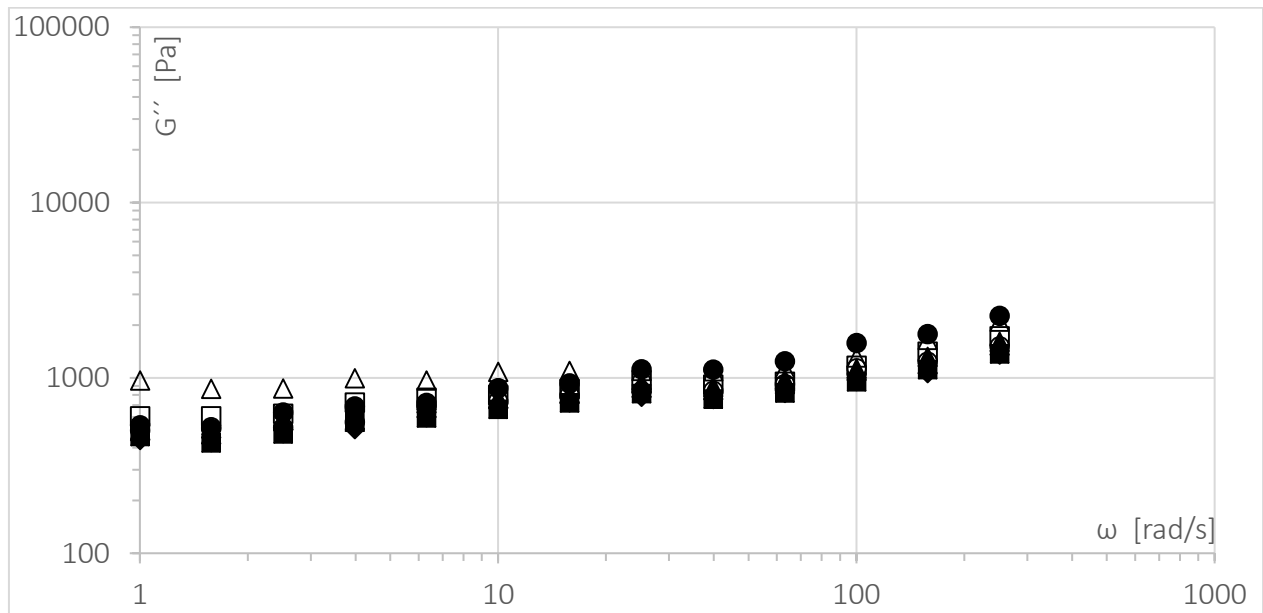


Figure 3.33. Loss modulus G'' during the frequency sweep test of the creams \bullet G0, \blacksquare H1, \blacktriangle H2, \blacklozenge H3, \circ H4, \square H5 and \triangle H6, 24 hours after preparation in the LVR at 20°C. The frequency ω increases logarithmically from 0.1 to 300 rad/s and the strain $\gamma = 0.001$ corresponds to a displacement angle of 1.77E-05 rad, such as $\gamma \ll \gamma_c$.

To assess if the $[L_\alpha] \rightarrow L_\alpha$ transition was spontaneously occurring after 6 months storage at RT, the frequency sweep test was repeated for all the nonionic aged creams. A representative example of the rheological behavior H3 is shown in [Figure 3.34](#), where G' , G'' and $|\eta^*|$ are plotted against ω at t_0 and 6 months. As demonstrated by Yuan et al. [86], a system composed of vesicles $[L_\alpha]$ only, would show a constant G' and G'' (with $G' > G''$) and a decreasing complex viscosity $|\eta^*|$ on the full range of frequencies. On the contrary, a system composed of planar lamellar L_α only, would show a slightly increasing G' and G'' (with $G' > G''$) and a decreasing complex viscosity $|\eta^*|$ on the full range of frequency. The nonionic creams showed, at t_0 and after 6 months, a L_α -phase rheological behavior with no obvious change of slope in the G' , G'' and $|\eta^*|$ plots. However, vesicles were clearly identified in the samples by means of microscopy. Therefore, one could assume that the nonionic systems are composed of mixed $[L_\alpha]$ and L_α phases transitioning partially in favor of L_α phases after six months storage at RT. This is consistent with the decrease of G' , G'' and $|\eta^*|$ after six months storage at RT on the full range of frequencies.

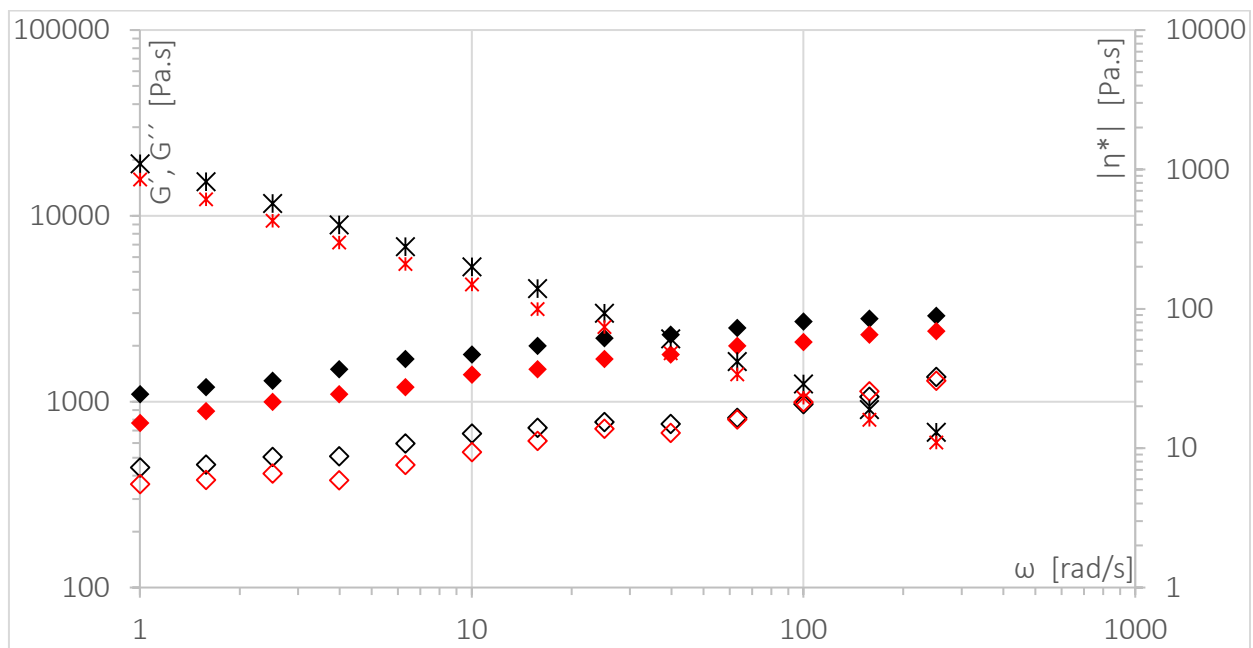


Figure 3.34. Storage modulus G' (\blacklozenge), loss modulus G'' (\diamond) and complex viscosity $|\eta^*|$ (*) of the cream H3 during the frequency sweep test, 24 hours after preparation ($\blacklozenge, \diamond, *$, respectively) and after 6 months storage at RT ($\redlozenge, \redlozenge, *$, respectively). The frequency sweep test is performed at 20°C in the LVR, with the strain $\gamma = 0.001$ corresponds to a displacement angle of $1.77\text{E-}05$ rad, such as $\gamma \ll \gamma_c$. The frequency ω increases logarithmically from 0.1 to 300 rad/s.

The loss factor: $\tan\delta$, was plotted in the high frequency range ($\omega = 250$ rad/s) in [Figure 3.35](#). When the storage and loss modulus are getting closer, $\tan\delta$ is approaching the unitless value 1 [69]. A noticeable decrease of $\tan\delta$ was observed under addition of salts: the salt-free sample G0 showed a larger $\tan\delta$ compared to H1 to H6. The samples

containing PTD exhibited $\tan\delta$ values scattering around 0.5. The aged samples showed a slight increase in $\tan\delta$ which was not always significantly different from t_0 . It is not clear whether this could be related to the partial $[L_\alpha] \rightarrow L_\alpha$ transition. All values, from the fresh and aged samples, remained largely under 1. Hence, all creams are metastable semi-solid systems independently of the electrolyte content and aging.

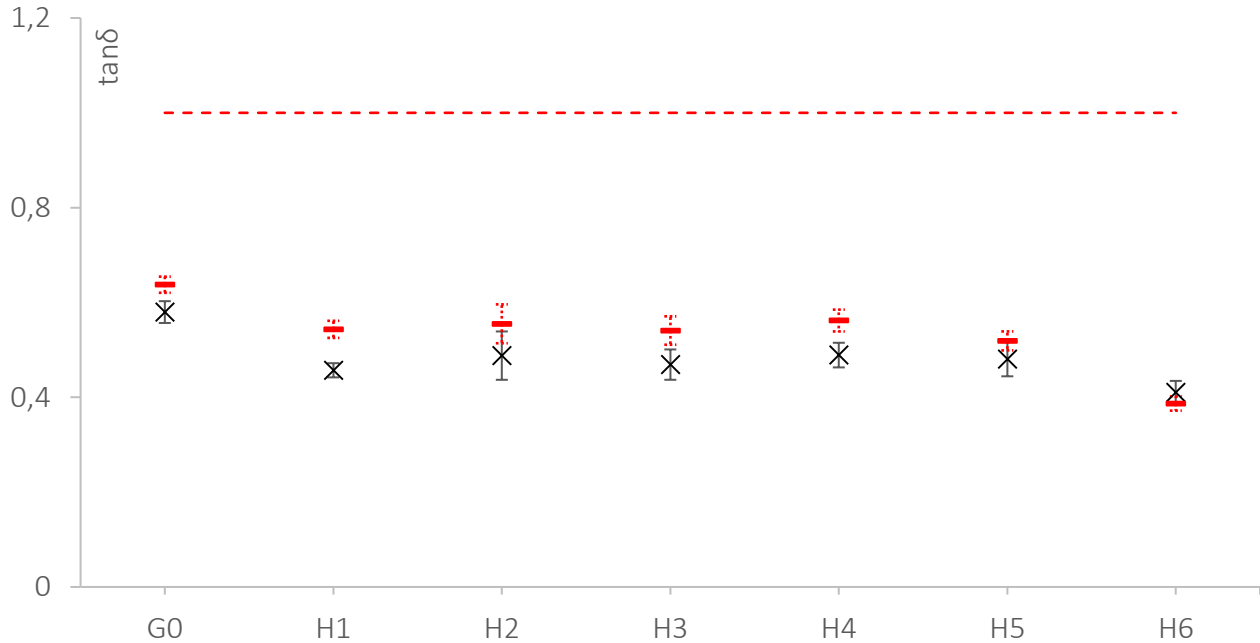


Figure 3.35. Loss factor ($\tan\delta$) at high frequency ($\omega = 250$ rad/s) for the creams G0 and H1 to H6 one day (X) and six months (—) after preparation. The whiskers above and below the average values define the $av. \pm$ std. dev.

All rheological data considered, the nonionic creams H1 to H6 showed a typical solid-like behavior likely to be composed of planar lamellar phases and vesicles. The rheological properties of the nonionic samples are robust towards organic salt addition and aging. However, it seems that the aged samples are subject to a partial spontaneous transition from $[L_\alpha]$ to L_α . Moreover, significant differences between the salt-free sample G0 and the other nonionic samples H1 to H6 were measured: higher viscosity and higher critical strain. This could be due to:

- The higher ratio of $[L_\alpha]$ (higher viscosity) than L_α phase. In fact, lamellar gel phases can be subject to spontaneous salt-induced transition from onion phase to lamellar phases [102].
- The existence of minor interactions between the nonionic surfactants and the PTD which would lower the stability (lower critical strain) of H1 to H6 compared to G0.

3.3.3. DSC

3.3.3.1. Thermal behavior of the raw materials contained in the nonionic creams

DSC was primarily used to determine the thermal behavior of the raw materials contained in the nonionic systems. Thermal cycling was performed. The results were taken during the third heating run and the second cooling run. The thermograms of glyceryl monostearate and PEG-50 cetyl/stearyl ether showed a single endothermic peak at 61 and 52°C, respectively. Both endotherms are broad. These two compounds have a single melting point. The melting enthalpy of glyceryl monostearate and PEG-50 cetyl/stearyl ether were equal to 100 J/g and 140 J/g, respectively, when averaging the three DSC attempts. Glyceryl monostearate showed two overlapping exotherms during cooling with a common onset temperature at 59°C. This revealed that glyceryl monostearate exhibits a polymorphism behavior with two close transition temperatures. This behavior was not observed during the melting process probably because both transitions are overlapping each other's. PEG-50 cetyl/stearyl ether showed a single narrow exotherm crystallization transition at 38°C. The thermal behavior of cetearyl alcohol was described earlier in [3.1.3. DSC in Figure 3.11.](#) PEG-2 cetyl/stearyl ether exhibited two endotherms: a first one at 28°C and a second one at 51°C. The thermal behavior of PEG-2 cetyl/stearyl ether is very similar to the one of cetearyl alcohol. This is not surprising as these two compounds are structurally alike: a 16 to 18 carbon chain and a small polar head; either composed of an alcohol functional group or an average of two OE functional groups. Therefore, PEG-2 cetyl/stearyl ether showed a polymorphism thermal behavior and exhibited both a configuration and a melting transition. The total melting enthalpies of this compound was equal to 173 J/g. The crystallization behavior of cetearyl alcohol and PEG-2 cetyl/stearyl ether are also similar and showed two transitions at 50-26°C and 50-25°C, respectively. Additionally, ammonium sulfate showed, at elevated temperatures, a single narrow endotherm at 366°C with a melting enthalpy equal to 29 J/g. PTD did not exhibit any endotherm peaking even at elevated temperature. All these results are summarized in [Table 3.11.](#) The thermogram of PEG-2 cetyl/stearyl ether is shown in [Figure 3.36.](#) The thermograms of all the other raw materials are showed in [Appendix 7.5.1.](#)

Table 3.11. Thermal behavior of the raw materials contained in the nonionic creams during the third heating and second cooling run (2K/min).

	T _{Melt. Max. 1} [°C]	T _{Melt. Max. 2} [°C]	ΔH _{Melt. Tot.} [J/g] *	T _{Cryst. Onset 1} [°C]	T _{Cryst. Onset 2} [°C]
Cetearyl Alcohol	29.62 ± 0.02	51.47 ± 0.04	191.63 ± 1.30	49.69 ± 0.04	25.62 ± 0.12
PEG-2 cetyl/stearyl ether	27.84 ± 0.06	51.23 ± 0.03	172.03 ± 1.25	49.63 ± 0.05	24.52 ± 0.04
PEG-50 cetyl/stearyl ether	52.59 ± 0.16	-	139.77 ± 4.80	38.23 ± 0.16	-
Glyceryl monostearate	60.96 ± 0.04	-	99.56 ± 1.26	59.21 ± 0.03	-

* The melting enthalpy reported in this table is the total melting enthalpy of each raw materials. For cetearyl alcohol and PEG-2 cetyl/stearyl ether exhibiting two melting endotherms, the ΔH_{Melt. Tot.} is the sum of ΔH_{Melt. 1} and ΔH_{Melt. 2}.

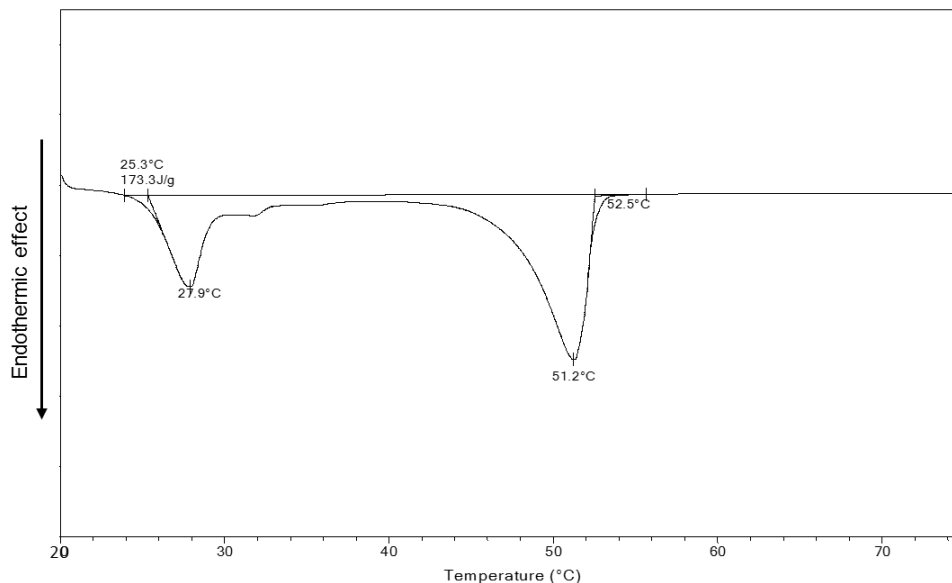


Figure 3.36. DSC thermograms of PEG-2 cetyl/stearyl ether measured between 20°C and 70°C at a heating rate of 2K/min.

3.3.3.2. Thermal behavior of the nonionic creams containing PTD

Subsequently, the DSC was used to establish the melting and crystallization behavior of the nonionic creams G0 and H1 to H6. Firstly, all the creams showed a reproducible melting behavior for the three repeated measurements. During the third heating, two broad and weak endotherms were observed for all the creams ([Figure 3.37.](#)). They will be called T_{c1} and T_{c2} . The absence of a phase transition in the 28 to 30°C region indicated that the hydrocarbon chains of cetearyl alcohol and PEG-2 cetyl/stearyl ether are in the α -form, i.e. crystal form. During heating, the first endotherms were visible between 48 and 50 °C. The second endotherms appeared between 60 and 66°C. While increasing the electrolytes concentration, the second endotherm shifted significantly to lower temperatures. Both endotherms from the nonionic creams had a low melting enthalpy. The total melting enthalpy was for all creams around 12 J/g. No significant difference in melting enthalpy was noticed towards addition of salts. As for the ionic systems, the nonionic samples showed a broad melting endotherm with low melting enthalpy between 60 and 70°C. This endotherm, T_{c2} , is related to the melting of the surfactants' bilayers. This thermal behavior is typical for lamellar gel phases composed of surfactants' bilayers.

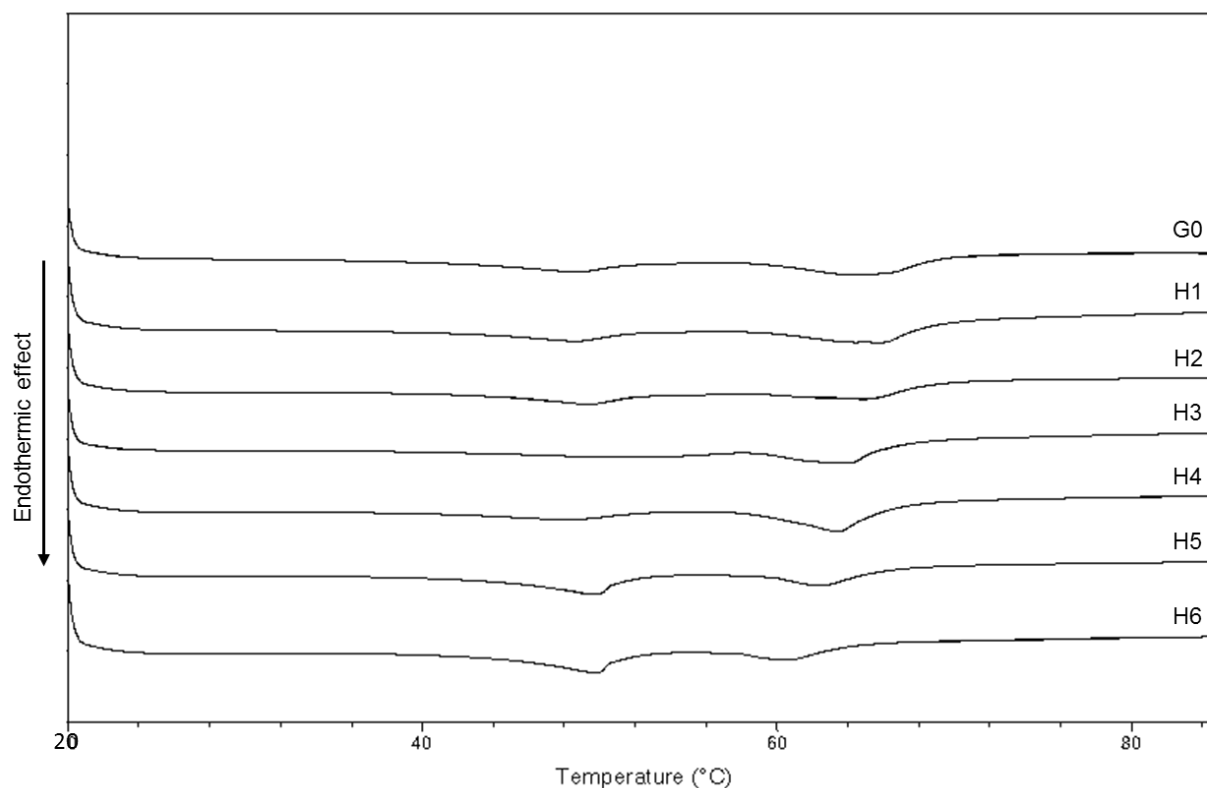


Figure 3.37. DSC thermograms of the nonionic samples G0 and H1 to H6 containing from 0 to 7.0 w% PTD in the third heating run. Heating run from 20 to 85°C at a constant heating rate of 2K/min.

The melting temperature of both endotherms and their related melting enthalpy are presented in [Figure 3.38](#). for the creams H1 to H6.

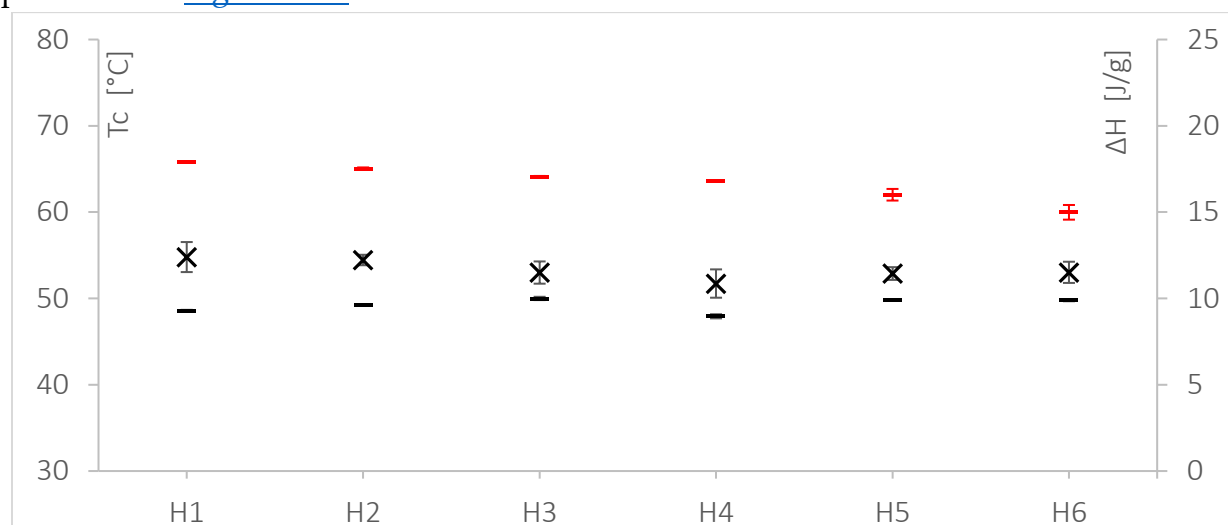


Figure 3.38. First and second thermal transitions: T_{c1} (—) and T_{c2} (—), and the total melting enthalpies ΔH (X) of the creams H1 to H6. The measurements were repeated three times. The whiskers above and below the average values define the av. \pm std. dev. The values presented were taken during the third heating run (2K/min).

The first endotherms T_{c1} at 49-50°C observed for the nonionic creams, correspond to the melting temperatures of the FA and/or PEG-2 cetyl/stearyl ether. Therefore, this first endothermic transition may prove the existence of a lipophilic gel phase melting before the lamellar gel phase (see [Fig. 1.7.](#) phase (c) and (e)). The existence of this phase will be further investigated in the following chapter [3.3.4. Spectroscopic imaging](#). Contrary to the ionic systems, the melting of this phase was visible in the heating run of all nonionic creams. The crystalline lipophilic phase might exist in a more significant amount in the nonionic samples than the ionic ones. Moreover, the first endotherms T_{c1} , did not show the tendency to shift in temperature under addition of electrolytes. Indeed, all the values oscillated around 49°C ± 1°C. If following the same argumentation discussed in [3.1.3.2. Thermal behavior of the ionic creams containing ammonium sulfate](#), the lipophilic gel phases from the nonionic creams might be all hydrated in an equivalent manner. The second endotherm, T_{c2} , observed between 60 and 66 °C correspond to the melting of the bilayers forming the lamellar gel phase. The onset, the melting and the offset temperatures of T_{c2} shifted to lower temperatures as the salt concentration increased. This shift is less significant than in the ionic systems. The decrease in T_{c2} , could be explained by the presence of additional lipophilic gel phases in the sample when adding electrolytes. However, as the lipophilic gel phase exists already in significant amount in H1 to H6, the diffusion of the FA and/or PEG-2 cetyl/stearyl ether out of the lamellae does not affect the melting enthalpy. The diffusion of FA from the bilayers to the crystalline phases is more likely to occur by migration of the cetearyl alcohol, in large excess in the samples, than by diffusion of the PEG-2 cetyl/stearyl ether. Moreover, the nonelectrical steric barrier existing between the POE polar head of the nonionic surfactants are rather strong interactions. Therefore, PEG-2 cetyl/stearyl ether is more likely to be present in the bilayers than in the crystalline phases.

The second cooling run showed for H1 to H4 a single broad exotherm peak and for H5 and H6, two tailed exotherms. The onset temperatures of the crystallization process are summarized in [Table 3.12.](#) and shown in [Appendix 7.5.2.](#)

Table 3.12. Crystallization temperatures of the creams H1 to H6 during the second cooling run (2K/min).

	H1	H2	H3	H4	H5	H6
Onset crystallization temperature [°C] *	57	55	55	54	59-49	58-49
Std. dev. [°C] *	0.3	0.1	0.2	0.4	0.1-0.0	0.6-0.0

* Av. values and std. dev. calculated from the three repeated measurements.

The second exotherms observed for H5 and H6 at 49°C corresponded to the crystallization temperatures of PEG-2 cetyl/stearyl ether and/or cetearyl alcohol. These findings prove the existence of a crystalline phase at least in H5 and H6. However, a double endotherm

was found at the same temperature during the heating run for all nonionic creams. Therefore, the lipophilic phase is most probably existing in all the samples. The two peaks might be not visible for H1 to H4 due to a temperature overlap.

DSC measurements demonstrated that the nonionic creams H1 to H6 containing PTD are composed of two phases: a lamellar gel phase and a lipophilic gel phase as presented in [Figure 1.7](#). (a)+(b) and (c)+(e), respectively.

3.3.3.3. Thermal behavior of the nonionic creams containing a mixture of hair-dyes

As the nonionic creams showed robust rheological, thermal and microscopic behavior, they were additionally formulated with a combination of hair-dyes. The nonionic simplified shades systems were studied under DSC ([Figure 3.39](#). and [Figure 3.40](#).).

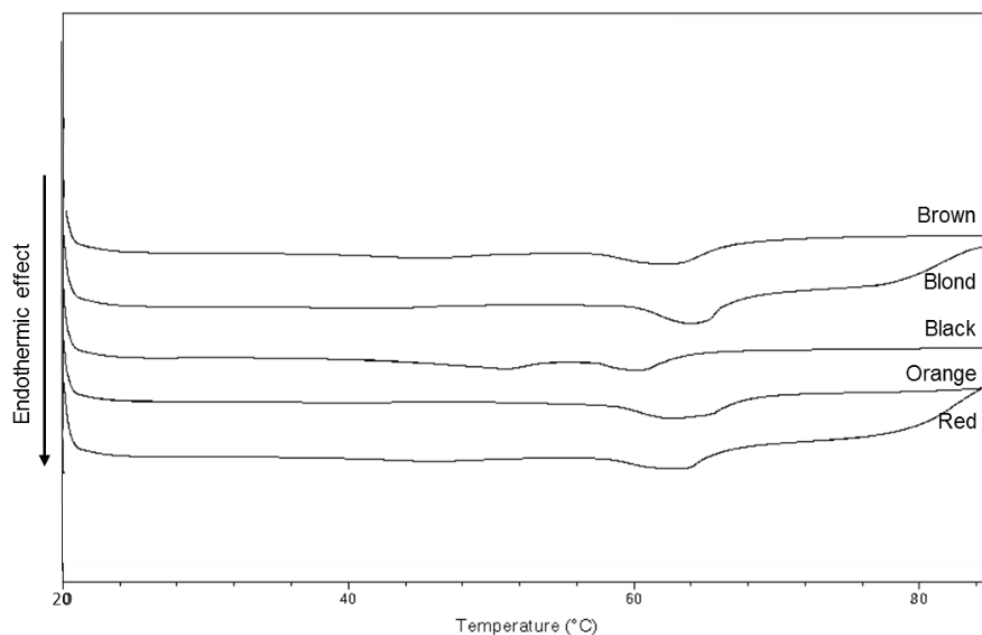


Figure 3.39. DSC thermograms of the nonionic samples containing different hair-dyes mixtures corresponding to the shades: brown, blond, black, orange and red in the third heating run. Heating run from 20 to 85°C at a constant heating rate of 2K/min.

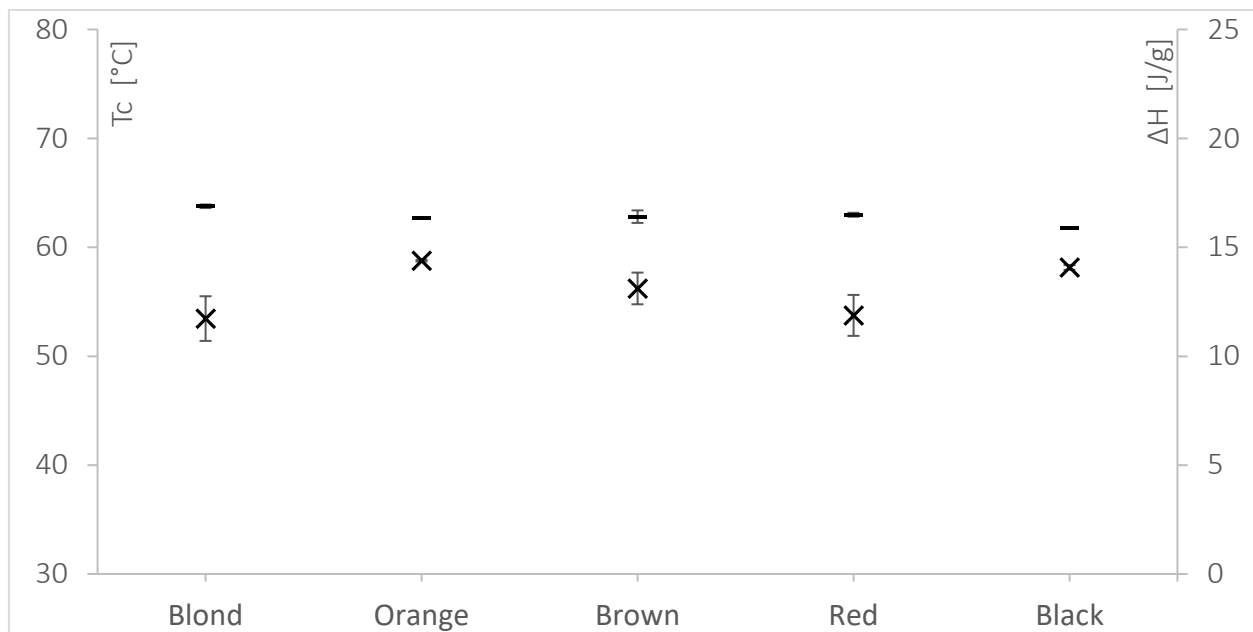


Figure 3.40. Melting temperatures (—) and melting enthalpies (X) of the nonionic creams containing hair-dyes mixtures. The measurements were repeated three times. The whiskers above and below the average values define the $av. \pm \text{std. dev.}$ The values presented were taken during the third heating run (2K/min).

The DSC results of the nonionic shades after three successive measurements were repeatable. The total hair-dyes concentration is going up from the blond (light) shade to the black (dark) shade. The nonionic simplified shades showed similar thermal behavior than the creams containing PTD only: melting enthalpy between 10 and 15 J/g and a significant decrease in melting temperature under addition of electrolytes (from 64 to 62°C). However, the first endotherm T_{c1} , observed previously was less visible.

The second cooling run showed for all the simplified nonionic shades a single broad exotherm. The onset temperatures of the crystallization process are summarized in [Table 3.13](#) and shown in [Appendix 7.5.2.](#)

Table 3.13. Crystallization temperatures of the nonionic creams containing hair dyes mixtures (shades) during the second cooling run (2K/min).

	Blond	Orange	Brown	Red	Black
Onset crystallization temperature [°C] *	57	57	55	56	59
Std. dev. [°C] *	0.1	0	0.1	0.1	0.1

* Av. values and std. dev. calculated from the three repeated measurements.

No double exotherm was observed. The crystalline phase was not visualized by means of DSC in the simplified nonionic shades, neither during heating nor cooling. These results are rather discussable and are not sufficient for assuming the absence of the crystalline phase in the nonionic systems containing hair-dyes mixtures. The onset of the

crystallization varied between 55°C to 59°C without any evident correlation to the dyestuff content.

The simplified nonionic shades showed typical lamellar gel phases thermal behavior. They are likely to be composed of surfactants bilayers. This chapter confirmed some similarities existing between the creams containing only PTD and the creams containing real dye-mixtures. The overall fluctuations in thermal behavior between these two systems remain acceptable if considering the radical changes in electrolytes composition. The nonionic surfactant systems are considered robust towards addition of salts from different natures and at different concentrations. The simplified nonionic shades will be further assessed in [7.7.2. Stability tests](#) and [7.7.3. Color delivery](#).

3.3.4. Spectroscopic imaging

The ATR-FTIR spectra of the raw materials contained in the nonionic creams are presented in [Appendix 7.6](#). The main IR absorption bands of each raw material are summarized in [Table 3.14](#). It was not possible to perform ATR-FTIR spectroscopy and microscopy with colored creams. Therefore, the nonionic cream containing 1.0 w% ammonium sulfate, G3, was studied. The nonionic cream G3 was observed under ATR-FTIR spectroscopy and microscopy. The intensity image under ATR-FTIR microscopy at 1420 cm⁻¹ and the ATR-FTIR spectra of the nonionic cream G3 are presented in [Figure 3.41](#) and [Figure 3.42](#) respectively.

Table 3.14. Main IR absorption bands of the raw materials contained in the nonionic creams

Wavenumber region [cm ⁻¹]	4000-3500	3500-3000	2000-1500	1500-1000	1000-500
Cetearyl alcohol		3270*, 2916, 2849		1472, 1060	730, 719
Ammonium sulfate		3015*		1403, 1061	610
PEG-50 cetyl/stearyl ether		2883		1341, 1102	958, 841
PEG-2 cetyl/stearyl ether		3271*, 2916, 2849		1472, 1061	719
Glyceryl monostearate		3304*, 2914, 2850	1730	1470, 1178, 1047	718
Water	3500		1650		

* Broad overtone of medium intensity

Note: The absorption bands typed in bold are the most intense bands of the spectrum.

The microscopy revealed the presence of three areas: a concentrated area (B in [Figure 3.41](#).) present everywhere in the sample, another concentrated but more diffuse area (A in [Figure 3.41](#).) and a completely diffuse area (C in [Figure 3.41](#).) present predominantly in the sample. These three phases/areas will be called concentrated, dispersed and diffuse phase, respectively.

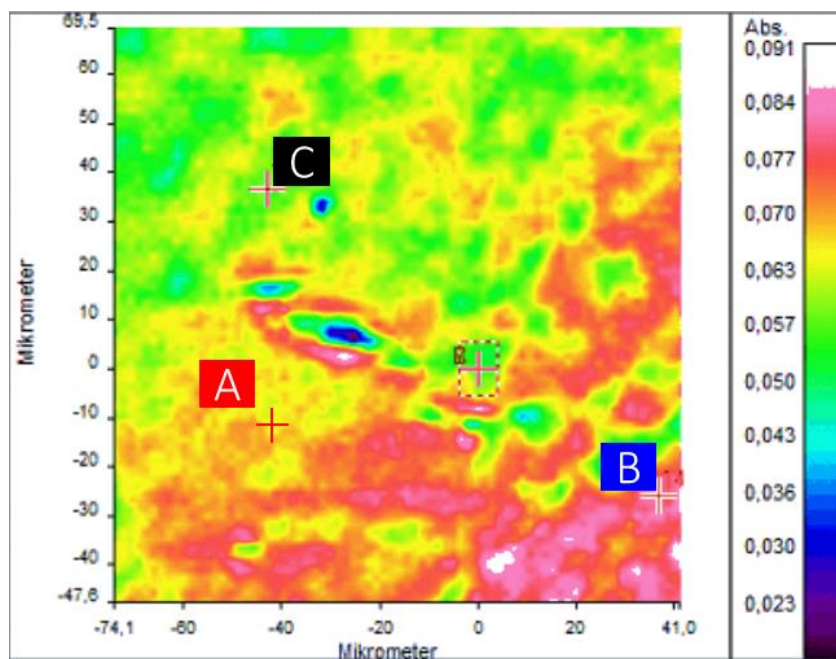


Figure 3.41. Intensity image under ATR-FTIR microscopy at 1420 cm^{-1} of the nonionic cream G3 containing 1.0 w% ammonium sulfate. The marked regions A, B and C correspond to the “dispersed”, the “concentrated” and the “diffuse” area, respectively. The color pattern corresponds to the color code used for the spectra in [Figure 3.42](#).

The intensity image was taken at 1420 cm^{-1} because all three areas showed different absorption bands at this specific wavenumber.

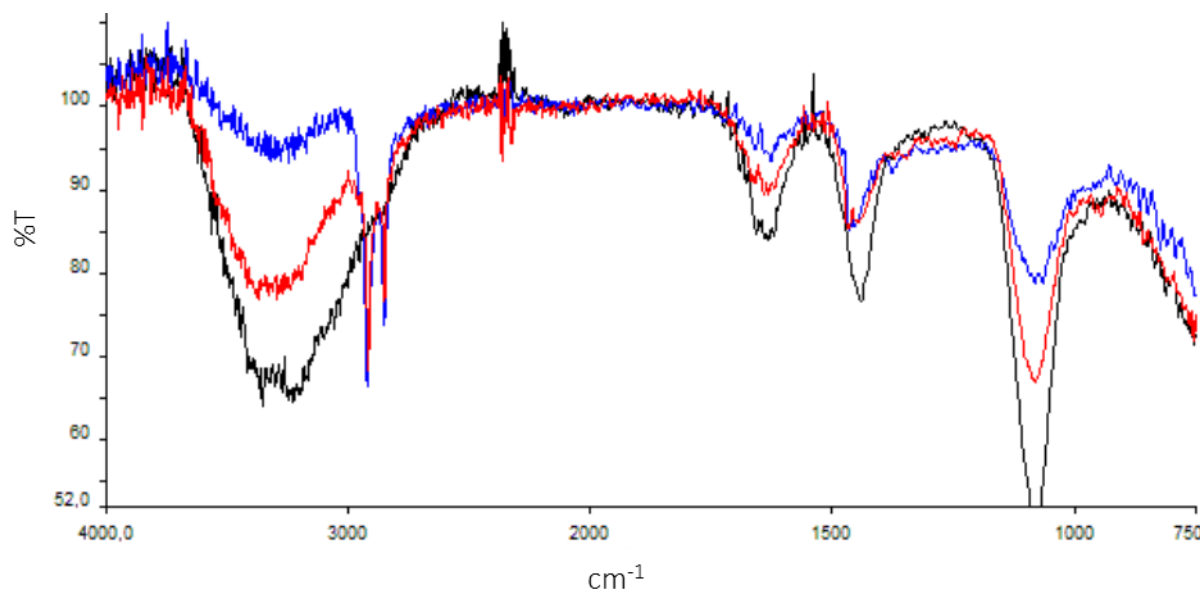


Figure 3.42. ATR-FTIR spectra of the nonionic cream G3 (1.0 w% ammonium sulfate) in three different regions of the sample: the “concentrated” (blue), the “dispersed” (red) and the “diffuse” (black) area. The color pattern corresponds to the color code used in [Figure 3.41](#). The spectra are measured at RT using UATR-technique with a diamond-KRS-5 (Thallium Bromoiodide) crystal.

The concentrated area showed typical absorbance bands of fatty alcohols e.g. cetearyl alcohol and long chain alcohol compounds e.g. PEG-50 cetyl/stearyl ether, PEG-2 cetyl/stearyl ether at 2950 and 2850 cm^{-1} . The broad peak between 3700 and 3100 cm^{-1} is characteristic for water. This band must not be mistaken with the ammonium sulfate broad peak which spreads until lower wavenumber: 2750 cm^{-1} . The second characteristic absorption band of the water is also identified in the IR spectrum of all the areas: 1650 cm^{-1} .

The diffuse area showed typical absorbance bands of ammonium sulfate especially the broad and intense peak between 3200 and 2750 cm^{-1} . This peak covered probably the water absorption band (after 3000 cm^{-1}). The typical long chain alcohol bands at 2950 and 2850 cm^{-1} are not visible. The bands between 1500 and 500 cm^{-1} are difficult to interpret as an overlap exists between the characteristic peaks of ammonium sulfate and the one of the long chain alcohols. The spectra's intensity for this phase is the highest, especially for the characteristic bands of ammonium sulfate and water. Therefore, the diffuse phase is more likely to be composed of the main amount of bulk-water and diluted electrolytes.

The dispersed area showed typical absorbance bands of both long chain alcohols and/or surfactants and ammonium sulfate. The wavenumber region down to 2850 cm^{-1} is difficult to interpret due to the overlap of the characteristic water, ammonium sulfate and the long chain alcohol bands. The pattern of the signal in this region ensure the presence of long chain alcohols (double narrow peaking at 2950 and 2850 cm^{-1}). However, one can read the spectrum in the two following ways:

- Presence in the dispersed phase of long chain alcohol (FA-amphiphiles and/or surfactants) and a low concentration of ammonium sulfate (compared to the diffuse phase).
- Presence in the dispersed phase of long chain alcohol and water only.

The first hypothesis is more likely to occur as the shoulder of the double peak representative of the long chain alcohols at 2850 cm^{-1} is rather distant from the spectrum baseline. This back shoulder might be the end of the ammonium sulfate absorption IR band at 3015 cm^{-1} .

Unlike the ionic systems, the ATR-FTIR spectra of G3 did not highlight the presence of both electrolytes and long chain alcohol compounds in the concentrated area. Indeed, it seems that the ammonium sulfate is present only in the diffuse and dispersed area. Considering that the diffuse area is the bulk-water phase (phase d in [Figure 1.7.](#)), that the

dispersed area is the lipophilic gel phase and/or aggregates of lipophilic crystalline compounds (phase c and e in [Figure 1.7.](#)) and that the concentrated area is the lamellar gel phases (phase a+b in [Figure 1.7.](#)), the ATR-FTIR spectroscopy and microscopy revealed that the salts are mainly diluted in the bulk-water and are not present in the interlamellar fixed water of the lamellar gel phase. These findings demonstrate that the electrolytes do not interact with the nonionic surfactants' bilayers. The presence of the characteristic absorption bands of FA and/or surfactants in the dispersed phase can be due to the presence of a crystalline hydrated lipophilic phase, as in the ionic creams. This assumption is in line with the DSC findings which demonstrated the existence of two distinct phases melting subsequently at 50 and 63°C. The presence of a lipophilic gel phase composed of crystalline fatty alcohols and/or surfactants may be due to the excess of FA and/or PEG-2 cetyl/stearyl ether or to the formulation process. As the FA are present in excess in all nonionic creams, the lipophilic phase is more likely to be composed of cetearyl alcohol in their crystalline α -form.

These results are in line with the rest of the chapter 3.3. which showed the independency of the microstructure, hence the rheological behavior, towards salt addition. In fact, ATR-FTIR imaging spectroscopy confirmed that salts are present mainly in the bulk-water and not in the fixed-water in the surfactants bilayers.

3.3.5. Conclusion

The characterization of the optimized hair coloring products revealed that the nonionic systems were behaving like typical lamellar gel phases composed of vesicles and/or lamellar structures. The microscopic investigations and the rheological and thermal analysis, all supported the existence of blended surfactants bilayers in the samples. The spectroscopic researches led to a deeper understanding of the repartition of the surfactants and the electrolytes in the sample. This latest method delivered crucial insights about the interactions between the self-arranged surfactants system and the salts. It enabled to explain the robustness and the non-dependency of the bilayers microstructures to the electrolytes content and nature.

To confirm theoretically the microstructural arrangement of the nonionic systems into vesicles and/or flexible bilayers, either the PP or the HLB of the system can be calculated. More literature is available about the HLB values of nonionic emulsifiers. Therefore, the "weighted HLB" will be calculated according to Frenkel et al. [124]. This value is calculated by incrementing the HLB of each emulsifier present in the system by their

respective weight fractions as a percentage of the total emulsifiers' content. The "weighted HLB" can be described by equation (18).

$$HLB_{w\%} = \sum_i \frac{[C_i]_{w\%} \times HLB_i}{100} \quad (18)$$

With $[C_i]_{w\%}$, the weight percentage of the surfactant i normalized on the total amount of surface-active substances contained in the system, and HLB_i , the HLB value of the surfactant i . In the scope of this study, as the nonionic systems is composed of two different surfactants: PEG-2 cetyl/stearyl ether and PEG-50 cetyl/stearyl ether, $i = 2$. Glyceryl stearate and cetearyl alcohol are considered as lipids (non-polar solvents i.e. hydrocarbons) and are therefore not taken in account in equation (18). A non-exhaustive list of the HLB values of classical PEG emulsifiers, from the literature and estimated according to Griffin [25], are listed in [Table 3.15.](#)

Table 3.15. HLB values of PEG-X cetyl/stearyl ether collected from the literature and estimated according to Griffin [25] ($X = 2, \dots, 100$).

Surfactant	HLB value*	Estimated HLB value**
PEG-2 cetyl/stearyl ether	4.9 [111], [112]	5.38
PEG-10 cetyl/stearyl ether	12.4 [111], [112]	12.96
PEG-12 cetyl/stearyl ether	13.5 [111]	13.77
PEG-20 cetyl/stearyl ether	15.5 [111]	15.73
PEG-25 cetyl/stearyl ether	16.2 [111]	16.43
PEG-30 cetyl/stearyl ether	16.3 [111]	16.93
PEG-40 cetyl/stearyl ether	17 [111]	17.61
PEG-50 cetyl/stearyl ether	-	18.04
PEG-100 cetyl/stearyl ether	18.8 [111]	18.97

* HLB values taken from the literature.

** Estimated HLB values according to Griffin (see equation (2) in [1.3.3. Hydrophilic-lipophilic Balance \(HLB\)](#)).

Consequently, by replacing the respective HLB values and weight fractions of each surfactant in equation (18), as described in [Table 3.16.](#), the estimated weighted HLB value of the complete nonionic system was found equal to 17.3.

Table 3.16. Weight fraction and HLB values of the surfactants and FA contained in the nonionic systems.

Surfactant	Estimated HLB value**	Weight fraction* [%]
PEG-2 cetyl/stearyl ether	5.38	6
PEG-50 cetyl/stearyl ether	18.04	94

* weight fraction normalized on the total amount of emulsifiers and FA contained in the system.

** Estimated HLB values according to Griffin (see equation (2) in [1.3.3. Hydrophilic-lipophilic Balance \(HLB\)](#)).

An HLB value between 10 and 20 is equivalent to a critical PP of $\frac{1}{2} < p < 1$ [73], [112]. Hence, the nonionic system is likely to assemble into vesicles and/or flexible bilayers. These calculation are supporting the results but remain approximations as the system contains more compounds than only two surfactants: PEG-2 cetyl/stearyl ether and PEG-

50 cetyl/stearyl ether. These estimations are however in line with the findings of this chapter.

In summary, the nonionic systems showed under addition of PTD:

- A broad particle size distribution which remained steady over aging
- A constant viscosity η (when PTD w% > 0.2)
- A constant critical strain γ_c (when PTD w% > 0.2)
- A slight decrease of the melting temperature and a stable melting enthalpy

The classical DLVO theory is not sufficient for describing the robustness and stability of the nonionic systems studied in this manuscript. In fact, as the surfactants are not charged, the main interactions driving the system to self-assemble in vesicles and flexible bilayers are not the electrostatic repulsions between the polar moieties. PEG surfactants can form a nonelectrical steric barrier which enable the system to assemble in a stable manner [33]. Polyethylene oxide functional groups can bind strongly with water. These nonelectrical interactions are twofold:

- Dragging water away from the lipophilic moieties of the bilayers which consolidates lamellae by promoting more and stiffer hydrophobic attractions.
- Forming a robust OE-water network/barrier in the hydrophilic interlamellar space.

This second reinforcement is driven by the formation of an extended POE-water and water-water network through hydrogen bounds formation. This network takes an helical conformation maintained even at high temperature [119]. The three-dimensional network is held together by electrostatic hydrogen bounds at a ratio of two molecules of water per OE unit [34]. The hydrogen bonds are occurring between the hydrogen atoms of the water and the highly electronegative oxygen atom of the OE unit. This network is not affected by the electrolyte concentration. In fact, as seen by means of ATR-FTIR spectroscopy and microscopy, the electrolytes are mainly diluted in the bulk-water phase and not in the bilayers themselves. Hence, the addition of salts is not influencing the structural backbone of the system. The replacement of the electrical driving forces of the ionic system by electrostatic nonelectrical POE-water and water-water interactions in the nonionic systems, led to an enhancement of the stability and a more robust rheological behavior towards salts addition.

The additional specific evaluations for cosmetic and industrial purposes are presented in [Appendix 7.7.](#)

4. Summary

Emulsions are widely used for numerous kind of industrial applications. Whether it concerns pharmaceuticals to ensure topical drug delivery, beauty products to carry cosmetic agents onto/into the human skin or hair or food supply which need to meet rigorous specifications, investigations about surfactants-containing systems are crucial to understand and control their phase-behavior. For hair coloring products, it is necessary to deliver specific salt-like active components i.e. hair dyes, into or onto the human hair fibers. Therefore, typical functional emulsions are used. Unfortunately, depending on their nature and concentration, hair dyes interact with common emulsifier systems and disrupt their stability, rheology and phase-behavior. The present work aimed to characterize the physicochemical behavior of classical hair coloration emulsions and to identify the key-parameters responsible of their rheological instability. Additionally, the classical hair coloring system has been optimized to obtain a cosmetic carrier with robust rheological and thermal phase-behavior nearly independently of the salt concentration and nature.

The characterization of the classical hair coloring system and evaluation of the optimized one was done by means of static and dynamic rheological measurements, microscopic observations i.e. cryo-TEM, TEM, PL and PC microscopy, DSC measurements and ATR-FTIR spectroscopic imaging. To identify the key-parameters impacting the phase-behavior, simplified emulsions have been studied. The simplification of a classical hair coloring system enabled to focus on the specific interactions existing between electrolytes and emulsifiers. Therefore, rheology modifier additives as well as the cosmetic claim ingredients or preservatives have been removed from the classical hair coloring formulation. The alkalizing agent, the oil and the water phases were preserved. The electrolyte composition was monitored either with an inorganic salt (ammonium sulfate), an organic salt (PTD) or a mixture of hair dyes.

Firstly, to characterize the classical hair coloring system, a ternary system containing blended ionic (SLES) and nonionic emulsifiers (PEG-20 cetyl/stearyl ether) with FA was studied. According to the literature review and the results of analytical method above-mentioned, this system was characterized as a semi-solid system composed of lamellar gel phases. It is mainly composed of a crystalline hydrophilic gel phase, a crystalline lipophilic phase, a bulk-water phase and a dispersed oil phase. The structural characterization of the classical hair coloring system was supported by the estimation of the PP. This theoretical approach confirmed the self-assembly of the surfactants in vesicles, flexible bilayers and planar bilayers. The properties of this system differed

considerably from a standard micellar emulsion's phase-behavior. Indeed, classical hair coloring system exhibited a typical shear thinning and solid-like behavior with a strong dependency to the aging and the overall electrolytes concentration. This system showed under addition of electrolytes: an expansion of the anisotropic structures visible under PL microscopy, a significant decrease of η , γ_c and T_c and a decrease of the hydration of the lipophilic phase. The ATR-FTIR imaging spectroscopic results demonstrated the presence of salts in the bilayers of the lamellar gel phase. This confirmed the direct interaction between the electrolytes and the emulsifiers and accordingly the strong dependency of the microstructure, hence the rheological behavior, towards salts addition. Further observations of the lamellar gel phases under PL microscopy revealed aggregation of the bilayers over time.

Subsequently, a systematic screening study of nonionic PEG-emulsifiers as replacement of the blended ionic and nonionic surfactants, enabled to formulate a more robust system. It showed that the rheological robustness was enhanced by combining two PEG-ether derivatives rather than a single nonionic surfactant: more precisely, it was observed that γ_c increased when the overall OE units present in the system increased and that the systems containing a combination of nonionic surfactants rather than a single nonionic surfactant were subject to less viscosity fluctuations over time. On the contrary, these fluctuations were more pronounced when the overall OE units present in the system increased. Moreover, it was shown that PEG-ether derivatives stabilized the salt-containing emulsions by two forces in synergy: the nonelectrical steric barrier in the interlamellar space of the bilayers and the enhanced Van der Waals forces in the lamellae. This latter occurred by reduction of the steric hindrances while using a short and a long PEG surfactant rather than a single long polar moiety. As a result, a schematic model of the nonionic surfactants' arrangement was proposed. The optimal system was composed of PEG-2 cetyl/stearyl ether and PEG-50 cetyl/stearyl ether (molar ratio 1:2.5) in combination with glyceryl monostearate and cetearyl alcohol. The molar ratio of the total surfactant content over the FA content was equal to 1:20.

Finally, the optimized nonionic hair coloring system was characterized as semi-solid system composed of lamellar gel phases. The PL, PC microscopy and cryo-TEM showed that the samples were composed of a coexisting $[L_\alpha]$ phase, having a broad particle size distribution scattering around 1 μm , and a L_α phase composed of 1-to-10nm-wide bilayers. The rheological measurements revealed a typical shear thinning and solid-like behavior with no dependency to the overall electrolytes concentration. Moreover, a systematic slight loss in η , G' , G'' and $|\eta^*|$ after six months storage at RT led to the assumption that the nonionic systems were composed more precisely of mixed $[L_\alpha]$ and

L_{α} phases transitioning partially in favor of L_{α} phases over time. All results taken together, the optimized system exhibited under addition of electrolytes: a stable but broad particle size distribution which remained steady over time, a constant η and γ_c (when PTD w% > 0.2), a slight decrease of T_c and a constant ΔH_{Melt} . Accordingly, the ATR-FTIR imaging spectroscopic results confirmed that salts were present mainly in the bulk-water and not in the fixed-water in the surfactants bilayers. The optimized system demonstrated a strong reduction of the viscosity fluctuations over time and under addition of the electrolytes: $\Delta\eta_{ionic} = 12.80$ Pa.s and $\Delta\eta_{nonionic} = 1.06$ Pa.s. A theoretical estimation of the HLB value of the system according to Frenkel was calculated. It confirmed that the nonionic hair coloring product might be composed of vesicles and/or flexible bilayers. Additional specific evaluations demonstrated the compatibility of the optimized nonionic system for cosmetic and industrial applications.

This thesis highlighted the importance of selecting a proper emulsifiers system for high-salt containing systems like hair coloring products. The improved systems showed a promising potential for being used as a universal carrier for salt-like actives for the hair cosmetic. This study gave a closer-to-reality look on multi-component finish-goods, which are usually, as such, not studied in the literature.

5. Zusammenfassung

Emulsionsbasierte Systeme werden in industriellen Anwendungen weit verbreitet eingesetzt. Ganz gleich, ob es sich dabei um pharmazeutische Formulierungen zum gerichteten, topischen Wirkstofftransport in die Haut, um Kosmetikprodukte, die den Stofftransport in die Haut oder auf das Haar sicherstellen sollen oder um den Einsatz von Emulsionen in Nahrungsmitteln, trägt die detaillierte Kenntnis des Verhaltens von tensidhaltigen Systemen grundlegend dazu bei, das Phasenverhalten von Emulsionen zu verstehen und zu kontrollieren. In Haarfarbprodukten werden Farbstoffvorstufen, die in der Mehrzahl Salze sind, in und auf die Haarfaser übertragen. Zu diesem Zweck verwendet man geeignete funktionale Emulsionen. Je nach Art und Konzentration interagieren Haarfarbstoffe jedoch mit herkömmlichen Emulgator-Systemen und beeinflussen deren Stabilität, Rheologie und deren Phasenverhalten. Gegenstand der vorliegenden Arbeit war es, das physikalisch-chemische Verhalten eines klassischen Haarfärbesystems zu charakterisieren und die für die rheologische Instabilität verantwortlichen Schlüsselparameter zu identifizieren. Des Weiteren wurde auf Basis dieser Erkenntnisse ein Haarfärbesystem dahingehend optimiert, dass die resultierende Emulsion ein robusteres rheologisches und thermisches Phasenverhalten aufweist, welches weitestgehend von der Art der verwendeten Salze sowie deren Konzentration unabhängig ist.

Sowohl die Charakterisierung des klassischen Haarfärbesystems als auch die Optimierung der Formulierung und deren anschließende Charakterisierung wurden mittels statischer und dynamischer rheologischer Messungen, mikroskopischer Beobachtungen, d. h. Kryo-TEM-, TEM, PL- und PC-Mikroskopie, DSC-Messungen und ATR-FTIR-Spektroskopie beurteilt. Um die Schlüsselparameter zu identifizieren, die das Phasenverhalten maßgeblich bestimmen, wurden Modell-Emulsionen untersucht. Dadurch war es möglich, sich auf die spezifischen Wechselwirkungen zwischen Elektrolyten und Emulgatoren zu konzentrieren. Bei diesen Modellformulierungen wurden die Bestandteile der Öl- und Wasserphase sowie das Alkalisierungsmittel beibehalten; auf Zusatzstoffe, die die Rheologie beeinflussen, kosmetische Pflege- oder Aktivstoffe und Konservierungsmittel wurde verzichtet. Die Elektrolytzusammensetzung wurde entweder mit einem anorganischen Salz (Ammoniumsulfat), einem organischen Salz (PTD) oder ausgewählten Farbstoffen kontrolliert.

Zur Charakterisierung eines klassischen Haarfärbesystems wurde im ersten Schritt ein ternäres System aus gemischten ionischen (SLES) und nichtionischen Emulgatoren (PEG-

20-Cetyl/Stearylether) mit Fettalkoholen (FA) untersucht. Im Einklang mit der wissenschaftlichen Literatur und mittels der oben genannten analytischen Methoden wurde diese Formulierung als halbfestes System, bestehend aus lamellaren Gelphasen, charakterisiert. Dieses System besteht hauptsächlich aus einer kristallinen hydrophilen Gelphase, einer kristallinen lipophilen Phase, einer Phase aus freiem Wasser, die den Hauptbestandteil der Formel bildet, und einer dispergierten Ölphase. Die strukturelle Charakterisierung des klassischen ionischen Systems wurde ebenfalls durch die Abschätzung des Packungsparameters (PP) untermauert. Dieser theoretische Ansatz bestätigte die Selbstorganisation der Tenside in Vesikeln, flexiblen Doppelschichten und planaren Doppelschichten. Die Eigenschaften dieses Systems unterscheiden sich erheblich vom Phasenverhalten einer mizellaren Emulsion. Im Gegensatz dazu weist das klassische Haarfärbesystem ein typisches scherverdünnendes (strukturviskos), feststoffähnliches Verhalten auf, das stark von der Gesamtkonzentration der Elektrolyte und Alterung der Formel abhängt. Die Zugabe von Elektrolyten bewirkte eine Ausdehnung der anisotropen Strukturen, die durch PL-Mikroskopie sichtbar gemacht werden konnten, eine signifikante Abnahme von η , γ_c und T_c und eine Abnahme der Hydratation der lipophilen Phase. Die ATR-FTIR-Spektroskopie zeigte das Vorhandensein von Salzen in den Doppelschichten der lamellaren Gelphase. Dies bestätigte die direkte Wechselwirkung zwischen den Elektrolyten und den Emulgatoren und dementsprechend die starke Abhängigkeit der Mikrostruktur und somit auch des rheologischen Verhaltens von der Salzzugabe. Die Visualisierung der lamellaren Gelphasen mittels PL-Mikroskopie zeigten eine Aggregation der Doppelschichten im Zeitverlauf.

Das anschließende systematische Screening mit nichtionischen PEG-Emulgatoren als Ersatz für die gemischten ionischen und nichtionischen Tenside ermöglichte die Formulierung eines robusteren Systems. Die rheologische Robustheit wurde durch die Kombination zweier PEG-Ether-Derivate anstelle der Verwendung eines einzelnen nichtionischen Tensids erhöht: Es zeigte sich, dass γ_c anstieg, je mehr EO-Einheiten sich insgesamt im System befanden, und dass die Systeme, die eine Kombination von nichtionischen Tensiden anstelle eines einzelnen, nichtionischen Tensids enthielten, im Laufe der Zeit weniger Viskositätsschwankungen unterlagen. Im Gegensatz dazu waren diese Schwankungen umso ausgeprägter, wenn die Gesamtzahl der im System vorhandenen EO-Einheiten zunahm. Des Weiteren ergab sich aus dem Screening, dass PEG-Ether-Derivate salzhaltige Emulsionen generell durch zwei synergistisch wirkende Kräfte stabilisieren: durch die nichtelektrische sterische Barriere im interlamellaren Raum der Doppelschichten und erhöhte Van-der-Waals-Kräfte in den Lamellen. Letztere traten durch die Verringerung der sterischen Wechselwirkungen bei der Kombination jeweils

eines kurzen und eines langen PEG-Tensids anstelle der Verwendung eines einzelnen, langen polaren Molekülanteils auf. Als Ergebnis wurde ein schematisches Modell der Anordnung nichtionischer Tenside entwickelt. Als optimal erwies sich ein System, das aus PEG-2-Cetyl/ Stearylether und PEG-50-Cetyl-/ Stearylether (molares Verhältnis 1: 2.5) in Kombination mit Glycerylmonostearat und Cetearylalkohol besteht. Das molare Verhältnis des Gesamtgehalts an Tensid im Verhältnis zum Gehalt an Fettalkoholen war 1:20.

Das optimierte, nichtionische Haarfärbesystem wurde abschließend als halbfestes System bestehend aus lamellaren Gelphasen charakterisiert. PL-, PC-Mikroskopie und Kryo-TEM zeigten, dass die Proben aus einer koexistierenden $[L_\alpha]$ -Phase mit einer breiten Partikelgrößenverteilung, die um einen Mittelwert von 1 μm streut, und einer L_α -Phase mit einer Schichtdicke zwischen 1 und 10 nm bestehen. Die rheologischen Messungen belegten ein typisches scherverdünnendes (strukturviskos) feststoffähnliches Verhalten unabhängig von der Gesamtkonzentration der Elektrolyte. Ein systematischer, leichter Verlust von η , G' , G'' und $|\eta^*|$ nach sechsmonatiger Lagerung bei Raumtemperatur führte zu der Annahme, dass die nichtionischen Systeme aus einer Mischung von $[L_\alpha]$ - und L_α -Phasen bestanden, wobei der Anteil an L_α durch einen Phasenübergang im Laufe der Lagerung zunahm. Zusammengefasst zeigte das optimierte System unter Zugabe von Elektrolyten eine stabile, aber breite Partikelgrößenverteilung, die über die Zeit konstant blieb, sowie konstante Werte für η und γ_c (PTD w% > 0.2), eine leichte Abnahme von T_c und eine konstante ΔH_{Melt} . Die Ergebnisse der ATR-FTIR-Bildgebungsspektroskopie bestätigten, dass sich die Salze hauptsächlich im Wasseranteil außerhalb der Tensid-Doppelschichten befanden. Das optimierte System zeigte eine starke Abnahme der Viskositätsschwankungen im Zeitverlauf der Lagerung und unter Zugabe von Elektrolyten ($\Delta\eta_{\text{ionic}} = 12.80 \text{ Pa}\cdot\text{s}$ und $\Delta\eta_{\text{nonionic}} = 1.06 \text{ Pa}\cdot\text{s}$ im Vergleich). Zusätzlich wurde eine theoretische Abschätzung des HLB-Wertes des nichtionischen Systems nach Frenkel vorgenommen. Diese bestätigte, dass das nichtionische Haarfärbesystem aus Vesikeln und/oder flexiblen Doppelschichten bestehen sollte. Weitere Untersuchungen belegten die Eignung des optimierten, nicht-ionischen Systems für den Einsatz in kosmetischen Anwendungen.

Diese Arbeit unterstreicht die Wichtigkeit der Auswahl eines geeigneten Emulgatorsystems für Produkte mit einem hohen Salzgehalt, wie er üblicherweise in Haarfärbeprodukten auftritt. Die verbesserten Systeme zeigen ein hohes Potential für den Einsatz als universelle Formulierungsgrundlage für salzartige Wirkstoffe in der Haarkosmetik. Diese Arbeit leistet einen wichtigen Beitrag zur praxisbezogenen

Untersuchung von komplexen Mehrkomponenten-Fertigprodukten, die in der Literatur als solche meist nicht beschrieben werden.

6. Outlook

Hair coloring products are finished goods of great interest for the cosmetic industry. The present work is the first attempt to characterize high-salt containing ternary systems especially focusing on hair-dyes as salt-like compounds. This study opens a room for research in the field of cosmetic carriers for delivery of salt-like active substances onto or into the human hair. The following topics would be interesting for additional investigations:

- Further study about the influence of other salt-like active substances of interest for the hair-care and hair-color industry such as: aluminum, magnesium, lanthanum salts etc.
- Further characterization of the surfactants' bilayers by X-ray scattering. This would give insights about the degree of swelling of the bilayers under addition of salt in different concentrations and nature. This approach could reinforce the statement that the nonionic system is more robust than the ionic one. However, regarding the thickness and the opacity of these creams, this method would be challenging to apply on those systems.
- Testing APG derivatives emulsifiers as an alternative to the PEG ether surfactants to obtain milder emulsions for the skin.
- Additional scale-up tests at an industrial scale to confirm the results obtained in the pilot plant study.

7. Appendices

7.1. List of 114 substances allowed for restricted use in hair dye products according to the European Commission. Regulation (EC) No. 1223/2009 updated in March 2017.

No.	INCI Name	CAS No.
1	N-Phenyl-p-phenylenediamine	101-54-2; 2198-59-6; 4698-29-7
2	p-Phenylenediamine	106-50-3
3	2,6-Dihydroxyethylaminotoluene	149330-25-6
4	Toluene-2,5-diamine	95-70-5
5	1-Naphthol	90-15-3
6	Resorcinol	108-46-3
7	Acid Yellow 23	1934-21-0
8	Acid Blue 9	3844-45-9
9	Curry Red	25956-17-6
10	Acid Red 18	2611-82-7
11	Acid Red 52	3520-42-1
12	Acid Blue 62	4368-56-3
13	N,N-bis(2-hydroxyethyl)-p-phenylenediamine sulfate	54381-16-7
14	4-Chlororesorcinol	95-88-5
15	2,4,5,6-Tetraaminopyrimidine sulfate	5392-28-9;1004-74-6
16	2-chloro-6-ethylamino-4-nitrophenol	131657-78-8
17	6-Methoxy-2-methylamino-3-aminopyridine HCl	90817-34-8; 83732-72-3
18	Dihydroxyindoline HBr	29539-03-5
19	Hydroxyethyl-p-phenylenediamine sulphate	93841-25-9
20	Dihydroxyindole	3131-52-0
21	5-Amino-4-chloro-o-cresol	110102-85-7
22	6-Hydroxyindole	2380-86-1
23	2,3-Indolinedione (Isatin)	91-56-5
24	2-Amino-3-hydroxypyridine	16867-03-1
25	1-Acetoxy-2-methoxynaphthalene	5697-02-9

No.	INCI Name	CAS No.
26	2-Methyl-1-naphthol	7469-77-4
27	Acid Yellow 1	846-70-8
28	4-amino-3-nitrophenol	610-81-1
29	2,7-Naphthalenediol	582-17-2
30	m-Aminophenol	591-27-5; 51-81-0; 68236-81-6
31	2,6-Dihydroxy-3,4-dimethylpyridine	84540-47-6
32	4-Hydroxypropylamino-3-nitrophenol	92952-81-3
33	HC Blue No.11	23920-15-2
34	Hydroxyethyl-2-nitro-p-toluidine	100418-33-5
35	2-Hydroxyethylpicramic acid	99610-72-7
36	p-Methylaminophenol	150-75-4; 55-55-0
37	HC Violet No.2	104226-19-9
38	HC Blue No. 12	104516-93-0; 132885-85-9
39	1,3-Bis-(2,4-diaminophenoxy)-propane, 4 HCl	74918-21-1; 81892-72-0
40	3-Amino-2,4-dichlorophenol HCl	61693-42-3
41	Phenyl methyl pyrazolone	89-25-8
42	2-Methyl-5-hydroxyethylaminophenol	55302-96-0
43	Hydroxybenzomorpholine	26021-57-8
44	HC Yellow No.10	109023-83-8
45	2,6-Dimethoxy-3,5-pyridinediamine HCl	56216-28-5
46	HC Orange No.2	85765-48-6
47	HC Violet No 1	82576-75-8
48	3-Methylamino-4-nitrophenoxy-ethanol	59820-63-2
49	2-Hydroxyethylamino-5-nitroanisole	66095-81-6
50	HC Red No. 13	94158-13-1

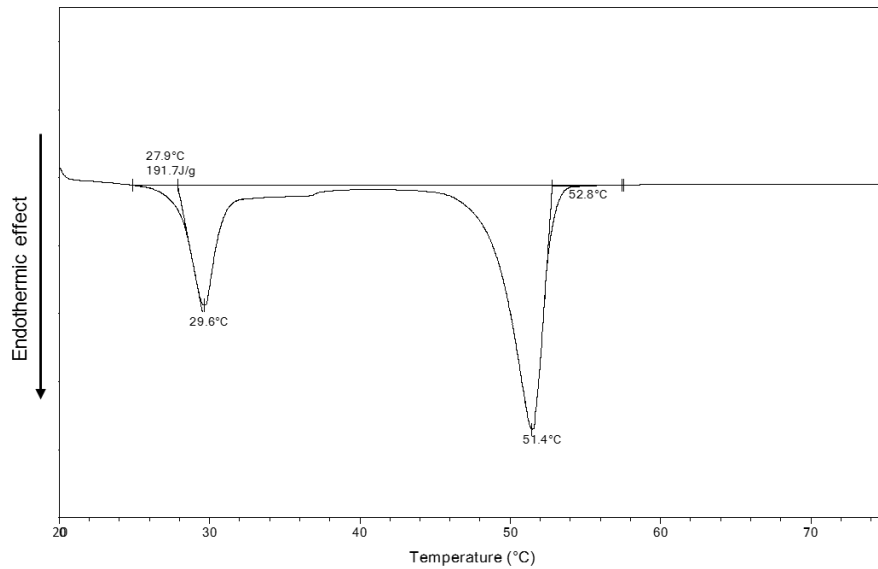
No.	INCI Name	CAS No.
51	1,5-Naphthalenediol	83-56-7
52	Hydroxypropyl bis(N-hydroxyethyl-p-phenylenediamine), HCl	128729-28-2; 128729-30-6
53	4-Nitro-o-phenylenediamine sulphate	99-56-9
54	4-Amino-2-hydroxytoluene	2835-95-2
55	2,4-Diaminophenoxyethanol	66422-95-5; 70643-20-8
56	2-Methylresorcinol	608-25-3
57	4-Amino-m-cresol	2835-99-6
58	2-amino-4-hydroxyethyl aminoanisole	83763-48-8; 83763-47-7
59	Hydroxyethyl-3,4-methylenedioxyaniline HCl	94158-14-2
60	HC Blue No. 2	33229-34-4
61	3-Nitro-p-hydroxyethylaminophenol	65235-31-6
62	4-Nitrophenyl aminoethylurea	27080-42-8
63	HC Red No.10 + HC Red No.11	95576-89-9; 95576-92-4
64	HC Red No. 7	24905-87-1
65	2-Amino-6-chloro-4-nitrophenol	6358-09-4
66	HC Yellow No. 4	59820-43-8; 52551-67-4
67	Acid Red 33	3567-66-6
68	HC Yellow No. 2	4926-55-0
69	HC Orange No. 1	54381-08-7
70	HC Red No. 1	2784-89-6
71	HC Yellow No. 9	86419-69-4; 141973-33-3
72	HC Yellow No. 7	104226-21-3
73	HC Yellow No. 13	10442-83-8
74	Basic Yellow 57	68391-31-1

No.	INCI Name	CAS No.
75	Disperse Black 9	20721-50-0
76	HC Blue No 14	99788-75-7
77	Disperse Violet 1	128-95-0
78	HC Red No 3	2871-01-4
79	Basic Red 76	68391-30-0
80	Basic Red 51	77061-58-6
81	2-Amino-5-Ethylphenol HCl	149861-22-3
82	Acid Red 92	18472-87-2
83	Disperse Blue 377 is a mixture of three dyes: (1) 1,4-bis[(2-hydroxyethyl)amino]anthra-9,10-quinone (2) 1-[(2-hydroxyethyl)amino]-4-[(3-hydroxypropyl)amino]anthra-9,10-quinone (3) 1,4-bis[(3-hydroxypropyl)amino]anthra-9,10-quinone	(1) 4471-41-4 (2) 67674-26-4 (3) 67701-36-4
84	p-Aminophenol	123-30-8
85	1-Hydroxyethyl-4,5-Diamino Pyrazole Sulfate	155601-30-2
86	4-Formyl-1-Methylquinolinium-p-Toluenesulfonate	223398-02-5
87	Basic Yellow 87	68259-00-7
88	Basic Orange 31	97404-02-9
89	2,6-Diamino-3-((Pyridine-3-yl)azo)Pyridine	28365-08-4
90	Basic Violet 2	3248-91-7
91	2,3-Diaminodihydropyrazolopyrazolone Dimethosulfonate	857035-95-1
92	Picramic Acid and Sodium Picramate	96-91-3
93	2-Nitro-5-Glyceryl Methylamine	80062-31-3
94	HC Blue 16	502453-61-4
95	5-Amino-6-Chloro-o-Cresol; 5-Amino-6-Chloro-o-Cresol HCl	84540-50-1; 80419-48-3
96	2,2'-Methylenebis-4-aminophenol HCl	27311-52-0
97	2,6-Diaminopyridine	141-86-6
98	HC Blue No 17	16517-75-2

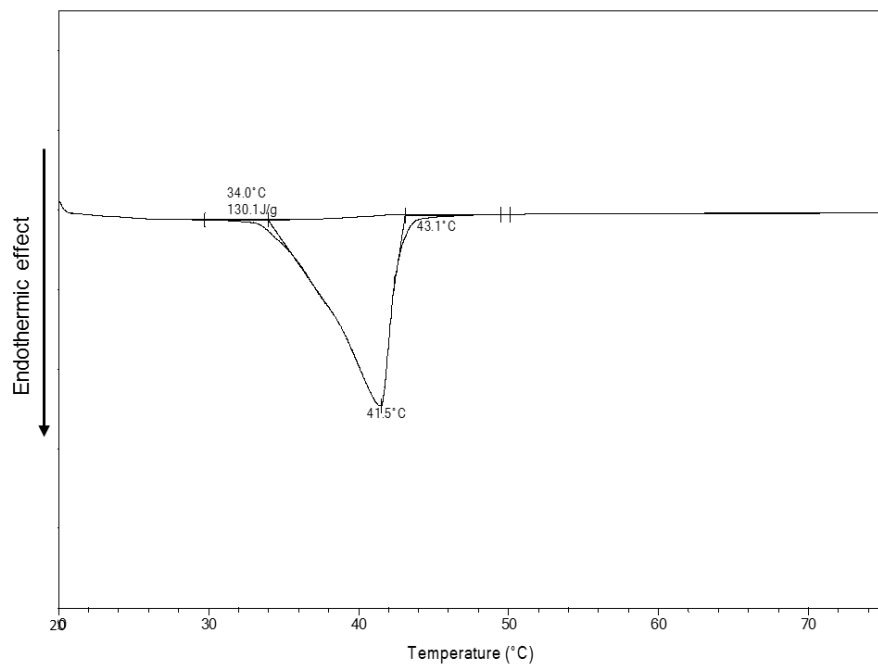
No.	INCI Name	CAS No.
99	HC Blue No 15	74578-10-2
100	Acid Green 25	4403-90-1
101	Acid Violet 43	4430-18-6
102	2-Methoxy-Methyl-p-Phenylenediamine 2-Methoxy-Methyl-p-Phenylenediamine Sulfate	337906-36-2 337906-37-3
103	Hydroxyanthraquinone-aminopropyl Methyl Morpholinium Methosulfate (38866-20-5)	38866-20-5
104	Disperse Red 17	3179-89-3
105	Acid Black 1	1064-48-8
106	Pigment Red 57	5858-81-1
107	HC Red No 17	1449471-67-3
108	HC Yellow No 17	1450801-55-4
109	1-Hexyl 4,5- Diamino Pyrazole Sulfate	1361000-03-4
110	2,5,6-Triamino- 4-Pyrimidinol Sulfate	1603-02-7
111	Hydroxyethoxy Aminopyrazolopyridine HCl	1079221-49-0
112	3-Amino-2,6- Dimethylphenol	6994-64-5
113	Basic Brown 17	68391-32-2
114	Basic Blue 124	67846-56-4

7.2. Thermal behavior of the ionic system

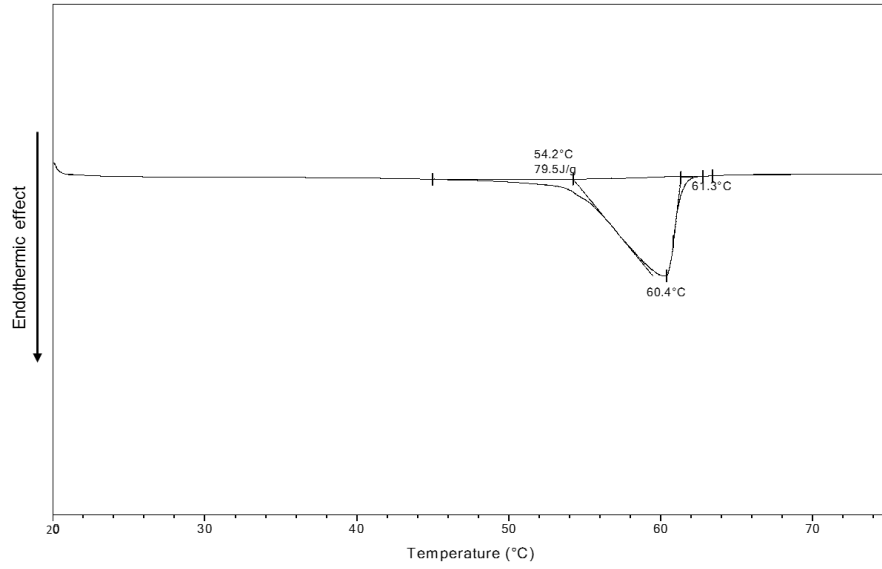
7.2.1. DSC thermograms of the raw materials contained in the ionic systems



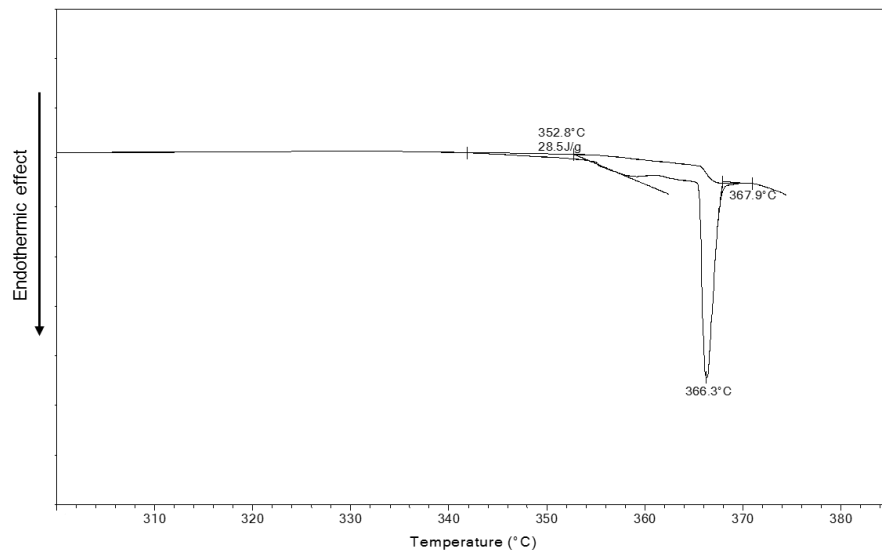
Appendix 7.2.i. DSC thermograms of ceteryl alcohol measured between 20°C and 70°C at a heating rate of 2K/min.



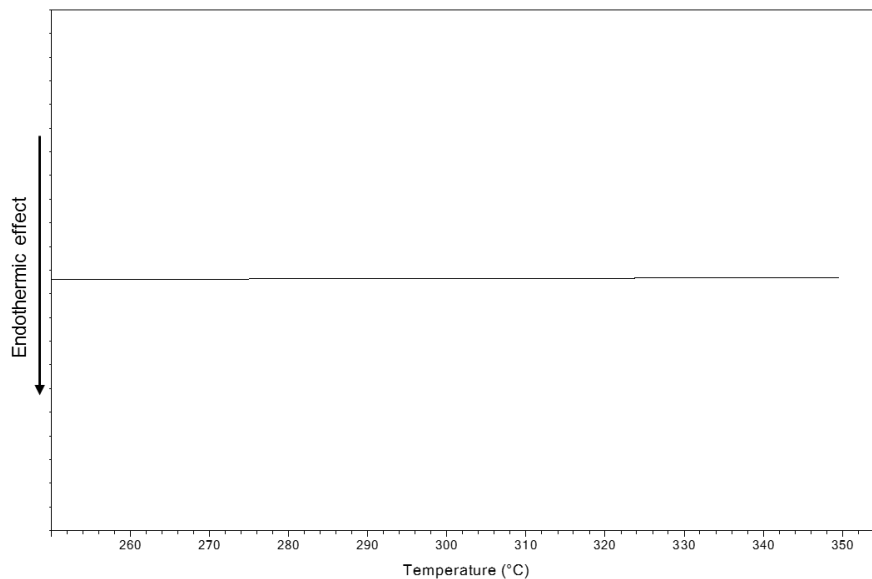
Appendix 7.2.ii. DSC thermograms of PEG-20 cetyl/stearyl ether measured between 20°C and 70°C at a heating rate of 2K/min.



Appendix 7.2.iii. DSC thermograms of glyceryl monostearate measured between 20°C and 70°C at a heating rate of 2K/min.

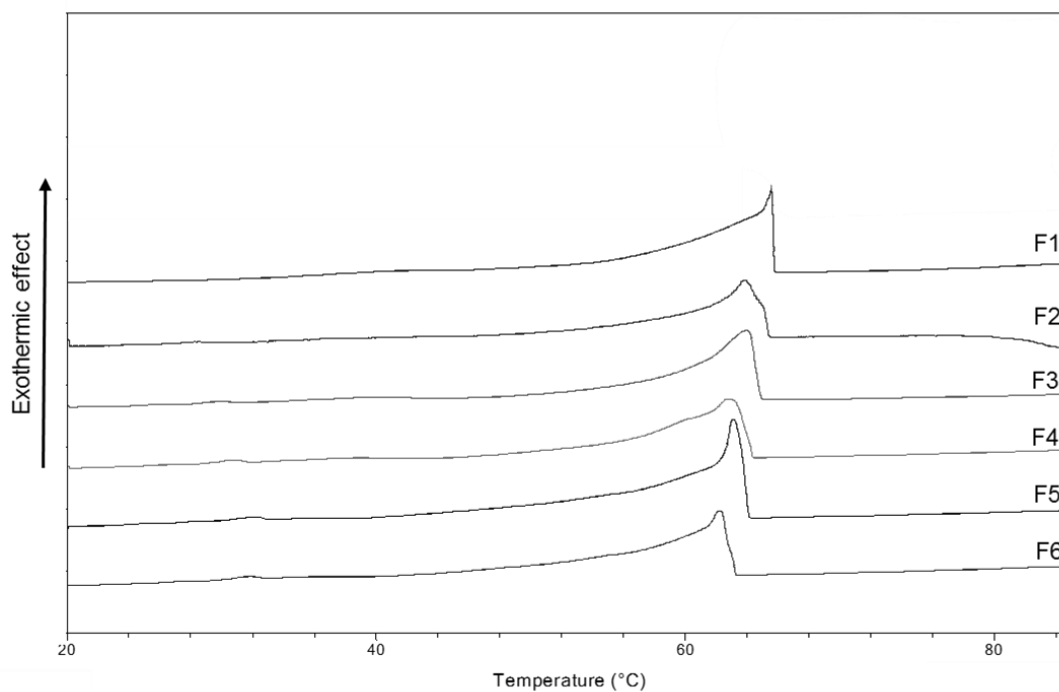


Appendix 7.2.iv. DSC thermograms of ammonium sulfate measured between 20°C and 70°C at a heating rate of 2K/min.



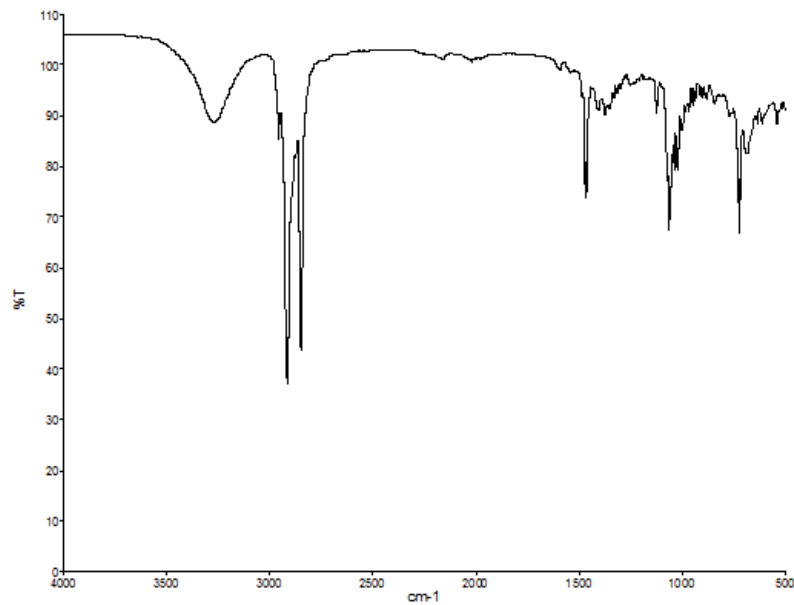
Appendix 7.2.v. DSC thermograms of PTD measured between 20°C and 70°C at a heating rate of 2K/min.

7.2.2. DSC thermograms of the ionic systems – Cooling run

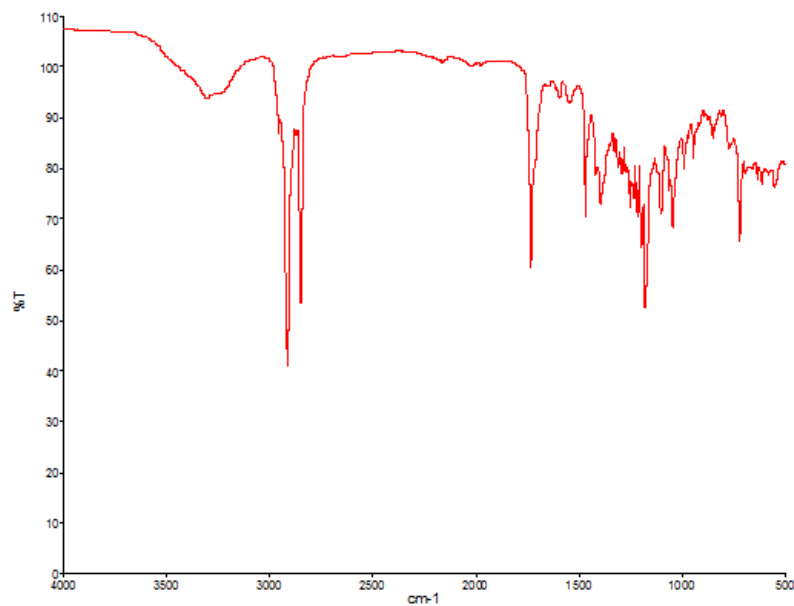


Appendix 7.2.vi. DSC thermograms of the ionic samples F1 to F6 containing from 0 to 7.0 w% PTD in the second cooling run. Cooling run from 85 to 20°C at a constant heating rate of 2K/min.

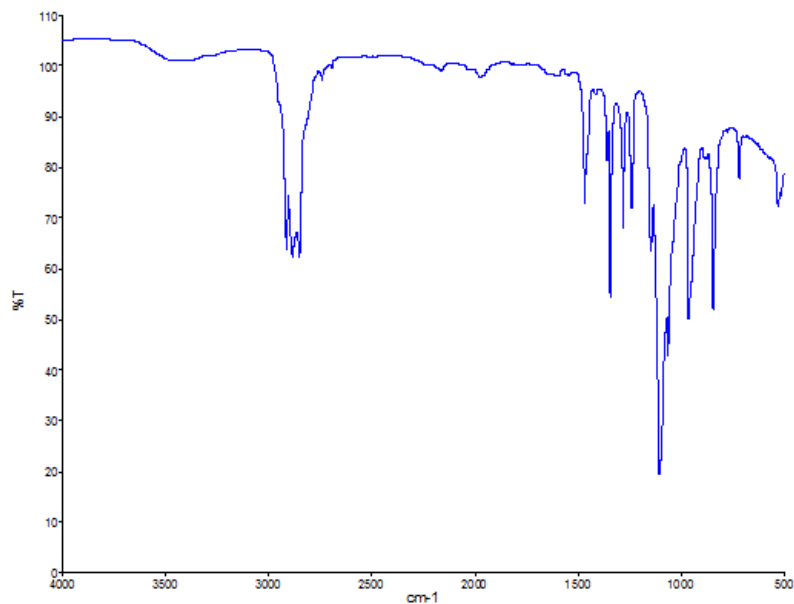
7.3. ATR-FTIR spectra of the raw materials contained in the ionic system



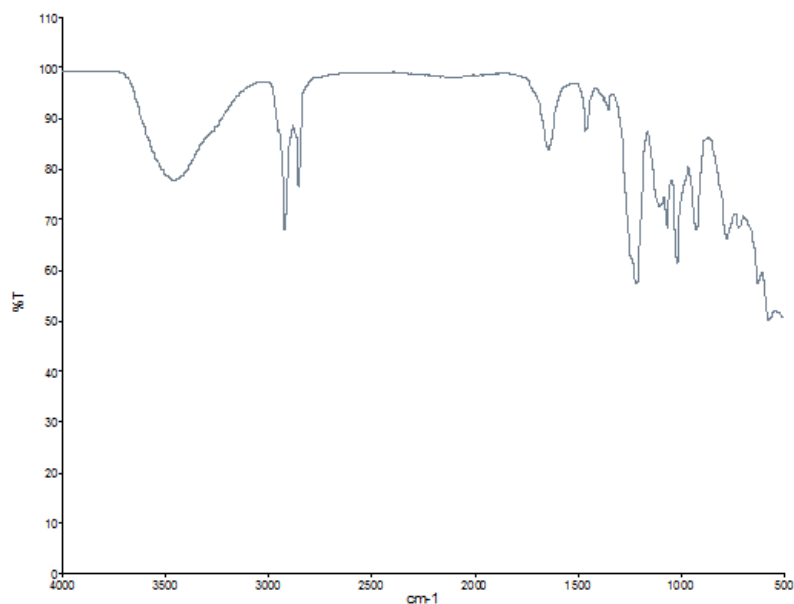
Appendix 7.3.i. ATR-FTIR spectrum of ceteryl alcohol. The spectrum is measured at RT using UATR-technique with a diamond-KRS-5 (Thallium Bromoiodide) crystal.



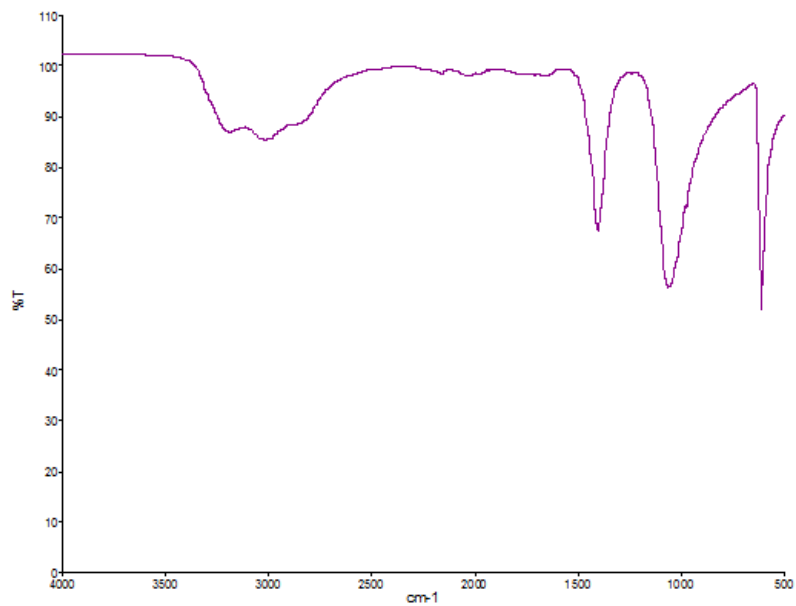
Appendix 7.3.ii. ATR-FTIR spectrum of glyceryl monostearate. The spectrum is measured at RT using UATR-technique with a diamond-KRS-5 (Thallium Bromoiodide) crystal.



Appendix 7.3.iii. ATR-FTIR spectrum of PEG-20 cetyl/stearyl ether. The spectrum is measured at RT using UATR-technique with a diamond-KRS-5 (Thallium Bromoiodide) crystal.

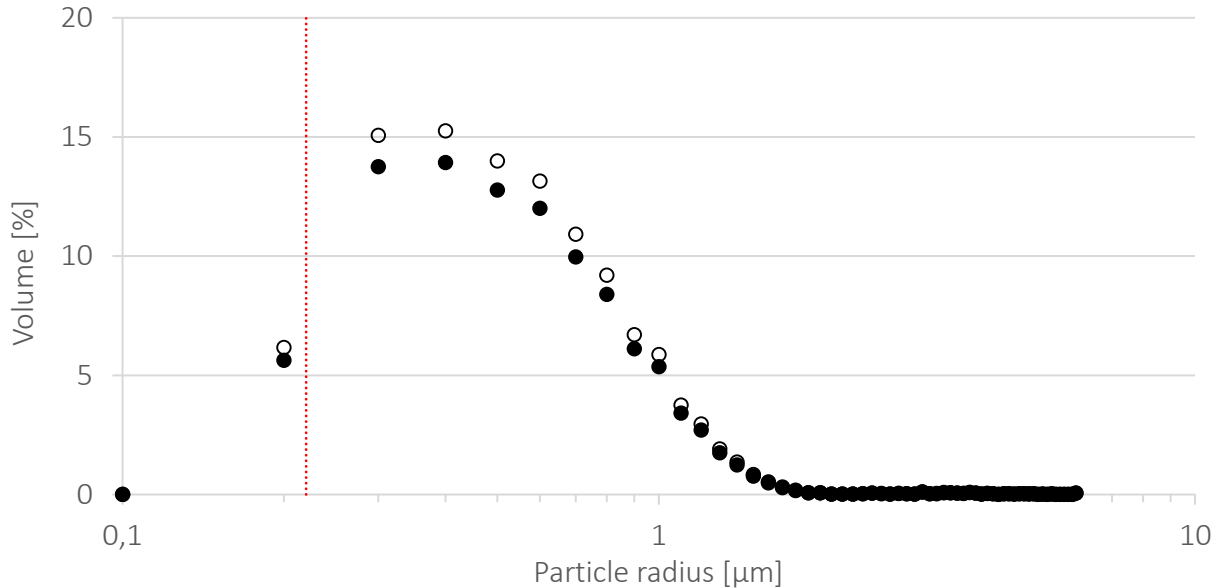


Appendix 7.3.iv. ATR-FTIR spectrum of SLES. The spectrum is measured at RT using UATR-technique with a diamond-KRS-5 (Thallium Bromoiodide) crystal.

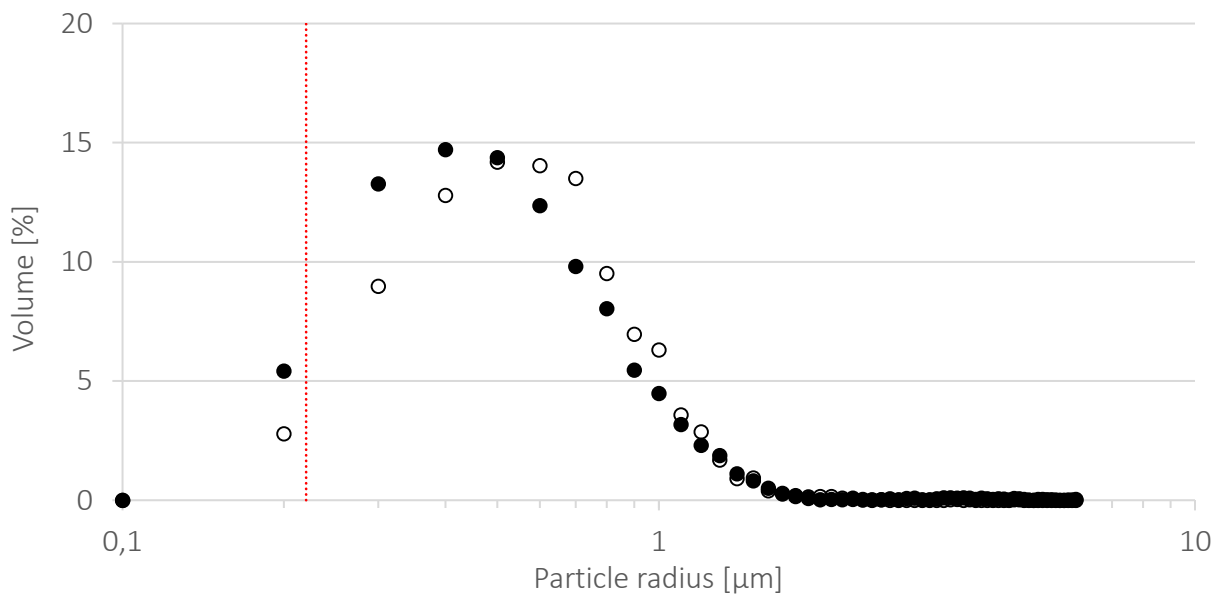


Appendix 7.3.v. ATR-FTIR spectrum of ammonium sulfate. The spectrum is measured at RT using UATR-technique with a diamond-KRS-5 (Thallium Bromoiodide) crystal.

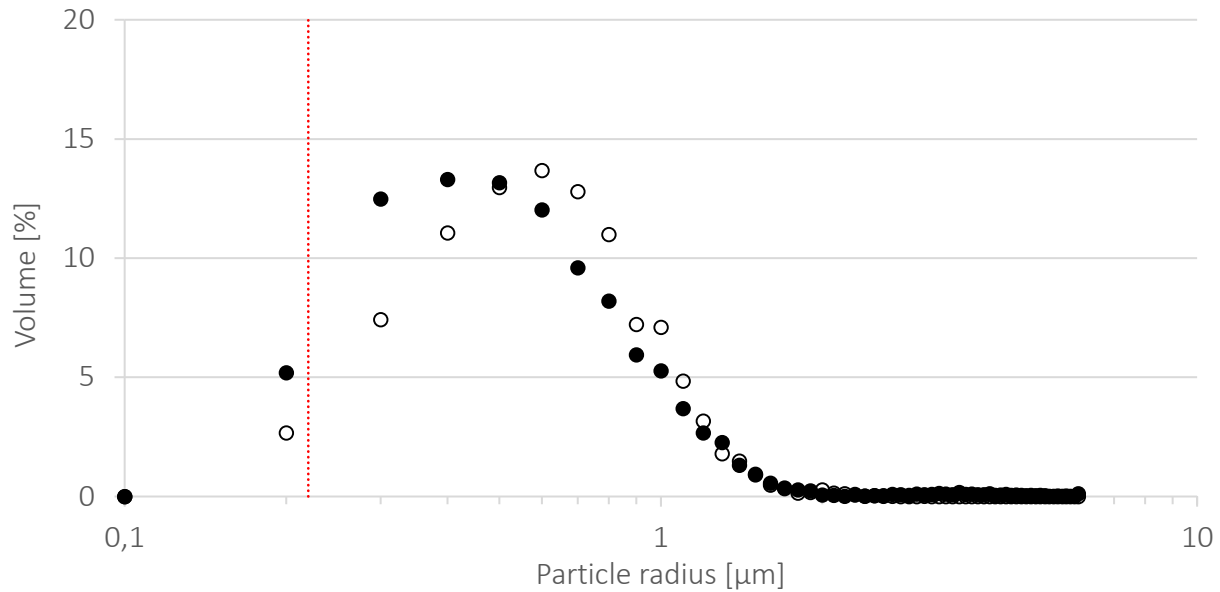
7.4. Particle size measurement of the nonionic hair coloring product



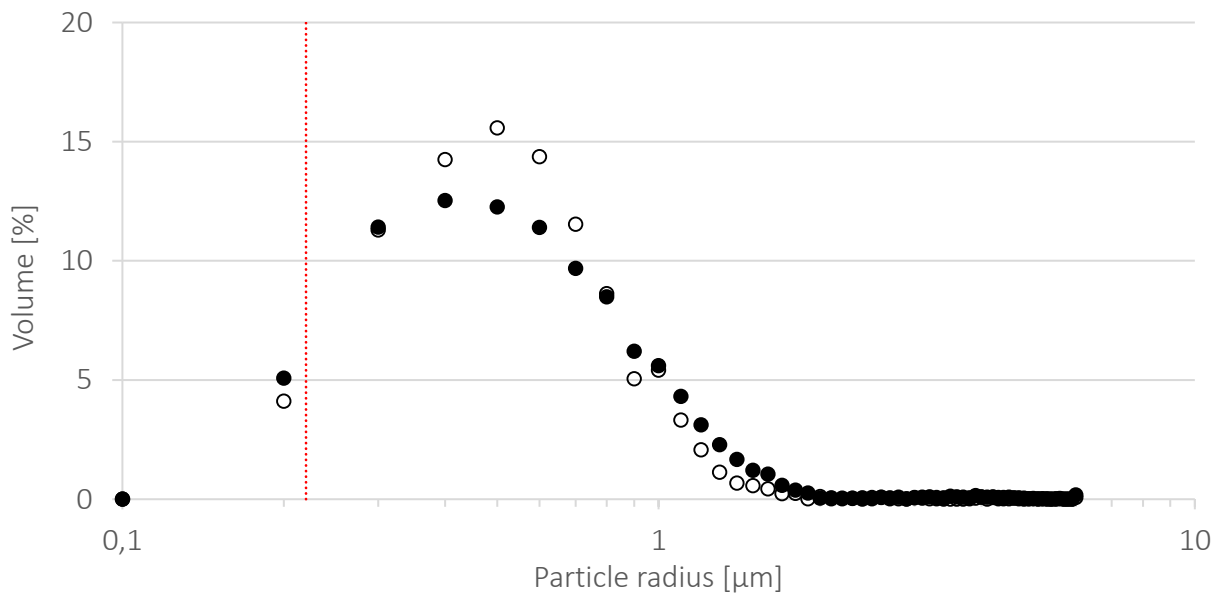
Appendix 7.4.i. Size distribution (radius [μm]) of G0 (0.00 w% PTD) using PC microscopy (total magnification x200) at t0 (●) and after 3 months storage at RT (○). Number of particles counted at t0 and 3 months: 13873, 12661, respectively. The red dotted line represents the microscope limit of detection: particles with radius smaller than 0.22 μm .



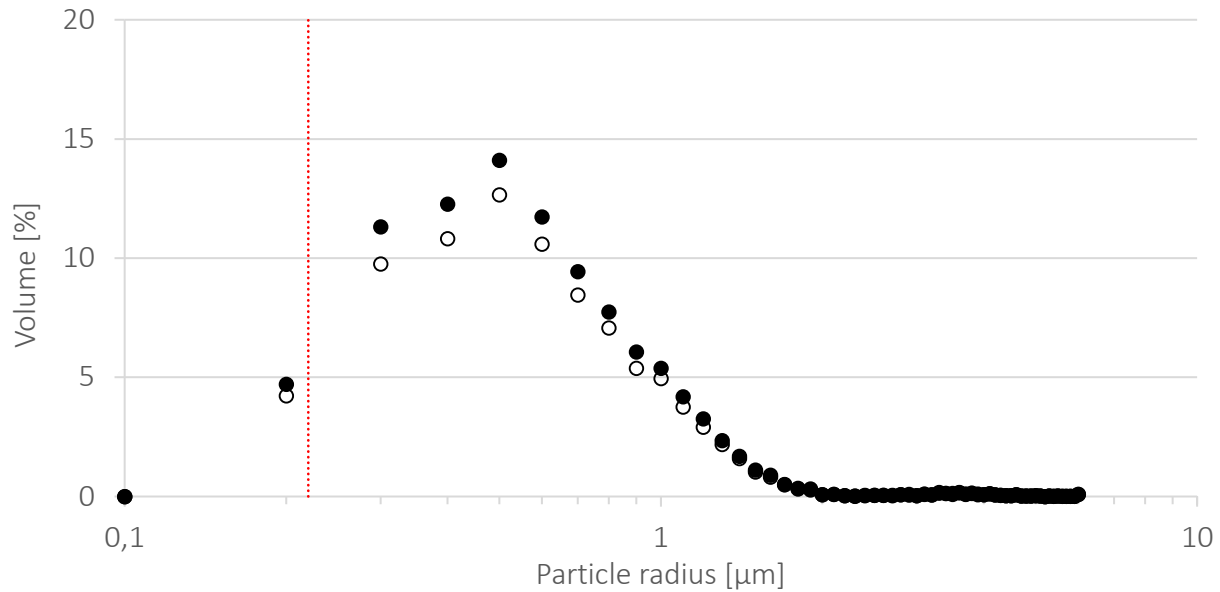
Appendix 7.4.ii. Size distribution (radius [μm]) of H1 (0.17 w% PTD) using PC microscopy (total magnification x200) at t0 (●) and after 3 months storage at RT (○). Number of particles counted at t0 and 3 months: 10392, 8582, respectively. The red dotted line represents the microscope limit of detection: particles with radius smaller than 0.22 μm .



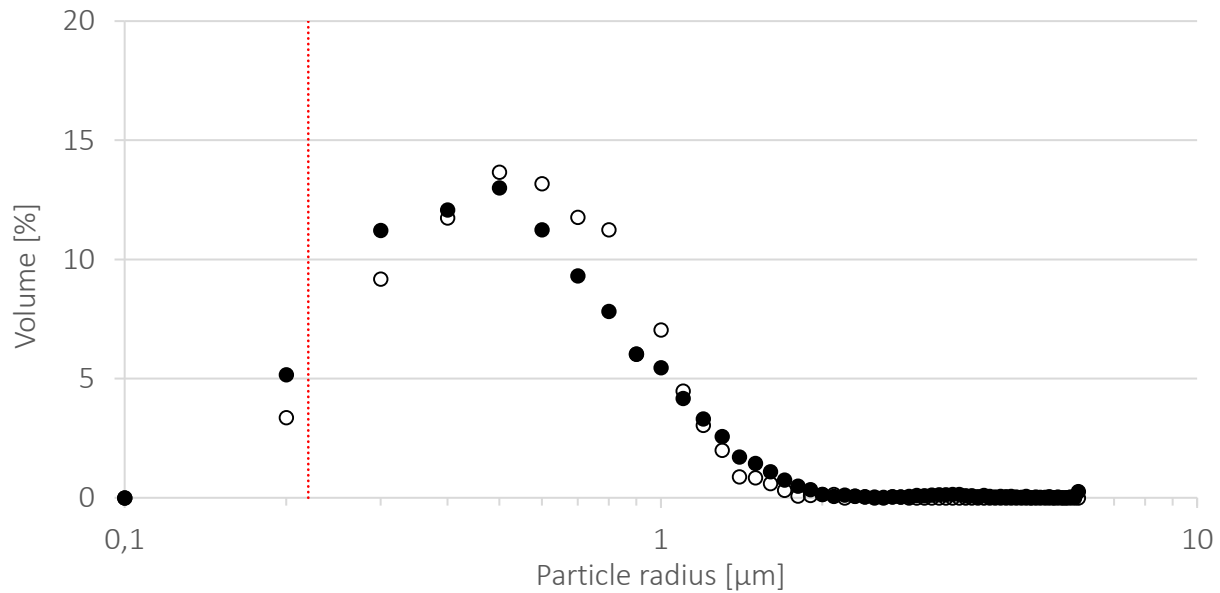
Appendix 7.4.iii. Size distribution (radius $[\mu\text{m}]$) of H2 (0.83 w% PTD) using PC microscopy (total magnification $\times 200$) at t0 (\bullet) and after 3 months storage at RT (\circ). Number of particles counted at t0 and 3 months: 10689, 7229, respectively. The red dotted line represents the microscope limit of detection: particles with radius smaller than $0.22 \mu\text{m}$.



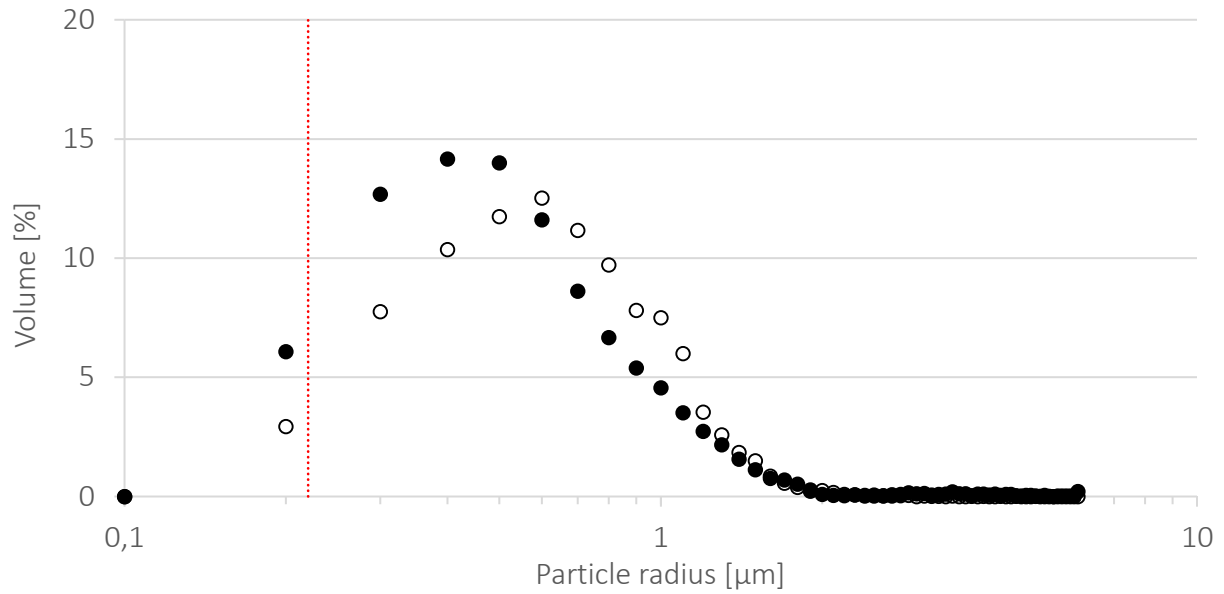
Appendix 7.4.iv. Size distribution (radius $[\mu\text{m}]$) of H3 (1.67 w% PTD) using PC microscopy (total magnification $\times 200$) at t0 (\bullet) and after 3 months storage at RT (\circ). Number of particles counted at t0 and 3 months: 12434, 7428, respectively. The red dotted line represents the microscope limit of detection: particles with radius smaller than $0.22 \mu\text{m}$.



Appendix 7.4.v. Size distribution (radius [μm]) of H4 (3.33 w% PTD) using PC microscopy (total magnification x200) at t0 (●) and after 3 months storage at RT (○). Number of particles counted at t0 and 3 months: 12457, 8824, respectively. The red dotted line represents the microscope limit of detection: particles with radius smaller than 0.22 μm.



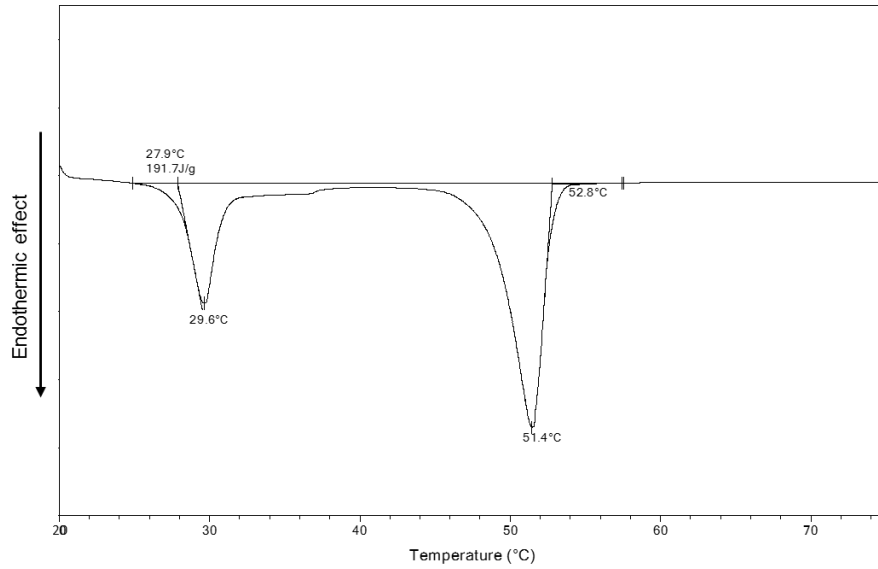
Appendix 7.4.vi. Size distribution (radius [μm]) of H5 (5.00 w% PTD) using PC microscopy (total magnification x200) at t0 (●) and after 3 months storage at RT (○). Number of particles counted at t0 and 3 months: 13452, 7854, respectively. The red dotted line represents the microscope limit of detection: particles with radius smaller than 0.22 μm.



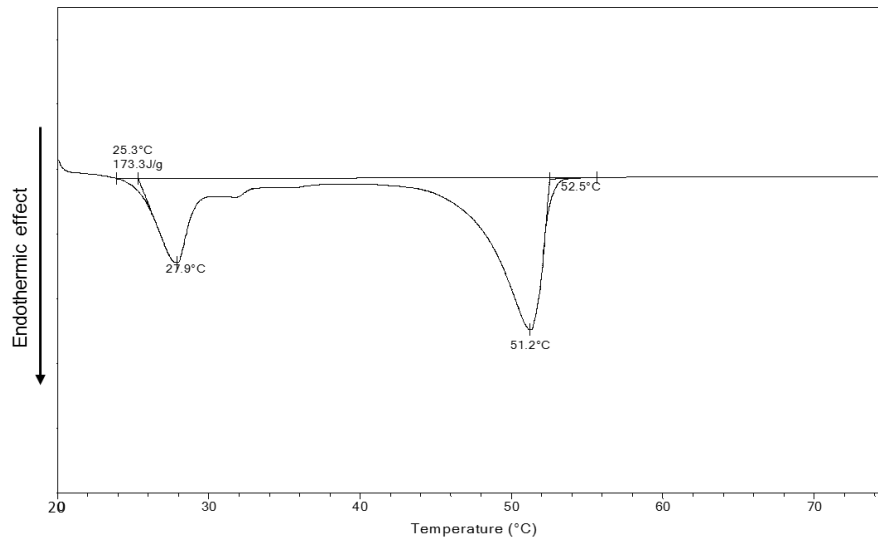
Appendix 7.4.vii. Size distribution (radius [μm]) of H6 (6.67 w% PTD) using PC microscopy (total magnification $\times 200$) at t0 (●) and after 3 months storage at RT (○). Number of particles counted at t0 and 3 months: 12973, 8484, respectively. The red dotted line represents the microscope limit of detection: particles with radius smaller than $0.22 \mu\text{m}$.

7.5. Thermal behavior of the nonionic system

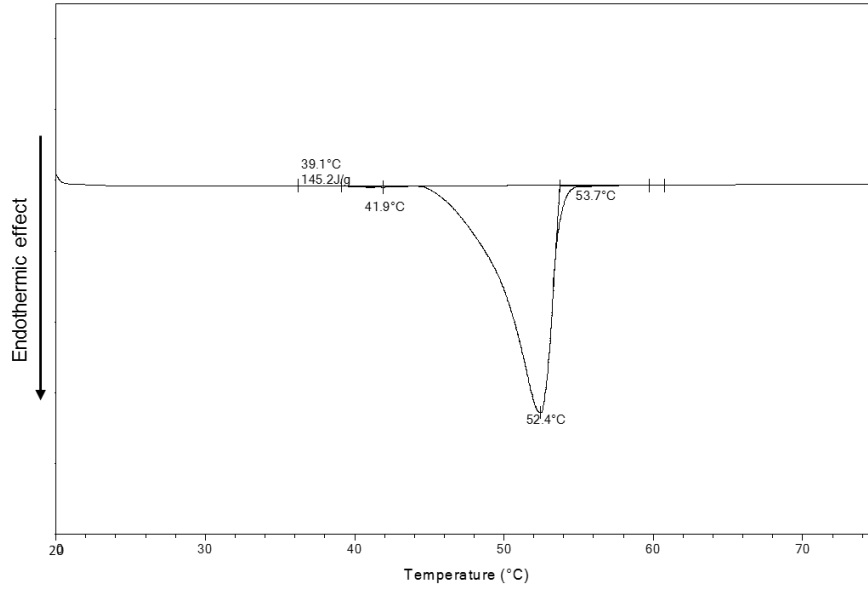
7.5.1. DSC thermograms of the raw materials contained in the nonionic system



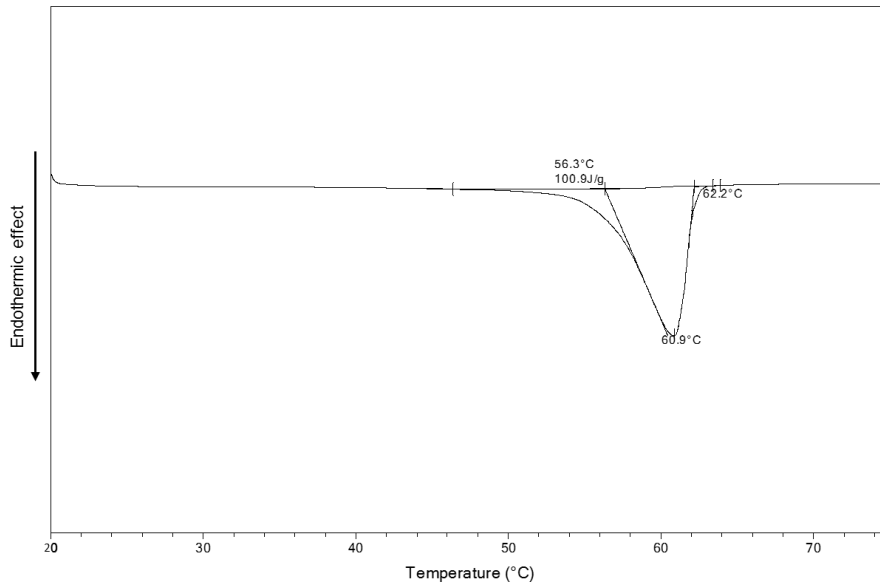
Appendix 7.5.i. DSC thermograms of cetaryl alcohol measured between 20°C and 70°C at a heating rate of 2K/min.



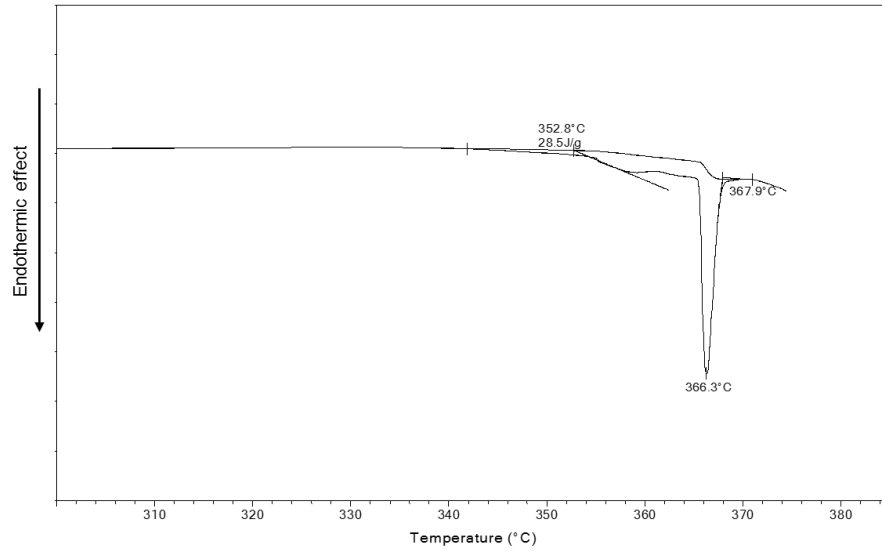
Appendix 7.5.ii. DSC thermograms of PEG-2 cetyl/stearyl ether measured between 20°C and 70°C at a heating rate of 2K/min.



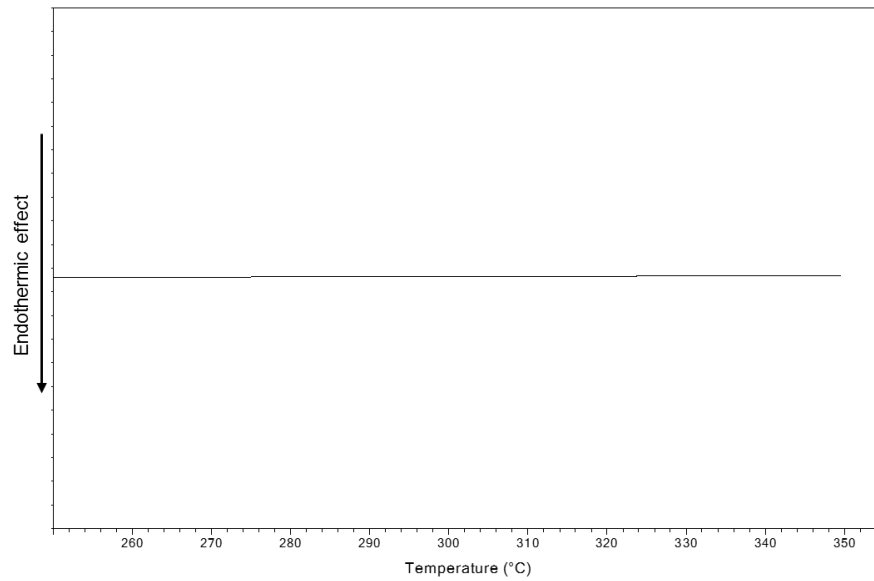
Appendix 7.5.iii. DSC thermograms of PEG-50 cetyl/stearyl ether measured between 20°C and 70°C at a heating rate of 2K/min.



Appendix 7.5.iv. DSC thermograms of glyceryl monostearate measured between 20°C and 70°C at a heating rate of 2K/min.

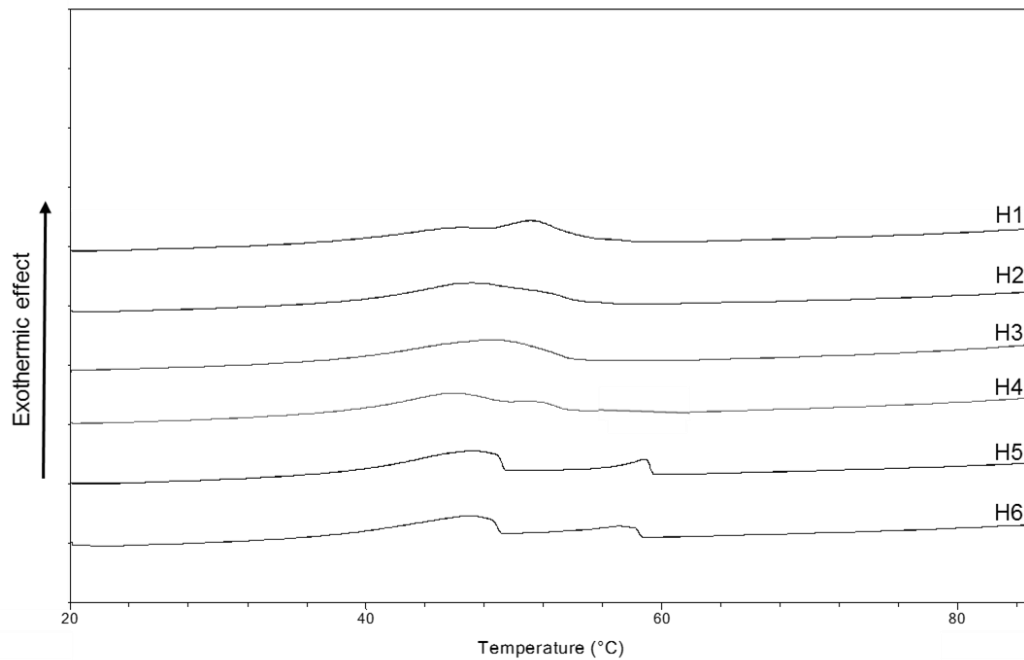


Appendix 7.5.v. DSC thermograms of ammonium sulfate measured between 20°C and 70°C at a heating rate of 2K/min.

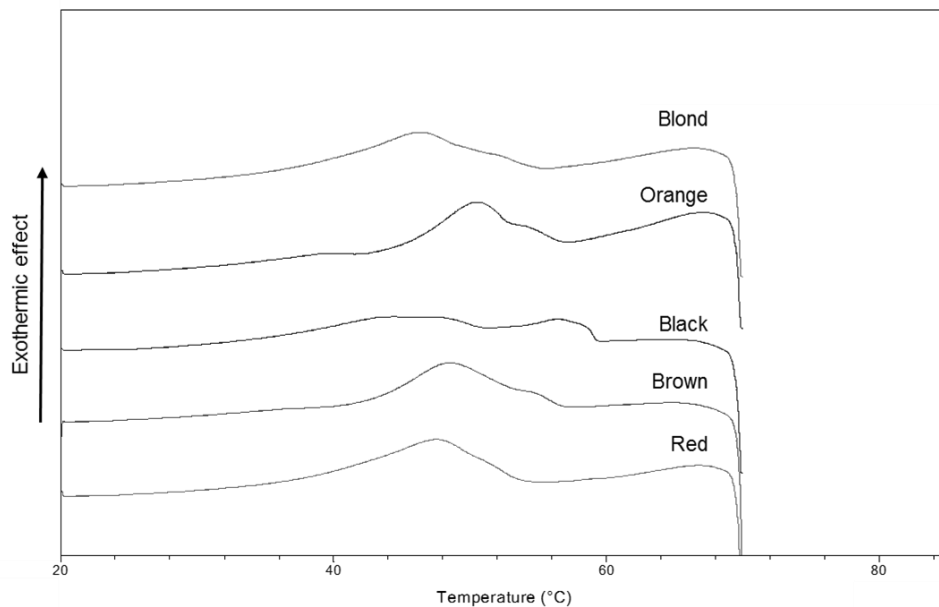


Appendix 7.5.vi. DSC thermograms of PTD measured between 20°C and 70°C at a heating rate of 2K/min.

7.5.2. DSC thermograms of the nonionic systems - Cooling run

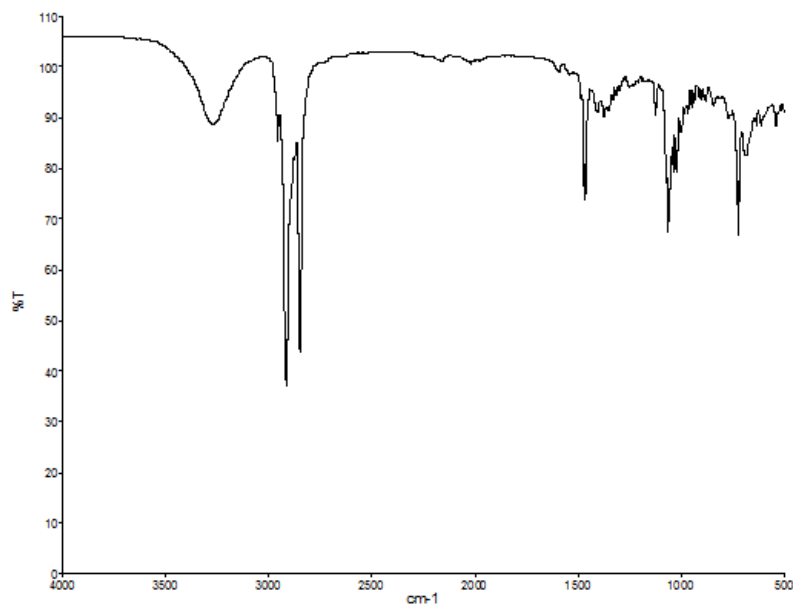


Appendix 7.5.vii. DSC thermograms of the ionic samples H1 to H6 containing from 0 to 7.0 w% PTD in the second cooling run. Cooling run from 85 to 20°C at a constant heating rate of 2K/min.

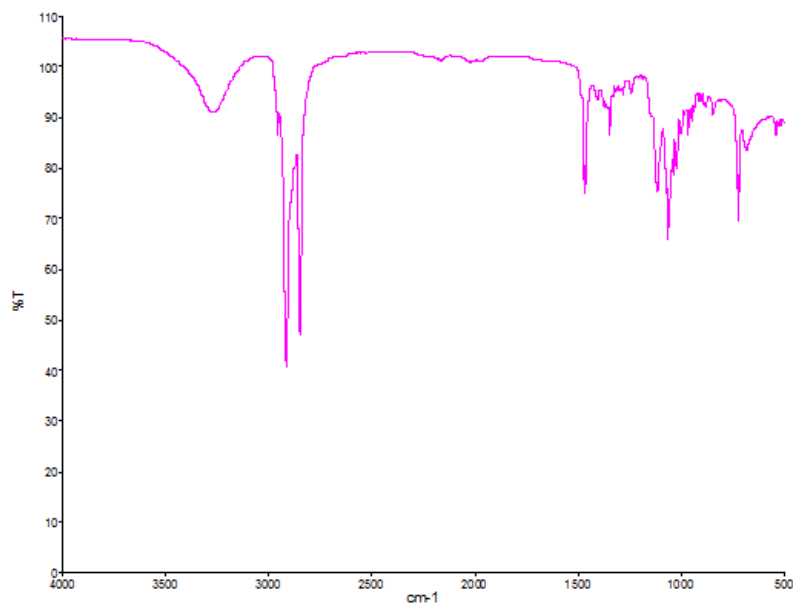


Appendix 7.5.viii. DSC thermograms of the ionic samples H1 to H6 containing different hair dyes mixtures (shades: black, brown, red, orange, blond) in the second cooling run. Cooling run from 70 to 20°C at a constant heating rate of 2K/min.

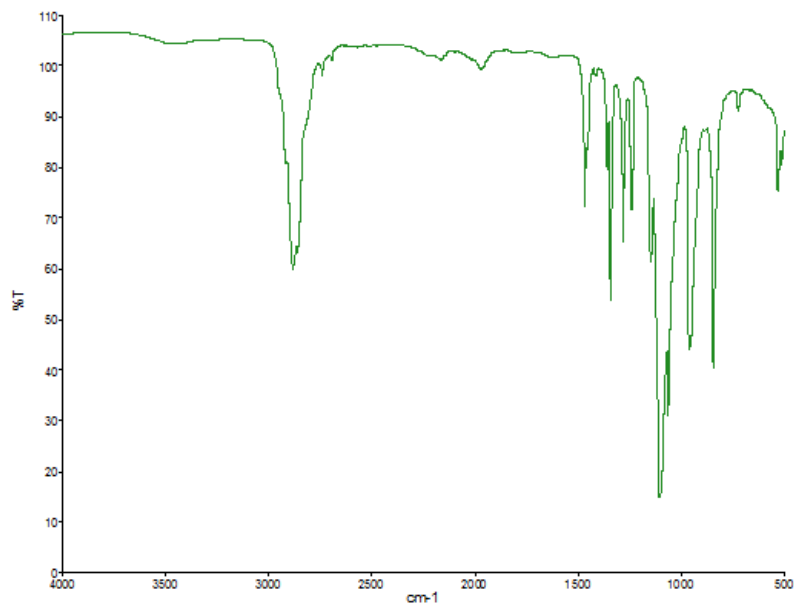
7.6. ATF-FTIR spectra of the raw materials contained in the nonionic system



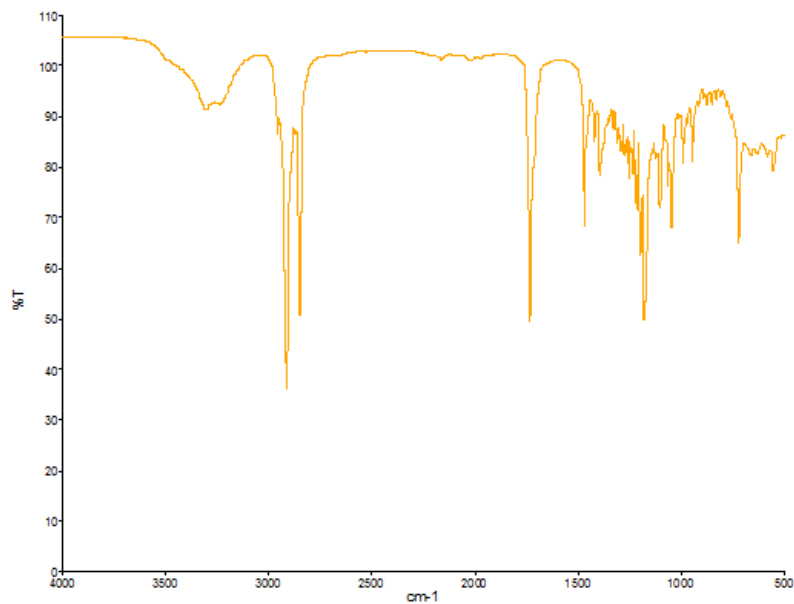
Appendix 7.6.i. ATR-FTIR spectrum of ceteryl alcohol. The spectrum is measured at RT using UATR-technique with a diamond-KRS-5 (Thallium Bromoiodide) crystal.



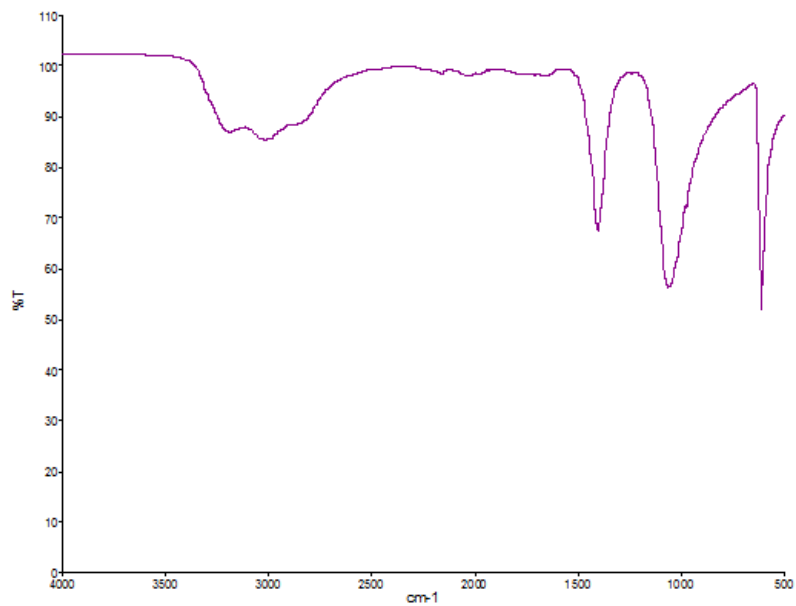
Appendix 7.6.ii. ATR-FTIR spectrum of PEG-2 cetyl/stearyl ether. The spectrum is measured at RT using UATR-technique with a diamond-KRS-5 (Thallium Bromoiodide) crystal.



Appendix 7.6.iii. ATR-FTIR spectrum of PEG-50 cetyl/stearyl ether. The spectrum is measured at RT using UATR-technique with a diamond-KRS-5 (Thallium Bromiodide) crystal.



Appendix 7.6.iv. ATR-FTIR spectrum of glyceryl monostearate. The spectrum is measured at RT using UATR-technique with a diamond-KRS-5 (Thallium Bromiodide) crystal.



Appendix 7.6.v. ATR-FTIR spectrum of ammonium sulfate. The spectrum is measured at RT using UATR-technique with a diamond-KRS-5 (Thallium Bromoiodide) crystal.

7.7. Additional specific evaluations for cosmetic and industrial purposes

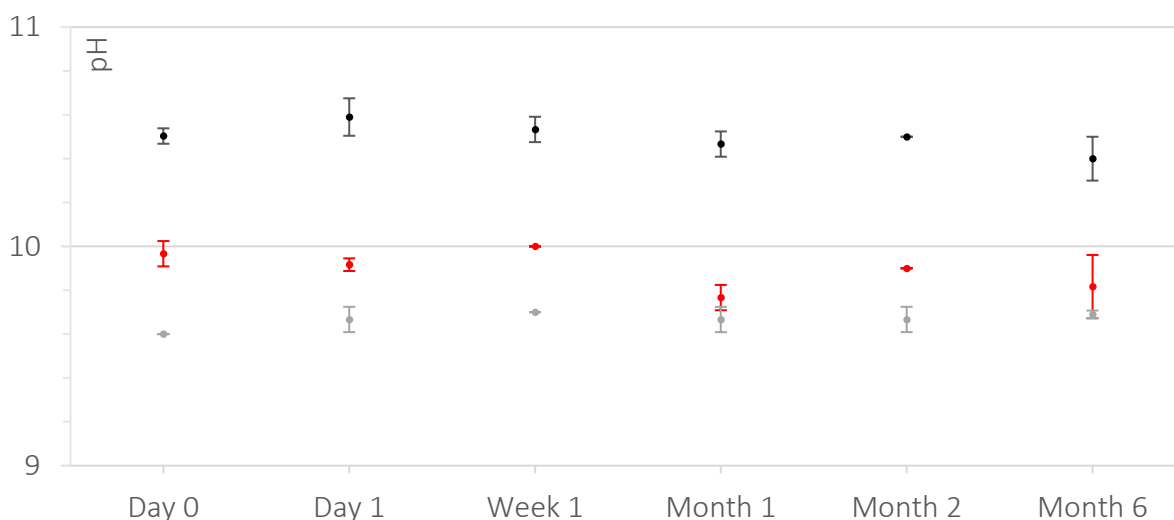
Additional specific evaluations are necessary to assess whether the optimized nonionic systems are compatible with further industrial developments. Firstly, a scale-up study enabled to test the robustness of some nonionic systems containing PTD. Subsequently, classical stability tests and a color delivery assessment were performed with systems containing real existing hair-dyes-mixtures. These changes in salt content and nature are bringing gradually the optimized system closer to a marketable formula.

The given specifications were:

- (i) pH of the hair coloring creams such as: $9.0 < \text{pH} < 11.0$
- (ii) Viscosity of the coloring creams such as: $8.0 < \eta < 30.0 \text{ Pa}\cdot\text{s}$
- (iii) Visual macroscopic evaluation showing no inhomogeneity
- (iv) Satisfying color delivery on real human hair strands (in-vitro, in the laboratory and in-vivo in a specialized test-salon) compared to reference hair coloring products
- (v) Toxicity acceptance

7.7.1. Scale-up

For ensuring the possibility to transfer the optimized nonionic formulation to an industrial scale, a simple scale-up study was performed. To do so, 15 kilos of H3, H5 and H6 were formulated in a pilot reactor. Each cream was formulated three times in the same processing conditions. The pH, storage modulus, critical strain, cream viscosity and mixture viscosity (hair coloring product and developer), were monitored at day 0, day 1, week 1, month 1, month 2 and month 6, after production. The key factors for the product development (η and pH) will be discussed in this chapter. All the other factors are summarized in tables in [Appendix 7.7.4.](#) The cream viscosity and the pH values of the nonionic creams are presented in [Appendix 7.7.i.](#) and [Appendix 7.7.ii.](#), respectively.

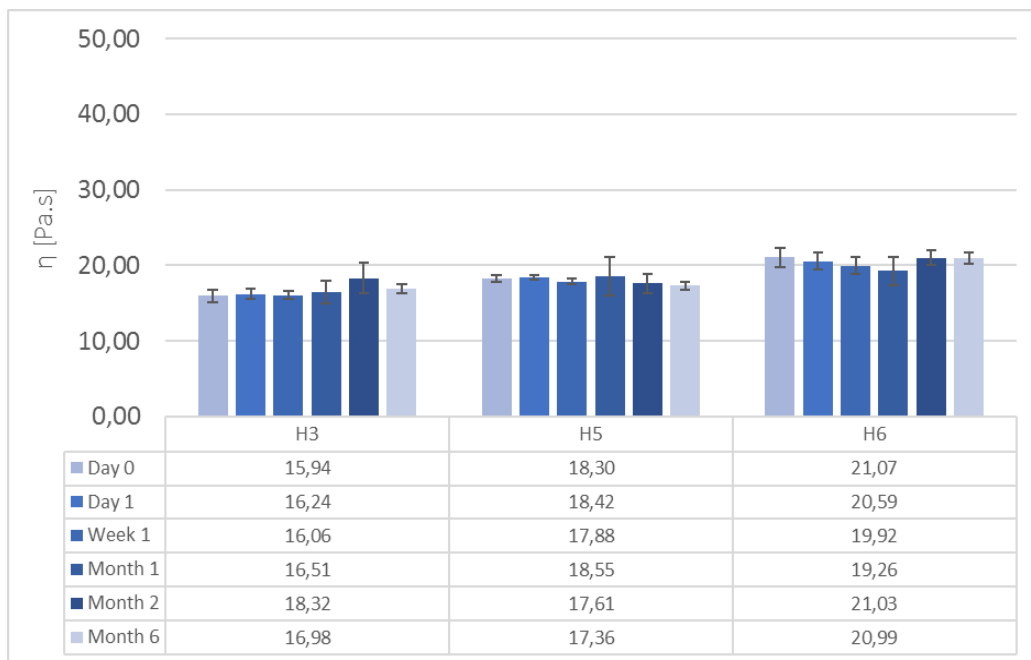


Appendix 7.7.i. Average pH values of (•) H3, (•) H5 and (*) H6 directly after production and up to 6 months storage at RT. pH values were measured at 20°C. The whiskers above and below the average pH values define the $av. \pm std. dev.$

The pH value of the hair coloring products is crucial for the colorants delivery in the hair fiber. The color delivery will be assessed in [7.7.3. Color delivery.](#) Directly after production, H3, H5 and H6 showed significant different average pH values of 10.50, 9.97 and 9.60, respectively. Over time, some minor fluctuations were observed. These fluctuations were significantly different only for H5 at week 1 and month 1. Overall, all pH values ranged between 9.6 and 10.5. These values were fulfilling the conditions postulated in the beginning of this chapter. It is interesting to note that the significant decrease of the pH-value was in correlation with the increasing PTD concentration. This might be due to the acid-base neutralization of the sulfuric counter-ions associated to the PTD hair-dyes.

The second key factor for product development is the viscosity of the hair coloring product directly after production and over time. Indeed, this factor impacts the efficacy

of the production line, the good color delivery, the ease of mixing with the developer and the proper application of the product on the hair. Directly after production, the nonionic creams exhibited viscosities between 16 and 21 Pa.s. This gap was minimized after 6 months, as H3, H5 and H6 showed viscosities between 17 and 21 Pa.s. It was shown earlier that the nonionic creams containing at least 0.1 w% of salts exhibited viscosities between 14 and 18 Pa.s. These differences were expected as more energy is transmitted in the 15 kg batches during the homogenization step than with a simple propeller in the lab-scale samples. However, the gap in viscosities between low and high electrolytes content remained low $\Delta\eta_{\text{nonionic 15kg}} = 5 \text{ Pa.s}$.



Appendix 7.7.ii. Average viscosity η of H3, H5 and H6 directly after production and up to 6 months storage at RT. η values were measured at 20°C. The whiskers above and below the average η values define the av. \pm std. dev.

Note: all the viscosity values are in Pa.s

In conclusion, all data i.e. pH, η , $\eta_{\text{mix.}}$, G' , and γ_c showed few significant differences after 6 months of storage at RT. Therefore, it can be assumed that:

- The nonionic creams can be formulated at a bigger scale in a reproducible manner
- The salt content is having minor impact on the hair coloration products
- The nonionic creams are robust towards salt addition and ageing at a pilot scale

The scale-up study confirmed that the nonionic creams are fulfilling the conditions (i), and (ii) listed in the [beginning of this chapter](#).

7.7.2. Stability tests

The viscosity at RT, -10°C and +40°C and the pH values at RT were monitored at t0 (24 hours after the preparation), week 4, 8, 12 and 24 for all the nonionic creams containing a dye stuff mixture. These measurements have been conducted only once. Therefore, no statistical evaluation was done. The viscosity measurements at RT are presented in [Appendix 7.7.iii.](#) All the data concerning the viscosity and pH measurements are summarized in tables in [7.7.5. Storage tests results of the nonionic creams containing hair dyes mixtures.](#)



Appendix 7.7.iii. Viscosity of the nonionic creams and the reference ionic creams (shades: black, brown, orange, red, and blond) from t0 to month 6 storage at RT. The viscosity η is measured at $\dot{\gamma} = 7,2 \text{ s}^{-1}$ at 20°C.

Note: all the viscosity values are in Pa.s

The reference chosen as a comparison for the viscosity measurement is a classical ionic hair coloring product containing the same dye-stuff mixtures than the nonionic creams. Their viscosities were measured at t ∞ , which is equivalent to the week 24 for the nonionic system. For the nonionic creams, some fluctuations in viscosities were observed at RT. It is interesting to note that the nonionic creams containing a dye mixture exhibited higher viscosities than H1 to H6. These differences could come from the processing techniques: H1 to H6 were prepared in small batches and mixed with a propeller. On the other hand, the nonionic shades were prepared in larger amount with a laboratory mixer equipped with a homogenization stirrer. Therefore, the viscosities of the nonionic shades are similar to the creams formulated during the scale-up study. The differences between the lowest and the highest viscosities, all shades included, were equal to 4.68 Pa.s (RT, t ∞) for the

nonionic creams. The reference creams exhibited a $\Delta\eta$ equal to 16.40 Pa.s (RT, t_∞). This means, that the viscosity fluctuations between several shades containing hair-dyes mixtures of different concentrations and natures, were reduced of 70% by using a nonionic surfactant system. These results are detailed in [Appendix 7.7.iv.](#) This table highlights the benefit of using a nonionic surfactant system rather than a ionic one in terms of viscosity robustness.

Appendix 7.7.iv. Comparison of the viscosity fluctuations $\Delta\eta$ for the two hair-coloring systems: ionic surfactant system vs nonionic surfactant system containing different kind of electrolytes.

	Ionic system		Nonionic system	
Ammonium sulfate	X*			
PTD			X***	
Hair-dyes mixture	X**		X	
$\Delta\eta$ **** [Pa.s]	12.80	16.40	1.06	4.68
Reduction of η fluctuations compared to the ionic classical system [%]	-	-	-92	-71

* Ionic systems E1 to E7.

** Reference hair coloring products.

*** Nonionic systems H1 to H6.

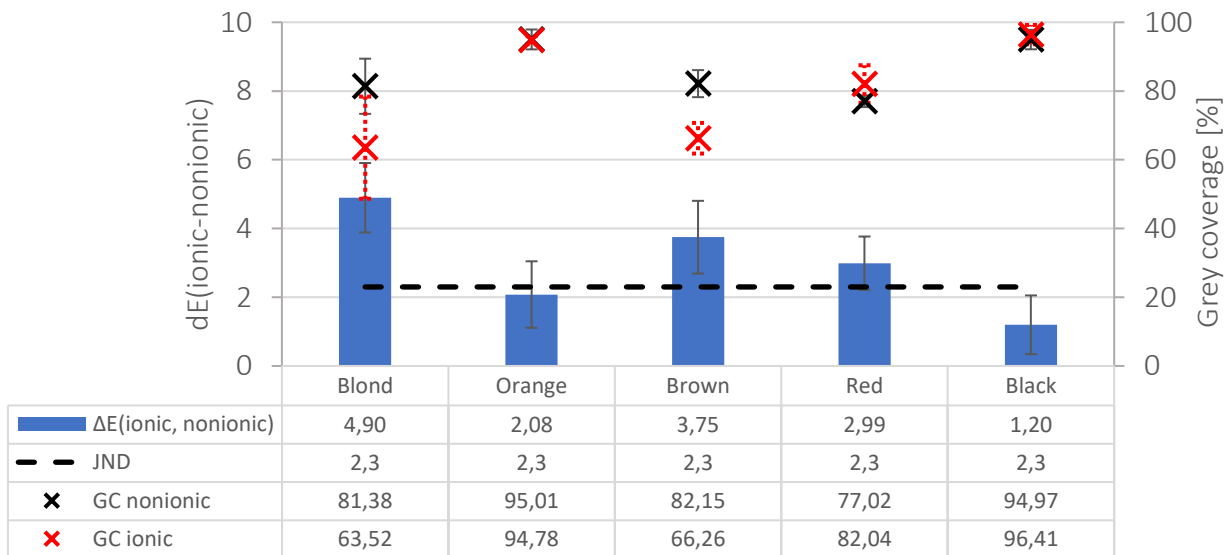
**** $\Delta\eta$ is defined by the difference between the highest and the lowest viscosity of a system containing different concentrations of salts.

The pH values of the new nonionic creams containing hair-dyes mixtures were fulfilling the conditions postulated in the [beginning of this chapter](#) for all storage temperatures between t_0 and week 24. They ranged between 9.43 and 10.87. Moreover, no macroscopic instability factors (change of color, inhomogeneity, phase separation etc.) were observed during the storage test. The stability tests confirmed that the nonionic creams are fulfilling the conditions (i), (ii) and (iii) listed in the [beginning of this chapter](#).

7.7.3. Color delivery

The batches from the above-chapter ([7.7.2. Stability tests](#)) were used for the color delivery assessment. The creams were tested on human hair strands in the laboratory (in-vitro) and subsequently on models in a specialized test salon (in-vivo). Beforehand, the safety data of each raw material contained in the nonionic and ionic creams were evaluated and cleared by toxicological experts. All ingredients were judged as safe for this product category i.e. hair coloring products, especially with respect to each ingredient's concentration and with respect to the intended and reasonably foreseeable use conditions. Two parameters were calculated to evaluate the color delivery of the nonionic creams: the grey coverage (GC) and the color difference (ΔE) between the ionic reference shades and the nonionic shades. The results are presented in [Figure 7.7.v.](#). The detailed colorimetric data are presented in tables in [7.7.6. Color delivery data](#).

It was empirically proven that the human eye can visualize a difference in color when ΔE is greater than 2.3. This limit is called the just noticeable difference (JND) [125]. As showed in [Figure 7.7.v.](#), only the black shade and the orange shade from the nonionic system were below the JND limit. The red shade exhibited a higher ΔE than 2.3 but in a not significant way. The brown and especially the blond shades exhibited a significant too high ΔE value. No correlation could be found between the amount of hair-dyes contained in the shades and ΔE . Therefore, the differences in colors probably depend on the nature of the colorants themselves.



Appendix 7.7.v. Grey coverage (GC) of the ionic reference (✕) and the nonionic (✕) shades containing different hair-dyes mixtures (blond, orange, brown, red and black), applied on human hair strands in the laboratory and the color difference ΔE (■) between these two formulations. The dashed line represents the limit of just noticeable difference (JND) at 2.3 on the ΔE axis. The whiskers above and below the average values define the $\text{av.} \pm \text{std. dev.}$

Even though the nonionic creams showed a more robust rheological behavior, they seemed to perform differently in terms of color delivery. These observations do not reveal that the nonionic systems are a not suitable system for color delivery but rather that they deliver it differently. To evaluate the color delivery performance, one must calculate the GC. This factor reveals the ability to cover gray hair, hence to deliver hair-dyes into the cortex. One can assume that, the higher the GC the more colorants are delivered in the cortex. The black, orange and red nonionic shades did not show significant differences in GC compared to the ionic reference. The blond nonionic shade exhibited a not significantly higher GC than the ionic reference. Finally, the brown nonionic shade showed a significant higher GC than the reference. Surprisingly, the GC for both systems was not in correlation with the amount of hair dyes contained in each shade. Overall, the nonionic system performed better in terms of GC than the ionic reference. This revealed that the new hair coloring product is an efficient system for hair colorants delivery. Nevertheless, the measured color results were visibly different. This color shift could be due to the different hair-dyes' repartition in the distinct phases of the nonionic system. Indeed, it was demonstrated in this study that the salts-like compounds are likely to diffuse in the interlamellar space and in the bulk-water in the ionic system. On the contrary, the hair-dyes are likely to be present only in the bulk-water in the nonionic system. The presence of a significant amount of the hair-dyes in the fixed-interlamellar water in the ionic system could be related to the less efficient color delivery. This hypothesis is in line with the GC values observed: $GC_{\text{ionic}} < GC_{\text{nonionic}}$.

To assess the color shift in real conditions (in-vitro), the same nonionic shades were tested in a blind-test in a specialized test-salon against the ionic references. The evaluation was only visual and performed by color experts under specific and controlled light conditions. The report revealed that both systems performed equally in term of GC. The same color shifts were observed, especially for the blond and brown shades.

It was already demonstrated in the literature that the hair coloring products' base components e.g. surfactants, solvent, oil, have a substantial impact on the color delivery [9]– [11]. The results of this chapter are in line with this statement. The color delivery tests did not confirm that the nonionic creams are fulfilling condition (iv) mentioned at the beginning of [7.7. Additional specific evaluation for cosmetic and industrial purposes](#).

7.7.4. Scale-up data

		i1	i2	i3	Av.	Min	Max	Std. Dev.
pH	Day 0	10,47	10,54	10,50	10,50	10,47	10,54	0,04
	Day 1	10,67	10,50	10,60	10,59	10,50	10,67	0,09
	Week 1	10,50	10,50	10,60	10,53	10,50	10,60	0,06
	Month 1	10,40	10,50	10,50	10,47	10,40	10,50	0,06
	Month 2	10,50	10,50	10,50	10,50	10,50	10,50	0,00
	Month 6	10,50	10,40	10,30	10,40	10,30	10,50	0,10
	G' [Pa]	Day 0	5536,3	4238,1	5041,9	4938,7	4238,1	5536,3
Day 1		4531,3	4770,7	4969,1	4757,0	4531,3	4969,1	219,22
Week 1		4955,2	4697,8	4219,5	4624,1	4219,5	4955,2	373,34
Month 1		3748,6	3791,8	3864,6	3801,6	3748,6	3864,6	58,63
Month 2		3646,6	3542,6	2998	3395,7	2998,0	3646,6	348,35
Month 6		2783,9	2991,1	2875	2883,3	2783,9	2991,1	103,85
γ_c		Day 0	0,0364	0,0327	0,0411	0,0367	0,0327	0,0411
	Day 1	0,0356	0,0412	0,0360	0,0376	0,0356	0,0412	0,0031
	Week 1	0,0335	0,0300	0,0335	0,0323	0,0300	0,0335	0,0020
	Month 1	0,0349	0,0312	0,0324	0,0328	0,0312	0,0349	0,0019
	Month 2	0,0367	0,0355	0,0396	0,0373	0,0355	0,0396	0,0021
	Month 6	0,0313	0,0249	0,0325	0,0296	0,0249	0,0325	0,0041
	η [Pa.s]	Day 0	15,82	15,18	16,83	15,94	15,18	16,83
Day 1		16,07	15,61	17,03	16,24	15,61	17,03	0,73
Week 1		16,56	15,44	16,19	16,06	15,44	16,56	0,57
Month 1		17,57	17,12	14,83	16,51	14,83	17,57	1,47
Month 2		19,54	19,38	16,04	18,32	16,04	19,54	1,98
Month 6		16,77	17,65	16,52	16,98	16,52	17,65	0,59
η_{mix} [Pa.s]		Day 0	12,89	12,30	12,55	12,58	12,30	12,89
	Day 1	14,94	14,26	14,22	14,48	14,22	14,94	0,40
	Week 1	15,52	15,00	12,48	14,33	12,48	15,52	1,63
	Month 1	14,88	14,80	13,57	14,41	13,57	14,88	0,73
	Month 2	14,22	13,67	12,86	13,58	12,86	14,22	0,69
	Month 6	14,33	13,54	13,52	13,80	13,52	14,33	0,46

Appendix 7.7.vi. pH values, storage modulus G' , critical strain γ_c , viscosity η and mixture viscosity η_{mix} of the nonionic cream H3 (1.7 w% PTD) formulated with the Symex production mixer CML 20 (15kg), at t0, day1, week 1 and month 1, 2, 6. The formulation was repeated 3 times (i1, i2 and i3) in the exact same conditions. The mixture viscosity η_{mix} is the viscosity of the hair coloring cream and the developer mixed together (weight mixing ratio 1:1) immediately before the measurement. All measurements are performed at 20°C and the formulations were stored at RT.

		i1	i2	i3	Av.	Min	Max	Std. Dev.
pH	Day 0	9,90	10,00	10,00	9,97	9,90	10,00	0,06
	Day 1	9,95	9,90	9,90	9,92	9,90	9,95	0,03
	Week 1	10,00	10,00	10,00	10,00	10,00	10,00	0,00
	Month 1	9,80	9,80	9,70	9,77	9,70	9,80	0,06
	Month 2	9,90	9,90	9,90	9,90	9,90	9,90	0,00
	Month 6	9,90	9,90	9,65	9,82	9,65	9,90	0,14
G' [Pa]	Day 0	4653,7	5002,4	4754,6	4803,6	4653,7	5002,4	179,43
	Day 1	5224,8	4619,5	4451,3	4765,2	4451,3	5224,8	406,81
	Week 1	4641,2	4323,0	4008,1	4324,1	4008,1	4641,2	316,55
	Month 1	3374,7	3156,9	3479,7	3337,1	3156,9	3479,7	164,65
	Month 2	3446,4	2736,6	3683,5	3288,8	2736,6	3683,5	492,72
	Month 6	2364,7	2238,2	3125,0	2575,9	2238,2	3125,0	479,67
Y _c	Day 0	0,0367	0,0360	0,0369	0,0365	0,0360	0,0369	0,0005
	Day 1	0,0400	0,0432	0,0387	0,0406	0,0387	0,0432	0,0023
	Week 1	0,0413	0,0482	0,0322	0,0406	0,0322	0,0482	0,0080
	Month 1	0,0441	0,0532	0,0356	0,0443	0,0356	0,0532	0,0088
	Month 2	0,0451	0,0512	0,0343	0,0435	0,0343	0,0512	0,0085
	Month 6	0,0443	0,0357	0,0359	0,0386	0,0357	0,0443	0,0049
η [Pa.s]	Day 0	17,82	18,71	18,37	18,30	17,82	18,71	0,45
	Day 1	18,48	18,02	18,75	18,42	18,02	18,75	0,37
	Week 1	18,16	18,05	17,42	17,88	17,42	18,16	0,40
	Month 1	21,24	18,14	16,26	18,55	16,26	21,24	2,51
	Month 2	17,73	18,86	16,25	17,61	16,25	18,86	1,31
	Month 6	17,91	17,32	16,85	17,36	16,85	17,91	0,53
η _{mix.} [Pa.s]	Day 0	9,02	9,88	7,59	8,83	7,59	9,88	1,16
	Day 1	8,72	8,39	7,39	8,17	7,39	8,72	0,69
	Week 1	9,58	7,73	8,18	8,50	7,73	9,58	0,97
	Month 1	9,68	8,94	7,19	8,60	7,19	9,68	1,28
	Month 2	9,17	8,87	7,89	8,65	7,89	9,17	0,67
	Month 6	9,06	8,64	8,35	8,68	8,35	9,06	0,35

Appendix 7.7.vii. pH values, storage modulus G' , critical strain γ_c , viscosity η and mixture viscosity η_{mix} of the nonionic cream H5 (3.3 w% PTD) formulated with the Symex production mixer CML 20 (15kg), at t0, day1, week 1 and month 1, 2, 6. The formulation was repeated 3 times (i1, i2 and i3) in the exact same conditions. The mixture viscosity η_{mix} is the viscosity of the hair coloring cream and the developer mixed together (weight mixing ratio 1:1) immediately before the measurement. All measurements are performed at 20°C and the formulations were stored at RT.

		i1	i2	i3	Av.	Min	Max	Std. Dev.
pH	Day 0	9,60	9,60	9,60	9,60	9,60	9,60	0,00
	Day 1	9,70	9,60	9,70	9,67	9,60	9,70	0,06
	Week 1	9,70	9,70	9,70	9,70	9,70	9,70	0,00
	Month 1	9,60	9,70	9,70	9,67	9,60	9,70	0,06
	Month 2	9,70	9,60	9,70	9,67	9,60	9,70	0,06
	Month 6	9,67	9,70	9,70	9,69	9,67	9,70	0,02
G' [Pa]	Day 0	4054,9	5842,0	7136,8	5677,9	4054,9	7136,8	1547,49
	Day 1	4456,5	4075,8	5771,1	4767,8	4075,8	5771,1	889,49
	Week 1	4021,1	3946,2	3814,5	3927,3	3814,5	4021,1	104,59
	Month 1	3320,7	3980,4	3813,4	3704,8	3320,7	3980,4	342,99
	Month 2	3396,0	3803,1	2298,7	3165,9	2298,7	3803,1	778,14
	Month 6	3170,9	3769,0	2548,0	3162,6	2548,0	3769,0	610,54
γ_c	Day 0	0,0382	0,0347	0,0325	0,0351	0,0325	0,0382	0,0029
	Day 1	0,0400	0,0384	0,0412	0,0399	0,0384	0,0412	0,0014
	Week 1	0,0457	0,0376	0,0483	0,0438	0,0376	0,0483	0,0056
	Month 1	0,0454	0,0389	0,0400	0,0415	0,0389	0,0454	0,0035
	Month 2	0,0441	0,0353	0,0314	0,0370	0,0314	0,0441	0,0065
	Month 6	0,0495	0,0316	0,0353	0,0388	0,0316	0,0495	0,0095
η [Pa.s]	Day 0	22,33	21,18	19,71	21,07	19,71	22,33	1,32
	Day 1	20,44	19,51	21,82	20,59	19,51	21,82	1,17
	Week 1	20,27	18,66	20,83	19,92	18,66	20,83	1,12
	Month 1	18,05	18,36	21,36	19,26	18,05	21,36	1,82
	Month 2	19,86	21,58	21,64	21,03	19,86	21,64	1,01
	Month 6	20,16	21,43	21,38	20,99	20,16	21,43	0,72
η_{mix} [Pa.s]	Day 0	7,45	8,43	8,29	8,06	7,45	8,43	0,53
	Day 1	6,79	7,09	6,33	6,74	6,33	7,09	0,38
	Week 1	7,34	6,90	7,03	7,09	6,90	7,34	0,23
	Month 1	6,87	6,37	7,71	6,98	6,37	7,71	0,68
	Month 2	6,93	6,70	6,64	6,75	6,64	6,93	0,15
	Month 6	7,05	7,32	7,15	7,17	7,05	7,32	0,14

Appendix 7.7.viii. pH values, storage modulus G' , critical strain γ_c , viscosity η and mixture viscosity η_{mix} of the nonionic cream H6 (5.0 w% PTD) formulated with the Symex production mixer CML 20 (15kg), at t0, day1, week 1 and month 1, 2, 6. The formulation was repeated 3 times (i1, i2 and i3) in the exact same conditions. The mixture viscosity η_{mix} is the viscosity of the hair coloring cream and the developer mixed together (weight mixing ratio 1:1) immediately before the measurement. All measurements are performed at 20°C and the formulations were stored at RT.

7.7.5. Storage tests results of the nonionic creams containing hair-dyes mixtures

	Black												
	t0	Week 4			Week 8			Week 12			Week 24		
	RT	-10°C	RT	40°C	-10°C	RT	40°C	-10°C	RT	40°C	-10°C	RT	40°C
pH value	10,01	9,74	9,57	9,66	9,71	9,66	9,54	9,71	9,75	9,67	9,77	9,43	9,81
Viscosity η [Pa.s]	20,39	22,68	22,84	23,65	22,51	21,66	24,34	22,19	22,62	26,97	27,54	23,54	25,67
Stability	OK												
Appearance	thick, glossy												
Color	light beige												

Appendix 7.7.ix. Storage test results of the black nonionic shade at t0, week 4, 12 and 24. The formulation was stored at RT, -10°C and +40°C.

	Brown												
	t0	Week 4			Week 8			Week 12			Week 24		
	RT	-10°C	RT	40°C	-10°C	RT	40°C	-10°C	RT	40°C	-10°C	RT	40°C
pH value	10,33	9,75	9,46	9,81	9,56	9,50	9,93	10,66	10,23	10,34	10,32	10,45	10,61
Viscosity η [Pa.s]	22,87	17,53	21,14	18,30	19,28	20,79	21,39	18,68	19,54	20,93	17,36	18,88	20,63
Stability	OK												
Appearance	thick, glossy												
Color	light beige												

Appendix 7.7.x. Storage test results of the brown nonionic shade at t0, week 4, 12 and 24. The formulation was stored at RT, -10°C and +40°C.

	Orange												
	t0	Week 4			Week 8			Week 12			Week 24		
	RT	-10°C	RT	40°C	-10°C	RT	40°C	-10°C	RT	40°C	-10°C	RT	40°C
pH value	10,53	10,62	10,32	10,29	10,36	10,18	10,47	10,24	10,37	10,32	10,38	10,61	10,46
Viscosity η [Pa.s]	23,39	23,36	23,77	23,95	24,31	25,67	23,94	24,32	23,94	22,14	23,51	23,56	22,12
Stability	OK												
Appearance	thick, glossy												
Color	light orange												

Appendix 7.7.xi. Storage test results of the orange nonionic shade at t0, week 4, 12 and 24. The formulation was stored at RT, -10°C and +40°C.

Red

	t0	Week 4			Week 8			Week 12			Week 24		
	RT	-10°C	RT	40°C	-10°C	RT	40°C	-10°C	RT	40°C	-10°C	RT	40°C
pH value	10,43	10,37	10,27	10,63	10,52	10,42	10,47	10,42	10,56	10,51	10,56	10,38	10,27
Viscosity η [Pa.s]	22,90	20,87	23,86	23,01	24,44	24,43	24,31	20,71	19,85	19,93	22,23	22,65	21,39
Stability	OK												
Appearance	thick glossy												
Color	orange-brown												

Appendix 7.7.xii. Storage test results of the red nonionic shade at t0, week 4, 12 and 24. The formulation was stored at RT, -10°C and +40°C.

Blond

	t0	Week 4			Week 8			Week 12			Week 24		
	RT	-10°C	RT	40°C	-10°C	RT	40°C	-10°C	RT	40°C	-10°C	RT	40°C
pH value	10,52	10,37	10,24	10,27	10,27	10,51	10,41	10,87	10,77	10,79	10,68	10,63	10,73
Viscosity η [Pa.s]	23,74	18,03	19,44	21,62	19,96	20,87	22,57	17,46	18,00	20,10	18,76	20,41	21,64
Stability	OK												
Appearance	thick, glossy												
Color	white, beige												

Appendix 7.7.xiii. Storage test results of the blond nonionic shade at t0, week 4, 12 and 24. The formulation was stored at RT, -10°C and +40°C.

7.7.6. Color delivery data

			Av.	Std. dev.	1	2	3	4	5	6
Black	BH	L	14,88	2,52	17,75	14,59	11,90	14,32	18,74	16,61
		a	-0,07	0,01	-0,07	-0,08	-0,08	-0,08	-0,06	-0,07
		b	-0,68	0,22	-0,73	-0,28	-0,83	-0,80	-0,43	-0,62
	IH	L	16,09	0,53	17,56	16,56	16,42	17,25	16,26	16,39
		a	-0,07	0,07	0,08	0,04	-0,13	0,01	-0,02	0,01
		b	-0,71	0,08	-0,82	-0,59	-0,73	-0,69	-0,64	-0,63
	WH	L	72,92	0,91	72,41	72,01	73,64	73,16	71,33	71,54
		a	1,38	0,52	1,52	1,02	0,95	1,64	1,27	0,19
		b	12,88	0,38	13,17	12,86	12,77	13,25	12,17	12,96
	Brown	BH	L	28,64	1,68	32,48	28,74	28,91	30,27	31,30
a			24,82	0,92	25,71	25,23	26,40	23,67	25,04	24,69
b			22,52	3,23	19,77	27,17	23,97	21,11	24,04	18,44
IH		L	23,47	0,73	24,07	22,37	22,04	23,42	23,17	22,97
		a	13,39	0,22	13,84	13,39	13,27	13,65	13,32	13,48
		b	11,53	0,09	11,45	11,30	11,43	11,35	11,56	11,46
WH		L	72,92	2,68	71,10	72,09	77,35	75,60	75,40	71,08
		a	1,38	0,13	1,47	1,32	1,20	1,40	1,58	1,45
		b	12,88	0,63	12,38	12,78	11,56	13,37	12,39	13,05
Orange		BH	L	21,37	0,41	21,09	21,37	20,44	21,32	21,31
	a		5,79	0,86	6,50	6,81	5,14	5,69	5,52	4,48
	b		7,71	0,49	8,27	7,46	7,55	7,71	7,45	8,62
	IH	L	20,80	1,24	21,83	20,03	20,15	18,36	21,40	19,75
		a	4,98	0,65	5,16	5,22	3,91	4,87	4,35	5,72
		b	5,82	0,27	5,91	5,95	6,06	6,29	5,58	5,60
	WH	L	72,92	1,22	72,66	71,42	71,63	73,87	74,44	73,43
		a	1,38	0,12	1,20	1,36	1,58	1,36	1,33	1,39
		b	12,88	0,86	12,99	12,10	13,21	11,12	12,82	13,44
	Red	BH	L	21,11	0,11	20,91	20,94	21,11	20,82	21,09
a			24,35	1,26	26,91	24,96	23,20	23,86	24,77	24,88
b			10,44	0,21	10,57	10,42	10,26	10,35	10,86	10,54
IH		L	21,31	0,81	21,77	20,79	20,79	21,62	22,35	20,15
		a	15,35	1,86	12,33	17,09	15,99	16,29	16,98	14,19
		b	7,45	0,35	7,54	7,34	7,40	7,69	8,09	7,07
WH		L	72,92	1,33	73,68	74,71	74,81	72,89	75,33	71,83
		a	1,38	0,30	1,36	1,33	1,65	1,24	0,98	1,84
		b	12,88	1,60	15,51	11,58	12,28	11,21	13,85	13,30
Blond		BH	L	76,81	0,92	75,82	77,16	75,14	77,10	77,36
	a		-1,12	0,01	-1,11	-1,13	-1,11	-1,12	-1,13	-1,12
	b		2,31	0,28	2,05	2,63	1,97	2,35	2,23	2,61

	L	74,49	0,63	73,90	73,11	74,07	74,61	73,53	74,78
IH	a	-1,69	0,22	-1,60	-1,50	-1,92	-1,74	-1,36	-1,40
	b	4,83	0,65	3,61	4,79	4,17	3,66	5,28	4,14
	L	72,92	1,46	71,70	75,08	71,98	72,37	72,03	74,52
WH	a	1,38	0,10	1,39	1,31	1,21	1,33	1,10	1,29
	b	12,88	0,67	12,38	12,88	12,25	11,41	13,33	12,90

Appendix 7.7.xiv. Colorimetric results of the ionic reference creams containing hair dyes mixtures applied on real hair strands measured with the spectrophotometer Datacolor Elrepho. Six colorimetric measurements were done per hair strand. The terms BH, IH and WH stand for the different hair types: buffalo hair, ideal hair color and 100% white hair, respectively.

		Av.	Std. dev.	1	2	3	4	5	6	
Black	BH	L	14,58	2,76	13,10	9,48	17,12	12,53	15,71	15,46
		a	-0,05	0,08	0,02	0,00	0,07	-0,16	-0,07	-0,04
		b	-0,75	1,64	0,43	0,25	-1,64	0,82	-1,66	-3,39
	IH	L	15,43	0,58	15,12	15,31	15,85	15,33	15,82	16,71
		a	-0,02	0,01	-0,03	-0,04	-0,01	-0,01	-0,01	-0,02
		b	-0,68	0,27	-0,86	-0,97	-0,31	-1,00	-0,55	-0,68
WH	L	72,92	0,65	71,96	73,02	72,17	73,35	72,07	71,71	
	a	1,38	0,42	1,78	1,74	2,67	1,69	1,48	2,09	
	b	12,88	0,89	13,45	11,21	13,52	13,26	12,32	12,49	
Brown	BH	L	24,97	1,55	22,87	26,33	26,38	25,25	25,08	23,01
		a	22,61	1,04	21,91	24,76	22,20	22,19	22,48	22,62
		b	17,33	2,33	13,61	14,57	18,70	15,58	14,04	18,84
	IH	L	24,55	0,92	24,97	25,95	26,64	25,05	23,97	25,58
		a	15,26	0,41	15,11	15,68	15,18	15,49	15,28	14,49
		b	13,08	1,78	15,39	11,65	11,96	14,53	11,14	11,58
WH	L	72,92	2,90	73,57	75,58	72,06	68,48	75,58	70,14	
	a	1,38	0,29	1,43	1,43	1,29	1,46	0,94	1,85	
	b	12,88	1,28	12,04	12,19	10,41	13,38	13,15	14,03	
Orange	BH	L	20,54	0,93	21,18	21,73	21,57	20,32	21,88	19,52
		a	5,91	0,30	6,22	5,65	5,71	5,99	5,38	5,97
		b	7,72	0,87	9,19	8,23	7,55	7,30	9,50	8,39
	IH	L	20,85	1,72	24,76	22,10	22,07	20,40	21,00	19,97
		a	5,25	0,16	5,47	5,44	5,09	5,18	5,23	5,15
		b	6,42	1,14	6,47	7,60	4,56	7,40	6,20	5,57
WH	L	72,92	1,97	75,75	71,21	73,34	70,39	72,29	74,16	
	a	1,38	0,26	1,33	1,63	0,93	1,57	1,19	1,35	
	b	12,88	1,06	12,84	13,59	13,76	14,64	11,70	12,33	
Red	BH	L	20,64	0,48	21,07	20,58	20,63	20,73	20,43	19,65
		a	25,13	1,03	25,92	26,36	24,00	24,36	25,84	24,27

		b	11,11	1,61	9,77	11,66	10,33	11,37	9,20	13,69
		L	20,04	1,31	20,37	20,74	18,39	19,79	22,01	18,90
	IH	a	13,83	0,10	13,80	13,92	13,61	13,85	13,76	13,77
		b	6,06	1,24	7,47	5,44	7,46	8,61	6,44	5,56
		L	72,92	2,72	71,16	74,01	68,58	69,82	75,89	70,96
	WH	a	1,38	0,52	2,70	1,38	1,70	1,27	1,79	1,48
		b	12,88	0,85	13,36	15,50	13,54	13,25	13,85	13,40
		L	73,31	1,14	73,48	73,84	74,25	71,72	73,00	75,07
	BH	a	0,41	0,93	-0,80	0,56	0,13	0,66	1,24	1,93
		b	0,13	0,20	-0,01	0,21	0,28	-0,10	0,26	0,44
		L	72,53	2,13	71,84	72,89	71,01	69,53	72,39	75,86
Blond	IH	a	0,86	0,44	0,81	1,32	1,21	1,78	0,49	1,14
		b	1,27	0,21	0,93	0,96	0,99	1,23	1,28	1,45
		L	72,92	2,19	72,53	69,88	75,36	73,13	70,78	69,72
	WH	a	1,38	0,10	1,59	1,46	1,44	1,30	1,46	1,37
		b	12,88	1,36	10,41	12,56	12,33	13,27	12,57	14,59

Appendix 7.7.xv. Colorimetric results of the nonionic creams containing hair-dyes mixtures applied on real hair strands measured with the spectrophotometer Datacolor Elrepho. Six colorimetric measurements were done per hair strand. The terms BH, IH and WH stand for the different hair types: buffalo hair, ideal hair color and 100% white hair, respectively.

7.8.List of Tables

Table 1.1. Emulsifiers typical usage according to their HLB values - Classification	7
Table 1.2. Authorized and most common hair dyestuffs for hair coloring products.	30
Table 2.1. Classical hair coloring products containing a blend of ionic and nonionic emulsifiers and different amounts of ammonium sulfate.....	34
Table 2.2. Classical hair coloring products containing a blend of ionic and nonionic emulsifiers and different amounts of PTD.....	35
Table 2.3. Nonionic emulsifiers used for the optimization of the surfactant system of the classical hair coloring product.	35
Table 2.4. Nonionic simplified hair coloring systems containing either one or two PEG surfactants.....	36
Table 2.5. Nonionic hair coloring products containing a blend of nonionic emulsifiers and different amount of salts: either inorganic (ammonium sulfate) or organic (PTD).	37
Table 2.6. Nonionic hair coloring products containing a blend of nonionic emulsifiers and different hair-dyes mixtures. The reference hair coloring products contain a blend of ionic and nonionic emulsifiers and the same hair-dyes mixtures than the nonionic formulations.	37
Table 3.1. Thermal behavior of the raw materials contained in the ionic creams (E0 to E7) during the third heating and second cooling run (2K/min).....	51
Table 3.2. Crystallization temperatures of the creams E0 to E7 during the second cooling run (2K/min). ..	54
Table 3.3. Crystallization temperatures of the creams F1 to F6 during the second cooling run (2K/min)....	56
Table 3.4. Main IR absorption bands of the raw materials contained in the ionic creams E0 to E7.....	57
Table 3.5. Rheological properties of the nonionic systems containing a single emulsifier.	62
Table 3.6. Rheological properties of the nonionic systems containing a combination of two emulsifiers....	64
Table 3.7. Rheological properties of nonionic additional systems containing a combination of two emulsifiers (including PEG-20 oleyl ether or PEG-23 lauryl ether).....	66
Table 3.8. Rheological properties of the nonionic systems containing PEG-2 and PEG-50 cetyl/stearyl ether in combination, at different molar ratio.	67
Table 3.9. Particle size distribution in the creams G0 and H1 to H6, 24 hours after production.	75

Table 3.10. Particle size distribution in the creams G0 and H1 to H6, 3 months after preparation (storage at RT).	75
Table 3.11. Thermal behavior of the raw materials contained in the nonionic creams during the third heating and second cooling run (2K/min).....	84
Table 3.12. Crystallization temperatures of the creams H1 to H6 during the second cooling run (2K/min).	87
Table 3.13. Crystallization temperatures of the nonionic creams containing hair dyes mixtures (shades) during the second cooling run (2K/min).	89
Table 3.14. Main IR absorption bands of the raw materials contained in the nonionic creams	90
Table 3.15. HLB values of PEG-X cetyl/stearyl ether collected from the literature and estimated according to Griffin [25] (X = 2, ...100).....	94
Table 3.16. Weight fraction and HLB values of the surfactants and FA contained in the nonionic systems.	94

7.9. List of Figures

- Figure 1.1. Schematic plot of the total potential energy $V=V_{TOT}$ (plain line) between two particles as a function of the distance H . The dotted lines represent V_A and V_R . (modified from Rosen et al. [29])... 8
- Figure 1.2. Influence of electrolytes concentration on the energy of interaction V_{TOT} between two spherical particles as a function of the distance H . (Taken from Rosen et al. [29]) 10
- Figure 1.3. Illustration of the geometrical PP and the related shapes of surfactants aggregates (Taken from Hiemenz et al. [41]) 12
- Figure 1.4. Liquid crystalline aggregate with different morphologies: (A) spherical micelles, (B) rodlike micelles, (C) disks, (D) inverted micelles L_2 , (E) fragment of a rhombohedral phase, (F) lamellae planar bilayer L_α , (G) inverted hexagonal phase H_{II} , (H) inverted micellar cubic phase I_{II} , (J) bilayer cubic $Im3m$ phase, (K) bilayer cubic $Pn3m$ phase also called sponge phase, (L) bilayer cubic $Ia3d$ phase. (Taken from Tenchov [42]) 13
- Figure 1.5 Schematic representation of a colloidal arrangement containing (A) pure FA (cetyl and stearyl alcohol 1:1), (B) pure nonionic type emulsifier and (C) a mixture of FA and nonionic type surfactants used as co-emulsifiers in water. \circ are the FA polar head, $—$ the long hydrophobic carbon tail of the FA, \sim the POE or hydrophilic moiety and \sim the hydrated POE or hydrophilic moiety (Redrawn from de Vringer et al. [47])..... 14
- Figure 1.6. Schematic diagram of a multiple-phase-o/w emulsion containing ionic surfactant to illustrate the composition of the viscoelastic continuous phase with (A) the crystalline/hydrophilic successive gel phase, (B) the bulk-water, (C) the crystalline phase and (D) the dispersed oil-phase (redrawn and modified Eccleston [24]). Refer to Figure 1.5. for more details of phase (A). 17
- Figure 1.7. Schematic diagram of a multiple-phase-o/w emulsion containing nonionic e.g. PEG surfactants illustrating the composition of the viscoelastic continuous phase with (a) mixed crystal bilayers of PEG surfactants and FA, (b) interlamellarly fixed water (a+b form together the lamellar gel phase), (c) the lipophilic gel phase, (d) the bulk-water, (e) lipophilic components (taken from Eccleston [24])..... 18
- Figure 1.8. Photomicrograph of (left) Maltese crosses and (right) faint Maltese crosses, typical patterns formed by lamellar phases, under PL (Taken from Park et al. [81])..... 23
- Figure 1.9. Different Maltese crosses shape under SALS from planar bilayers to single vesicles densely packed vesicles phase (PP increases) (taken from (Taken from Richtering [82]). 23
- Figure 1.10. (A) Schematic representation of the formation of different lamellar domains from planar lamellar to entangled not flexible bilayers (a) or flexible bilayers and/or round vesicles (b). (B) Typical region of vesicles and lamellar coexistence under optical microscopy (taken from Nagai [83])..... 24
- Figure 1.11. Cryo-TEM micrographs of (a) small micelles, (b) and (c) bilayers, (d) uni-lamellar vesicles (the arrow shows a perforated vesicle) and (e) multi-lamellar vesicles ((a),(b),(d) taken from Gustaffson et

al. [85] and (c),(e) taken from Yuan et al. [86]). (a), (b) and (d) Colloidal system are formed by egg lecithin and cetyltrimethylammonium chloride in brine (NaCl). (c) and (e) Colloidal system are formed by cationic surfactant di-(2-ethylhexyl) phosphoric acid and cationic trimethyltetradecylammonium hydroxide in a salt-free solution..... 25

Figure 1.12. Thermal behavior of C₁₆OH and C₁₈OH pure, blended in a 1:1 mixture and in a ternary system containing 6% ionic surfactants and a large amount of water during (left) the second heating run (heating rate: 5°C/min) and (right) the first cooling run (cooling rate: 5°C/min). (Redrawn from Wunsch et al. [87]). 26

Figure 1.13. Schematic diagram of the sample set-up for ATR-FTIR measurements and the IR light path from the light source to the detector..... 28

Figure 3.1. Photomicrographs of the creams (a) E1, (b) E3, (c) E4, (d) E5, (e) E6 and (f) E7 using PL microscopy 24 hours after preparation (magnification x200)..... 43

Figure 3.2. Photomicrographs of the cream E4 under PL microscopy after one-year storage at RT (magnification x200)..... 44

Figure 3.3. Photomicrographs of the creams (a) E3 and (b) E6 using PL microscopy after dilution 1:1 for the TEM study (magnification x200). 45

Figure 3.4. Photomicrographs of the diluted (1:1), centrifuged and negatively stained creams (left) E3 (right) E6, under TEM. The arrows are indicating the lamellar phases (magnification of the TEM x20000)... 45

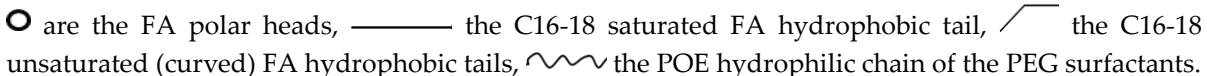
Figure 3.5. Rotational sweep measurement of the creams • E0, ■ E1, ▲ E2, ◆ E3, ○ E4, □ E5, △ E6 ◇ E7, 24 hours after preparation at 20°C. 46

Figure 3.6. Viscosity of the creams E0 to E7 from t0 to month 6 of storage at RT. The viscosity is measured at $\dot{\gamma} = 7,2 \text{ s}^{-1}$ at 20°C. The whiskers above and below the average values define the av. \pm std. dev. 47

Figure 3.7. Critical strain γ_c of the creams E0 to E7 one day (X) and 6 months (—) after preparation (storage at RT). γ_c is expressed as a percent of the total strain range during the amplitude test (γ from 0 to 5) and taken at $\tan\delta = 1$, $\omega = 1.6 \text{ Hz}$ 47

Figure 3.8. Storage modulus G' during the frequency sweep test of the creams • E0, ■ E1, ▲ E2, ◆ E3, ○ E4, □ E5, △ E6 and ◇ E7, 24 hours after preparation in the LVR at 20°C. The frequency ω increases logarithmically from 0.1 to 300 rad/s and the strain $\gamma = 0.001$ corresponds to a displacement angle of $1.77\text{E-}05 \text{ rad}$, such as $\gamma \ll \gamma_c$ 49

Figure 3.9. Loss modulus G'' during the frequency sweep test of the creams • E0, ■ E1, ▲ E2, ◆ E3, ○ E4, □ E5, △ E6 and ◇ E7, 24 hours after preparation in the LVR at 20°C. The frequency ω increases logarithmically from 0.1 to 300 rad/s and the strain $\gamma = 0.001$ corresponds to a displacement angle of $1.77\text{E-}05 \text{ rad}$, such as $\gamma \ll \gamma_c$ 49

Figure 3.10. Loss factor ($\tan\delta$) at high frequency ($\omega = 250$ rad/s) for the creams E0 to E7 one day (X) and six months (—) after preparation. The whiskers above and below the average values define the av. \pm std. dev.	50
Figure 3.11. DSC thermograms of ceteryl alcohol measured between 20°C and 70°C at a heating rate of 2K/min.....	52
Figure 3.12. DSC thermograms of the ionic samples E0 to E7 containing from 0 to 5.0 w% ammonium sulfate in the third heating run. Heating run from 20 to 85°C at a constant a heating rate of 2K/min.	53
Figure 3.13. Melting temperatures T_c (—) and melting enthalpies ΔH (X) of the creams E0 to E7. The measurements were repeated three times. The whiskers above and below the average values define the av. \pm std. dev. The values presented were taken during the third heating run (2K/min).	53
Figure 3.14. DSC thermograms of the ionic samples E0 and F1 to F6 containing from 0 to 7.0 w% PTD in the third heating run. Heating run from 20 to 85°C at a constant a heating rate of 2K/min.	56
Figure 3.15. Melting temperatures T_c (—) and melting enthalpies ΔH (X) of the creams F1 to F7. The measurements were repeated three times. The whiskers above and below the average values define the av. \pm std. dev. The values presented were taken during the third heating run (2K/min).	56
Figure 3.16. Intensity image under ATR-FTIR microscopy at 1420 cm^{-1} of the ionic cream E3 containing 1.0 w% ammonium sulfate. The marked regions A and B correspond to the “concentrated” and the “diffuse” area, respectively. The color pattern corresponds to the color code used in Figure 3.17..	58
Figure 3.17. ATR-FTIR spectra of the ionic cream E3 (1.0 w% ammonium sulfate) in two different regions of the sample: the “concentrated” (red) and the “diffuse” (blue) area. The color pattern corresponds to the color code used in Figure 3.16.. The spectra are measured at RT using UATR-technique with a diamond-KRS-5 (Thallium Bromoiodide) crystal.	58
Figure 3.18. Photomicrographs of (a) S2, (b) S3, (c) S4 and (d) S12 one day after preparation t_0 (above row) and after 6 months storage at RT (below row) under PL microscopy (magnification x200).	63
Figure 3.19. Photomicrographs of (a) S6, (b) S7, (c) S8, (d) S9 and (e) S10 one day after preparation t_0 (above row) and after 6 months storage at RT (below row) under PL microscopy (magnification x200).	66
Figure 3.20. Photomicrographs of (a) S3, (b) S13, (c) S14 and (d) S8 one day after preparation t_0 (above row) and after 6 months storage at RT (below row) under PL microscopy (magnification x200).	68
Figure 3.21. Schematic representation of the bilayers containing (A) a short POE chain single nonionic emulsifier like S1, (B) a long POE chain single nonionic emulsifier like S3 or S4, (C) a medium POE chain single emulsifier having an unsaturated carbon chain like S12 and (D) a short POE chain nonionic emulsifier combined with a long to medium POE chain nonionic emulsifier like S6, S7, S8, S9 and S10. 	

di1, di2 and di3 are the interlamellar distances of the hydrophilic part of the bilayers (where the water is fixed) in system like S1, S3 or S4 or S6 or S7 or S8 or S9 or S10 and S12, respectively. dc1, dc2 and dc3 are the distances between a nonionic emulsifier and successive FA in the hydrophobic part of the bilayer in system like S1, S3 or S4 or S6 or S7 or S8 or S9 or S10 and S12, respectively. Distances are drawn so that $di1 < di3 < di2$ and $dc1 < dc2 < dc3$ 70

Figure 3.22. Photomicrographs of the creams (a) G0, (b) G3, (c) H1, (d) H2, (e) H3, (f) H4, (g) H5 and (h) H6, 24 hours after production, using PL microscopy (magnification x200). 71

Figure 3.23. Photomicrographs of the creams (a) G0, (b) G3, (c) H1, (d) H2, (e) H3, (f) H4, (g) H5 and (h) H6, 6 months after production using PL microscopy (magnification x200). 72

Figure 3.24. Cryo-TEM photomicrographs of the nonionic cream H3 at different magnification. The yellow arrows point the vesicles/flexible bilayers (uni- or multi-lamellar): $[L_{\alpha}]$ phase in (a), (b) and (c). The red arrows point the linear bilayers forming lamellae: L_{α} phase in (d) and (e). The magnifications of the TEM microscope are as follow: (a) x2100, (b) x4200, (c) x10000, (d) 20000, (e) x20000, and (f) x2900. 73

Figure 3.25. Photomicrographs of the creams (a) G0, (b) H1, (c) H2, (d) H2 (e) H4, (f) H5, (g) H6 and (h) F1, 24 hours after preparation under PC light microscopy (magnification x200). 74

Figure 3.26. Description of the automatic particle recognition process for particle size distribution calculation in the nonionic creams using the software ZEN (image analysis module Blue) from Zeiss. Left and middle photomicrographs: PC pictures of the cream H3 before and after isolation of the “objects” (i.e. isolation of the particles from the background). Right: Automatic particle recognition. The yellow dots show the particle with a radius such as $R \geq 2.0 \mu\text{m}$, the green dots show the particles with a radius such as $1 \mu\text{m} \leq R < 2 \mu\text{m}$. The red dots show the particles with a radius such as $R < 1 \mu\text{m}$ 74

Figure 3.27. Average value of the radius of the particles R, for the cream G0 and H1 to H6, (●) one day and (●) 3 months after preparation. The whiskers above and below the average value define the av. \pm std. dev. 76

Figure 3.28. Average, min. and max. radius of the particles for the cream G0 and H1 to H6, (●) one day and (●) 3 months after preparation. The inner circles represent the min. radius, the outer circles represent the max. radius and the circles in between represent the average of the particles’ radius in μm 77

Figure 3.29. Rotational sweep measurement of the creams ● G0, ■ H1, ▲ H2, ◆ H3, ○ H4, □ H5, △ H6, 24 hours after production at 20°C. 78

Figure 3.30. Viscosity of the creams G0 and H1 to H6 from day 1 to month 6 storage at RT. The viscosity η is measured at $\gamma = 7,2 \text{ s}^{-1}$ at 20°C. The whiskers above and below the average values define the av. \pm std. dev. 79

- Figure 3.31. Critical strain γ_c of the creams G0 and H1 to H6 one day after the preparation (X) and after 6 months storage (—) at RT. γ_c is expressed as a percent of the strain range during the strain test (γ from 0 to 5) and taken at $\tan\delta = 1$ 80
- Figure 3.32. Storage modulus G' during the frequency sweep test of the creams • G0, ■ H1, ▲ H2, ◆ H3, ○ H4, □ H5 and △ H6, 24 hours after preparation in the LVR at 20°C. The frequency ω increases logarithmically from 0.1 to 300 rad/s and the strain $\gamma = 0.001$ corresponds to a displacement angle of $1.77E-05$ rad, such as $\gamma \ll \gamma_c$ 81
- Figure 3.33. Loss modulus G'' during the frequency sweep test of the creams • G0, ■ H1, ▲ H2, ◆ H3, ○ H4, □ H5 and △ H6, 24 hours after preparation in the LVR at 20°C. The frequency ω increases logarithmically from 0.1 to 300 rad/s and the strain $\gamma = 0.001$ corresponds to a displacement angle of $1.77E-05$ rad, such as $\gamma \ll \gamma_c$ 81
- Figure 3.34. Storage modulus G' (◆), loss modulus G'' (◇) and complex viscosity $|\eta^*|$ (*) of the cream H3 during the frequency sweep test, 24 hours after preparation (◆,◇,*, respectively) and after 6 months storage at RT (◆,◇,*, respectively). The frequency sweep test is performed at 20°C in the LVR, with the strain $\gamma = 0.001$ corresponds to a displacement angle of $1.77E-05$ rad, such as $\gamma \ll \gamma_c$. The frequency ω increases logarithmically from 0.1 to 300 rad/s. 82
- Figure 3.35. Loss factor ($\tan\delta$) at high frequency ($\omega = 250$ rad/s) for the creams G0 and H1 to H6 one day (X) and six months (—) after preparation. The whiskers above and below the average values define the av. \pm std. dev..... 83
- Figure 3.36. DSC thermograms of PEG-2 cetyl/stearyl ether measured between 20°C and 70°C at a heating rate of 2K/min. 85
- Figure 3.37. DSC thermograms of the nonionic samples G0 and H1 to H6 containing from 0 to 7.0 w% PTD in the third heating run. Heating run from 20 to 85°C at a constant heating rate of 2K/min. 86
- Figure 3.38. First and second thermal transitions: T_{c1} (—) and T_{c2} (—), and the total melting enthalpies ΔH (X) of the creams H1 to H6. The measurements were repeated three times. The whiskers above and below the average values define the av. \pm std. dev. The values presented were taken during the third heating run (2K/min)..... 86
- Figure 3.39. DSC thermograms of the nonionic samples containing different hair-dyes mixtures corresponding to the shades: brown, blond, black, orange and red in the third heating run. Heating run from 20 to 85°C at a constant heating rate of 2K/min..... 88
- Figure 3.40. Melting temperatures (—) and melting enthalpies (X) of the nonionic creams containing hair-dyes mixtures. The measurements were repeated three times. The whiskers above and below the average values define the av. \pm std. dev. The values presented were taken during the third heating run (2K/min)..... 89

Figure 3.41. Intensity image under ATR-FTIR microscopy at 1420 cm^{-1} of the nonionic cream G3 containing 1.0 w% ammonium sulfate. The marked regions A, B and C correspond to the “dispersed”, the “concentrated” and the “diffuse” area, respectively. The color pattern corresponds to the color code used for the spectra in Figure 3.42. 91

Figure 3.42. ATR-FTIR spectra of the nonionic cream G3 (1.0 w% ammonium sulfate) in three different regions of the sample: the “concentrated” (blue), the “dispersed” (red) and the “diffuse” (black) area. The color pattern corresponds to the color code used in Figure 3.41. The spectra are measured at RT using UATR-technique with a diamond-KRS-5 (Thallium Bromoiodide) crystal. 91

7.10. List of publications and patents

Research Article

L. Bonnin, B. Mueller, T. Gassenmeier, R.H.H. Neubert, *“Simple and effective particle-size characterization of opaque emulsions”*, SOFW, 148 (2018).

L. Bonnin, B. Mueller, T. Gassenmeier, G. Hause, R.H.H. Neubert, *“Characterization of multi-component lamellar creams containing electrolytes”*, J. Soc. Cosmet. Chem., in final submission for 2018.

Poster presentation

L. Bonnin, B. Mueller, T. Gassenmeier, R.H.H. Neubert, *“Deep delivery – what can we learn about hair colorations?”*, IFSCC Congress 2018, 18.09.2018 – 21.08.2018, The INFINITY Hotel & Conference Resort in Munich, Germany.

Patents

L. Bonnin, B. Mueller, *“Lamellar o/w emulsion containing a high amount of inorganic/organic salt.”* DE Patent **PT033983**, issued August 16.

L. Bonnin, B. Mueller, *“Salt-tolerant nonionic o/w hair-coloration Emulsion with suitable and steady rheological properties independently of the different salt concentrations.”* DE Patent **102017209769.8**, issued June 17 – not published yet.

7.11. Acknowledgements

Firstly, I would like to address my deepest gratitude to my advisor Prof. Dr. Dr. h.c. Reinhard Neubert, Institute of Applied Dermatopharmacy at the Martin-Luther-University Halle-Wittenberg, for the continuous support of my Ph.D. study, for his insightful and valuable scientific guidance and his motivation and interest in the project. His willingness to supervise this thesis has been a great asset in this joint project between the Martin-Luther-University of Halle-Wittenberg and Henkel.

Besides my advisor, I would like to express my sincere gratitude to my supervisors, Dr. Burkhard Müller, Henkel, Düsseldorf, and Prof. Dr. Thomas Gassenmeier, University of Applied Sciences, Ostwestfalen-Lippe. Their immense knowledge and experience as well as their patience, extreme motivation and constant scientific critical feedback helped me to grow as a research scientist and widen my work from various perspectives. Their encouragements and advice on both my research and my career have been priceless. It was a real pleasure to work with them and I greatly value your time and guidance.

I would also like to thank Prof. Dr. Rolf Daniels to have reviewed my work and showed interest about my research area.

I would like to address a special thanks to Dr. Astrid Kleen and Dr. Mustafa Akram who initiated the research project, encouraged me to continue my study and offered me the opportunity to develop myself as a scientist within a successful chemical company. I greatly acknowledge Henkel in general for the financial support and for offering the possibility to students to grow, learn and take responsibilities in various and challenging R&D focus groups. I am also deeply thankful to my fellow labmates from Henkel R&D: Konstanze Neuba, Mark Krippahl, Udo Erkens, Juergen Schoepgens, Carsten Brake and Bernd Anderheggen, for their sincere and warm welcome, their patience, daily support and curiosity about my research topic. They made my stay in their team lively and enjoyable. Besides, I am thankful to Bruce Cox, Henkel Düsseldorf, and Dr. Thomas Hippe, Henkel, Hamburg, for their valuable insights and constant trust in the last step of the research project. Finally, I would like to thank Daniela Kessler-Becker and Georg Knuebel for translating the English version of the Summary into the German version.

My sincere thanks also go to Dr. Lothar Kintrup and his team, Dietmar Kirchhof, Burkhard Eschen, Dr. Oliver Seiler and Lena Reifenrath, Henkel, Düsseldorf, who provided me with excellent technical assistance and insightful scientific support on every

analytical topics. My deepest gratitude goes also to Dr. Gerd Hause, Biocenter of the Martin-Luther-University, Halle-Wittenberg, for his scientific and technical support on the TEM experimentations.

Finally, I am very grateful to my family, flatmates and friends for their emotional and moral supports. Special thanks to my mother Nathalie Le Bail, my brothers Simon Bonnin and Mathis Bonnin and my step-father Bertrand Sautier, for their help, encouragement, open-mindedness and understandings about my life-choices. Especially my mother who inspired me for doing a long academical journey. I would like to address a special thanks to my beloved partner Dominic Tiedemann, for sharing my feelings and for his perpetual spiritual support. My last thoughts are going to my father, Hervé Bonnin, who is unfortunately no longer with us and who always pushed me towards an international career.

7.12. Curriculum Vitae

<https://www.linkedin.com/in/lucile-bonnin-7b637b58/>

Personal Details:

Name	Lucile Claire Anne-Marie Bonnin
Date of Birth	11.01.1991
Place of Birth	La Roche sur Yon, France
Nationality	French
Marius Status	Single

Education:

04/2015 – 03/2019	PhD student at Henkel AG & Co. KGaA, Düsseldorf, Germany and at Institute of Pharmacy, Martin Luther University Halle-Wittenberg, Germany
09/2011 – 09/2014	MSc in Chemistry, CPE Lyon, Lyon, France and KTH Royal Institute of Technology, Stockholm, Sweden
09/2008 – 09/ 2011	BSc in Chemistry, CPE Lyon, Lyon, France and ENSCR, Rennes, France

Work Experience:

07/2017 – now	R&D Manager at Henkel AG & Co. KGaA, Düsseldorf, Germany
03/2014 – 09/2014	MSc student in R&D at Henkel AG & Co. KGaA, Düsseldorf, Germany
01/2013 – 07/2013	Laboratory assistant in R&D at Henkel AG & Co. KGaA, Düsseldorf, Germany
07/2012 – 12/2012	Laboratory assistant in R&D at L'Oréal Paris, Paris, France
07/2011 – 08/2011	Laboratory assistant in R&D at Sport Protect and at Faculty of Science of Montpellier, Montpellier, France

7.13. References

- [1] J. Halal, "Hair Structure and Chemistry Simplified," 5th ed., New York, NY, USA: Milady, 2009.
- [2] W.S. Lee and H.J. Ahn, "An ultrastructural study of hair fiber damage and restoration following treatment with permanent hair dye," *Int. J. Dermatol.*, vol. 2, pp. 88–92, 2002.
- [3] C.R. Robbins and R.J. Crawford, "Cuticle damage and the tensile properties of human hair," *J. Soc. Cosmet. Chem.*, vol. 42, pp. 59–60, 1991.
- [4] S. Harrison and R. Sinclair, "Hair coloring, permanent styling and hair structure," *J. Cosmet. Dermatol.*, vol. 8, pp. 180–185, 2004.
- [5] C. Boga *et al.*, "Investigation on the dyeing power of some organic natural compounds for a green approach to hair dyeing," *Dyes Pigment*, vol. 97, pp. 9–18, 2013.
- [6] L.J. Wolfram, "Hair cosmetics," in *Handbook of Cosmetic Science and Technology*, Marcel Dekker., New York, NY, USA: A.O. Barel, M. Paye, H.I. Maibach, 2001.
- [7] M.G. Navarre, "The chemistry and manufacture of cosmetics," Continental Press., 4 vols., Orlando, Florida, 1975, p. 864.
- [8] J.F. Corbett, "An historical review of the use of dye precursors in the formulation of commercial oxidation hair dyes," *Dyes Pigment*, vol. 41, no. 1–2, pp. 127–136, 1999.
- [9] G. Kuss and L. Hoehn, "Color reactions of oxidation dye intermediates," *J. Soc. Cosmetic Chem.*, vol. 12, pp. 146–154, 1960.
- [10] H. Tucker, "Hair color with oxidation dye intermediates," *J. Soc. Cosmetic Chem.*, vol. 18, pp. 609–628, 1967.
- [11] R. Goldenberg, "Effect of base component on the properties of oxidation hair dyes," *J. Soc. Cosmetic Chem.*, vol. 19, pp. 423–445, 1968.
- [12] G.M. Wis-Surel, "Some challenges in modern hair color formulations," *Int. J. Cosmetic Sci.*, vol. 21, pp. 327–340, 1999.
- [13] J.F. Corbett, "Chemistry of hair colorant process-science as an aid to formulation and development," *J. Soc. Cosmetic Chem.*, vol. 35, pp. 297–310, 1984.
- [14] J.N. Israelachvili, "Thermodynamic and geometric aspects of amphiphile aggregation into micelles, vesicles and bilayers, and the interactions between them," in *Physics of amphiphiles: micelles, vesicles and microemulsions*, Amsterdam, Holland: V. Degiorgio M. Corti, 1985, pp. 24–54.

- [15] M.L. Bender, "Mechanisms of catalysis of nucleophilic reactions of carboxylic acid derivatives," *Chem. Rev.*, vol. 60, no. 1, pp. 53–113, 1960.
- [16] S.K. Singh, *Handbook of cosmetics*, 1st ed. Delhi, India: Asia Pacific Business Press Inc., 2000.
- [17] M.M. Rieger and L. D. Rhein, "Surfactant chemistry and classification," in *Surfactants in Cosmetics*, 2nd ed., vol. 68, New York, NY, USA: Marcel Dekker, Inc., 1997, pp. 1–28.
- [18] C.R. Robbins, *Chemical and physical behavior of human hair*. New York, NY, USA: Springer, 1988.
- [19] H. Yasunaga, Y. Ishii, T. Komoda, T. Shinkawa, F. Kajiwara, and H. Urakawa, "Function of surfactants in hair dyeing by oxidation dyes 2. Effect on formation of oxidation dyes by p-aminophenol and 5-amino-o-cresol in dye bath," *Int. J. Cosmetic Sci.*, vol. 29, no. 4, pp. 301–309, 2007.
- [20] J. Toedt, D. Koza, and K. Van Cleef-Toedt, "Cosmetic and bathroom product," in *Chemical composition of everyday products*, USA: Greenwood Press, 2005, pp. 25–98.
- [21] P. Versluis and J.C. van de Pas, "Microstructure and rheology of lamellar liquid crystalline phases," *Langmuir*, vol. 13, pp. 5732–5738, 1997.
- [22] K. Holmberg, "Natural surfactants," *Curr. Opin. Colloid In.*, vol. 6, pp. 148–159, 2001.
- [23] M. Lukic, I. Pantelic, R. Daniels, C. Müller-Goymann, M. Savic, and S. Savic, "Moisturizing emulsion systems based on the novel long-chain alkyl polyglucoside emulsifier," *J. Thermal. Anal. Calorim.*, vol. 111, pp. 2045–2057, 2013.
- [24] G.M. Eccleston, "Multiple-phase oil-in-water emulsions," *J. Soc. Cosmetic Chem.*, vol. 41, pp. 1–22, 1990.
- [25] W.C. Griffin, "Classification of surface active agents by HLB," *J. Soc. Cosmetic Chem.*, vol. 1, pp. 311–326, 1949.
- [26] D.L. Courtney, "Emulsifier selection/HLB," in *Surfactant in cosmetics*, 2nd ed., New York, NY, USA: M.M. Rieger, L.D. Rhein, 1997, pp. 127–138.
- [27] J.T. Davies, "A quantitative kinetic theory of emulsion type. I. Physical chemistry of the emulsifying effect," in *2nd Int. Cong. Surf. Activity*, London, UK, 1957, vol. 1, pp. 417–421.
- [28] J.T. Davies, "A quantitative kinetic theory of emulsion type. II. Hydrodynamic factors," in *3rd Int. Cong. Surf. Activity*, London, UK, 1960, vol. 2, pp. 585–594.
- [29] M.J. Rosen, *Surfactants and interfacial phenomena*. New York, NY, USA, 2004.
- [30] J.N. Israelachvili, "Aggregation of amphiphile molecules into micelles, bilayers, vesicles and biological membranes," in *Intermolecular and surface forces*, 2nd ed., Santa Barbara, USA: Academic Press, 1991, pp. 366–394.

- [31] D. Henderson, "Recent progress in the theory of the electric double layer," *Prog. Surf. Sci.*, vol. 13, no. 3, pp. 197–224, 1983.
- [32] S. Ohki and H. Ohshima, "Interaction and aggregation of lipid vesicles (DLVO theory versus modified DLVO theory)," *Colloid Surface B*, vol. 14, pp. 27–45, 1999.
- [33] R.H. Ottewill and T. Walker, "The influence of non-ionic surface active agents on the stability of polystyrene latex dispersions," *Kolloid Z Z Polym*, vol. 227, no. 1–2, pp. 108–116, 1968.
- [34] T. de Vringer, J.G.H. Joosten, and H.E. Junginger, "A study of the hydration of polyoxyethylene at low temperatures by differential scanning calorimetry," *Colloid Polym. Sci.*, vol. 264, pp. 623–630, 1986.
- [35] M. Manciu and E. Ruckenstein, "Role of the hydration force in the stability of colloids at high ionic strengths," *Langmuir*, vol. 17, pp. 7061–7070, 2001.
- [36] Y. Park, R.H. Huang, D.S. Corti, and E.I. Franses, "Colloidal dispersion stability of unilamellar DPPC vesicles in aqueous electrolyte solutions and comparisons to predictions of the DLVO theory," *J. Colloid Interf. Sci.*, vol. 342, pp. 300–310, 2010.
- [37] C. Tanford, "Monolayers, micelles, lipid vesicles and biomembranes," in *Physics of amphiphiles: micelles, vesicles and microemulsions*, Bologna, Italy: V. Degiorgio, M. Coti, 1985, pp. 547–554.
- [38] S. Segota, "Spontaneous formation of vesicles," *Adv. Colloid Interfac.*, vol. 121, pp. 51–75, 2006.
- [39] M. Gradzielski, "Vesicle gels - phase behavior and process of formation," *Curr. Opin. Colloid In.*, vol. 9, pp. 149–153, 2004.
- [40] J.N. Israelachvili, D.J. Mitchell, and B.W. Ninham, "Theory of self-assembly of hydrocarbon into micelles and bilayers," *J. Soc. Cosmetic Chem.*, vol. 72, pp. 1525–1568, 1976.
- [41] P.C. Hiemenz and R. Rajagopalan, *Principles of colloid and surfaces chemistry*. New York, NY, USA: Marcel Dekker, Inc., 1997.
- [42] B. Tenchov, "On the reversibility of the phase-transitions in lipid-water systems," *Chem. Phys. Lipids*, vol. 57, pp. 165–177, 1991.
- [43] M. Mao, J.B. Huang, H.T. Shi, X. He, B.Y. Zhu, and H.L. Fu, "A study on organized assemblies in the sodium alkylcarboxylate/fatty alcohol/water systems," *Chinese J. Chem.*, vol. 18, no. 5, pp. 688–692, 2000.
- [44] H. Kunieda, A. Akahane, J. Feng, and M. Ishitobi, "Phase behavior of polyglycerol didodecanoates in water," *J. Colloid Interf. Sci.*, vol. 245, pp. 365–370, 2002.
- [45] J. Kötz, B. Tiersch, and I. Bogen, "Polyelectrolyte-induced vesicle formation in lamellar liquid crystalline model systems," *Colloid Polym. Sci.*, vol. 278, pp. 164–168, 2000.

- [46] F. Grewe, J. Ortmeier, R. Haase, and C. Schmidt, "Colloidal gels formed by dilute aqueous dispersions of surfactant and fatty alcohol," in *Colloid Process Engineering*, Berlin, Germany: Springer, 2015, pp. 21–43.
- [47] T. de Vringer, J.G.H. Joosten, and H.E. Junginger, "A study of the gel structure in a nonionic O/W cream by differential scanning calorimetry," *Colloid Polym. Sci.*, vol. 264, pp. 691–700, 1986.
- [48] H.E. Junginger, C. Führer, J. Ziegenmeyer, and S. Friebeg, "Strukturuntersuchungen an der wasserhaltigen hydrophilen Salbe DAB 7," *J. Soc. Cosmetic Chem.*, vol. 30, pp. 9–23, 1979.
- [49] R.J. Goetz and M.S. El-Aasser, "Dilute phase behavior of cetyl alcohol, sodium lauryl sulfate, and water," *Langmuir*, vol. 6, pp. 132–136, 1990.
- [50] D. Xia, F.C. Cui, Y. Gan, H. Mu, and M. Yang, "Design of lipid matrix particles for fenofibrate: effect of polymorphism of glycerol monostearate on drug incorporation and release," *J. Pharm. Sci.-US*, vol. 103, pp. 697–705, 2014.
- [51] D. Chapman, "The polymorphism of glycerides," *Chem. Rev.*, vol. 62, no. 5, pp. 433–456, 1962.
- [52] H. Wong, Y. Li, R. Bendayan, M. Rauth, and X.Y. Wu, "Solid lipid nanoparticles for anti-tumor drug delivery," in *Nanotechnology for cancer therapy*, USA: CRC Press, 2007, pp. 741–776.
- [53] V. Jenning and S. Gohla, "Comparison of wax and glyceride solid lipid nanoparticles (SLN®)," *Int. J. Pharm.*, vol. 196, no. 2, pp. 219–222, 2000.
- [54] V. Jenning, A. Gysler, M. Schäfer-Korting, and S. Gohla, "Vitamin A loaded solid lipid nanoparticles for topical use: occlusive properties and drug targeting to the upper skin," *Eur. J. Pharm. Biopharm.*, vol. 49, no. 3, pp. 211–218, 2000.
- [55] V. Jenning, K. Mäder, and S. Gohla, "Solid lipid nanoparticles (SLN™) based on binary mixtures of liquid and solid lipids: a ¹H-NMR study," *Int. J. Pharm.*, vol. 205, no. 1–2, pp. 15–21, 2000.
- [56] R. Shah, D. Eldridge, E. Palombo, and I. Harding, "Composition and structure," in *Lipid nanoparticles: production, characterization and stability*, vol. 4, USA: Springer, 2015, pp. 11–22.
- [57] S. Fukushima and M. Yamaguchi, "The effect of cetostearyl alcohol on cosmetic emulsions," *Cosmet. Toiletries*, vol. 98, pp. 89–102, 1983.
- [58] H.E. Junginger, "Multiple phase emulsion," in *Surfactants in cosmetics*, 2nd ed., vol. 68, New York, NY, USA: M.M. Rieger, L.D. Rhein, 1997, pp. 155–182.
- [59] G.M. Eccleston and L. Beattie, "The influence of emulsifier composition in the microstructure of nonionic semisolids," *J. Pharm. Pharmacol.*, vol. 12, p. 77, 1989.

- [60] T. de Vringer, J.G.H. Joosten, and H. Junginger, "Characterization of the gel structure in a nonionic ointment by small angle X-ray diffraction," *Colloid Polym. Sci.*, vol. 262, pp. 56–60, 1984.
- [61] T. de Vringer, J.G.H. Joosten, and H.E. Junginger, "A study of the gel structure in a nonionic O/W cream by X-ray diffraction and microscopic methods," *Colloid Polym. Sci.*, vol. 265, pp. 167–179, 1987.
- [62] T. de Vringer, J.G.H. Joosten, and H.E. Junginger, "A study of the ageing of the gel structure in a nonionic O/W cream by X-ray diffraction, differential scanning calorimetry and spin-lattice relaxation measurements," *Colloid Polym. Sci.*, vol. 265, pp. 448–457, 1987.
- [63] K. Mandani and S. Friberg, "Van der Waals interactions in three phase emulsions," *Progr. Colloid Polymer Sci.*, vol. 65, pp. 164–178, 1978.
- [64] F. Friberg and K. Larsson, in *Advances in liquid crystals*, vol. 2, London, UK: G.M. Brown, 1976, pp. 173–195.
- [65] M. Kónya *et al.*, "Study of the microstructure of oil/water creams with thermal and rheological methods," *J. Thermal. Anal. Calorim.*, vol. 73, pp. 623–632, 2003.
- [66] G.M. Eccleston and L. Beattie, "Microstructural changes during the storage of systems containing cetostearyl alcohol/polyoxyethylene alkyl ether surfactants," *Drug Develop. and Indust. Pharm.*, vol. 14, pp. 2499–2518, 1988.
- [67] J. Bergenholtz, "Theory of rheology of colloidal dispersions," *Curr. Opin. Colloid In.*, no. 5–6, pp. 484–488, 2001.
- [68] L.E. Silbert and J.R. Melrose, "The rheology and microstructure of concentrated, aggregated colloids," *J. Rheol.*, vol. 43, no. 3, pp. 673–688, 1999.
- [69] R. Brummer, *Rheology essentials of cosmetic and food emulsions*, Springer. Berlin, Germany, 2006.
- [70] H. Rehage and H. Hoffmann, "Viscoelastic surfactant solutions: model systems for rheological research," *Mol. Phys.*, vol. 74, pp. 933–973, 1991.
- [71] W.P. Cox and E.H. Merz, "Correlation of dynamic and steady flow viscosities," *J. Polym. Sci.*, vol. 28, pp. 619–622, 1958.
- [72] W.M. Kulicke and R.S. Porter, "Relation between steady shear flow and dynamic rheology," *Rheol. Acta*, vol. 19, no. 5, pp. 601–605, 1980.
- [73] P. Fernandez, N. Willenbacher, T. Frechen, and A. Kühnle, "Vesicles as rheology modifier," *Colloid Surface A*, vol. 262, 2005.

- [74] J. Zhao *et al.*, "Phase behavior and rheological properties of the lamellar liquid crystals formed in dodecyl polyoxyethylene polypropylene ether/water system," *Indian J. Chem.*, vol. 50A, pp. 641–649, 2011.
- [75] S. Kinzel and M. Gradzielski, "Control of phase behavior and properties of vesicle gels by admixing ionic surfactants to the nonionic surfactant Brij 30," *Langmuir*, vol. 24, pp. 10123–10132, 2008.
- [76] T.S. Awad, E.S. Johnson, A. Bureiko, and U. Olsson, "Colloidal structure and physical properties of gel networks containing anionic surfactant and fatty alcohol mixture," *J. Disper. Sci. Technol.*, vol. 32, pp. 807–815, 2011.
- [77] B. Medronho, M.G. Miguel, and U. Olsson, "Viscoelasticity of a nonionic lamellar phase," *Langmuir*, vol. 23, pp. 5170–5274, 2007.
- [78] P.S. Prestes *et al.*, "Rheological Measurements and Thermal Characterization of Lamellar Gel Phase Emulsions Developed with Cetearyl Alcohol/Nonionic Ethoxylated Surfactants," *J. Disper. Sci. Technol.*, vol. 33, no. 11, 2012.
- [79] M.G. Berni, C.J. Lawrence, and D. Machin, "A review of the rheology of the lamellar phase in surfactants systems," *Adv. Colloid Interfac.*, vol. 98, pp. 217–243, 2002.
- [80] A. Manosroi *et al.*, "Characterization of vesicles prepared with various non-ionic surfactants mixed with cholesterol," *Colloid Surface B*, vol. 30, pp. 129–138, 2003.
- [81] B.D. Park, J.K. Youm, S.K. Jeong, E.H. Choi, S.K. Ahn, and S.H. Lee, "The characterization of molecular organization of multilamellar emulsions containing pseudoceramide and type III synthetic ceramide," *J. Invest. Dermatol.*, vol. 121, no. 4, pp. 794–801, 2003.
- [82] W. Richtering, "Structure formation in colloidal systems," Christian-Albrechts-Universität zu Kiel, Kiel, Germany, 2002.
- [83] Y. Nagai, Y. Kawabata, and T. Kato, "Microscopic investigation on morphologies of bilayer gel structure in the mixed polyoxyethylene-type nonionic surfactant systems," *J. Phys. Chem. B.*, vol. 116, pp. 12558–12566, 2012.
- [84] L.E. Franken, E.J. Boekema, and M.C.A. Stuart, "Transmission electron microscopy as a tool for the characterization of soft materials: application and interpretation," *Adv. Sci.*, vol. 4, pp. 1600476–1600485, 2017.
- [85] J. Gustafsson, G.O.G. Lindblom, U. Olsson, and M. Almgren, "A defective swelling lamellar phase," *Langmuir*, vol. 13, pp. 852–860, 1997.
- [86] Z. Yuan, S. Dong, W. Liu, and J. Hao, "Transition from vesicle phase to lamellar phase in a salt-free cationic surfactant solution," *Langmuir*, vol. 25, no. 16, pp. 8974–8981, 2009.

- [87] K. Wunsch *et al.*, "Effect of surfactant on structure thermal behavior of cetyl stearyl alcohols," *J. Thermal. Anal. Calorim.*, vol. 123, no. 2, pp. 1411–1417, 2016.
- [88] S. Fukushima, M. Takahashi, and M. Yamaguchi, "Effects of cetostearyl alcohol on stabilization of oil-in-water emulsion I. Difference in the effect by mixing cetyl alcohol with stearyl alcohol," *J. Colloid Interf. Sci.*, vol. 57, pp. 201–206, 1976.
- [89] H.M. Ribeiro, J.A. Morais, and G.M. Eccleston, "Structure and rheology of semi-solid o/w creams containing cetyl alcohol/non-ionic surfactant mixed emulsifier and different polymer," *Int. J. Cosmetic Sci.*, vol. 26, pp. 47–59, 2004.
- [90] S.E. Glassford, B. Byrne, and S.G. Kazarian, "Recent application of ATR -FTIR spectroscopy and imaging to proteins," *Biochim. Biophys. Acta*, vol. 1834, pp. 2849–2858, 2013.
- [91] S.G. Kazarian and K.L.A. Chan, "Application of ATR-FTIR spectroscopic imaging to biomedical samples," *Biochim. Biophys. Acta*, vol. 1758, pp. 858–867, 2006.
- [92] A.R. Hind, A. McKinnon, and S.K. Bhargava, "At the solid/liquid interface: FTIR/ATR - the tool of choice," *Adv. Colloid Interfac.*, vol. 93, no. 1–3, pp. 91–114, 2001.
- [93] R.N. Lewis and R.N. McElhaney, "Fourier transform infrared spectroscopy in the study of lipid phase transitions in model and biological membranes: practical considerations," *Methods Mol. Biol.*, vol. 400, pp. 201–226, 2007.
- [94] T.R. Carale, Q.T. Pham, and D. Blankschtein, "Salt effects in intracellular interactions and micellization of nonionic surfactants in aqueous solutions," *Langmuir*, vol. 10, pp. 109–121, 1994.
- [95] A. Ray and G. Némethy, "Effect of ionic protein denaturants on micelle formation by nonionic detergents," *J. Am. Chem. Soc.*, vol. 93, no. 25, pp. 6787–6793, 1971.
- [96] I. Martinez, M.A. Ricardo, and J.M. Franco, "Effect of salts content on the rheological properties of salad dressing-type emulsions stabilized by emulsifier blends," *J. Food Eng.*, vol. 80, no. 4, pp. 1272–1281, 2007.
- [97] M.S. Brooks and G.D. Moggridge, "The effect of additives and the stability of multilamellar vesicles in a commercial surfactant system," *ICHemE*, pp. 139–146, 2006.
- [98] A.L. Márquez, A. Medrano, L.A. Panizzolo, and J.R. Wagner, "Effect of calcium salts and surfactant concentration on the stability of water-in oil emulsions prepared with polyglycerol polyricinoleate," *J. Colloid Interf. Sci.*, vol. 341, pp. 101–108, 2010.
- [99] P. Ghosh and M. Banik, "Effects of salts containing mono-, di- and trivalent ions on electrical and rheological properties of oil water interface in presence of cationic surfactant: importance in stability of oil-in -water emulsions," *J. Disper. Sci. Technol.*, vol. 35, no. 4, pp. 471–481, 2014.

- [100] A.K. Chattopadhyay, L. Ghaicha, S.G. Oh, and D.O. Shah, "Salt effects on monolayers and their contribution to surface viscosity," *J. Phys. Chem-US*, vol. 96, no. 15, pp. 6509–6513, 1992.
- [101] K. Katagiri, K. Ariga, and J. Kikuchi, "Novel class of organic-inorganic hybrid vesicle 'cerasome' derived from various amphiphiles with alkoxysilyl head," in *Proceedings of the international conference on colloid and surface science*, vol. 132, Amsterdam, the Netherlands: Elsevier, 2001.
- [102] E. van der Linden and C.J. Buytenhek, "Spontaneous formation of onion phases in a single surfactant system and their salt-induced transformation towards ordinary lamellar phase," *Physica A*, vol. 245, pp. 1–10, 1997.
- [103] E. Ullmann, K. Thoma, and O. Fickel, "Zum Mechanismus des Löslichkeitsvermittlung von Phenolen durch Polyäthylenglykolstearate," *Arch. Pharm. Res.*, vol. 303, no. 4, pp. 305–309, 1970.
- [104] K. Thoma, E. Ullmann, and O. Fickel, "Ausmaß und Ursache der Bindung von Phenolen durch Polyäthylenglykolstearate," *Arch. Pharm. Res.*, vol. 303, no. 4, pp. 297–304, 1970.
- [105] E. Azaz and M. Donbrow, "Solubilization of phenolic compounds in nonionic surface-active agents. I. Binding pattern and parameters of phenol, cresols and xylenols," *J. Colloid Interf. Sci.*, vol. 57, pp. 11–19, 1976.
- [106] V. Vitagliano, O. D'Errico, O. Ortona, and L. Paduano, "Physico Chemical properties of ethoxylated surfactants in aqueous solutions," in *Encyclopedia of surface and colloid science*, 2nd ed., vol. 6, Columbia University, USA: CRC Press, 2006.
- [107] J. Potschadel, "Inkompatibilitäten," presented at the Apothekerkammer Nordrhein für Pharmazeuten, NRW, Germany, 2015.
- [108] M. A. S. Abd El-Galeel, "Solubility and stability of natural food colorants in microemulsions," Rheinschen Friedrich-Wilhelms-Universität, Bonn, Germany, 2002.
- [109] P.P Constantinides and S.H. Yiv, "Particle size determination of phase inverted water-in-oil microemulsions under different dilution and storage conditions," *Int. J. Pharm.*, vol. 15, pp. 225–234, 1991.
- [110] S. Tomar, "25 fun facts about hair," *Madison-Reed*, 2015. .
- [111] T. Schmidts, D. Dobler, C. Nissing, and F. Runkel, "Influence of hydrophilic surfactants on the properties of multiple W/O/W emulsions," *J. Colloid Interf. Sci.*, vol. 338, pp. 184–192, 2009.
- [112] J.N. Israelachvili, "The science and applications of emulsions - an overview," *Colloid Surface A*, vol. 91, pp. 1–8, 1994.
- [113] "Emulsifiers, emollients and solubilizers for personal care." Kolb Distribution Ltd.

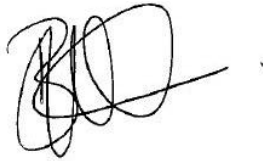
- [114] K. Aramaki *et al.*, "Formation of bilayer membrane and niosomes by double-tailed polyglyceryl-type nonionic surfactant," *Langmuir*, vol. 31, pp. 10664–10617, 2015.
- [115] R.G. Larson, *The structure and rheology of complex fluids*. New York, NY, USA: Oxford University Press, 1999.
- [116] Y. Iwasawa, N. Oyama, and H. Kunieda, "Proceedings of the International Conference on Colloid and Surface Science," presented at the Conference on Colloid and Surface Science, Tokyo, Japan, 2000, pp. 589–593.
- [117] C. Ballmann and B.W. Müller, "Stabilizing effect of cetostearyl alcohol and glycerylmonostearate as co-emulsifiers on hydrocarbon-free o/w glyceride cream," *Pharm. Dev. Technol.*, vol. 13, pp. 433–445, 2008.
- [118] A. Theodorou, "Mixed surfactant lamellar phases: studies under shear," University of Manchester, Manchester, UK, 2010.
- [119] K. Tasaki, "Poly(oxyethylene)–water Interactions: A molecular dynamics study," *J. Am. Chem. Soc.*, vol. 118, no. 35, pp. 8459–8469, 1996.
- [120] E. Evans and D. Needham, "Physical properties of surfactant bilayer membranes: thermal transitions, elasticity, rigidity, cohesion, and colloidal interactions," *J. Phys. Chem.*, vol. 91, pp. 4219–4228, 1987.
- [121] H. He *et al.*, "Cubosomes from hierarchical self-assembly poly(ionic liquid) block copolymers," *Nat. Commun.*, vol. 8, pp. 14057–14065, 2017.
- [122] M. Silvander, G. Karlsson, and K. Edwards, "Vesicle solubilization by alkyl sulfate surfactants: a cryo-TEM study of the vesicle to micelle transition," *J. Colloid Interf. Sci.*, vol. 179, pp. 104–113, 1996.
- [123] M. Vaccaro, C. von Corswant, and O. Söderman, "Investigation of the adsorption of PEG1500-12-acyloxystearate surfactants onto phospholipids bilayers: an ellipsometry and cryo-TEM study," *Biophys. J.*, vol. 93, pp. 4300–4306, 2007.
- [124] M. Frenkel, R. Shwartz, and N. Garti, "Multiple emulsions: I. Stability, apparent and weighted HLB," *J. Colloid Interf. Sci.*, vol. 94, no. 1, pp. 174–178, 1983.
- [125] G. Sharma, *Digital color imaging Handbook*. New York, NY, USA: CRC Press, 2003.

7.14. Declaration of academic integrity

With this statement I declare that I have independently completed the above PhD thesis entitled Optimization of stability and rheological robustness of cosmetic salt-containing lamellar gel phase emulsions. The thoughts taken directly or indirectly from external sources are properly marked as such. This thesis was not previously submitted to another academic institution and has also not yet been published.

Düsseldorf, 05.07.2018, Lucile Claire Anne-Marie Bonnin

X



Lucile Bonnin
Ph.D. Student, R&D Manager